

Michela Comune

# Wound healing and pro-angiogenic properties of LL37-conjugated nanoparticles

Tese de doutoramento em Biociências, Especialização em Biotecnologia, orientada pelo Doutor Lino Silva Ferreira e co-orientada pela Doutora Ana Luísa Monteiro Carvalho e Doutor Akhilesh Rai, apresentada ao Departamento de Ciências da Vida da Faculdade de Ciências e Tecnologia da Universidade de Coimbra.

Dezembro de 2015



UNIVERSIDADE DE COIMBRA





UNIVERSIDADE DE COIMBRA

MICHELA COMUNE

# **Wound healing and pro-angiogenic properties of LL37-conjugated nanoparticles**

Tese de doutoramento em Biociências, Especialização em Biotecnologia, orientada pelo Doutor Lino Ferreira e co-orientada pela Doutora Ana Luísa Carvalho e o Doutor Akhilesh Rai, apresentada ao Departamento de Ciências da Vida da Faculdade de Ciências e Tecnologia da Universidade de Coimbra.

Coimbra, Dezembro de 2015

**The following financial support are acknowledged:**



NANODRUG (Novel nanoparticles for drug delivery to the skin) is a research project funded by the European Commission, Marie Curie Actions, Seventh Framework Programme, Initial Training Network (project n° 289454, 2011-2015).

ERC (project n° 307384, Nanotrigger).



*Alla mia famiglia, Salvatore, Paola, Nicola, insostituibile fonte di forza, amore e sostegno.*

*Ai miei sogni. Al mio futuro...*

# Acknowledgements

I would like to express my sincere gratefulness to my advisor, Dr. Lino Ferreira for encouraging my research and for allowing me to grow as a research scientist. Thanks for your advices, suggestions, corrections, discussions and the innumerable brainstorming meeting. Thanks also for all the conflicts, the debate about different ideas and way of seeing things because I learned a lot even from that.

My thanks also goes to Dr. Akhilesh Rai to have introduced me to the fascinating world of gold nanoparticles, for his teaching, especially in the first years. Thanks to Prof. Dr. Ana Luisa Carvalho, for her courteousness, help, patience and kindness.

Thanks to the University of Coimbra, Biocant Park and CNC, their members and all the facilities because I could perform my work there, in a great environment.

A gigantic thanks to NANODRUG Family, to the coordinator Prof. Resmini, all the professors and fellows, for everything we lived together around Europe, for the science we made, for the friendships will stay for ever. NANODRUG is certainly one of the best experience that happened in my life. I would like to relive it! Thanks to Marie Curie Actions.

My sincere thanks also goes to Dr. Veronique Preat from the UCL (Brussels) and Dr. Jorge Rosenfeld from Sanofi Aventis (Toulouse), who provided me an opportunity to join their team, and who gave access to their laboratory and research facilities.

I would like to thank all the external collaborators of my papers: Kiran Kumar Chereddy, Andre F. Ferreira, Rodrigo A. Cunha, Juan Lerma, Ricardo J. Rodrigues, Pedro N. Simoes, Veronique Preat. Without their precious support it would not be possible to conduct this research. Thanks to all the people are not listed in the papers but they helped me. Thanks to my two wonderful technicians, Catarina Rebelo

---

and Joao Pedro Lopes.

I thank All the colleagues/friends, from the past and the present (nobody excluded), of the Biomaterials and Stem Cell-Based Therapeutics Laboratory for the hours we spent in the lab together, for the happy and stressful moments, for the fun and the crying, for your support, smiles, for your help, for having welcomed this crazy italian girl with open arms. Thanks for all the moments and experiences with also had outside of the lab. For the friendship.

Luis (our unique lab manager), Sandrinha (Bruno and Nuno), Sonia, Susana R., Susana S., Vitorrrr, Renato Renato, Adrianino, Josefina, Alessandra, Ivana, Sezin, Pedrinho, Miguelino, Zezinho, Cata R., Nina, Xica, Paty, Joao Maia, Joao R., Joao Sargento, Emanuelli, Hugo and Ana, Filipe and his group, Ricardo, Joana, Helena A. (with her beautiful family), Helenina V., Akhy, Tania, Carlos (and Vania), and all the students...Grazie a tutti!

Special Thanks goes to Cristiana. She introduced me to cell culture room and rules with her calm, patience and sweet smile. I will never forget that!

Thanks to all my aunts, uncles and cousins and all my relatives. I also thank my friends in Coimbra and all my friends in Sardinia, Italy and around the world. You were always with me, I really felt your support in these years. Un grazie speciale alle sempre presenti Porden e Laura. VVB

Special thanks to Josephine. My little german girl. I will never stop to thank "Marie Curie Project" because it made me meet you in Coimbra. You know what I think, you know what we lived together, don't need to write here. But I want to thank you for your friendship, your sweet eyes and heart, your help, support and because you are able to understand me just looking at me. Thanks for all the crazy days and nights out, for our trips :D. Thanks because you were with me in these portuguese years of my life. I leave Coimbra knowing I got a german sister in Portugal!!! TVB. Dank.

Special thanks also goes to my Spanish family, Adri and Vane, for all the funny moments we spent together. To be always available to help me and for the love and affection you gave to me, making me feel as part of your family. VVB.

My tender thanks to AMCS, for the help, support and love you gave to me. For

everything. To keep dreaming together. Love you.

Last but not the least, I would like to thank my family: my parents and my brother for supporting me and my life in general. Without you anything of this could be possible.

Un grazie speciale ai miei genitori e al mio fratellino, senza di loro nulla di ciò che ho fatto fino ad ora sarebbe stato possibile. Grazie per il sostegno che mi date, della forza, del coraggio, dell'amore e grazie per credere così tanto in me. Grazie per esserci sempre da vicino e da lontano, grazie per aiutarmi a tirarmi su quando a volte cado, grazie degli insegnamenti che mi avete dato. Grazie per non avermi mai messo limiti e avermi incoraggiato a seguire i miei sogni, anche se questo significava privarvi della mia presenza per tanto tempo. Un grazie infinito. Vi amo. E grazie per essere qui, ancora una volta, con me.

If I forgot someone, it was a mistake. My will was to thank all the people I met in these 5 years with whom I shared moments, conversations and experiences.

Obrigada Coimbra. Obrigada Portugal

## 0.1 Abstract

Impaired wound healing and its medical complications remain one of the most prevalent and economically burdensome healthcare issues in the world. In the United States alone, chronic wounds affect 6.5 million patients. More than US\$ 25 billion is spent annually on treatment of chronic wounds and the burden is growing rapidly due to increasing health care costs, an aging population and a sharp rise in the incidence of diabetes and obesity worldwide. Recent data indicate that 11.7% of the Portuguese population is diabetic. One of the most serious and debilitating complications of diabetes is the development of chronic non-healing wounds. In recent years, there have been efforts to develop new advanced methodologies to heal chronic wounds including the use of topic growth factors or cell-based therapies. Unfortunately, in many cases, the therapeutic efficacy is low, the therapies are expensive and require application in a clinical facility, and they have no antimicrobial activity. Therefore, development of new therapeutics is absolutely necessary and important to satisfy the unmet clinical need. Antimicrobial peptides (AMPs) synthesized in the skin provide a barrier to infection and some of them are very important for the regeneration of skin. LL37 is the most important AMP in skin, acts as first line of defense against bacteria, virus, fungi and plays an important role in immunomodulation, angiogenesis and wound healing properties. Recently, phase I/II clinical trials have demonstrated its therapeutic efficacy in chronic wounds; however, multiple topical administrations were required. The main goal of this thesis was to develop a LL37 nanoparticulate formulation with higher wound healing properties than the free peptide. The nanoparticulate formulation was prepared by a novel methodology in which thiol-terminated LL37 acts as capping agent during NP formation. This formulation has a gold (Au) core and a hydrophilic cationic LL37 peptide shell. We have selected Au NPs because it is relatively easy the immobilization of high concentrations of LL37 per surface area, the modification of their properties (including size, charge and morphology), and they have been used in the clinic for many years. LL37-Au NPs have controlled size (21 nm), low polydispersity, positive zeta potential (15 mV), high density of LL37 (250  $\mu$ g of peptide per mg of NP) and high stability in aqueous solutions and cell culture media. They showed antimicrobial activity against *E.coli* and high biological activity against mammalian cells, namely pro-angiogenic activity against endothelial cells and pro-migratory activity against keratinocytes. Remarkably, LL37-Au NPs have lower cytotoxicity than LL37 peptide. Our results further show that LL37-Au NPs are internalized by keratinocytes and endothelial cells, and in case of keratinocytes, the internalization

process is mostly mediated by scavenger receptors. The internalized LL37-Au NPs tend to accumulate in the endolysosomal compartment both in keratinocytes and endothelial cells. In both cell models, LL37-Au NPs induce the transactivation of EGFR. In case of keratinocytes, the process is initiated by the activation of P2X receptors that leads to a long-lasting phosphorylation of EGFR and ERK. This results in enhanced migratory properties of keratinocytes. In vivo results show that LL37-Au NPs have superior wound healing properties than LL37 peptide in a splinted mouse full thickness excisional model. In case of endothelial cells, LL37 peptide but not LL37-Au NPs activate FPRL1, intracellular accumulation of  $Ca^{2+}$  and secretion of  $VEGF_{165}$ . Yet, both LL37 and LL37-Au NPs have high pro-angiogenic activity as demonstrated in a Matrigel and chorioallantoic membrane (CAM) assays. It is likely that the pro-angiogenic activity of LL37-Au NPs is mediated by the transactivation of EGFR but further studies are needed to address this issue. The results presented here are an exciting first step toward the development of antimicrobial peptide-based nanotherapeutics for skin disorders paving the way for additional studies in more complex animal models. It is the first skin therapy that combines wound-healing efficacy and antimicrobial activity in the same formulation, it is cheaper than the actual advanced therapies, and may be administered only one time.

## 0.2 Resumo

Problemas de cicatrização de feridas e suas complicações médicas continuam a ser um dos problemas de saúde mais prevalentes e economicamente onerosos do mundo. Nos Estados Unidos, as feridas crónicas afectam 6.5 milhões de pacientes. Mais de 25 bilhões de dólares são gastos anualmente em tratamento de feridas crónicas e a despesa irá crescer rapidamente devido ao aumento dos custos de saúde, o envelhecimento da população e um aumento acentuado na incidência de diabetes e obesidade em todo o mundo. Dados recentes indicam que 11.7% da população Portuguesa é diabética. Uma das complicações mais graves e debilitantes da diabetes é o desenvolvimento de feridas crónicas e não cicatrizantes. Nos últimos anos, tem havido esforços para se desenvolver terapias avançadas para a cicatrização de feridas crónicas, incluindo o uso tópico de factores de crescimento ou terapias celulares. Infelizmente, em muitos casos, a eficácia terapêutica é baixa, as terapias são caras, requerem aplicação clínica e não possuem actividade antimicrobiana. Portanto, é imperativo o desenvolvimento de novas terapêuticas para responder a esta necessidade clínica. Os péptidos antimicrobianos (AMPs) sintetiza-

dos na pele podem constituir futuras terapias já que são moléculas que formam uma barreira à infecção e alguns deles são muito importantes para a regeneração da pele. O péptido LL37 é o AMP mais importante na pele, actuando como primeira linha de defesa contra bactérias, vírus, fungos e desempenha um papel importante na imunomodulação, angiogénese e cicatrização de feridas. Recentemente, foram publicados os resultados de um ensaio clínico fase I/II com o péptido LL37 que demonstram a sua eficácia terapêutica em feridas crónicas; no entanto, foram necessárias múltiplas administrações tópicas. O objectivo principal desta tese foi desenvolver uma formulação de nanopartículas conjugadas com LL37 de forma a possuir maior actividade de cicatrização da pele que o péptido livre (não imobilizado). A formulação de nanopartículas foi preparada por uma nova metodologia na qual foi utilizado o péptido LL37 com um terminal tiol, actuando o péptido como agente de revestimento durante a formação da nanopartícula. Esta formulação tem um núcleo de ouro (Au) e um escudo formado pelo péptido catiónico LL37. Durante esta tese seleccionámos nanopartículas de ouro porque é relativamente fácil a imobilização de altas concentrações de LL37 por unidade de superfície, a modificação das suas propriedades (incluindo tamanho, carga e morfologia), e pelo facto destas nanopartículas terem sido utilizadas na prática clínica há muitos anos. Estas nanopartículas possuem um tamanho controlado (21 nm), baixa polidispersão, um potencial zeta positivo (15 mV), alta densidade de LL37 (250  $\mu\text{g}$  de péptido por mg de nanopartícula) e alta estabilidade em soluções aquosas e meios de cultura celular. As nanopartículas mostraram actividade antimicrobiana contra *E.coli* e elevada actividade biológica contra células de mamíferos, ou seja, actividade pró-angiogénica em células endoteliais e actividade pró-migratória em queratinócitos. Surpreendentemente, as nanopartículas conjugadas com LL37 possuem menor citotoxicidade que o péptido LL37 livre. Os nossos resultados mostram ainda que as nanopartículas são internalizadas pelos queratinócitos e células endoteliais, e no caso de queratinócitos, o processo de internalização é mediado principalmente pelo receptor scavenger. As nanopartículas internalizadas tendem a se acumular no compartimento endolisosomal dos queratinócitos e das células endoteliais. Em ambos os modelos celulares, as nanopartículas induzem a transactivação do EGFR. No caso dos queratinócitos, o processo é iniciado pela activação de receptores P2X que levam a uma prolongada fosforilação de EGFR e de ERK. Isto leva a que os queratinócitos possuam maiores propriedades migratórias. Os resultados in vivo mostram que nanopartículas conjugadas com LL37 têm melhores propriedades cicatrizantes de feridas comparativamente ao péptido livre. No caso de células endoteliais, o péptido LL37, mas não

as nanopartículas conjugadas com LL37, levam à activação do receptor FPRL1, à acumulação de cálcio intracelular e à secreção de  $VEGF_{165}$ . No entanto, tanto o péptido LL37 como as nanopartículas conjugadas com LL37 têm elevada actividade pró-angiogénica, demonstrado num ensaio de Matrigel e de membrana corioalantóica (CAM). É provável que a actividade pró-angiogénica das nanopartículas conjugadas com LL37 seja mediada pela transactivação de EGFR, mas mais estudos são necessários para responder a esta questão. Os resultados apresentados nesta tese são um primeiro passo para o desenvolvimento de terapias baseadas em nanomedicina à base de péptidos antimicrobianos. Esta é a primeira terapia que combina propriedades de cicatrização de feridas e actividade antimicrobiana na mesma formulação, é mais barata do que as terapias avançadas actuais, e pode ser administrada uma única vez.



# Contents

<b>Acknowledgements</b>	<b>i</b>
0.1 Abstract . . . . .	iv
0.2 Resumo . . . . .	v
<b>List of Abbreviations</b>	<b>x</b>
<b>1 Introduction</b>	<b>1</b>
1.1 Aims and outline of the thesis . . . . .	1
<b>2 State of the Art</b>	<b>5</b>
2.1 Wound healing . . . . .	5
2.1.1 The wound healing process . . . . .	6
2.1.2 Acute and chronic wounds . . . . .	9
2.1.3 Wound healing treatments . . . . .	12
2.2 Nanotechnology and nanomedicine . . . . .	18
2.2.1 NPs for skin drug delivery . . . . .	20
2.2.2 Au NPs for skin drug delivery and regeneration . . . . .	23
2.2.3 Cytotoxicity of NPs . . . . .	26
2.2.4 Uptake of NPs . . . . .	30
2.2.5 Intracellular trafficking of NPs . . . . .	33
2.2.6 Peptide-conjugated Au NPs . . . . .	33
2.3 AMPs . . . . .	36
2.3.1 AMPs targeting skin diseases . . . . .	39
2.3.2 AMP-conjugated NPs . . . . .	41
2.4 LL37 AMP . . . . .	42
2.4.1 Antimicrobial properties of LL37 . . . . .	43
2.4.2 Biological role of LL37 . . . . .	44

<b>3</b>	<b>Antimicrobial peptide-nanoscale therapeutic formulation with high skin regenerative potential.</b>	<b>49</b>
3.1	Introduction . . . . .	49
3.2	Results and discussion . . . . .	50
3.2.1	Synthesis and characterization of LL37-Au NPs . . . . .	50
3.2.2	LL37-Au NPs are relatively non-cytotoxic to keratinocytes. . . . .	59
3.2.3	LL37-Au NPs are mostly internalized by scavenger receptor-mediated endocytosis in keratinocytes. . . . .	63
3.2.4	LL37-Au NPs accumulate in the endolysosomal compartment. . . . .	66
3.2.5	LL37-Au NPs, as LL37 peptide, promote HaCaT migration through P2X, ADAM17 and EGFR. . . . .	71
3.2.6	LL37-Au NPs prolong EGFR and ERK phosphorylation and HaCaT migration compared to LL37 peptide. . . . .	77
3.2.7	LL37-Au NPs have higher in vivo wound healing activity than LL37 peptide. . . . .	80
3.3	Conclusions . . . . .	87
3.4	Material and Methods . . . . .	87
<b>4</b>	<b>Interaction of antimicrobial peptide-conjugated nanoparticles with endothelial cells.</b>	<b>99</b>
4.1	Introduction . . . . .	99
4.2	Results and discussion . . . . .	100
4.2.1	LL37-Au NPs are less cytotoxic to endothelial cells than LL37 peptide. . . . .	101
4.2.2	Uptake and intracellular accumulation of LL37-Au NPs. . . . .	105
4.2.3	LL37 peptides but not LL37-Au NPs trigger an increase in intracellular levels of Ca <sup>2+</sup> in HUVECs. . . . .	110
4.2.4	Both LL37 peptide and LL37-Au NPs induce angiogenesis in a CAM assay. . . . .	113
4.3	Conclusions . . . . .	116
4.4	Methods . . . . .	116
<b>5</b>	<b>General Conclusions</b>	<b>123</b>
	<b>Bibliography</b>	<b>129</b>

# List of Abbreviations

ADP	adenosine diphosphate
ADSCs	adipose derived stem cells
Ag	silver
AM	acetoxymethyl
AMP	antimicrobial peptide
ARG	arginine
ATP	adenosine triphosphate
Au	gold
BBN	bombesin
BMSCs	bone marrow derived stem cells
BSA	bovine serum albumin
CAM	chorioallantoic membrane
CAV-1	caveolin-1
cDNA	complementary DNA
CFU	colony forming unit
CI	confidential interval
CLIC	clathrin-independent carriers
CLTC	clathrin heavy chain 1
CTAB	cetyltrimethylammonium bromide
CYS	cysteine
DAPI	4', 6'-diamidino-2-phenylindole
DCFH-DA	6-carboxy-2',7'-dichlorodihydrofluoresce in diacetate
DIOC	3,3'-dipentylloxacarbocyanine iodide
DLS	dynamic light scattering
DMEM	dulbecco's modified eagle medium
DMF	dimethylformamide

---

DMSO	dimethyl sulfoxide
DNA	deoxyribonucleic acid
EC	endothelial cell
ECM	extracellular matrix
EEA1	early endosome antigen 1
EGF	epidermal growth factor
EGFR	epidermal growth factor receptor
EGM-2	endothelial growth medium-2
EIPA	5-(N-Ethyl-N-isopropyl)amiloride
ELISA	enzyme-linked immunosorbent assay
EPC	endothelial progenitor cell
ERC	european research council
ERK	extracellular signal-regulated kinase
ESR	early stage researcher
FACS	fluorescence activated cell sorting
FBS	fetal bovine serum
FDA	Food and Drug administration
FGF	fibroblast growth factor
FITC	fluorescein isothiocyanate
FL2	fidgetin-like 2
FPRL1	formyl peptide receptor like 1
FPRL2	formyl peptide receptor like 2
FTRI	Fourier transformed infrared
GEEC	GPI-enriched early endosomal compartments
GM3	ganglioside-monosialic acid 3
HaCaT	human keratinocyte cell line
hBD	$\beta$ -defensin
HB-EGF	heparin-binding EGF
HEPES	4-(2-hydroxyethyl)-1-piperazineethanesulfonic acid
HTAB	hexadecyltrimethylammonium bromide
HUCPVCs	human umbilical cord perivascular cells
HUVEC	human umbilical vein endothelial cell
ICP-MS	inductively coupled plasma mass spectrometry
IGF	insulin-like growth factor
IgG	immunoglobulin G
IFN	interferon

---

IL	interleukin
JACOP	just another colocalization plugin
LDH	lactate dehydrogenase
LDLR	low-density lipoprotein receptor
LPS	lipopolysaccharides
LYS	lysine
MALDI-TOF	matrix assisted laser desorption ionization time-of-flight
miRNA	micro ribonucleic acid
MD	molecular dynamic
MIB	minimal inhibitory concentration
MMP	matrix metalloproteinase
MPO	myeloperoxidase
MSCs	mesenchymal stem cells
MT	Masson's Trichrome
NO	nitric oxide
NPs	nanoparticles
OEG	oligo(ethylene glycol)
PAA	poly(acrylic acid)
PBAE	poly(beta-amino esters)
PBS	phosphate buffer saline
PDGF	platelet-derived growth factor
PDMS	poly(dimethylsiloxane)
PEG	poly(ethylene glycol)
PFA	paraformaldehyde
PI	propidium iodide
PI3K	phosphatidylinositol 3-kinase
PIGF	placenta growth factor
PLA	poly(lactic acid)
PLGA	poly(lactic-co-glycolic acid)
PVA	poly(vinyl alcohol)
P2X7R	purinergic P2X7 receptor
qRT-PCR	quantitative real time polymerase chain reaction
RAB7	ras-related protein Rab-7
RNA	ribonucleic acid
ROS	reactive oxygen species
SCARAs	class-A scavenger receptors

siRNA	short interfering RNA
SPR	surface plasmon resonance
TEM	transmission electron microscopy
TGA	thermogravimetric analyses
TGF	transforming growth factor
TLR	toll-like receptor
TNF	tumor necrosis factor
UV	ultraviolet
VEGF	vascular endothelial growth factor

# Introduction

## 1.1 Aims and outline of the thesis

Impaired wound healing and its medical complications remain one of the most prevalent and economically burdensome healthcare issues in the world. Chronic wounds are those that have failed to proceed through an orderly and timely reparative process to produce anatomic and functional integrity of the injured site. In the United States alone, chronic wounds affect 6.5 million patients. More than US\$ 25 billion is spent annually on treatment of chronic wounds and the burden is growing rapidly due to increasing health care costs, an aging population and a sharp rise in the incidence of diabetes and obesity worldwide [1], [2]. Recent data indicate that 11.7% of the Portuguese population is diabetic [3]. One of the most serious and debilitating complications of diabetes is the development of chronic non-healing wounds. In recent years, there have been efforts to develop new advanced methodologies to heal chronic wounds including the use of topic growth factors or cell based therapies. Unfortunately, in many cases, the therapeutic efficacy is low, the therapies are expensive and require application in a clinical facility, and they have no antimicrobial activity. Therefore, the development of new therapies is necessary to address this unmet clinical need. LL37 is the most important AMP in skin and recently, phase I/II clinical trials have demonstrated its therapeutic efficacy in chronic wounds [4]; however required multiple topical administrations. The main goal of this thesis was to develop a LL37 nanoparticulate formulation with higher wound healing properties than the free peptide. The hypothesis was that LL37-conjugated NPs would have enhanced wound-healing properties than soluble LL37 peptide because they would prolong the biological activity of the peptide. So far no study has compared the in vivo performance of soluble AMP relatively to chemically im-

mobilized AMP formulations in terms of their regenerative potential. The results of this thesis describe for the first time the development of a novel nanoparticulate formulation for wound healing based on LL37-conjugated gold NPs (LL37-Au NPs). During this thesis, we have developed a novel methodology to produce stable LL37-Au NPs in which thiol-terminated LL37 acts as capping agent during NP formation. The production of our nanoparticulate formulation involved only a processing step, which facilitates the large-scale production of LL37-conjugated NPs at a relative low cost. We have evaluated initially the physico-chemical properties of LL37-Au NPs and the binding process of LL37 peptide to the NP formulation by molecular dynamic studies. The stability of the formulation in cell culture media, cytotoxicity properties against endothelial cells and keratinocytes as well as antimicrobial properties have been studied. To show the unique properties of this formulation, we have evaluated their pro-migratory properties against keratinocytes. Pro-angiogenic properties were also evaluated against endothelial cells. When these NPs are exposed to keratinocytes, they activate purinergic receptors which in turn trigger ADAM17 activity, the consequent release of EGF anchored to cell membrane and finally the activation of EGFR leading to a prolonged cell migration and enhanced wound healing. When these NPs are exposed to endothelial cells, they promote cord-like structures formation in a Matrigel assay and new vessel formation in a CAM assay. Importantly, LL37-Au NPs have higher wound healing activity than LL37 peptide in a splinted mouse full thickness excisional model.

The work conducted in this study is significant because it (i) shows that LL37 chemically conjugated to Au NPs have superior wound healing activity and lower cytotoxicity than LL37, a peptide that is currently being evaluated in clinical trials for wound repair, (ii) it shows for the first time that both LL37 and LL37-Au NPs mediate the migratory activity of keratinocytes through purinergic receptors and (iii) the activation of purinergic receptors by LL37-Au NPs but not LL37 peptide leads to long-lasting phosphorylation of EGFR and ERK which enhances the migratory properties of keratinocytes (iiii) LL37-Au NPs do not mediate pro-angiogenic properties of endothelial cells through FPRL1 as for LL37, meaning that a different receptor and signaling is involved.

The PhD thesis is divided in five chapters.

**Chapter 1** provides a general overview of the work, presents the problem addressed by the thesis and discusses the contributions to advance the state of the art.



**Chapter 2** reviews the state-of-the-art for the biological mechanism of wound healing and wound healing treatments. This section also describes novel formulation for drug delivery systems based on NPs and peptides, their impact on cell biology and their current applications mainly focusing on skin diseases. Moreover, this chapter also reviews recent progresses regarding the biology of LL37 and its biomedical applications.

**Chapter 3** provides information regarding the synthesis and characterization of LL37-Au NPs, NP cytotoxicity, internalization and intracellular trafficking in keratinocytes. Further, it describes the inductive properties of LL37-Au NPs and LL37 in the migration of keratinocytes, the underlying mechanisms and the in vivo regenerative potential of both approaches.

**Chapter 4** describes the cytotoxicity, internalization and intracellular trafficking of LL37-Au NPs in endothelial cells. It describes the results about the pro-angiogenic properties of LL37 and LL37-Au NPs evaluated in term of intracellular free  $Ca^{2+}$  and secretion of vascular endothelial growth factor (VEGF) in endothelial cells. Further, it presents the pro-angiogenic activity of LL37-Au NPs and LL37 in a Matrigel and chorioallantoic membrane model (CAM) assays.

**Chapter 5** provides a general discussion of the results collected during the thesis and discusses future opportunities.



## State of the Art

### 2.1 Wound healing

Despite an increasing awareness of the pathophysiologic events that take place in the development of wounds of various underlying etiologies, impaired wound healing and its medical complications remain one of the most prevalent and economically burdensome healthcare issues in the world. The annual wound care products market has reached to US\$ 15.3 billion by 2010 and still the need for post-surgical wound care is sharply on the rise. In the US alone, there are more than 100 million acute wounds annually, including surgical incisions, trauma, and burns, while chronic wounds affect 6.5 million patients being considered the “new global epidemic” [1]. More than US\$ 25 billion is spent annually on treatment of non healing wounds and the burden is growing rapidly due to increasing health care costs, an aging population and a sharp rise in the incidence of diabetes and obesity worldwide (Fig. 2.1) [2]. Recent data indicate that 11.7% of the Portuguese population is diabetic [3]. One of the most serious and debilitating complications of diabetes is precisely the development of chronic non-healing wounds. More importantly, diabetes is the leading cause of non traumatic leg amputations in the United States. While the incidences of diabetic ulcers are sharply on the rise, pressure ulcers in critical care and intensive care patients are also increasing. Chronic wounds have many psychosocial consequences, including stress, negative mood, pain, and social isolation [5].

Current treatment options are limited, costly, and inefficient. Considering the increase in the incidence of diabetes and obesity, investigation into tissue regeneration in chronic wound repair is vital as well as the development of new therapeutics is absolutely necessary and important to satisfy the unmet clinical need.

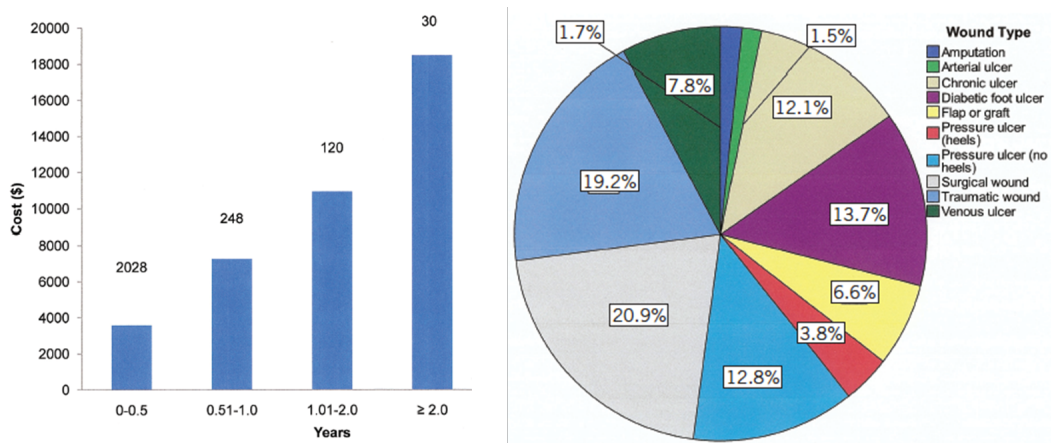


**Figure 2.1: Incidence of different types of non-healing wounds and costs among patients treated in US Outpatient Wound Centers.** Right side of the figure shows cumulative cost care. Numbers in boxes represent number of wounds for each column. Among patients followed for long periods, the cost of care increased as treatment duration lengthened. Although data from patients in treatment for more than 2 years were available in only 30 cases, the cost of care per patient was more than \$18,000. In the left side the distribution of wound and ulcer types are shown. Non-healing surgical wounds represent the largest category at 20.8% of the total, followed by pressure ulcers on the body at 19.2%. Diabetic foot ulcers are the next most common ulcer type at 13.7% of the total while traumatic wounds or chronic ulcers represent 12.8% and 12.1%, respectively. Venous ulcers represented 7.8% and arterial ulcers and non-healing amputations 1.5% each (adapted from [2]).

### 2.1.1 The wound healing process

Disruption of the integrity of skin, mucosal surfaces or organ tissue results in the formation of a wound. Skin is the largest plastic organ in the human body that serves as protective barrier to the environment and external stimuli. Loss of the integrity of large portions of the skin as a result of injury or illness may lead to major disability or even death [6]. When healthy skin is injured a normal wound healing response, consisting of a well-organized interaction of cells and tissues, begins immediately [7]. Cytokines, growth factors and proteases are also closely involved in the wound-healing process to complete normal tissue repair after damage [8]. The normal wound repair process takes around 7 to 14 days to complete and it consists of different continuous, sometimes overlapping, phases that comprise a series of cellular and biochemical events. These are haemostasis, inflammation, proliferation, and remodeling [9].

Haemostasis occurs immediately after injury. The exposure of subendothelial

collagen and the formation of thrombin lead to the activation of platelets, located in the intravascular space. Activated platelets are able to initiate the coagulation cascade leading to the formation of a fibrin clot that protects the denuded wound and serves as provisional scaffold for other cells that later can migrate there during the repair process. Importantly, the clot also serves as a reservoir of cytokines, growth factors vasoactive substances such as platelet-derived growth factor (PDGF), transforming growth factor- $\beta$  (TGF- $\beta$ ), fibroblast growth factor (FGF), endothelial growth factor (EGF), serotonin, thromboxane A<sub>2</sub>, platelet factor IV, prostaglandins, and histamine that are released from activated platelets degranulate [10]. This cocktail released from platelets initiate the early events of wound closure process providing chemotactic cues to recruit circulating inflammatory cells to the wound site. Additionally, it promotes the tissue movements of reepithelialization and connective tissue contraction, and stimulates the characteristic wound angiogenic response [9], [10].

The inflammatory phase begins in the first hours after injury and may continue for up to 6 days. This inflammatory response consists in regional vasodilation and increased capillary permeability, and a leukocyte infiltrate that occurs in response to specific chemotactic factors generated in the wound. In fact, growth factors released from the platelets diffuse into tissues surrounding the wound promoting the recruitment of inflammatory cells into the injured area. Neutrophils are the first inflammatory cells to enter the wound, followed by monocytes. Neutrophils role has long been considered to be confined to clearing the initial rush of contaminating bacteria, but studies have shown that they are also a source of pro-inflammatory cytokines that probably serve as the earliest signals activating local fibroblasts and keratinocytes [11]. More, activated neutrophils release a number of lysosomal enzymes (such as elastase, neutral proteases, and collagenase) which proteolytically remove damaged components of extracellular matrix (ECM) [12]. Subsequently, activated monocytes are differentiated to macrophages, and recruited at the injured sites and help in host defense. Macrophages play an important role in tissue debridement and in augmenting the inflammatory response releasing a variety of proinflammatory cytokines (IL-1 and IL-6) and growth factors (FGF, EGF, TGF- $\beta$ , and PDGF). Macrophages also initiate the development of granulation tissue and they are strongly essential for effective wound healing; if macrophage infiltration is prevented, then healing is severely impaired [13].

The main events of the proliferation phase are the formation of the new ECM and hence a new permeability barrier (reepithelialization), the beginning of angiogenesis and reinforcement of the injured dermal tissue. The cells are involved in

this phase are mainly fibroblasts and endothelial cells. They proliferate in response to growth factors and cytokines that are released from macrophages, platelets and mesenchymal cells, or have been stored in the fibrin clot. During the first 2-3 days after injury, fibroblasts activity predominantly involves migration and proliferation. After this time, fibroblasts release collagen and glycosaminoglycans (mainly hyaluronic acid, chondroitin-4-sulphate, dermatan sulphate, and heparin sulphate) in response to macrophage-released growth factors, hypoxia and by-products of anaerobic metabolism. New collagen production remains the dominant process in wound healing until approximately 6 weeks after wounding. The combination of collagen and fibronectin forms the new ECM, which is essential for the development of granulation tissue that eventually fills the wound [14]. Then fibroblasts stop producing collagen and undergo apoptosis. Angiogenesis accompanies fibroblast proliferation and allows nutrients and healing factors to enter the wound space. It is also essential for the growth of granulation tissue. The main growth factors that regulate angiogenesis are FGF, released by damaged endothelial cells and macrophages, and vascular endothelial growth factor (VEGF) which is released by keratinocytes and macrophages [9].

The remodelling phase usually begins 3 weeks after injury and can take up to 2 years to complete. Unlike non-injured skin, the arrangement of newly formed collagen fibers in the wound is random and disorganised. The remodelling of collagen fibres into a more organised lattice structure gradually increases the tensile strength of the scar tissue, though this never exceeds 80 percent of the strength of intact skin. Remodelling of the ECM involves a balance between collagen synthesis and degradation, which is operated by several proteolytic enzymes, like matrix metalloproteinases (MMPs), neutrophil-released elastase and gelatinase, collagenases and stromelysins [15]. The results of remodelling phase is a scar formation less cellular than normal skin and never achieves the same tensile strength as uninjured skin.

In summary, the normal healing cascade begins with an orderly process of hemostasis and fibrin deposition, which leads to an inflammatory cell cascade, characterized by neutrophils, macrophages and lymphocytes within the tissue. This is followed by attraction and proliferation of fibroblasts and collagen deposition, and finally remodeling by collagen cross-linking and scar maturation. Despite this orderly sequence of events responsible for normal wound healing, pathologic responses leading to fibrosis or chronic ulcers may occur if any part of the healing sequence is altered.

### 2.1.2 Acute and chronic wounds

Wounds were classified mainly in two types: acute wounds and chronic wounds. By definition, acute wound are the ones that proceeds through an orderly and timely reparative process to establish sustained anatomic and functional integrity, and a chronic wound as one that has failed to proceed through an orderly and timely reparative process to produce anatomic and functional integrity or has proceeded through the repair process without establishing a sustained anatomic and functional result [17].

Acute wounds are categorized based on causes and type according to size and depth (superficial or deep). Acute wound care is indicated in all patients with surgical and traumatic wounds, abrasions, or superficial burns [1]. Acute wounds heal in a very orderly, timely and efficient manner following a normal wound healing process characterized by the four phases previously described. The well organized cascade of physiological events results in full epithelization in about 2 weeks. Any disturbances in these events may result in an incomplete and improper restoration of the injured part. Therefore, any acute wound can reach a chronic state if it does not heal within the expected time due to some important factors that can influence the healing process: nutrients, hypoxia, poor blood supply, hygiene, infection, immunosuppression (HIV), chronic diseases (diabetes), age, genetics, wound management and surgical complications (Fig. 2.2) [16]. Whereas acute wounds go through the linear progression of overlapping biological and molecular events, chronic wounds do not progress through the orderly process. Some areas of chronic wounds are in different phases at the same time and, presumably, progression to the next phase does not occur in synchrony. All type of wounds that not heal within three months are considered chronic wounds. Chronic wounds are classified into pressure ulcers, vascular ulcers (eg. venous and arterial ulcers) and diabetic ulcers (Table. 2.1) [18].

A pressure ulcer is a localized injury in the skin and/or underlying tissue usually over a bony prominence, as a result of pressure, or pressure in combination with shear and/or friction. Pressure ulcers are common in aged patients, stroke victims, patients with diabetes, dementia, impaired mobility or sensation. Pressure ulcers can lead to infection and lead to complications such as septicaemia, osteomyelitis and, even death. It is estimated that there are over 7.4 million of patients with pressure ulcers in the world where estimation was possible i.e. excluding the vast number of developing countries [1].

Venous valvular incompetence in the deep and superficial veins can lead to venous ulcers characterized with a constant blood backflow resulting in an increase

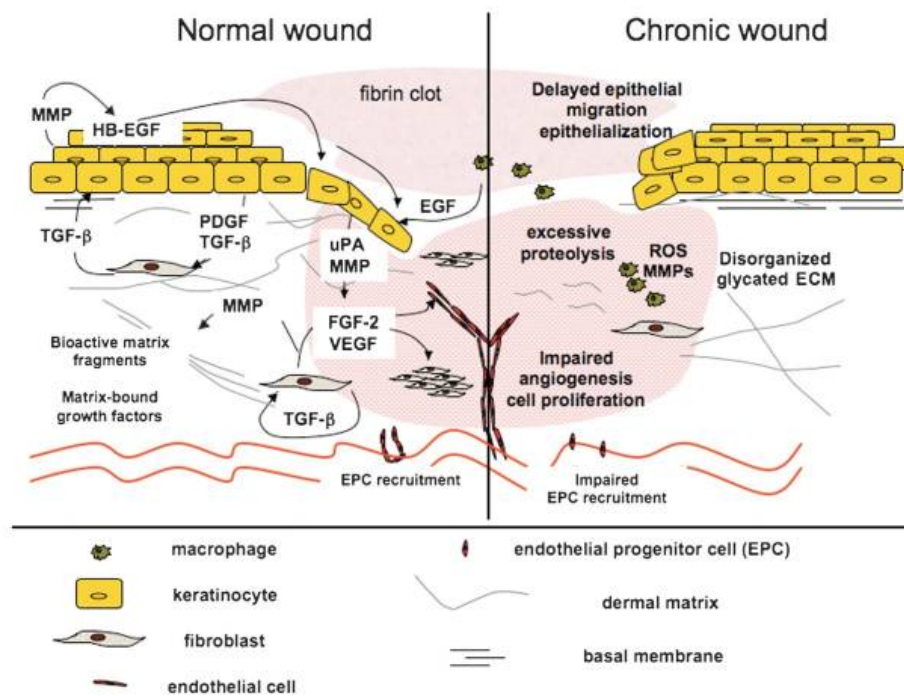


**Figure 2.2: Normal versus chronic wound.** Panel on the left displays the normal wound microenvironment characterized by numerous growth factors, a well-organized ECM, and active cell populations. Matrix synthesis in this scenario surpasses degradation, MMP activity is regulated by the presence of MMP inhibitors (TIMPs). Phenomenon of angiogenesis/neovascularization in normal wounds occurs in a synchronous actions through well-regulated sprouting of existing blood vessels and recruitment of endothelial progenitor cells (EPC), and by low bacterial burden. Chronic wounds here represented by the panel on the right, are often characterized by a high incidence of bacterial infection creating biofilms, which in turn lead to a persistent inflammation, excessive proteolysis, and ultimately to the degradation of critical growth factors, receptors, and/or ECM. The inability of the resident cells to proliferate and/or migrate effectively, creates a scenario where matrix synthesis is ineffective, because of the absence of functional receptors or appropriate promigratory matrix substrates. Angiogenesis/neovascularization impairment, are hallmarks of chronic wounds, resulting into oxygen and nutrient deprivation for the cells residing within the wound bed, leading to further wound bed mutilation and impaired healing (adapted from [18]).

in venous pressure. Pressure-induced changes in blood vessel wall permeability causing the leakage of fibrin and other plasma components into the perivascular space [21]. Arterial ulcers are less common than chronic venous wounds. They are due to arterial insufficiency caused by atherosclerosis or embolism that can progress to narrowing of arterial lumen and ischemia, which impair timely healing of minor traumatic injuries. Venous ulcers generally arise between the knee and the ankle



while arterial leg wounds can appear at any spot distal to arterial perfusion like a tip of a toe. It is estimated 100,000 Americans annually are affected by arterial ulcers [19].

MAJOR TYPES OF CHRONIC WOUNDS

Wound Type	Pathology	No. of Affected Patients	Cost of Treatment	Total Annual Cost
Venous ulcers	Venous insufficiency, thrombosis, varicosis	400,000–600,000	\$5000–\$10,000	\$1.9 billion to \$2.5 billion <sup>94</sup>
Arterial ulcers	Macroangiopathy, atherosclerosis, arterial insufficiency	100,000 <sup>33</sup>	\$9000–\$16,000	
Diabetic ulcers	Neuropathy, microangiopathy, hyperglycemia	2 million ( <a href="http://www.feetnet.com/statistics.php">http://www.feetnet.com/statistics.php</a> )	\$6000/patient	\$150 million <sup>95</sup>
Pressure ulcers	Immobility, excessive pressure	1.3 million to 3 million	Up to \$70,000 <sup>96</sup>	\$3.5 billion to \$7.0 billion annually <sup>96</sup>

**Table 2.1:** Table showing types of chronic wounds, pathology associated to the occurrence of those wounds and their socio-economical impact (adapted from [18]).

Diabetic ulcers are another type of chronic wounds do not follow an orderly and reliable progression of wound healing. In patients with diabetes (diabetes mellitus) wound healing is severally impaired. In fact, diabetic patients often have neuropathy, which could be causative, or often linked to vascular impairment, deficiencies in muscle metabolism, and a number of microvascular pathologies often caused by hyperglycemia [20]. The diabetic foot ulcer is a leading cause of hospital admissions for people with diabetes in the developed world and is a major morbidity associated with diabetes, often leading to pain, suffering, and a poor quality of life for patients. Diabetic foot ulcers are estimated to occur in 15% of all patients with diabetes and precede 84% of all diabetes-related lower leg amputations [22].

Common features are shared by all type of chronic wounds including the absence of linear progression of healing, prolonged or excessive inflammatory phase, persistent infections, formation of drug-resistant microbial biofilms, and the inability of dermal and/or epidermal cells to respond to reparative stimuli [18]. In addition, chronic wounds have higher concentrations of proteases (such as MMPs) and lower levels of growth factors and cytokines in the inflammatory phase than acute wounds [16]. Therefore, pressure, vascular and diabetic ulcers showing peculiar phenomena that make a different wound, they need of a specific management and care. It has been shown that dermis of venous ulcers exceed in TGF- $\beta$ 1 and it may cause fibrosis [31]. It is known that chronic wound fibroblasts contain aberrantly high levels of metalloproteinases [32] and lack the integrin receptor for fibronectin binding [33]. More, diabetic fibroblasts show impairment in cellular migration, VEGF production and in hypoxia response [30] leading to impaired angiogenesis and abnormalities in granulation tissue and decrease in collagen. More importantly,

some cells in chronic wounds are phenotypically altered. Keratinocytes on the edge of chronic wounds are unable to migrate properly; therefore, the wound cannot be closed. One reason for the inability of non-healing keratinocytes to migrate is because they are, for one reason or another, non-responsive to activation signals that promote cell migration [34]. It is thus critical to understand all the abnormalities occurring at the wound bed to better understand the reasons of the delayed and/or non-healing processes and to implement an effective therapies.

The optimal way to treat non-healing wounds is based on a multidisciplinary concept consisting in a specific treatment plan including modern wound care products and well-educated personnel. Considerable developments have occurred in wound healing and care over the last few decades that lead innovative technologies, debated in the next section, to the clinic. These technologies have been advantageous, but even the most advanced and sophisticated product requires proper wound care and wound bed preparation in order to function optimally, contributing to the huge economic burden of this medical area.

### 2.1.3 Wound healing treatments

#### Clinical treatments

Currently, chronic and acute wounds of different etiologies are treated using a multistep approach based on contemporary knowledge of wound healing and known by the acronym TIME. First, nonviable tissues (T) from within and around a wound are removed using surgical debridement or debriding agents, such as bacterial collagenase. Second, infection and inflammation (I) are minimized with antibiotics and anti-inflammatory preparations. Third, moisture (M) imbalance is corrected, generally with carefully selected dressings. Last step, epithelialization (E) and granulation tissue formation are promoted by the application of specific therapies, such as cell-based therapies or growth factors [23].

The use of TIME and current therapies are not always effective in some wounds. In fact, the success of a therapy depends on a detailed understanding of the molecular and cellular components present in each wound bed. Recent advances in understanding those components using novel diagnostic approaches as for example the "bar coding", can lead to personalized diagnosis and therapies and therefore better therapeutic outcomes [24]. Depending on the type of wounds, current treatments consist of specific dressings, skin substitutes and growth factors. There is a variety of wound dressings in the market, all of which function to preserve hydration within

the wound in order to optimize regeneration, warm, protect against infection, and avoid disruption of the wound base. The most currently available bioactive wound dressings are made using chitosan as “HemCon® Bandage”, hyaluronic acid, collagen and silicon as the product “Biobrane” [25]. In addition, other biomaterials that are currently being investigated for wound dressings consist of alginates, heparin, cellulose, and gelatin [26]. Being these materials biodegradable and part of the natural tissue matrix, they play an active part in the new tissue formation.

Dressings cannot replace lost tissue, particularly missing dermis as occurs in chronic wounds. For the treatment of these cases, bioengineered skin substitutes and growth factors represent the only Food and Drug Administration (FDA) approved products nowadays. Skin substitutes consists in autograft, allograft, xenograft, and bioengineered skin substitutes such as polymers, naturals or synthetic, acting as scaffolds for tissue engineered substrates that replace lost tissue rather than just facilitate wound healing (Table. 2.2). Autograft is currently the preferred option, but in many instances there is an insufficient amount of tissue available for grafting, or the patient’s condition precludes the use of autograft. Allografts and xenografts can provide a temporary coverage option, but they come with issues regarding rejection, and possible disease transfer, availability, as well as cultural and ethical considerations [27]. A gold standard in chronic wound management is the use of a full split-thickness autograft from a donor site and grafting it over the compromised region. Other options for chronic wounds are the use of donor keratinocytes or cultured epithelial autografts. This has been applied in form of confluent sheets of cells applied directly to the wound bed or onto a pre-prepared wound base made of allograft dermis. Limitations of tissue grafting are quantity of donor skin available, the risk of complications including pain and infection, high cost, need of multiple applications [27]. To avoid some of these problems bioengineered skin substitutes, both biosynthetic and cultured autologous engineered skin, are available to provide temporary or permanent coverage, in large quantities and negligible risk of infection or immunologic issues. The main limitation of these products is their costs and still limited efficacy. Nowadays, some examples of FDA approved products are:

- Apligraf®, a bilayered living human skin equivalent indicated for the treatment of diabetic foot and venous leg ulcers;
- Dermagraft®, a human fibroblast-derived dermal substitute, which is indicated only for use in the treatment of full-thickness diabetic foot ulcers;
- REGRANEX® Gel, a human platelet-derived growth factor for the treatment

of deep neuropathic diabetic foot ulcers [28].

Dressing	Type	Major Components	Manufacturers
Integra™	Artificial skin	Collagen/chondroitin-6 sulphate matrix overlaid with a thin silicone sheet	Integra LifeScience (Plainsborough, NJ)
Biobrane™	Biosynthetic skin substitute	Silicone, nylon mesh, collagen	Dow Hickham/Bertek Pharmaceuticals (Sugar Land, TX)
Alloderm™	Acellular dermal graft	Normal human dermis with all the cellular material removed	Lifecell Corporation (Branchberg, NJ)
Dermagraft™	Dermal skin substitute	Cultured human fibroblasts on a biodegradable polyglycolic acid or polyglactin mesh	Advanced Tissue Sciences (LaJolla, CA)
Epicel™	Epidermal skin substitute	Cultured autologous human keratinocytes	Genzyme Biosurgery (Cambridge, MA)
Myskin™	Epidermal skin substitute	Cultured autologous human keratinocytes on medical grade silicone polymer substrate	Celltran Limited (University of Sheffield, Sheffield, UK)
TranCyte™	Human fibroblast derived skin substitute (synthetic epidermis)	Polyglycolic acid/polylactic acid, extracellular matrix proteins derived from allogenic human fibroblasts and collagen	Advanced Tissue Sciences
Apligraf™	Epidermal and dermal skin substitutes	Bovine type I collagen mixed with a suspension of dermal fibroblasts	Organogenesis (Canton, MA)
Hyalograft 3-D™	Epidermal skin substitute	Human fibroblasts on a laser-microperforated membrane of benzyl hyaluronate	Fidia Advanced Biopolymers (Padua, Italy)
Laserskin™	Epidermal skin substitute	Human keratinocytes on a laser-microperforated membrane of benzyl hyaluronate	Fidia Advanced Biopolymers
Bioseed™	Epidermal skin substitute	Fibrin sealant and cultured autologous human keratinocytes	BioTissue Technologies (Freiburg, Germany)

**Table 2.2: Tissue Engineered skin substitutes available commercially.** Table displays the new generation of engineered skin substitutes, their categorization by type of scaffold or matrices, a brief description of the major components involved and the manufacturers responsible for the development and commercialization (adapted from [27]).

REGANEX® Gel, recombinant human platelet-derived growth factor-BB in a sodium carboxymethylcellulose gel, is the first and the only topical growth factor therapy approved by FDA (Fig. 2.3). It has been shown to promote a rapid wound healing and more completely heal of diabetic neuropathic ulcers [35]. It is currently under investigation for the treatment of decubitus (pressure) ulcers, while it has been demonstrated that is not effective in diabetic ischemic ulcers. However, there is a concern about the regular use of this product because of risk of skin cancer [36].

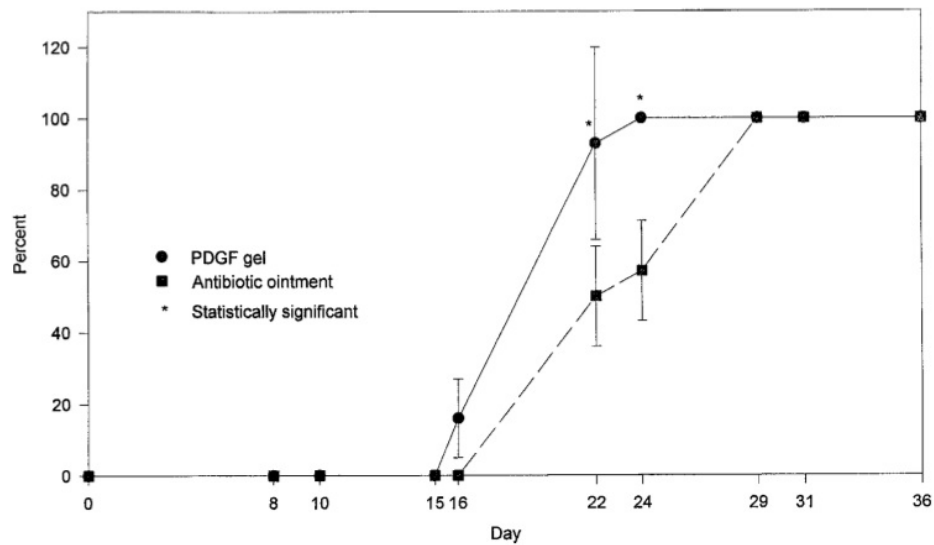


**Figure 2.3: Percentage of complete wound healing after PDGF gel and antibiotic ointment treatments.** A 4 mm punch biopsy instrument was used to make 2 full-thickness wounds on each arm of each volunteer. Fourteen wounds treated with PDGF gel were compared with 14 wounds treated with antibiotic ointment. Healing was evaluated by visual determination of the global percentage healed and wound depth. Wounds treated with PDGF gel showed a significantly faster rate of healing on each of the initial 6 follow-up visits. The greatest difference was on day 10 when PDGF-treated wounds were 71% healed compared with 28% for antibiotic-treated wounds ( $P=0.0005$ ). At days 22 and 24, 92.9% and 100% of the PDGF gel-treated wounds were healed, compared with 50% and 57%, respectively ( $P=0.0313$  and  $P=0.0313$ ), in the antibiotic ointment group. By day 29, both PDGF gel and antibiotic-treated wounds were healed. (Adapted from [35]).

Another important class of treatments is represented by antibiotics and antimicrobials used to prevent and combat infections often associated with diabetic foot ulcers and surgical and accident wounds [27]. Antibiotics from paraffin based ointments such as bismuth subgallate are known to have significant effect in the wound healing process [37]. Other antibiotics used consist of gentamycin from collagen sponges [42]. Generally, antibiotics are delivered to the wounds preferably by antibiotic incorporated dressing products. Some examples are dialkylcarbamoylchloride into Cutisorb1 (cotton wool dressing), povidone-iodine used with fabric dressing and silver used with most of the modern dressings [27]. The use of silver to prevent and treat infection is documented as early as 69 BC, and it is still one of the most technologies currently used for antimicrobial prophylaxis [38]. Silver is a very effective against a wide variety of bacteria, viruses, fungi, and molds, with low toxicity and low bacterial resistance [29]. Nanocrystalline silver dressings developed

and introduced in the late 1990s, are still the latest used silver wound dressings. The products currently in use consist of two layers of high-density polyethylene net sandwiching a layer of rayon/polyester gauze [39]. The outer layer is coated with a nanocrystalline (<20 nm), noncharged form of silver ( $\text{Ag}^0$ ), and the inner layer helps maintain a moist environment for wound healing. A higher therapeutic effect and a less frequent dressing changes are some advantages of nanocrystalline silver based dressing compared with silver sulfadiazine and silver nitrate. To date, there have been developed several new silver containing wound products as silver impregnated modern dressings available on the UK Drug Tariff include Fibrous Hydrocolloid, Polyurethane Foam Film and Silicone gels [41]. Topical delivery of antibiotics by dressings is preferred to their systemic administration to avoid the risk of systemic toxicity, to promote tissue compatibility, low occurrence of bacterial resistance and ineffective systemic antibiotic therapy resulting from poor blood circulation at the extremities in diabetic foot ulcers [40].

Regarding antimicrobial products, novel dressings reported include, freeze-dried fibrin discs for the delivery of tetracycline [27] and lactic acid based system for the delivery of ofloxacin and the inhibition of *S. aureus* and *P. aeruginosa* in split-thickness wounds in rats [44]. It has been demonstrated antimicrobial releasing silicone gel sheets promotes epithelization of superficial burns [43]. Minocycline incorporated in chitosan-polyurethane film dressing has also been developed for treating severe burn wounds [45].

### **Treatments in pre-clinical testing**

Some exploratory therapies are being tested in clinical trials. For example, FGF loaded in absorbable collagen increased the complete wound closure by 68% after 3 weeks compared to the placebo group in patients with traumatic ulcers [46]. A similar study showed diabetic foot ulcers treated with topical application of gel containing human EGF healed faster and higher than placebo group (Fig. 2.4) [47].

Other biomolecule as siRNA, miRNA, genetic material, antimicrobial peptides (AMPs) could be delivered at the wound bed to target a specific phase or molecular mechanism of the wound healing process. Delivery of growth factors or other biomolecules presents some important limitations difficult to overcome as their fast degradation by proteases or dilution by tissue fluid [51]. Moreover, they are able to target just a molecular pathway but since wound repair is the result of a complex set of interactions among cytokines, formed blood elements extracellular matrix and cells, future therapies for chronic wounds and their complications will have to be

based on correcting multiple deficits simultaneously. In conclusion, even if recently different drugs and delivery systems have been extensively investigated targeting the different phases of wound healing and to improve outcome, yet the standard available wound procedure remains costly, limited and ineffective. Therefore, the development of novel therapeutic strategy to satisfy the unmet clinical needs are urgently and continuously required.



**Figure 2.4: Clinical outcome of topical application of recombinant human EGF in diabetic foot ulcers.** Comparative study of two groups of 25 patients each. Group 1 was the experimental group: patients in this group received topical application of recombinant human epidermal growth (rhEGF) gel. Group 2 was the control group in which patients received betadine dressing. Clinical follow up after every two weeks for eight weeks. Left picture shows diabetic foot ulcer prior to start of therapy while the right picture shows diabetic foot ulcer of experimental group completely healed after 6 weeks of application of recombinant human epidermal growth; thus rhEGF gel appliance shortens wound healing time significantly and the mean closure was significantly higher in the EGF group compared with control (adapted from [47]).

### Cell therapies

The unique capability of stem cells to differentiate into various tissues has been also explored for skin regeneration and wound healing application. To date, bone marrow, peripheral blood, and umbilical cord blood have been used as source of stem cells to apply for healing acute and chronic wounds [48]. Mesenchymal stem cells derived from bone marrow (BMSCs) either autologous or allogenic demonstrate to enhance wound healing, increase blood vessel and granular tissue formation in chronic wounds [26]. Limitations of BMSC use consisting in their difficult harvesting from living tissue and donor site associated morbidity led scientists to explore other types of MSCs. An example, it is the use of adipose derived stem cells (ADSCs) that are present in major quantity and they can be harvested with easier procedures. Several studies have shown the capacity of ADSCs to promote angio-

genesis by releasing angiogenic factors in wounds and to reduce scar formation by releasing numerous cytokines and other cellular components [49]. ADSCs have been also tested on a cellular derived matrix in a full thickness cutaneous murine model. Results showed an improvement in wound healing, angiogenesis and vascularization [26].

MSCs isolated from umbilical cord Wharton's jelly have been also used in a poly(vinyl alcohol) (PVA) hydrogel membrane to promote wound healing in two dogs showing non-healing large skin lesions after standard treatments. MSC-PVA treatment significantly enhanced the skin regeneration in both the dogs [50]. Other studies demonstrated that MSCs from umbilical cord Wharton's jelly promoted higher wound healing, less inflammation and a thinner granulation tissue formation in goat when compared with the control wounds [26].

Human umbilical cord perivascular cells (HUCPVCs) have also been used in mouse excisional splinted wounds, showing faster wound healing compared with human skin-fibroblast (hSFb)-treated and phosphate buffered saline (PBS)-injected controls [50].

## 2.2 Nanotechnology and nanomedicine

«What I want to talk about is the problem of manipulating and controlling things on a small scale... What I have demonstrated is that there is room that you can decrease the size of things in a practical way... I will not discuss how we are going to do it, but only what is possible in principle... We are not doing it simply because we haven't yet gotten around to it...».

With this words at the annual meeting of the American Physical Society, at Caltech, on 1959, Nobel Prize winner *Richard Feynman* introduce the principles of a new science, known nowadays as nanotechnology. In his visionary lecture entitled "*There is Plenty of Room at the Bottom*" [52], Feynman speculated about the possibility to miniaturize object and the convergence of physical, chemical and biological processes at the molecular level. However, it was only later with the publication of the Eric Drexler's book titled "*Engines of Creation*" to rise an active interest of many scientists in the new field of nanotechnology [53]. Four decades after *Feynman's* lecture, scientists have learnt to manipulate materials on the same unimaginably small scale which is used by nature as atoms, molecules, and clusters on surfaces and new fundamental physics that governs the properties of nanoobjects are known. Therefore, by definition, nanotechnology is the science able to deal with matter that range



from 1 to 1000 nm (although in many studies, authors refer to objects in the range of 1 to 100 nm) permitting the design, synthesis, characterization and application of new materials and devices [54].

In the past 30 years, nanotechnology grew in several fields bringing innovation in pharmacology, chemistry, biology, physics, materials science and engineering. In recent years, burgeoning interest in the medical applications of nanotechnology has led to the emergence of a new scientific field of "Nanomedicine". Nanomedicine, as the most important cross-link subject between nanoscience and biomedicine, is defined as the process of disease prevention, diagnosis, and therapeutic using nanomaterials or nanotechnology [55]. The great potential of nanotechnology in medicine is contributing to the improvement in health and make remarkable achievements in new-generation of biological materials, artificial internal organ, interventional therapy, drug carrier systems, blood purification, and biomacromolecule separation. Furthermore, nanotherapies can increasingly be tailored to each patient's need enhancing currently available medical treatments, like those for impaired wound healing. So far nanomedicine in the skin therapy area has mainly been attributed to the use of scaffolds and nanomaterials such as biocompatible nanoparticles for drug delivery able get into the cells and modulate cell activity [57].

Nanoparticles (NPs), due to their small size and their unusual physical and chemical properties, exhibit differential biological activities. In fact, high surface area to volume ratio for a given mass of NPs augment the binding sites for multiple cargos in order to modulate biological properties. More, the increased cell surface interactions permit NPs to access into the cytoplasmic space crossing cellular barriers and activate specific transport mechanisms [56]. This permits to achieve temporal and spatial site-specific delivery of biologically active compounds and tune their interaction with cell features resulting in significant biomedical effects. NPs can offer the following advantages in the area of medicine:

- a tailored drug loading;
- reduced dosage and reduced frequency of dosing;
- improved drug solubility and high efficiency;
- controlled drug delivery and less side effects;
- less invasive, cheaper and faster disease treatments.

### 2.2.1 NPs for skin drug delivery

NPs are defined as the particulate dispersions, or solid particles with a size in the range of 1-1000 nm [106]. In the past two decades, FDA approved 24 nanoparticle-based therapeutic products for clinical use. Among these products, liposomal and polymeric drug conjugates are two dominant classes, accounting for more than 80% of the total amount [117]. Liposomes, spherical lipid vesicles with a bilayered membrane structure composed of natural or synthetic amphiphilic lipid molecules, were the first to be proposed as carriers for drug delivery for therapeutical purpose in 1960. So far, they have been already widely used, alone or functionalized, to encapsulate and protect both hydrophilic and hydrophobic therapeutic agents with high efficiency [118]. Small molecule drugs conjugated to several polymeric based nanocarriers are the second most used NP-based drug delivery systems. Many polymers have been proposed as drug delivery carriers, such as poly(ethylene glycol) (PEG), polyglutamic acid, polysaccharides, poly(allylamine hydrochloride) and N-(2-hydroxypropyl) methacrylamide [119].

Besides drug-encapsulated liposomes and polymer drug conjugates, other nanoparticle platforms such as micelles, dendrimers, engineered viral NPs and inorganic NPs like iron oxide, gold NPs (Au NPs), silica, alumina NPs have also shown therapeutic potential [120]. First generation of NPs for drug delivery were able to prolong drug half-life, improving solubility of hydrophobic drugs, reducing potential immunogenicity, and/or releasing drugs in a sustained or stimuli-triggered fashion compared with the conventional approach of drug delivery. Second generation of NPs for drug delivery consists of more advanced systems for (a) gene therapy, (b) active targeting of cells by specific ligands and (c) co-delivery [117]. One such material being studied for gene therapy is poly(lactic-co-glycolic acid) (PLGA), a specific polymer that can be applied to form NPs densely loaded with DNA or siRNA for sustained gene silencing [121]. Combination of lipid and/or polymer-based nanoscale systems, previously developed for single drug delivery, have been applied to facilitate co-delivery of two therapeutics or combine targeted imaging and therapeutic agents [122].

For skin drug delivery, NPs must be able to penetrate the skin barrier, mostly in the form of the complex structural arrangement of the stratum corneum, deliver efficiently their payload or actively target specific cells and then be cleared from the body without adverse side effects. Research in NPs for skin delivery has focused in three main areas: (1) skin cancer imaging and targeted therapeutics, (2) immunomodulation and vaccine delivery, and (3) antimicrobials and wound hea-

ling [124].

Wound healing is one of the fields that will most benefit from clinical application of NPs. A trend in skin repair is to use innate properties of nanocarriers or use them to deliver specific biomolecules, growth factors, antimicrobials and antibiotics targeting the main phases of wound repair with their cellular signaling involved (Fig. 2.5).

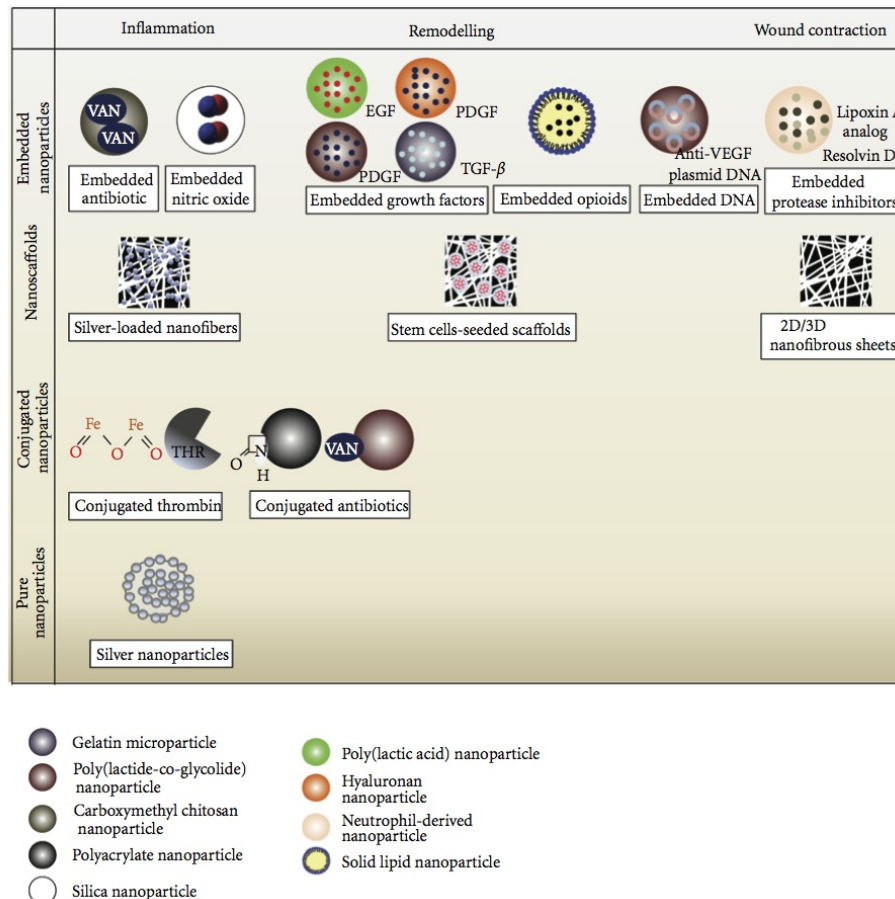


**Figure 2.5: Examples of nanoparticles currently under study for wound healing treatment.** Current NPs strategies for wound healing consist on both pure, conjugated or embedded NPs and scaffold as illustrated in this panel. Nanoparticle-bearing endogenous molecules, nanosphere-based strategies and nanoscaffolds are emphasized highlighting a correlation with the different healing phases that they may target. In the bottom of the figure, materials commonly developed for nanoparticulate-delivery systems are listed. Different structures (two- and three-dimensional) of nanofibrous sheets can be produced by both degradable and nondegradable nanofibers (adapted from [123]).

Another current trend is to develop and use NPs for gene therapy and knock-down of specific genes that are up-regulated or down-regulated in some phases of

chronic wounds phenotype. Several studies have described the use of NPs in wound healing. At the inflammation phase, iron oxide NPs conjugated with thrombin have been developed to prolong its half life in human plasma. In fact, thrombin, essential to convert fibrinogen to fibrin and create the platelet clot, is rapidly degraded by natural protease inhibitors. Thrombin-conjugated iron oxide NPs accelerated the healing of incisional wounds than free thrombin [123]. An other example of the use of NPs for wound healing is related to NPs for the release of nitric oxide (NO). NO is a critical molecule for wound healing, involved in collagen formation, cell proliferation and wound contraction. Previous studies showed diabetic wounds are characterized by a decrease in NO production and therefore by decreased wound reparative collagen deposition [125]. A new therapeutic approach, consisting in hydrogel based NPs containing NO, accelerated wound healing in mice promoting angiogenesis and increasing fibroblasts migration and collagen deposition [126]. NPs bearing antibiotics and silver NPs are also vastly used to treat wound infections, that often impede the final wound closure, and with the aim to reducing the risk of antibiotic resistance. Beside antimicrobial properties, studies in vivo demonstrated also a direct acceleration of wound healing and reduction on hypertrophic scarring by silver NPs mediated by cytokine-modulated inflammation [123]. Strategies to improve proliferation and remodeling phases of wound healing have used NPs to guarantee long-term protection from enzymatic degradation and prolonged delivery of exogenous growth factors at the wound bed. Growth factors are important to accelerate the healing process by attracting cells into the wound site, promoting cell migration, stimulating the proliferation of epithelial cells and fibroblasts (FGF and PDGF), as well as initiating the formation of new blood vessels (FGF and VEGF), and finally participating in the remodelling of the scar [127]. Some of the formulations used are PDGF-embedded PLGA nanospheres and PLGA NPs conjugated with VEGF and EGF [123]. PLGA NPs have been also used to encapsulate LL37 AMPs or curcumin with the aim to combine their bioactive properties and supplement the wound of exogenous lactate, known to accelerate angiogenesis [129], [128]. Curcumin (diferuloylmethane) is a well-known topical wound healing agent for both normal and diabetic-impaired wounds. Encapsulation of curcumin in PLGA NPs improves its solubility and showed a twofold higher wound healing activity compared to that of PLGA or curcumin in a full thickness excisional wound. PLGA-LL37 NPs significantly accelerated wound healing compared to PLGA or LL37 administration alone. PLGA-LL37 NP-treated wounds displayed advanced granulation tissue formation, high collagen deposition, re-epithelialized and neovascularized composition. LL37

has been also used also to create stabilized silver NPs (AgNP) for skin infections. LL37-immobilized AgNPs showed similar antimicrobial activity of clinically used ionic silver while LL37 on AgNPs promote fibroblast proliferation, compared to bare silver NPs due to LL37 biological activity [130]. Wound healing properties of LL37 peptides and advantages to use LL37 conjugated NPs will be further discussed in a subsequent section of this chapter.

### 2.2.2 Au NPs for skin drug delivery and regeneration

Au compounds are still used nowadays to treat rheumatoid arthritis [90], although Au colloids were introduced to treat several arthritis as early as the 1920s by Forestier [79]. Over the last century, Au NPs have been synthesized by different methods in a variety of sizes and shapes including Au nanospheres, nanorods, nanobelts, nanocages, nanoprisms, and nanostars (Fig. 2.6) [80]. These Au NPs have been extensively investigated for biomedical application [81]. The most common method to prepare Au spherical NPs is a single-phase water-based reduction method using citrate reduction as described by Turkevich and Frens [83], [84]. Varying the concentration of citrate and Au for the thermal reduction, size, shapes and absorption peak can be tuned passing by an absorption peaks near 540 nm to a peak closer to the optical window of tissue which is between 700 and 800 nm.

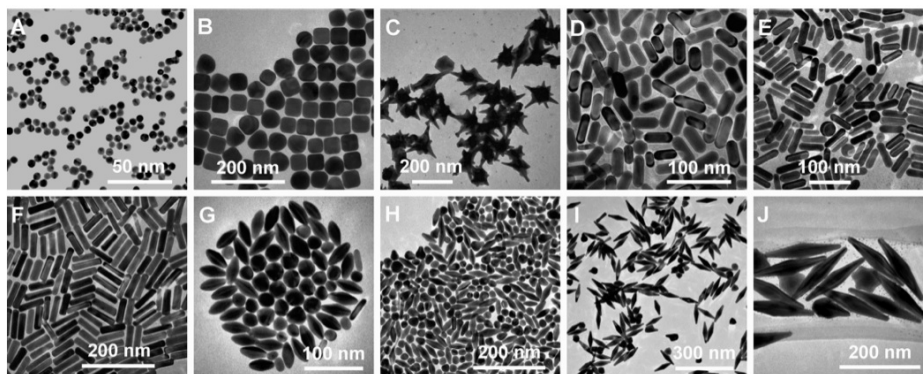


**Figure 2.6: TEM images of Au NPs ranging several shapes and different sizes.** (A) Nanospheres. (B) Nanocubes. (C) Nanobranches. (D) (E) (F) Nanorods with different aspect ratio. (G) (H) (I) (J) Nanopyramids with different aspect ratio (adapted from [75]).

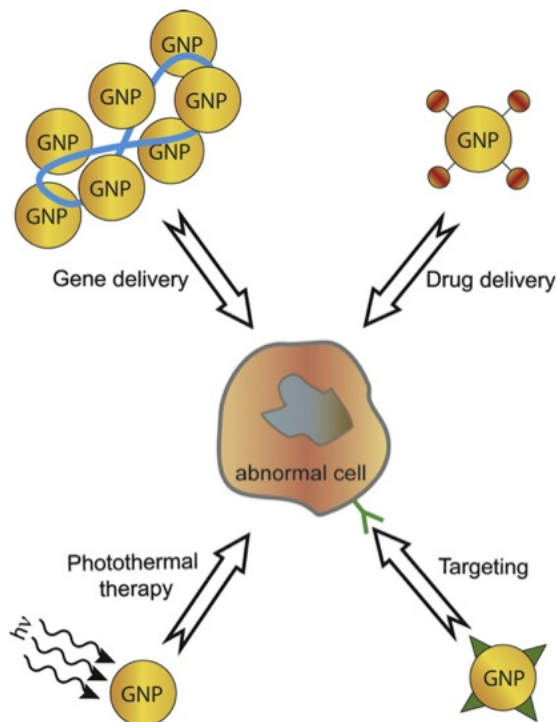
In the last 15 years, Au NPs have received considerable attention for their physical and chemical properties. Au NPs surface is easy to chemically modified with ligands containing functional groups such as thiols, phosphines, and amines, which

exhibit affinity for Au surfaces [85] and hence be used for the delivery of oligonucleotides, proteins, and peptides [86], [87], [88]. These properties, enabled Au NPs to be used in various therapeutic and diagnostic applications. Au NPs have been mostly explored for the treatment of cancer [87], rheumatoid arthritis [90], antimicrobial infections, inflammations and HIV therapies [93]. They have been used as carriers for the delivery of drugs or biomolecules as peptides, proteins, oligonucleotides, genetic materials and antigens, responding to endogenous or external chemical or physical stimuli [89]. *Rotello* and co-workers have developed a cationic 2 nm Au nanoconjugate functionalized with thiol-modified alkyl amines that possess photoactive o-nitrobenzyl ester linkages, which can be cleaved with near-UV irradiation [91]. An alternative method of releasing molecules from Au NPs consists of a mixed monolayer of amine-terminated and fluorophore-labeled alkyl thiol ligands on Au NPs that after entering in contact with intracellular environments containing an elevated glutathione concentration (a thiol-possessing peptide) results in substitution and the passive release of the nanoconjugate ligands [92]. Generally, approaches used for using Au NPs as a drug delivery vehicle include systems based on covalent binding, drug encapsulation, electrostatic adsorption, and other non-covalent assemblies [131].

In the area of transdermal delivery, it has been recently reported that Au NPs have a high potential to be absorbed in the skin, penetrate the stratum corneum, enter the epidermis and deliver efficiently the drug in the dermis [124]. Size, shape and coating of Au NPs also influence their absorption and penetration into the skin. *Dean et al.* showed that DNA coated Au NPs could enhance the penetration of vaccines from the layer of the skin to Langerhans cells introducing an innovative approach of epidermal delivery of particle mediated vaccine [94]. In general, studies have shown that spherical and smaller Au NPs (< 15 nm) present higher and faster permeation in rat and mouse skin than larger Au NPs [74], [75]. Au NPs of 6 and 15 nm with different chemistries could penetrate the stratum corneum and migrate in the deeper layer of human skin due to their interaction with skin lipids and increased skin permeability [244].

In addition to immunomodulation and vaccine delivery, Au NPs have been used on diagnostic [96] and treatment of skin cancer (Fig. 2.7) [95]. Melanocyte-stimulating peptide conjugates Au NPs are specifically internalized by receptor-mediated active targeting of melanoma cells and to be an efficient system for selective photothermal ablation in vivo. There are various strategies for combining biomolecule on Au NPs, however most of Au complexes for active targeting are based on covalent binding

of small peptides directly on Au surface or on PEGylated Au NPs. Therapeutic platforms based on Au NPs covalently conjugates with peptide will be discussed in a subsequent section of the thesis.



**Figure 2.7: Main biomedical applications of Au NPs.** Au NPs have been used in drug delivery and gene therapy applications either in vitro or in vivo (adaptated from [104]).

Au NPs have been also explored for skin therapy as new antimicrobials for skin infections and wound healing treatments. In fact, both applications are associated because diabetic chronic wounds are frequently colonized with bacteria infections. Au NPs are a potential candidate to treat effectively these pathologies both for their innate antimicrobial and anti-inflammatory properties as metal based NPs both for being a tunable system for topical delivery of specific drugs, antioxidants and siRNA. Previous studies have demonstrated that Au NPs display excellent antibacterial potential for both Gram negative bacteria *E.coli* and the Gram positive bacteria and they did not induce bacterial resistance even after 20 generations [98], [99]. In addition, 21 nm Au NPs have the capacity to reduce macrophage infiltration and inflammation, inhibiting pro-inflammatory cytokine expression as IL-6 and TNF- $\alpha$ , characteristics of non-healing wounds pro-inflammatory phenotype [102].

Conjugated Au NPs can act as anti-inflammatory and anti-oxidants agents. Stu-

dies showed that Au NPs conjugated with a mixture of antioxidants, epigallocatechin gallate, and  $\alpha$ -lipoic acid, significantly accelerated diabetic wound healing through anti-inflammation and angiogenesis modulation than antioxidants alone. Au NPs have enhanced the functionality of antioxidants serving as an adjuvant to increase the skin absorption [97].

Au NPs can be used for the efficient delivery of siRNA and miRNA in order to modulate wound healing. For example, Au NPs of conjugated with a specific siRNA to silence Fidgetin-like 2 (FL2) gene, a fundamental regulator of cell migration, improved wound healing in a murine burn wound model. By knocking down the production of this enzyme, epithelial cell migration was improved, as well as the rate and quality of wound closure [100]. In addition, Au NPs (13 nm) conjugated with ganglioside-monosialic acid 3 (GM3) siRNA, efficiently knockdowned GM3 expression in type 2 mice diabetic wounds and accelerate wound closure as compared to non-treated wounds [101].

### 2.2.3 Cytotoxicity of NPs

As the development of NPs and their biological applications are rapidly expanding, several studies and then a new science called "Nanotoxicology" has emerged to study the toxicity mechanism of nanomaterials in living organism and other biological organism [58]. Nanotoxicology focuses on correlating the physiochemical properties of NPs with biological response such as kinetics of their accumulation and elimination, and biological targeting (cells, tissues, organs) (Fig. 2.8). Several in vitro and in vivo tests have been proposed to evaluate the toxicology of nanomaterials that typically consist in colorimetric methods to evaluate features as plasma membrane integrity (LDH release assay), cell viability (annexinV/propidium iodide) and cell metabolism (MTT, ATP kits). Further, cellular secretion of cytokines and chemokines can be used to evaluate the pro-inflammatory activity of nanomaterials. The pro-inflammatory molecules such as IL-6, TNF- $\alpha$ , IL-8, IL-1, among others can be evaluated by ELISA kits or Multiplex kits commercially available. The biological impact of NPs can also be evaluated at gene level. In this case, a small number of genes, typically involved in cytotoxic response, or whole gene microarrays can be performed [59].

The first step to evaluate the biocompatibility of NPs involves cell cultures studies. In many cases NPs when dispersed in cell culture medium aggregate and change their physical properties or they can sediment affecting the NP concentration that cells are exposed to [61]. Because cytotoxicity of NPs depends on parameters



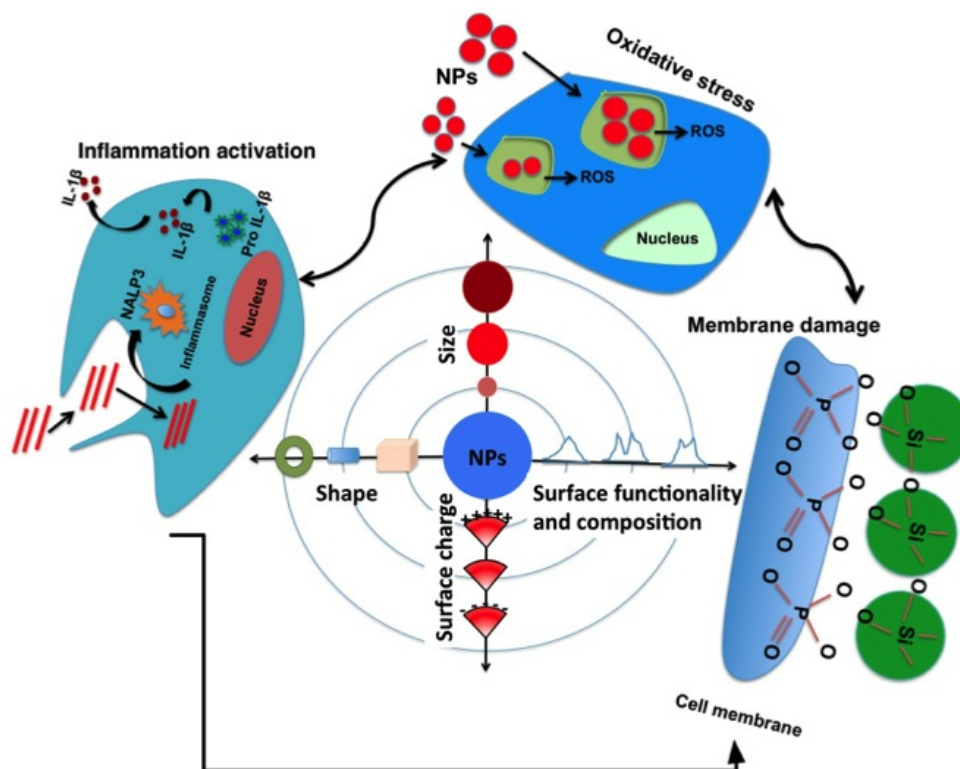


Figure 2.8: Summary of the toxicity pathways induced by NPs.

such as size, shape, surface area, agglomeration state, chemical composition, surface chemistry and dose [60], it is very important to perform stability studies of NPs in the cell culture media before assessing their toxicity profile. Spherical Au NPs of size ranging from 4 to 100 nm are in general relatively not cytotoxic and do not create any morphological change of various cells such as HeLa, human leukemia, human dermal endothelial and mouse macrophage cells up to 100  $\mu\text{g}/\text{mL}$  [62], [63]. This is similar to other biocompatible NPs. For example, organic PLGA NPs with the overage diameter or 100 nm are substantially non-cytotoxic against several type of cells for concentrations up to 100  $\mu\text{g}/\text{mL}$ . PLGA NPs with surface area between 3 and 10  $\text{m}^2/\text{g}$  and concentration ranging from 1 to 100  $\mu\text{g}/\text{mL}$  are non-toxic to Caco-2 and HeLa cells [64]. Importantly, the size of NPs affects oxidative stress. Au NPs with diameter of 1.4 nm induce higher oxidative stress than Au NPs with a diameter of 15 nm [62].

The shape of Au NPs is an other important parameter for their internalization and Au NPs cytotoxicity response. The uptake of rod-shaped Au NPs is lower than their spherical counterpart [63] may likely due to the larger contact area that rod-shaped NPs have with the cell receptors than the spherical NPs. Another reason

might be due to differences in the surface chemistry either from the synthesis process of both nanomaterials or the adsorption of proteins from cell culture media. Positively charged Au NPs functionalized with long carbon chains are more toxic to cells at a lower concentration due to the strong electrostatic interaction with negatively charged cell membrane and hydrophobicity induced toxicity [65]. They are able to depolarize the membrane potential in a dose dependent manner on different types of cells. Furthermore, cationic Au NPs increased the intracellular  $\text{Ca}^{2+}$  concentration by stimulating  $\text{Ca}^{2+}$  plasma membrane influx as well as  $\text{Ca}^{2+}$  release from the endoplasmic reticulum [66]. Compared to inorganic NPs, organic NPs such as PLGA NPs do not have significant impact on structural properties of cell membrane. Smaller size PLGA NPs trigger intracellular  $\text{Ca}^{2+}$  flux in RAW 264.7 and BEAS-2B cells through ROS generation but do not cause any cell death or damage to organelles [67]. On the other hand, negatively charged, and short carbon chain functionalized Au NPs have low internalization and exert no toxicity effect on cells [65]. NPs with high hydrophobicity induce high levels of ROS. Not only inorganic but also organic NPs such as PLGA NPs of different sizes (60, 100 and 200 nm) induce the production of ROS. Mouse macrophages RAW264.7 and human bronchial epithelial BEAS-2B cells incubated for 24 hrs with bare PLGA NPs with different sizes (60, 100 and 200 nm) show a cytotoxic profile that was size dependent [67]. The smallest NPs were the most effective in inducing cell damage, by the generation of superoxide radicals, a decrease in mitochondrial membrane potential and an increase in cytosolic  $\text{Ca}^{2+}$ . PLGA NPs coated with chitosan, poloxamer, poly(vinyl alcohol), and cetyltrimethyl-ammonium bromide having positive, neutral and negative charges do not induce cytotoxicity to cells [68]. Importantly, the ligand present at the surface of the NP has an important role in their cytotoxicity. It was found that cetyltrimethylammonium bromide (CTAB) capped Au nanorods are cytotoxic to HeLa cells; however, the level of cytotoxicity was reduced after being modified with PEG, phosphatidylcholine, poly(acrylic acid) or poly(allylamine hydrochloride), indicating that the chemicals involved in the synthesis of Au nanorods play a role in their cytotoxicity [69]. It has been shown that PLGA NPs coated with Tween-20 and poly (beta-amino esters) (PBAE) exhibit also toxicity to brain endothelial and COS-7 cells respectively with the increasing concentration of functionalized ligands and NP doses (Table. 2.3) [67].

NPs may act as immunomodulators. For example, it is well known organogold compounds have been used to treat rheumatic diseases since 1930 [70]. Au NPs with a diameter of 5 nm interact with extracellular IL-1 and down regulate the in-

flammatory pathways in THP-1 cells, a human myeloid leukaemia cell line [71]. This is dependent on the size of the NPs since Au NPs with 15 or 35 nm have no effect. In addition poly(acrylic acid) (PAA) coated Au NPs bind to and induce unfolding of fibrinogen, which promotes interaction with integrin receptor (Mac-1) of monocytes, resulting in release of inflammatory cytokines [72]. In some cases, the immunomodulatory properties of NPs depends on their capacity to interact with cellular toll-like receptors (TLRs). For example, Au NPs provoke specific inhibition of TLR9 (CpG oligodeoxynucleotides) [73].

Beside the evaluation of NPs toxicity *in vitro*, it is of utmost importance the *in vivo* evaluation of NP biodistribution, circulation, toxicity and elimination to determine their biological impact, since it is impossible to predict it or correlate with *in vitro* results. Typically, these studies are performed in mice or rats and evaluated by changes in blood serum chemistry and histological analysis. Different routes of administration can result in various effects on biodistribution of NPs in body. Generally, systemically administrated NPs are taken up by liver and spleen in a large amount and small amounts distributed in kidney, lung, heart and brain after single administration [75]. The biodistribution of Au NPs is also found be influenced by size, surface charge and coating. A large amount of small Au NPs (15 nm) was also accumulated in blood, liver, lung, spleen, kidney, and stomach and was able to pass blood-brain barrier, however, a tiny amount of 200 nm Au NPs was found in brain, stomach and kidney. In another study, 1.4 nm Au NPs were able to cross the air-blood barrier of the respiratory tract while 18 nm Au NPs were trapped in the lungs [74]. Neutral and zwitterionic Au NPs (2 nm in diameter core; overall hydrodynamic diameter of 9-10 nm) have longer circulation time via both intraperitoneal and intravenous injections, whereas negatively and positively charged NPs have relatively short half-lives [76]. PEG-coated Au NPs (13 nm) induced acute inflammation and apoptosis in liver and accumulated in liver and spleen up to 7 days after injection [77]. Regarding transdermal delivery of NPs, long term effects and side effects of applying Au NPs *in vivo* via the skin needs further investigation.

Cell Line	Morphology of GNPs	Surface Functionalization	Cell Culture Conditions	GNP Concentration and Average Size		Cytotoxicity Assay	Toxicity Results	Refs.
Human liver carcinoma, HepG2	Spherical	BSA, 4 nuclear targeting peptides,	85% confluency	N/A	20-25 nm	LDH	95% viable	[54,60]
COS-1, Red blood cells		NH <sub>3</sub> and COOH containing molecules	80% confluency	0.38, 0.75, 1.5 and 3 $\mu$ M	2 nm	MTT, trypan blue, Cos-1 viability assay	LC50:anionic-1 $\mu$ M and cationic> 7.5 $\mu$ M	
COS-7 cells	Spherical	PEI	3 x 10 <sup>5</sup> cells/well	N/A	4 nm	MTT	70-78% viability	[54]
Human breast carcinoma xenograft cells, MDA-MB 231, RAW 264.7 macrophage cells	Spherical	Coumarin-PEG thiol, m-PEG-thiol	10 <sup>5</sup> cells/well	50-200 $\mu$ g/mL	10 nm	Cell titer	Non-toxic up to 200 $\mu$ g/mL	[80]
		Lysine, PLL	10 <sup>5</sup> cells/well	10, 25, 50 and 100 $\mu$ M	4 nm	MTT	Toxic 85 % viable, 100 $\mu$ M after 72 hrs	
Human dermal fibroblast	Spherical	Citrate	N/A	0-0.8 mg/mL	13 nm	Microscopy	Viability decreases with dose	[81]
Human dermal microvascular endothelial cells	Spherical	Glucosamine, ethanediamine, hydroxylpropylamine,	N/A	10-250 $\mu$ g/mL	20-63 nm	MTS	99 % cell viable after 24 hrs	[50]
Human embryonic kidney	Rod	AEDP, plasmid, rhodamine	3x10 <sup>5</sup> cells/well	44 $\mu$ g/mL	200 nm	WST	LD50= 750 $\mu$ g/mL	[82]
HeLa cells	Rod	CTAB, PEG	5x10 <sup>3</sup> cells/well	0.01-0.5 mM,	65 $\pm$ 5 nm	WST	CTAB-Rod: 80% cell died at 0.05 mM, PEG-Rod: 10/ died at 0.05 mM	[83, 84]
HeLa cells	Rod	Phosphatidylcholine	5x10 <sup>3</sup> cells/well	0.09-1.45 mM	65 $\pm$ 5 nm	MTT	20% cell died at 1.45 mM	[84]

**Table 2.3: Cytotoxicity of Au NPs.** Toxicity profile of NPs having variable morphology, surface functionalization, charge, shape and size against different cell lines.

## 2.2.4 Uptake of NPs

Cellular uptake, intracellular pathway and final location of NPs in the cells play an important role in the delivered dose of the cargo and its bioactivity. Cells have several compartments, therefore it is important NPs, after cross the plasma membrane target the right place in order to obtain the desired effect with specificity and efficiency. Studies have shown that the charge of NPs influences the driving force

for the uptake and define their intracellular pathway [78]. This is due to the NPs electrostatic interactions are created with the cell membrane and because charge contributes for the adsorption of specific proteins, present in the cell medium, at the NPs surface that might enhance or reduce their cellular uptake. Size and surface functionality of the NPs affect their cellular uptake and intracellular fate. Endocytosis is a process by which materials are engulfed by a cell through the invagination of a portion of the plasma membrane, with subsequent formation of vesicles with these materials inside the cell. The internalization of the NPs can be mediated by one of the following pathways: (i) receptor mediated endocytosis (clathrin-, caveolin-, and raft- dependent), (ii) non-specific endocytosis, and (iii) internalization under endocytosis-inhibiting conditions (Fig. 2.9) [106], [103].

Another classification of endocytosis mechanisms consists in distinctions based on the proteins required for a certain pathway (for example dynamin, clathrin, caveolin, or actin), the type of cargo being internalized (large versus small, specific receptors or extracellular fluid sampling), the morphological appearance of the endocytic process (vesicular or tubular appearance, or a ruffled appearance as seen in circular dorsal ruffles), or the sub-cellular compartment/organelle it is associated with (such as the primary cilium). Clathrin-independent endocytic pathways are further divided in phagocytosis (actin-dependent, professional endocytosis) and macropinocytosis (receptor-independent), for internalization of large-sized particles, and pinocytosis for the uptake of fluids and solutes [107].

Uptake mechanisms of Au NPs into mammalian cells have been deeply reviewed [103]. Several studies have shown as charge and hydrophobicity contributes to determining the cellular uptake of functionalized Au NPs [104]. In addition, *Chan et al.* have reported size of Au NPs plays likewise an important role in their cellular uptake [105]. Au NPs get internalized through receptor specific or non-specific endocytosis pathways, depending on chemical composition of ligands present on NP surface, size, shape, protein corona adsorbed and accumulate at endocytic vesicles, cytoplasm or perinuclear regions of cells [63]. Furthermore, nanocomplexes, made of cell-penetrating peptides complexed with Au NPs to deliver oligonucleotides, turning negative charged in transfection medium, implied that their uptake in HeLa cell is mediated by scavenger receptors, specifically class-A scavenger receptors like SCARA3 and SCARA5 [114]. Scavenger receptors are one of the six types of phagocytosis receptors that are able to bind modified lipoproteins such as oxidized and acetylated LDLs, and they demonstrate promiscuous binding of polyanionic ligands [115]. In another study, *Patel et al.* demonstrated that the mammalian cell

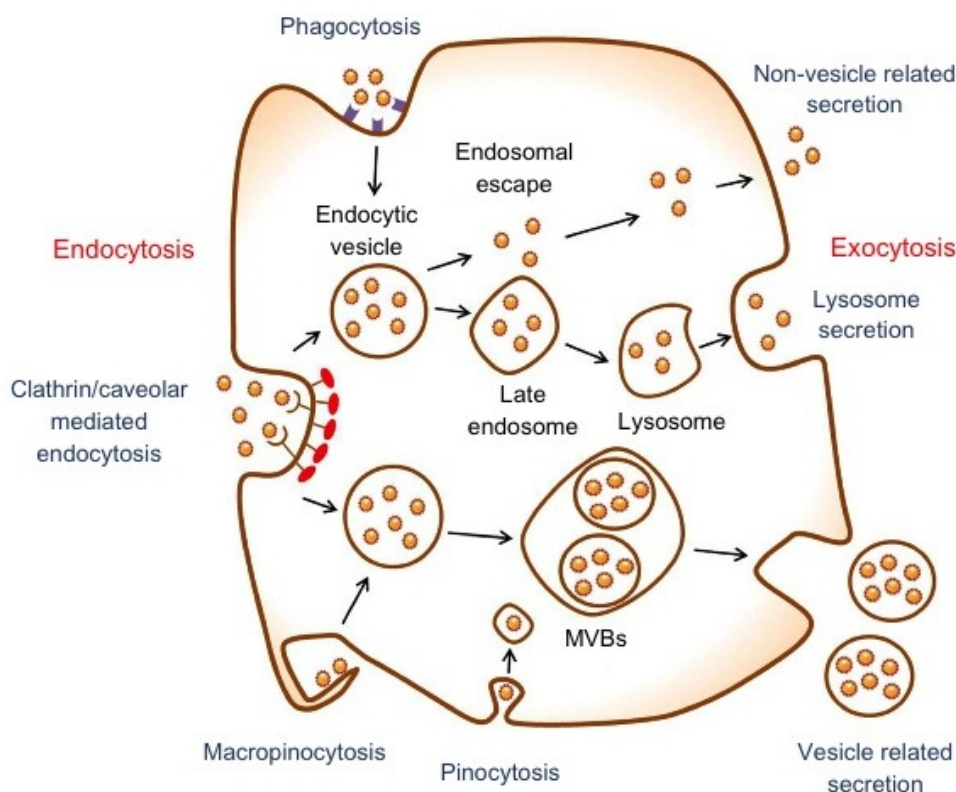


**Figure 2.9: Pathways of endocytosis and intracellular fate.** A number of endocytic pathways have been described, each mechanistically distinct and highly regulated at the molecular level. These pathways facilitate cellular signalling and cargo transport. Controlling the route of NP uptake is important for both mediating their intracellular fate as well as their biological response. After internalization via one or more of the endocytic pathways, NPs are trafficked along the endolysosomal network within vesicles with the help of motor proteins and cytoskeletal structures. Vesicles can transport their contents into sorting endosomes, or excrete/recycle them back to the cell surface by fusing with the plasma membrane. Alternatively, endosomes can mature into lysosomes via luminal acidification and recruitment of degradative enzymes, which target the vesicle contents for degradation. In order to access cytoplasmic or nuclear targets, NPs must be capable of escaping from the endolysosomal network as well as traverse through the crowded cytoplasm (adapted from [63]).

uptake of Au NPs functionalized with polyvalent oligonucleotides is also mediated primarily by scavenger receptors. Cells preincubated with polyinosinic acid, which are agonist for these receptors, decreased the level of Au NPs uptake by 60% [116].

### 2.2.5 Intracellular trafficking of NPs

Independently of the mode of entry, endocytosed NPs are usually delivered to the early endosome, where the fate of the cargo is decided in the first instance. From the early endosome, NPs can (i) be trafficked to the late endosome and then to acidic and oxidative environments of peroxisome and lysosomes for degradation, (ii) be expelled by exocytosis, or (iii) they can escape from the endo-lysosome compartment and travel to other intracellular locations including cell nuclei [108].

In most of the case, Au NPs are trapped in endosomes, fuse with lysosomes for processing, and leave the cell via the exocytosis process [112]. Several studies showed that citrate-capped Au NPs travel through the regular endolyso path causing NPs to become trapped in either endosomes or lysosomes [63]. A different intracellular path, consisting in endosome escape and cytoplasm localization, has been demonstrated for peptide conjugated Au NPs [109]. For example, Au NPs conjugated with peptides containing integrin binding domain can enter the cell via the endocytosis process followed by escaping into the cytoplasm from endosomes [110], [111]. *Brust* and co-workers also have suggested that an effective approach of evading the well-established endolyso pathway of uptake to a significant extent is by surface modification of NPs by cell penetrating peptides often used to deliver Au NPs loaded with target molecules via the cytoplasm to the cell nucleus [112]. Modified Au NPs with the cell-penetrating peptide TAT enhances HeLa cell uptake and leads to an unusual distribution pattern, by which particles are found initially in the cytosol, the nucleus, and the mitochondria and later within densely filled vesicles, from which they can be released again [113].

### 2.2.6 Peptide-conjugated Au NPs

Au NPs have been conjugated with peptides for drug delivery systems or active cell targeting and cell bioactivity. Peptides are relatively cheap compared to proteins, easy to produce in laboratory (using solid state chemistry) and their small size minimally compromise the overall size of the resulting peptide-conjugated NPs. Moreover the high surface volume ratio of NPs permits a high density of peptides on their surface. Therefore, multiple different peptide species can be easily immobilized on Au NPs surface, they prevent aggregation of Au NPs induced by salts and are amenable to serve as intermediary linkers between Au NPs and other active biomolecules [134]. So far, there have been developed three main approaches to prepare peptide Au nanoconjugates:

- ligand exchange method;
- chemical reduction method;
- and chemical conjugation method [135].

The ligand exchange method consists in using peptides with a cysteine moiety in order to reach a spontaneous reaction of the thiol group with GNP surface. Thiols form strong Au-S bonds with Au NPs [132], [133]. In general, a cysteine, at the N-terminus is preferred to create strong Au-S covalent bonds as well as a core of hydrophobic amino acids for packing and polar amino-acids at the C-terminus of peptide to provide solubility in physiological environments [133]. In 2004, *Levy* and colleagues reported the synthesis of CALNN, a peptide forming a self-assembled monolayer on Au nanoparticles [136]. CALNN, a pentapeptide thiol capping ligand, was developed to tune citrate-stabilized Au NPs into stable and water-soluble Au NPs with chemical properties comparable to proteins following this design: (i) a thiol group in the side chain of the N-terminal cysteine (C) to make a covalent bond to the Au surface, (ii) alanine (A) and leucine (L) in positions 2 and 3 with hydrophobic side chains to promote the self-assembly of the peptide, (iii) the uncharged but hydrophilic amino acid asparagine (N) in positions 4 and 5, with the amide group on the side chain, C-terminal asparagine in position 5 can bear a negative charge due to the terminal carboxylic group [137]. Successively, *Shaheena Parween et al.* replaced the internal hydrophobic residues of CALNN peptide with hydrophobic non-natural amino acids in order to avoid its degradation from Cathepsin L protease [141].

The chemical reduction method consist in one-step method (one-pot synthesis) in which peptides are not only able to interact with surface but they are employed as reducing agents and/or capping reagents. It has been found that the formation of Au NPs by short peptides is primarily determined by two basic functionalities of the amino acid residues: reducing capability for tetrachloroaurate (III) anions ( $AuCl_4^-$ ) and capping (binding) capability for the Au NPs formed [142]. Several studies have demonstrated the capacity of peptide sequences to control the composition, shape, and size of Au NPs during the synthesis process [148]. Following this approach, Au NPs are generally synthesized at room temperature, in water or in reducing buffer such as 4-(2-hydroxyethyl)piperazine-1-ethanesulfonic acid (HEPES), known to dominate the reduction of Au(III), and in the presence of specific peptide residues acting as capping and stabilizing agents that solubilize the growing NP [137]. *Serizawa et al.* found that reductions of  $AuCl_4^-$  by HEPES in the presence of adequate amounts of Cys-terminal peptides led to the production of peptide functionalized



Au NPs under ambient conditions [138].

Both linear and cyclic peptides containing arginine, tyrosine and tryptophan residues are strong metal binders and they can reduce  $AuCl_4^-$  to the gold atoms, which eventually combine to form Au NPs [149], [142]. *Amir et al.* were also the first to evaluate L-cyclic peptides as simultaneous reducing and capping agents for generation of cyclic peptide-capped Au NPs (CP-Au NPs), into aqueous solution, with the aim to develop a drug delivery system with cell penetrating properties and able to entrap antiviral or anticancer drugs without any chemical modification and functionalization on Au NPs surface [139].

Recently, functional Au NPs for the detection of *Staphylococcus aureus* were created due to the ability of thiol group, from cysteine of the peptide DVFLGDVFLGDEC (DD) to interact with Au ions and generate DD-immobilized Au NPs, while methicillin resistant *S. aureus* (MRSA) was used as the reducing agent and protective group [140]. Another study reported the efficient strategy to develop in one-pot synthesis Au NPs ideal for gene delivery and efficient transfection using positively charged polypeptides (e.g., poly-L-lysine, PLL) that serve not only as capping agents but also as reductants without the need for an external reducing agent [143].

In the chemical conjugation method, Au NPs are capped with a linker, which is then activated and functionalized with the peptide. Linkers contained a thiol group (e.g., thiol-containing oligoethylene glycols as PEG or OEG) to bind the gold surface of the NP and a terminal functional group (e.g. amine or carboxylic group) to bind the peptide. In earlier studies, peptides have been covalently coupled first to bovine serum albumin (BSA), which was subsequently adsorbed onto Au NPs via electrostatic interactions [145]. The frequent instability of peptide-BSA-Au nanoparticle conjugates in biological media prompted scientists to explore the alternative approaches. An example is the use of PEG as a co-adsorbate to create a mixed peptide/PEG monolayers on Au NPs surfaces [146]. *Bartczak* and *Kanaras* successfully coupled KPQPRPLS peptide, relevant for angiogenic genes activation, to carboxy-terminated oligoethylene glycol Au NPs (OEG NPs) using EDC/sulfo-NHS coupling reaction, one of the most common used chemical conjugation technique [147]. *Kumar et al.* have also successfully conjugated two peptides, therapeutic (p12) and targeted (CRGDK) for cancer treatment, on the surface of tiopronin capped Au NPs without changing the properties of peptides by the EDC/NHS coupling strategy [151]. There are other chemical conjugation methods available for cross-linking peptide to Au NPs including click chemistry and biotin-avidin coupling [150].

Ligands, such as the TAT sequence (which enhances intracellular delivery), cyclic

RGD peptide (which increases cell spreading and differentiation and enhances DNA synthesis), Bombesin (BBN) peptide (which bind with high affinity gastrin-releasing receptors), REV peptide (targeting ovarian surface epithelial cell) have been also successfully attached to Au NPs [152], [153], [154], [155].

Beside being used in chemical sensing and biomedical imaging applications, peptide functionalized Au NPs have been used to delivery biomolecules in specific cellular compartments and tumors. Therefore, CPPs as TAT or RGD (arginine-glycine-aspartic acid) functionalized Au NPs have used to delivery drugs to a nuclear location [152], [153]. The possibility to further functionalize the surface of peptide-conjugated Au NPs with other specific biomolecules (e.g. oligonucleotides, peptides, proteins) permit their delivery in the correct cellular target localization and tackle a variety of therapeutic applications. For instance, *Mirkin et al.* have designed a heterofunctionalized AuNP consisting of a 13-nm Au NPs containing both thiolated antisense oligonucleotides and cysteine-terminated basic peptides [156]. The heterofunctionalized AuNPs were prepared easily and showed perinuclear localization and an enhanced gene regulation activity when tested in a cellular model. In the area of tumor targeting, peptide-conjugated Au NPs have been reported to recognize specific receptors highly expressed on a variety of neoplastic and non-neoplastic cells. RGD short peptides can specifically bind to integrin  $\alpha_3$ , an important biomarker overexpressed in sprouting tumor vessels and most tumor cells. It has been demonstrated that RGD-(GC)<sub>2</sub> coupled to Au NPs show a high level of internalization in the cancer cells by receptor-mediated entrance with huge potential as novel method for tumor diagnosis and therapy [157].

A class of peptides of utmost importance for skin care applications is AMPs. Some formulations of AMP-conjugated NPs have been recently developed and used for skin infections and wound healing. An overview of AMPs properties together with some examples of application both in soluble form and nanoformulation will be discussed in the next sections.

## 2.3 AMPs

AMPs are peptides produced by bacteria, insects, plants and vertebrates with antimicrobial properties. In a broader sense, AMPs refer to all oligo or polypeptides that kill microorganisms or inhibit their growth, including peptides that result from cleavage of larger proteins or peptides synthesized non-ribosomally [158]. Even if the first report on AMPs is from 1930, only in the last 15-20 years researchers

started to explore therapeutical potentials of AMP against pathogens [159]. Currently, more than 800 natural AMPs of different origins have been isolated and characterized from practically all-living organisms, ranging from prokaryotes to humans and they are cataloged in a specific database located in Trieste, Italy [160]. Most of AMPs are small (usually containing less than 50 aminoacids), positively charged, with an excess of basic residues like lysine and arginine and about 50% of hydrophobic aminoacids and heat-stable (100°C, 15 min) [161], [162].

AMPs can be classified considering their origin, size, secondary structure or their aminoacid structure. AMPs have been also described into two classes, nonribosomally synthesized peptides and ribosomally synthesized natural peptides [163]. Based on their gross composition and secondary structure AMPs are grouped into four major classes: (i) linear peptides with an amphipathic  $\alpha$ -helical structure such as cecropin, magainins, human ubiquicidin and histatins, (ii)  $\beta$ -sheet structures stabilised by disulphide bridges such as  $\beta$  defensin, (iii) peptides with predominance of one or more amino acids such as the tryptophan-rich indolicidin of bovine neutrophils and the proline-arginine-rich peptide PR39 of pig neutrophils and (iv) peptides with loop structures such as gramicidin [158], [164].

In humans, the most prominent innate AMPs are the cathelicidins and defensins produced primarily by cells of the immune system and the histatins produced and secreted into the saliva by the parotid, mandibular, and submandibular salivary glands [161]. These peptides are normally synthesized in the skin at sites of potential pathogens entry, providing a chemical barrier to keep human skin healthy. In case of infection or injury, skin cells, including keratinocytes, sebocytes and mast cells increase the synthesis of AMPs. Circulating cells as neutrophils and natural killer cells give also an important contributions on secreting AMPs. Secretion of these peptides is also induced in response to microbial products such as lipopolysaccharide, proinflammatory cytokines as tumour necrosis factor, interferon and interleukin [158]. They have potent activities against a broad range of microorganism, both gram-positive and gram-negative bacteria, fungi and viruses hence representing essential effectors of innate immunity [166]. The minimal inhibitory concentrations of the more effective AMPs are in the range from 0.1-10  $\mu\text{g}/\text{ml}$ .

The precise mechanism of action remains unknown, although electrostatic interactions between the positively charged peptide and the negatively charged molecules at the surface membranes of the target organisms are thought to be responsible to initiate the process. A secondary step results in the modification of the biophysical properties of the membrane that lead to loss of membrane function including break-

down of membrane potential, pore formations leakage of metabolites and ions and alteration of membrane permeability, therefore killing the pathogen [158]. Proof of the host defence function of AMPs in living organisms have been already demonstrated both in vitro and in vivo. Studies in knock-out mice deleted for CRAMP, the murine LL37 cathelicidin, showed a significant infection after bacteria inoculation [169]. In addition, mice deficient  $\beta$ -defensin-1 (mBD-1), revealed delayed clearance of *Haemophilus influenzae* from lung [167].

In addition to their antimicrobial activity and rapid killing of microbes, AMPs can also neutralize endotoxin and the ones that act in microorganism membrane are less susceptible to microorganism resistance [168]. Besides the antimicrobial properties, AMPs have recently gained interests of scientists due to their immunomodulatory activities, their involvement in several inflammatory conditions as psoriasis, atopic dermatitis, atherosclerosis and in wound healing and diabetic foot ulcer [170]. In fact, low concentrations of AMPs bind to cellular receptors and activate intracellular signaling pathways and certain cellular functions. High concentrations of AMPs have been described to be cytotoxic for eukaryotic cells [171]. Defensins are able to attract human immature dendritic cells [174] and monocytes [172] and to induce release of interferon (IFN)- $\gamma$ , IL-6 and IL-10 from T cells [173]. In addition, cathelicidin such as LL37 was found to bind to formyl peptide receptor like 1 (FPRL1), G-protein coupled receptor, and to attract neutrophils, monocytes and CD4<sup>+</sup>T cells, and to activate mast cells [175]. Properties and biological function of LL37 will be discussed below.

AMPs are very attractive to a number of therapeutic applications because they have low propensity to induce bacteria resistance and they have a broad spectrum of microorganism activity. To date, small biotech companies in association with larger pharmaceutical companies carried out animal and human studies using AMPs with the aim to evaluate their potential as useful drugs for clinical application including infected and chronic diabetic foot ulcers, oral mucositis, stomach and intestinal disorders, acne and fungal infections [158]. So far, no AMP has yet reached the drug market; however, pharmaceutical companies remain enthusiastic about the prospect of understanding more about AMPs molecular processing, mechanism of action and regulation in order to use these novel agents as a new generation of medications, especially for skin therapy.

### 2.3.1 AMPs targeting skin diseases

AMPs play an important role both in normal skin function and in various non-healthy skin conditions. AMPs were first observed in mammalian skin when cathelicidin PR-39 was discovered in porcine wound fluid. By that moment, human cathelicidin LL37 was observed in epidermal keratinocytes as well as human  $\beta$ -defensins (hBD). hBD-2 has been found in human skin, lung, uterus, and trachea epithelia, and elevated hBD-2 expression in human keratinocytes exposed to pathogenic bacteria. hBD-2 and hBD-3 are very low at the steady state and typically inducible in the skin during infection, inflammation, and wounding. Other peptides with antimicrobial properties like cystatin, adrenomedullin are also produced in skin [176].

In general, mainly defensins and cathelicidin (LL37) are secreted by skin, not only, to serve as antimicrobial agents and contribute to innate immunity, but to stimulate and regulate inflammation, angiogenesis and wound healing. Altered production and availability of these appears to be associated with various skin diseases ranging from chronic inflammatory skin disorders to infectious complications. In this sense, controlling the secretion of AMPs may offer new therapeutic approaches in skin diseases, dermatology, wound healing and in cosmetic applications. Changes in the expression of AMPs are already examined in a variety of skin conditions to understand their involvement in the etiology of several diseases and hence to envisage innovative therapies. More, the association of AMPs with inflammation, led to the evidence that abnormal expression of AMPs is implicated in the pathogenesis of diseases as psoriasis, atopic dermatitis, rosacea and lupus [170].

Cathelicidins and hBDs are well known to be strongly induced in psoriatic lesions in comparison with normal skin. LL37 and hBD-2 were found abundant in the superficial epidermis from patients suffering of psoriasis. At the contrary, the same AMPs were found downregulated in acute and chronic atopic dermatitis lesions than expected, despite the presence of skin inflammation. This lack in the expression of AMPs following inflammation may explain the susceptibility of patients with atopic dermatitis to skin infections, as those due to *Staphylococcus aureus* colonization [177]. It has also been demonstrated that patients with atopic dermatitis have increased viral infections as manifested by the characteristic clinical symptoms of eczema herpeticum and eczema vaccinatum, likely due to a deficiency of AMPs in the skin [180]. An excess of LL37 have been also showed in rosacea, and this drives inflammation and abnormal blood vessel growth by mechanisms of cell activation involving the abnormal pattern recognition by TLRs, and proteases that process hCAP18, the inactive form of LL37 [178]. Also in cutaneous lupus erythe-

matosus, the higher amount of LL37 in the neutrophils, eosinophils, and dendritic cells in the skin of lead to an upregulated autoinflammatory signaling, contributing to the disease [179]. Expression of AMPs is also induced within the epidermis during viral infectious diseases such as condyloma acuminatum and verruca vulgaris. Studies have reported that human and mouse cathelicidin reduces vaccinia virus plaque formation in vitro and in mice lacking cathelicidin [180].

AMPs can have an important contribution in angiogenesis and wound healing. AMPs not only kill bacteria but also promote wound healing itself inducing angiogenesis, stimulating cell proliferation and migration and regulating inflammatory response at the wound area. Application of LL37 promotes angiogenesis important for wound healing and tissue repair [183]. Mice skin transfected with a plasmid leading to the expression of LL37 peptide showed improved skin healing [184]. In contrast, mice lacking LL37 or in which LL37 was inhibited by LL37 antibody showed a decreased in vascularisation and re-epithelisation during wound repair.

Burn wounds are also characterized by AMPs deficiency that increases the risk of infections and the healing time [180]. LL37, defensins hBD-2, -3, and -4 also increase human keratinocyte migration and proliferation along with intracellular calcium mobilization and EGFR phosphorylation [186]. Both defensins and cathelicidins have effect in promoting expression of collagen and decreased the expression of matrix metalloproteinase-1 in cultured human fibroblasts, an other important cell type in wound healing process [180]. These observations suggest that the induction and activation of AMPs after injury has a dual function, both preventing infection and assisting wound healing.

Importantly, the pleiotropic actions of AMPs, the many examples of relevance in animal models, and their associations with several skin disorders, all point toward this class of molecules as a new target for therapy. In fact, in case of infectious disease, atopic dermatitis or diabetic foot ulcer, the stimulation of AMP expression or the deliver of exogenous AMP itself at the unhealthy skin lesion may be promising. At the contrary, in case of psoriasis, rosacea or lupus, treatments targeting AMP down-regulation by using siRNA knockdown would be beneficial.

New therapies based on AMP for skin diseases will require the synthesis of these peptides, or in some cases chemicals capable of inhibiting their action. It is of utmost importance to develop efficient ways of delivering these drugs in active form to the skin.

### 2.3.2 AMP-conjugated NPs

The biomedical application of AMPs is limited due to the fact that they show low activity in presence of serum [198] and proteases [199], they are susceptible to pH changes and plasma components [201] and they show low stability and potential toxicity [200]. AMPs suffer also from poor pharmacokinetics [170]. Therefore, an efficient way of delivering AMPs in active form to their target sites at the skin is necessary. As many of these peptides are greater than 500 Da and hydrophilic in character they will not diffuse passively across intact skin, therefore their delivery will require an enhancement system [197]. One of the most promising strategies to increase the stability and antimicrobial/pro-regenerative properties of AMPs is by the conjugation to NPs. Therefore, polymeric, lipidic or inorganic NPs have been developed in recent years as AMPs carriers.

To date some formulations of AMP-NPs have been already tested for antitumor, anti-infections and wound healing application. Dermaseptin encapsulated-chitosan NPs have been shown to possess excellent antitumor activities [194]. Chitosan-based NPs have been also used to encapsulate frog-skin derived AMP temporin B against *Staphylococcus epidermidis* [192]. AMP encapsulation in NPs demonstrates a higher and sustained antibacterial action for at least 4 days compared to bare chitosan NPs and a reduced cytotoxicity against mammalian cells. PLGA NPs have been also explored to encapsulate plectasin for the treatment of airway *S. aureus* infections [193]. An other example consists in lactoferrin functionalized to the surface of PEG-PLA NPs used to mediate blood-brain barrier (BBB) and blood-brain tumor barrier (BBTB) and glioma cell dual targeting [195]. In addition, lipid NPs have been conjugated with LL37, melitin or bombolitin V for endosomal escape and thus for gene delivery [196].

Physical immobilization, both electrostatic and hydrophobic interactions, of AMPs in carbohydrate NPs was used to minimize the loss of peptide during storage and meanwhile realize an effective release of AMPs overtime [188]. In this study, Phytyglycogen (PG) based NPs were evaluated for their capability for loading nisin and prolonging its efficacy against *L. monocytogenes* bacteria. Although, this approach prolonged the in vitro activity of the AMP, its efficacy was never demonstrated in vivo may due to a reduced efficacy mediated dilution effect of AMP after being released. On the contrary, in vivo anti-infective activity of AMPs chemically conjugated with NPs has been already evaluated for the treatment of meningitis [190], [191]. Antimicrobial core-shell structured NPs self-assembled from the amphiphilic peptide CG3R6TAT showed to be able to cross the blood brain barrier

in a *S. aureus*-induced meningitis rabbit model and suppress bacterial growth in the brain with a high therapeutic index (50).

So far, only one formulation of AMP loaded NPs has been proposed for wound healing treatment. In 2014, *Cherreddy et al.* used PLGA NPs for the delivery of LL37 to promote wound closure [129]. LL37 has been also used to create silver NPs. LL37-conjugated silver NPs showed similar antimicrobial properties as ionic silver. Yet, LL37-conjugated NPs have higher capacity to induce fibroblast proliferation than bare silver NPs [130]. To date, this was the first example of LL37 immobilization in inorganic based NPs and it is the only one published.

## 2.4 LL37 AMP

LL37 is the active form of the unique human AMP belonging to the cathelicidin family. In 1995, the proprotein form of LL37 was identified for the first time in human and named hCAP-18 [202]. The hCAP-18 is encoded by the CAMP gene and comprises a signal peptide, a highly conserved N-terminal prosequence termed the cathelin domain and a highly variable C-terminal peptide domain in which the antimicrobial activity is found [203]. LLGDFFRKSKEKIGKEFKRIVQRIKDFLRN-LVPRTES, resulting from the hCAP-18 clavage by serine protease. The discovery of LL37 marked the beginning of more than two decades of research on this exciting AMP, in term of cell expression, structure and biological potential.

LL37 expression was found both in epithelial cells (intestine, airway, genitals, ocular surface, keratinocytes and eccrine glands) and in cells from immune system (neutrophils, NK cells, mast cells, dendritic cells, monocytes and macrophages) justifying LL37 prominent role in the innate immune response [204]. Expression in most epithelia is constitutive, although the expression in keratinocytes is induced, where the cathelicidin precursor is stored in granules and lamellar bodies, in response to several conditions. Activation of TLR receptors and/or an alteration in the cytokine milieu, contact with bacteria or bacterial cell wall constituents such as LPS, stress, inflammation, wounds, cell damage, provides a trigger that activates the cell to degranulate [207]. This leads to the release of the inactive hCAP18 precursor in the extracellular environment, where it can be processed by specific proteases into the active LL37 peptide, hence enhancing its expression.

It has been demonstrated that LL37 adopts an  $\alpha$ -helical structure to exert his function in lipid membranes, micelles, and ions such as hydrocarbonate, sulfate and to a lesser extent chloride, but is a random coil in pure water [205]. The common am-



phipathic structure of LL37 consist of a N-terminal  $\alpha$ -helix followed by a C-terminal  $\alpha$ -helix, and a C-terminal tail. The two helices are separated by a bend or break. The concave hydrophobic surface of LL37 is bordered by predominately positively charged residues, enabling interaction with negatively charged molecules or structures, such as LPS, genetic material and bacterial cell walls. The hydrophobic surface of LL37 is formed by the four aromatic phenylalanine side chains that all point in the same direction [206]. Many of the effects of LL37, either the antimicrobial action or the effect on host immunity, can be attributed to its cationic and hydrophobic nature. Studies have reported that N-terminal helix is involved in chemotaxis, peptide oligomerisation, proteolytic resistance and hemolytic activity while the C-terminal helix is responsible for the antimicrobial, anticancer and antiviral effect [208].

### 2.4.1 Antimicrobial properties of LL37

The effects of LL37 on microbial membranes and its antibacterial properties were established only two years after their discovery. Acting on Gram-positive and Gram-negative bacteria, they provide protection against a wide variety of pathogens and could serve as a template for the development of novel antibiotics, especially to overcome the bacterial resistance to current antibiotics. LL37 also has other antimicrobial properties including antifungal and antiviral activities and the inhibition of biofilm formation [204].

The antibacterial activity of LL37 is derived from its secondary structure. In fact, it has been shown that the replacement of L-amino acids in the sequence by D-amino acids did not result in a loss of the antibacterial effect [208]. At the contrary, small changes in charge, helicity and hydrophobicity have a large impact on the activity of LL37 [203]. LL37 firstly approaches the outer membrane as oligomers and/or monomers and covers the surface, secondly bind parallel to the surface, with the positively charged amino acids in contact with the head groups of the phospholipids [210]. LL37 coats the phospholipid membrane surface until a threshold concentration is reached when it induces such a high degree of membrane curvature that toroidal pores in the membrane are formed. This mechanism is known as toroidal pore carpet-like mechanism and it is commonly used by other cationic AMPs [204]. Other studies have shown that the mechanism of LL37 depends on the exact nature of bacteria membrane composition. In some cases, no evidence could be found for the destruction of the membrane into small fragments indicating a non-pore mechanism, while in the case of the fungal membrane found in *Candida albicans*, LL37 induced rapid phase separation and ultimately disintegration of membrane

into discrete vesicles, resulting in the formation of large pores or channels in the cytoplasmic membrane [203]. Aside from the pore-forming action of LL37, electrostatic interaction with protein complexes responsible for electron transport, generating ATP, could lead to the disruption of membrane homeostasis.

### 2.4.2 Biological role of LL37

LL37 differs from most  $\alpha$ -helical AMPs because of the relatively low specificity of LL37 to distinguish between bacterial and eukaryotic cells. Generally, LL37 favorably interacts with bacterial membranes at lower concentrations because these contain negatively charged lipopolysaccharides (Gram -) or teichoic acid (Gram +), as opposed to the zwitterionic eukaryotic membranes. The only exception is the membrane of erythrocytes, which contains sialic acid [211]. Therefore, a high concentration of LL37 in blood causes hemolysis. Furthermore, high concentration of sterols, notably cholesterol and spingomyelin, in the outer layer of mammalian cell membranes decreases the ability of LL37 to insert into the lipid bilayer, minimizing the toxic effect [203]. Further, serum and apolipoprotein-1 bind the AMP effectively reducing the concentration of free LL37 in vivo.

Although high concentrations of LL37 cause cytotoxicity in mammalian cells, LL37 interactions with eukaryotic cells, at low concentration, stimulate a wide range of cell receptors, transcriptional factors and relevant intracellular signaling. LL37s are able to signal tissue and cell damage through chemoattraction, as well as stimulation and modulation of cytokine release from cells of the innate and adaptive immune system [204]. LL37 is considered an alarmin because it is able to attract cells around the site of infection, such as monocytes, neutrophils, T-cells and dendritic cells, capable of dealing with the microbial threat to the site of infection [212]. Moreover, LL37 is able to indirectly attract more innate immune cells by inducing secretion of IL-8 by macrophages, fibroblasts [213] and epithelial cells [214]. Beside the function of attract immune cells, LL37 stimulates and modulates their action due to a directly inducing production and secretion of pro- and anti-inflammatory cytokines in a number of cell types. LL37 causes production and release of IL-1 $\beta$  in monocytes and keratinocytes and TNF- $\alpha$  in macrophages and secretion of IL-6 in keratinocytes, epithelial cells, human gingival fibroblasts [204]. LL37 has also an effect on the release of TNF- $\alpha$ , IL-6 and IL-12 in mesenchymal stem cells [215].

About LL37 modulatory role, studies have shown that treatment with LL37 decreases the TNF- $\alpha$  and nitric oxide levels, reducing the inflammation in macrophage-like cell lines previously treated with lipopolysaccharide (LPS) [216]. Epithelial cells

and fibroblasts also release less IL-8 after treatment with LPS and LL37 [218]. In addition, epithelial cells pretreated with flagellin and subsequently treated with LL37, produce less IL-6 than without LL37 treatment [217]. In addition, one group reports the ability of LL37 to enhance the activation of intracellular TLR4 by LPS in epithelial cells, while several other studies report the opposite [204].

Apart chemotactic effect and modulation of cytokine release, LL37 also regulates apoptosis of cells involved in infection, promotes angiogenesis and enhances wound healing. LL37 is able to suppress apoptosis of epithelial cells and neutrophils, hence prolonging the production of chemokines and cytokines and the clearance of pathogens at the site of infection, respectively. This suppression is realized through the action of LL37 on the N-formyl peptide receptor 2 (FPR2) and Purinergic P2X7 Receptor (P2X7R) with a mechanism that involves ERK1/2 activation leading to a decreased caspase-3 activity and an increased bcl-xL anti-apoptotic protein expression [219].

LL37 plays also an important role in several important processes, aiming to repair the impaired tissue, like migration and proliferation of epithelial cells [234], angiogenesis [233], and the inhibition of collagen production by fibroblasts to avoid too much scar tissue [222]. Additionally, LL37 is involved in diseases like chronic ulcers and cystic fibrosis as well, where its action is impaired [220].

The formation of new blood vessels is a prerequisite of tissue repair and wound healing. Angiogenic properties of LL37 have been associated with binding via formyl peptide receptor-like 1 (FPRL1), a G protein-coupled found in endothelial cells [183]. More, LL37 is able to recruit endothelial progenitor cells to the site of wound healing and induces their proliferation through the activation of NF $\kappa$ B dependent pathway [221].

Proliferation and migration of keratinocytes are other important steps in skin wound healing and they most depends on the epidermal growth factor receptor (EGFR) transactivation [223]. Activation of the EGFR on epithelial cells, endothelial cells and fibroblasts results in the activation of several intracellular pathways such as p38 MAPK, ERK1/2 and PI3K [204]. This causes the cells to migrate, proliferate, and hence repair the tissue damage.

Previous studies have shown that LL37 activates keratinocyte migration by the transactivation of epidermal growth factor receptor (EGFR) [224], [225]. The insertion of LL37 on the cell membrane activates a metalloproteinase (likely ADAM10 and/or ADAM17) [226] which cleaves epidermal growth factor anchored to cell membrane into a heparin-binding EGF (HB-EGF), by a recently elucidated pro-

cess called ectodomain shedding, which then binds and phosphorylates EGFR. This leads to the phosphorylation of STAT3, translocation into the nucleus and finally the initiation of the transcription of target genes. In addition, there is the phosphorylation of ERK1/2. All of these signaling pathways lead to enhanced keratinocyte migration to the wound site and cell proliferation (Fig. 2.10). Recently, studies with another AMP (mellitin) suggest that the activation of the metalloproteases involves the activation of purinergic receptors, in particular P2X receptor (ATP-gated ion channel), although it is unclear which pathway/molecule links purinergic receptors with the activation of metalloproteases [227]. It has been also shown LL37 promotes similar proliferative effects as EGFR activation after activation of FPR2 and P2X7 on epithelial cells and fibroblasts [228].

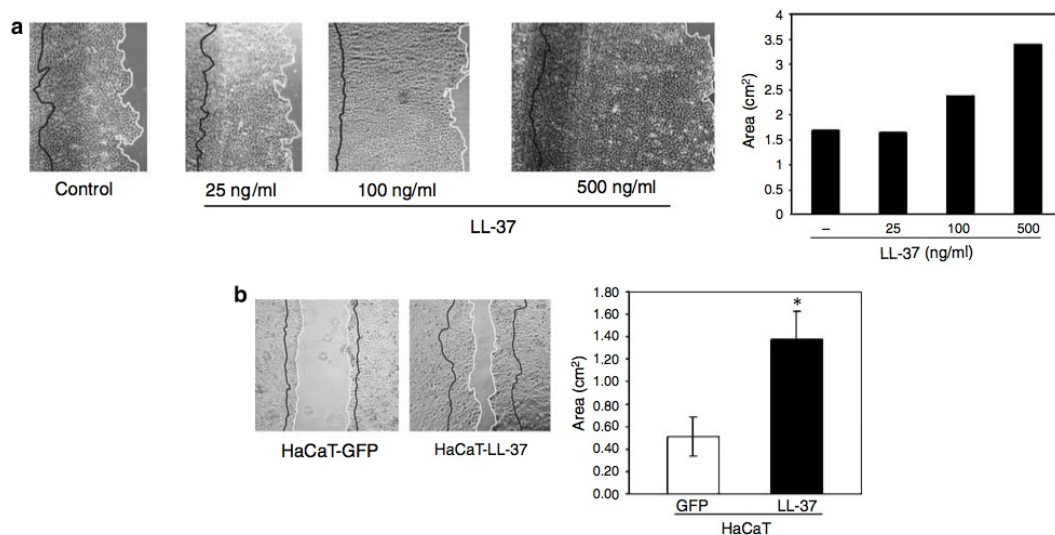


**Figure 2.10: LL37-induced migration of HaCaT cells in an in vitro wound model.**

(a) HaCaT cells were grown to confluence on fibronectin-coated six-well tissue culture plates. Cells were serum-starved for 12 hours. Different concentrations of the synthetic LL37 AMP ranging from 25 to 500 ng/ml were used in an in vitro wound assay, where half of each well was denuded from cells and then re-coated with fibronectin. Migration was monitored for up to 72 hours. (b) Retrovirus-transduced HaCaT cells were used in a similar assay. Cells were grown to confluence on collagen I-coated 24-well tissue culture plates. Cells were treated with mitomycin C to inhibit cell proliferation and then an in vitro wound was produced using a sterile pipette tip. Cell migration was monitored for up to 48 hours and quantified by image analysis. Results showed a clear induction of migration either on fibronectin or collagen type I by LL37 (adapted from [234]).

P2X7 mediates also LL37 internalization in macrophages and leads to the release of IL-1 $\beta$  and IL-8 promoted by the interaction with endogenous LL37 in monocytes

and human gingival fibroblast, respectively [229] [213]. The precise mechanism by which LL37 activates P2X7 is still an ongoing debate. It is suspected that LL37, thanks to its hydrophobic nature, is able to interact with the C-terminal end of the purinergic receptor, by inserting into the membrane. In fact, LL37 maintains its effect even if the affinity of the peptide to the ligand-binding site is altered when all aminoacids and sequence are substituted by their enantiomers, while the physico-chemical characteristics remain unaltered.

The wide range of responses caused by LL37 are fascinating and how one peptide is able to have multiple effects is still subject of debate. A number of potential different pathways have been proposed. Generally, the enormous potential of LL37 is due to its ability to activate multiple receptors, in a simultaneous or successive manner, and consequently activate different transcription factors, downstream pathways, causing cross-talk, resulting in a cell type- and context-specific response. Receptors activation by LL37 can be obtained by a direct or indirect mechanism of interaction.

Indirect mechanism is the one demonstrated for EGFR transactivation and previously described in this section [225]. Moreover, insertion of the LL37 into the lipid membrane can increase membrane fluidity resulting in leakage of intracellular signaling components, as the release of ATP and  $Ca^{2+}$ , which can then modulate P2X7 receptor (an ATP activated ion channel) [232].

Other studies have shown that the effect of exogenous ATP but not LL37 on P2X7 can be inhibited, suggesting that LL37 acts with a more direct interaction [231] [229]. Recent inhibitor studies have been also revealed a direct interaction of LL37 with the G protein coupled receptor FPRL1, leading then to direct initiation of a signaling cascade [183].

Furthermore, the concentration of LL37 and the duration of the stimulus further affect the response. In the end, LL37 action results in a surprisingly tightly regulated and balanced immune response, capable of effectively killing bacteria, fungi and viruses, promoting wound healing and participating in the tumor surveillance system. Due to this wide range of properties, many groups have recognized the therapeutic potential of exogenous LL37 in several application such as novel antibiotics, anti-HIV drugs, in melanoma and in chronic wounds applications [203]. A Sweden company (Pergamum AB) has reported recently the results of phase I/II clinical trials [4]. The company announced that the primary safety and tolerability end-point for LL37 was met for patients with venous leg ulcers. The results further show that patients treated with LL37 (twice per week; 0.5 mg/mL) had a statistically

significant improved healing rate compared with placebo. However, the peptide was administered twice per week and new systems for the sustained release of the peptide while potentiating its activity may be need.

Therefore, to translate LL37 based therapeutics in the market, challenges as the need to simplify the structure preserving helicity and hydrophobic nature (reducing production costs) and reduce host-cell toxicity whilst maintaining stability to general proteolysis and enhancing activity and selectivity remain to be overcome.

One possible solution is represented on the use of nanoparticles. The nanotechnology is necessary to present high density of AMPs per surface area to activate and prolong the regenerative mechanism and to reduce the degradation of the peptide by proteases in the wound. A NP formulation for the delivery of LL37 has been developed by our collaborators in 2014. The hypothesis of this thesis is that the chemical immobilization of LL37 on NPs will enhance its stability and bioactive properties to a level not achievable by the sustained release of LL37 from a conventional NP formulation.

# Antimicrobial peptide-nanoscale therapeutic formulation with high skin regenerative potential.

## 3.1 Introduction

LL37 is an antimicrobial peptide (AMP) predominantly found in human skin that acts at different levels for the homeostasis of the skin [204]. LL37 acts as first line of defense against bacteria, virus and fungi [253]. Importantly, LL37 plays an important role in immunomodulation, angiogenesis and wound healing properties. It has been shown that LL37 is a chemoattractant for mast cells, monocytes, T lymphocytes and neutrophils [255]. Furthermore, they contribute to regulation of inflammation and promote wound healing and angiogenesis [183], [233]. Angiogenic properties of LL37 have been associated with binding via formyl peptide receptor-like 1 (FPRL1) in endothelial cells [183], while the immunomodulatory and chemotactic properties have been associated with binding via P2X7, epidermal growth factor receptor (EGFR) or FPRL1 [225], [229]. Although the wound healing properties of LL37 peptide have been demonstrated [225], [234], only recently the peptide has been immobilized on NPs; however, the regenerative potential of the formulation was not demonstrated [130]. To the best of our knowledge, indeed no AMP-conjugated NPs have been tested in the context of their regenerative potential. The conjugation of AMPs to NPs may offer a prolonged activation of signaling cascades and thus potentiate their regeneration potential.

Here, we investigated the wound healing potential of LL37-conjugated NPs that have a gold (Au) core and a hydrophilic cationic LL37 peptide shell. We have se-

lected Au NPs because it is relatively easy the immobilization of high concentrations of LL37 per surface area, the modification of their properties (including size, charge and morphology), and they have been used in the clinic for many years [70]. The production of our nanoparticulate formulation involved only a processing step (which included the mixing of the peptide with gold salts, at room temperature) for one day followed by a centrifugation step. The simplicity of the process makes possible the large-scale production of LL37-conjugated NPs at a relative low cost. We hypothesize that LL37-conjugated NPs have enhanced wound-healing properties than LL37 peptide because they prolong in time the biological activity of the peptide. So far no study has compared the *in vivo* performance of soluble AMP relatively to chemically immobilized AMP formulations in terms of their regenerative potential. To verify this hypothesis we have evaluated initially the physico-chemical properties of LL37-Au NPs and the binding process of LL37 peptide to the NP formulation by molecular dynamic studies. The cytotoxicity properties of LL37-Au NPs and LL37 peptide against keratinocytes have been evaluated by cell viability, metabolism, stress oxidative, cell membrane and platelet activation assays. The internalization and intracellular trafficking of both LL37-Au NPs and LL37 have been evaluated in keratinocytes by chemical and genetic inhibition, immunofluorescence and transmission electron microscopy analyses. To show the unique properties of LL37-Au NPs we have evaluated their pro-migratory properties against keratinocytes and evaluated their mechanism relatively to LL37 peptide. Finally, we have evaluated *in vivo* the regenerative potential of LL37 and LL37-Au NPs in a splinted mouse full thickness excisional model.

## 3.2 Results and discussion

### 3.2.1 Synthesis and characterization of LL37-Au NPs

LL37 peptide modified with a cysteine at C-terminus was used to prepare in a single step LL37-conjugated Au NPs (Fig. 3.1a). In the absence of the LL37 peptide, Au NPs with different sizes and zeta potentials were synthesized rapidly in HEPES buffer within 30 min (Table. 3.1). In the presence of LL37, the formation of NPs was slower than in the absence of the peptide. Several reaction conditions, including initial concentration of Au ions (Fig. 3.2), LL37 (Fig. 3.3) and pH (Fig. 3.4) were screened to obtain rapidly Au NPs with low size, relatively low polydispersity and high incorporation of LL37 (Fig. 3.1a). In the absence of HEPES buffer, no reduction of Au ions was observed by LL37 peptide, indicating that HEPES and LL37

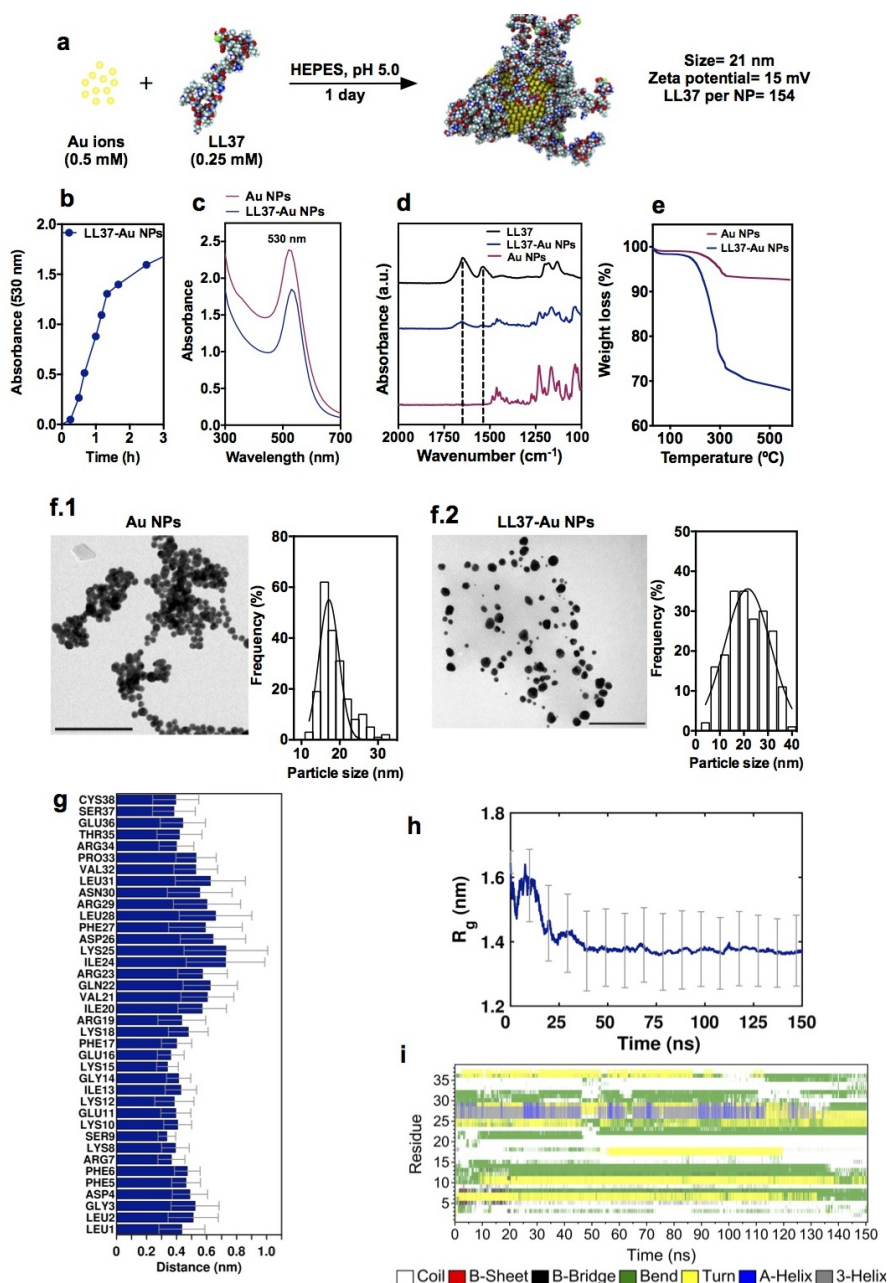


peptide act as reducing and capping agents, respectively. In the presence of HEPES buffer, we initially screened several concentrations of Au ions and LL37. We selected HEPES buffer pH 5 for this initial screening since at this pH the formation of NPs was faster than at pH 6 or 7.5 (see below). Concentrations of Au ions of 0.5 mM and LL37 of 0.25 mM were selected for further screenings since NPs were formed in less than 1 day and showed a relatively low polydispersity (Figs. 3.2, 3.3). Next, we screened the effect of pH in the growth kinetics of LL37-Au NPs. It is known that the reaction pH affects the charge of LL37 peptide and species of gold ions, which in turn influences the interaction of peptide with Au (0), leading to the formation of Au NPs at different synthesis rates. NPs were rapidly formed at pH 5 with saturation being reached in 2 h. In contrast, at pH 6 or pH 7.5, the saturation of NP formation was observed after 1 and 9 days, respectively (Figs. 3.1b-f, 3.4). Based in these results we selected pH 5.0 to generate LL37-Au NPs for subsequent tests. For subsequent tests we have also prepared Au NPs with similar size, shape and homogeneity to our LL37-conjugated Au NPs using citrate reduction (Fig. 3.1c-f). The reduction reaction at pH 5.0 reached a steady state at 2-3 h (Fig. 3.1b), and the NPs formed had a SPR band centered at 530 nm (Fig. 3.1c). As determined by transmission electron microscopy (TEM) analyses, the Au NPs reached an average diameter of  $21 \pm 8$  nm ( $n \geq 100$ ) (Fig. 3.1 f.2). Fourier transformed infrared (FTIR) analyses indicated that LL37-Au NPs typically had a random coil structure (amide-I and amide-II bands at 1650 and 1582  $\text{cm}^{-1}$ ) as did LL37 peptide in aqueous solution (Fig. 3.1d). Thermogravimetric analysis (TGA) was then used to determine the composition of the NPs, showing that from 180°C to 300°C LL37-Au NPs lost approximately 25% of its organic mass, likely LL37 peptide (Fig. 3.1e). The remaining mass is inorganic, likely gold. Au NPs showed a 10% organic weight loss due to citrate and water, the remaining mass is gold material. Zeta potential analyses (DLS) showed that the NPs were positively charged ( $+15.4 \pm 2$  mV). The number of Au atoms per 21nm LL37- Au NP was 106876 calculated using the equation described in [254]. Quantification by spectrophotometry of LL37 peptides that were not conjugated to the Au NPs after reaction indicates that each LL37-Au NP had approximately 154 peptides conjugated.

To evaluate the binding process of the LL37 peptide during NP growth process we performed molecular dynamic (MD) studies. These studies have been a valuable tool to study the binding process of peptides to metal surfaces [256], [257], [258]. Most of the aminoacid residues took 50 ns to achieve a stable position (Fig. 3.5). At the end, some cationic residues of LL37 (ARG7, LYS8, LYS10, LYS12, LYS15, ARG19

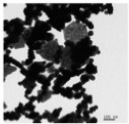
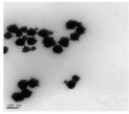
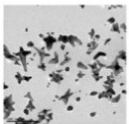
and ARG34) as well as CYS38 (the terminal residue of LL37) were in contact (below 0.3 nm) with the surface of the NP while other cationic residues (LYS18, ARG23, LYS25 and ARG29) were distant (Fig. 3.1g). Evaluation of the radius of gyration (Rg) profile, which measures the mass of atoms relative to the center of mass of the complex [259], also suggest that the peptide conformation changes during the interaction with the Au NP, adopting a more compact structure after the immobilization process (Fig. 3.1h). Although some regions of the peptide (the ones that are distant from the surface of the NP) seem to adopt an alpha-helix structure during the immobilization process, such structure is not present at the end of the simulation, suggesting that no clear secondary structure exists in the immobilized peptide (Fig. 3.1i).

To evaluate whether LL37-Au NPs maintained the bioactivity of LL37, we assessed their antimicrobial properties. The antimicrobial properties of LL37-Au NPs (10  $\mu\text{g}/\text{mL}$  which corresponds to an immobilized concentration of 2,5  $\mu\text{g}/\text{mL}$ ) have been assessed against  $10^5$  CFU of *E. coli*, a gram-negative bacteria. Both soluble LL37 and Au NPs (without peptide) have been used as controls. As expected, Au NPs had no antimicrobial activity while LL37 showed a minimal inhibition concentration (MIC) of 5  $\mu\text{g}/\text{mL}$  (Fig. 3.6). On the other hand, LL37-Au NPs have high antimicrobial activity killing more than 75% of the microorganisms in 4 h. No antimicrobial activity was observed in the supernatant of the LL37-Au NPs, which indicated that the peptide was not leached from the NP surface (data not shown).



**Figure 3.1: Synthesis and characterization of LL37-Au NPs.** (a) Schematic representation of Au NP synthesis in the presence of LL37 peptide. (b) Time dependent absorbance for the synthesis of LL37-Au NPs in HEPES buffer pH 5.0 (Au ions=0.5 mM; LL37=0.25 mM). (c) UV-visible spectra of Au NPs (1mg/mL) synthesized using citrate buffer and LL37-Au NPs (1mg/mL) synthesized in HEPES buffer pH 5. (d) FTIR and (e) TGA analyses of Au NPs and LL37-Au NPs. (f.1 and f.2) Representative TEM images of Au NPs (f.1) and LL37-Au NPs (f.2) and particle size analysis. (g) Distance of LL37 aminoacid residues to the Au surface at the end of the simulation. The line at 0.3 nm represents the cut-off used to define direct contact between the atoms of the amino acids and the Au surface. (h) Gyration radius profile of LL37 in LL37-Au NPs. Results are Average  $\pm$ 95% CI,  $n=20$ . (i) Time course of LL37 peptide secondary structure in LL37-Au NPs. Aminoacid residues are identified by numbers that are displayed in Fig. 3.1g.

---

Au NP	pH (HEPES 100mM)	Au	Zeta Potential (mV)
	5	0.5 mM	-16.77 ± 2.8
	6	0.5 mM	- 43.73 ± 0.36
	7.5	0.5 mM	- 3.5 ± 1.1

---

**Table 3.1: Au NPs synthesised in HEPES.** The Au NPs showed a SPR band at 720, 650 and 920 nm for pH 7.5, 6 and 5, respectively. TEM analyses showed the formation of irregular shapes Au NPs for pH 6 and 7.5 conditions and of large clusters of heterogeneous and aggregated Au NPs synthesized at pH 5.0.

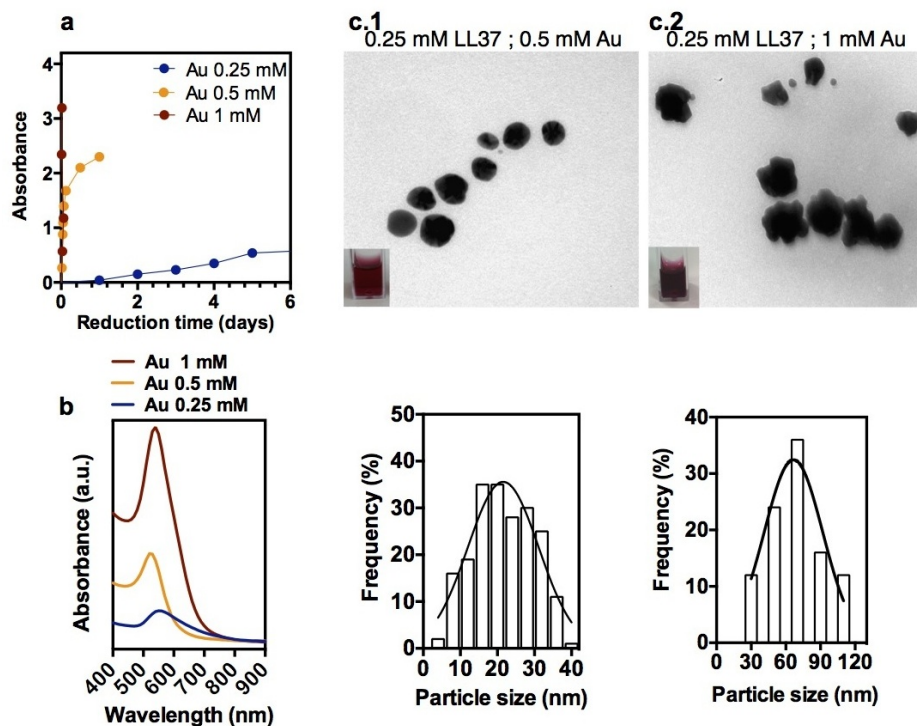


**Figure 3.2: Screening conditions for the preparation of LL37-Au NPs: effect of concentration of Au in the growth of LL37-Au NPs.** The reactions were performed in HEPES buffer pH 5 in the presence of 0.25 mM LL37 and three different concentration of Au (0.25 mM, 0.5 mM and 1 mM). (a) Growth kinetic of Au NPs under different conditions, followed by UV Vis spectroscopy. The reduction rate was faster for reactions having high concentrations of Au. (b) Absorbance peaks of the NPs at the end of the reactions (Au 1mM: 20 min; Au 0.5 mM: 1 day; Au 0.25 mM: 6 days). The absorbance peak of LL37 AuNPs (1 mM Au) at 550 nm confirms a large diameter and not homogenous LL37-Au NPs. (c) TEM images and histograms showing the distribution of NP diameters.

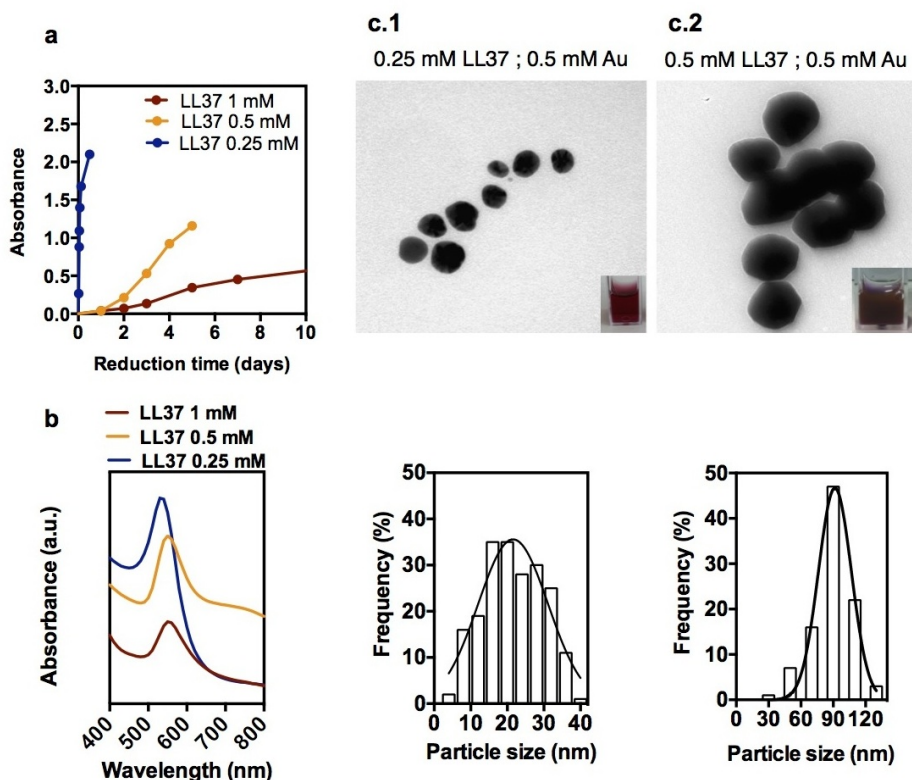


**Figure 3.3: Screening conditions for the preparation of LL37-Au NPs: effect of concentration of LL-37 in the growth of LL37-AuNPs.** The reactions were performed in HEPES buffer pH 5 in the presence of 0.5 mM Au and three different concentration of LL-37 (0.25 mM, 0.5 mM and 1 mM). (a) Growth kinetic of Au NPs under different conditions, followed by UV-Vis spectroscopy. The reduction rate was faster for the lowest concentration of LL-37 tested showing smaller, spherical and homogenous LL-37 NPs after 1 day of reaction. (b) Absorbance peak of the NPs at the end of the reaction (LL37 1 mM: 10 days; LL37 0.5 mM: 5 days; LL37 0.25 mM: 1 day). (c) TEM images and histograms showing the distribution of NP diameters.

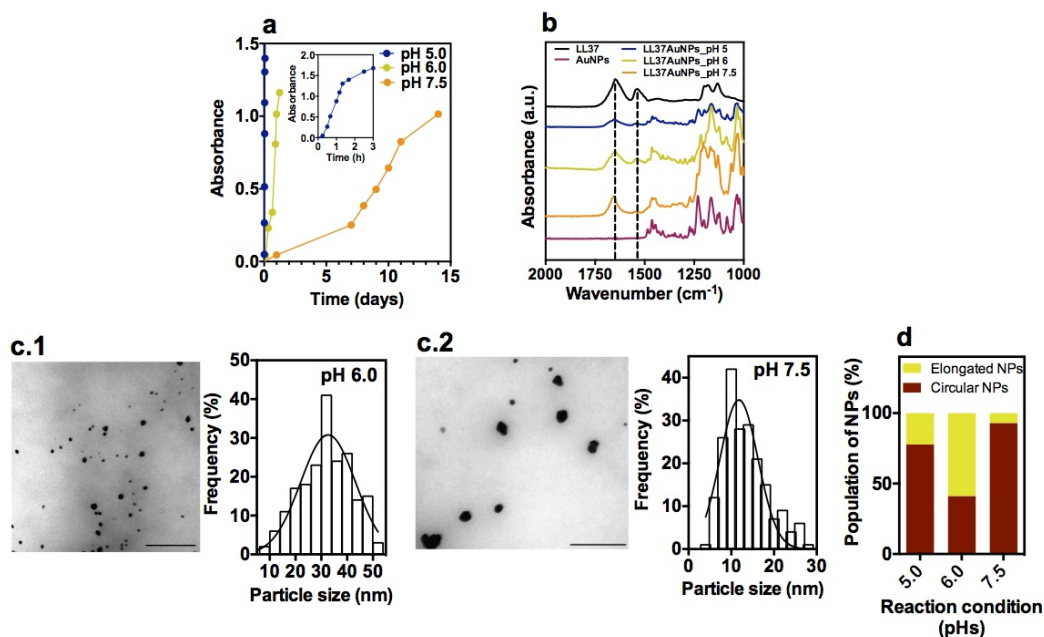


**Figure 3.4: Screening conditions for the preparation of LL37-Au NPs: effect of pH.**

The reactions were performed in HEPES buffer pH 5, 6 or 7.5 in the presence of 0.25 mM LL37 and Au (0.5 mM). (a) Growth kinetic of Au NPs under different conditions, followed by UV-Vis spectroscopy. Time dependent absorbance at 530 nm was recorded with reaction time. In the presence of peptide, the rate of reduction of Au ions was dependent on the aqueous conditions, being faster for pH 5.0 and slow for pH 7.5. (b) FTIR analysis. FTIR results indicate that LL37 conjugated to Au NPs have a random coil structure (amine-I band at 1646) as it is usually observed by AMPs in aqueous solution. (c) TEM images and histograms showing the distribution of NP diameters. The average diameters for LL37-Au NPs obtained at pH 5.0 (shown in Fig. 3.1), 6.0 and 7.5 were  $21 \pm 8$ ,  $35 \pm 7$  and  $12 \pm 3$  nm ( $n \geq 100$  NPs), respectively. (d) Percentage of NPs with a circular or elongated morphology obtained at different pH conditions.



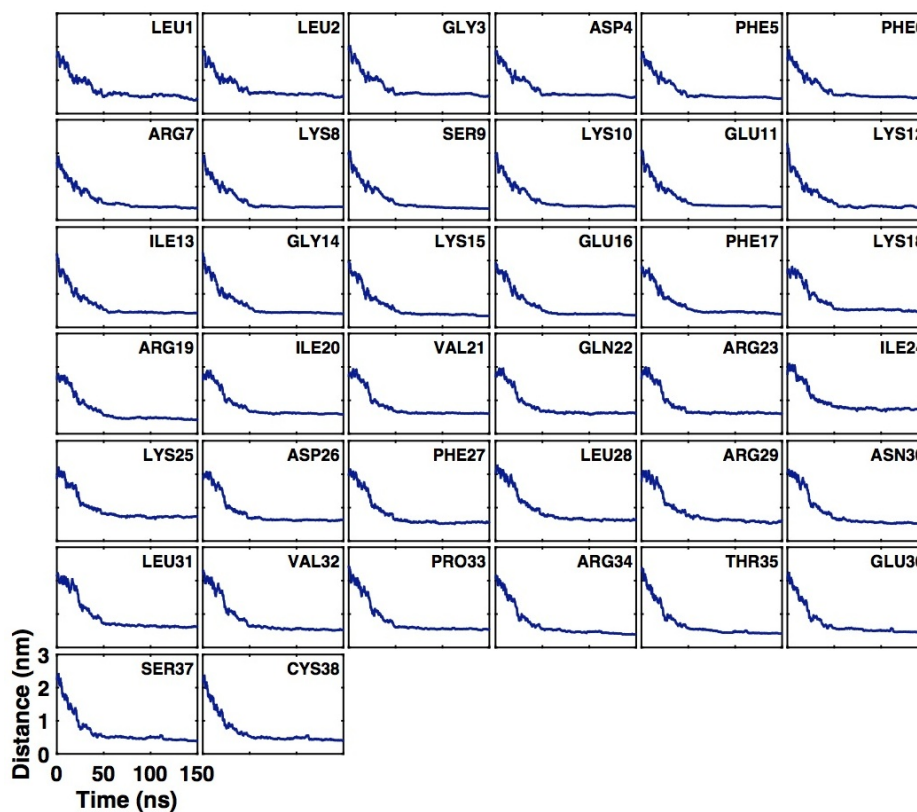


**Figure 3.5: MD trajectories for the interaction of one Au NP with six LL37 peptides.** The trajectories for averaged distances of each amino acids residue of LL37 to the Au NPs surface are represented.



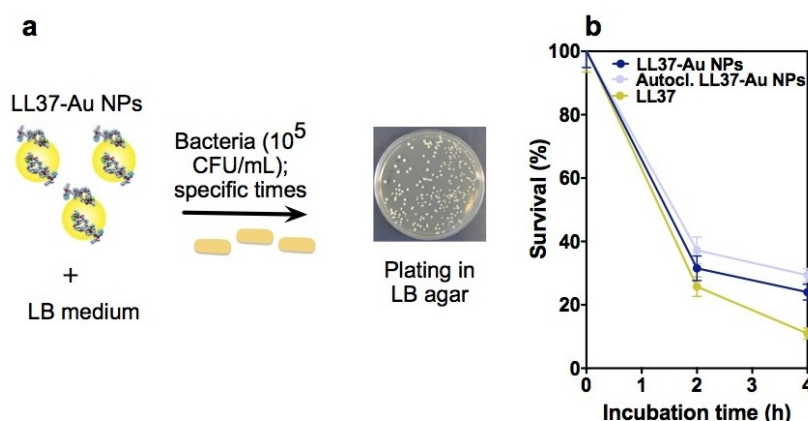


**Figure 3.6: Antimicrobial activity of LL37 and LL37-Au NPs.** (a) Scheme showing the general procedure. LL37-Au NPs ( $10 \mu\text{g}/\text{mL}$  in PBS which corresponds to  $2,5 \mu\text{g}/\text{mL}$  of immobilized LL37) or LL37 ( $5 \mu\text{g}/\text{mL}$  in PBS) were added to LB medium containing *E.coli* (100.000 cells). After 2 or 4 h of incubation with NPs, aliquots of bacteria were plated on LB agar. (b) Colony forming units (CFU) counted in LB-agar plate. Results were normalised by the control (bacteria treated with PBS.) Results are average  $\pm$  SEM,  $n=3$ .

### 3.2.2 LL37-Au NPs are relatively non-cytotoxic to keratinocytes.

The cytotoxicity of NPs can be influenced by their physicochemical properties but also by their stability when resuspend in cell culture media. Therefore, it is of utmost importance to study NP stability in cell culture media. Initially, we studied the zeta potential, size and stability of Au NPs and LL37-Au NPs in keratinocyte culture medium (DMEM medium supplemented with 10% FBS) by dynamic light scattering (DLS). According to DLS studies, the LL37-Au NPs were positively charged when resuspended in HEPES; however, they became negatively charged after resuspension in cell culture medium likely due to formation of biomolecule corona on the surface of NPs (Fig. 3.7a). The Au NPs (produced by reduction of citric acid, average diameter of  $17.4 \pm 1.8 \text{ nm}$ ) resuspended in HEPES or cell culture media were negatively charged. Au NPs were more susceptible to sedimentation in cell culture media than LL37-Au NPs (Fig. 3.7b). LL37-Au NPs did not sediment but show some aggregation in cell culture media.

To evaluate the cytotoxicity of LL37-Au NPs, a human keratinocyte cell line (HaCaT) was incubated with increasing amounts of LL37-Au NPs for 48 h and cell viability was monitored by PI incorporation (Fig. 3.8a), cell metabolism by ATP production (Fig. 3.8b), and cellular oxidative stress by the production of reactive oxygen

species (ROS) using flow cytometry (Fig. 3.8d). LL37 and Au NPs have been used as controls. HaCaT cells treated with LL37 or LL37-Au NPs up to a concentration of 10  $\mu\text{g}/\text{mL}$  and 400  $\mu\text{g}/\text{mL}$  (ca. 100  $\mu\text{g}/\text{mL}$  of LL37), respectively, have no significant decrease in cell viability or increase in ROS production. Yet, a decrease in cell viability and an increase in ROS production were observed for concentrations of LL37 equal or above 10  $\mu\text{g}/\text{mL}$ . We complemented the previous studies by measuring the impact of soluble LL37, Au NPs and LL37-Au NPs on cell membrane (Fig. 3.8e). HaCaT cells become hyperpolarized after 5 h exposure to LL37 peptide in solution at concentrations above 25  $\mu\text{g}/\text{mL}$ , while the effect is lost at 48 h. Interestingly, the membrane potential of HaCaT cells is depolarized after exposure to LL37-Au NPs or Au NPs for 48 h. These results suggest a likely interaction of NPs with cell membrane. Finally, we evaluated the hemocompatibility of Au NPs and LL37-Au NPs by assessing their capacity to induce platelet activation. This was evaluated by quantifying the expression of CD62P (P-selectin) in mononuclear cells by FACS. Our results show no significant effect of the LL37-Au NPs in platelet activation, as the percentage of CD62P<sup>+</sup> platelets was similar to TCPS (Fig. 3.8c).

Overall, our results show that LL37-Au NPs are relatively non-cytotoxic to HaCaT cells for concentrations up to 400  $\mu\text{g}/\text{mL}$  (this means 100  $\mu\text{g}/\text{mL}$  of immobilized LL37) in HaCaT cells. This suggests that the immobilized LL37 might not be able to form secondary structures and punch the human cell membrane. In contrast, LL37 is relatively cytotoxic for concentrations above 10-30  $\mu\text{g}/\text{mL}$ . These results are in line with previous ones showing that LL37 is cytotoxic for human keratinocytes in concentrations of 45  $\mu\text{g}/\text{mL}$  when exposed for 6 h [230]. In addition, LL37 has been reported to be cytotoxic to human peripheral blood leukocytes and T-cells for concentrations above 45  $\mu\text{g}/\text{mL}$  when exposed for 12-15 h [260].

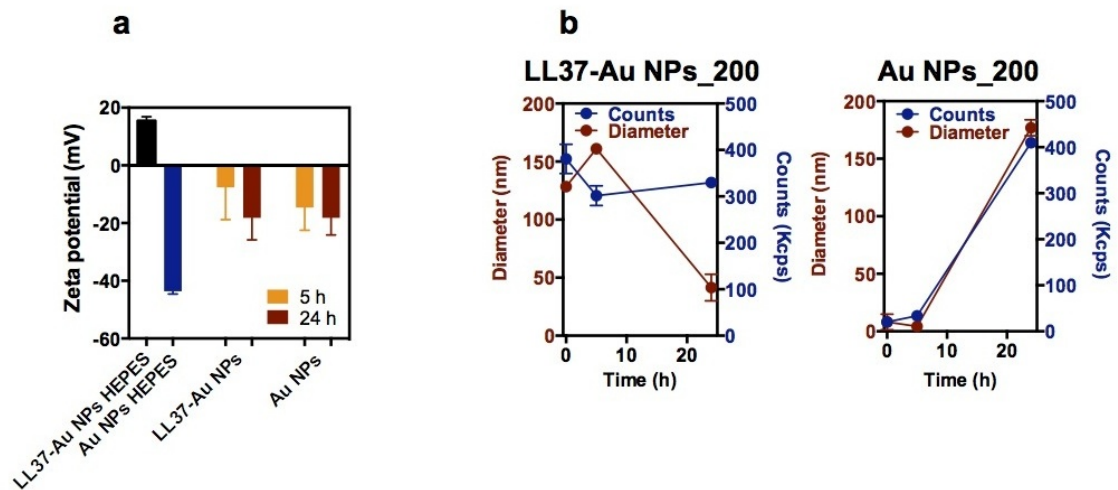


**Figure 3.7: Stability of NPs suspended in culture medium.** (a) Zeta potential of LL37-Au NPs and Au NPs suspended in HEPES or DMEM medium containing 10% (v/v) FBS (HaCaT cell medium). (b) Diameter and counts (Kcps) of LL37-Au NPs and Au NPs in DMEM containing 10% (v/v) FBS. The average diameter of NPs ( $200\mu\text{g}/\text{mL}$ ) suspended in 2 mL of cell culture media was determined by a dynamic light scattering method (DLS) using a Zeta Plus analyzer (Brookhaven), from six independent measurements. In a and b, results are Average  $\pm$  SEM,  $n=3$ .

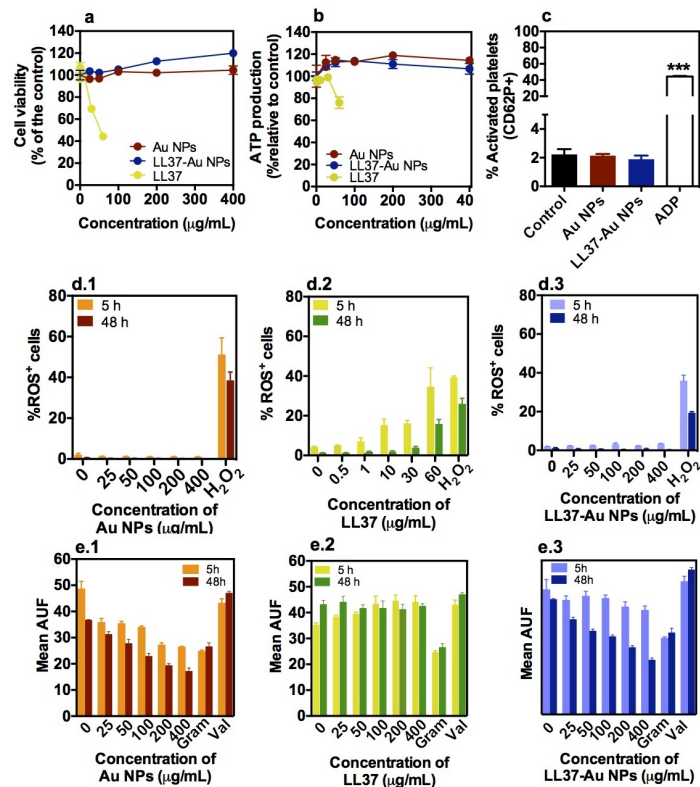


**Figure 3.8: Cytotoxicity of soluble LL37, Au NPs and LL37-Au NPs.** HaCaT cells were exposed for 48 h to different concentrations of soluble LL37, Au NPs and LL37-Au NPs, followed by the quantification of viability (PI staining) (a) or ATP (b). (c) Human peripheral blood was in contact with LL37, Au NPs or LL37-Au NPs for 1 h and the percentage of activated platelets quantified by the flow cytometric quantification of CD62P (P-selectin) expression, using ADP as mild activator. Results show no significant effect of Au NPs or LL37-Au NPs in platelet activation. As positive control we used ADP, a platelet activator, which induced the activation of 40% of the platelets. (d) Percentage of HaCaT cells expressing ROS. Untreated cells and hydrogen peroxide-treated cells were used as negative and positive controls, respectively. Cells cultured with Au NPs or LL37-Au NPs show low capacity to generate ROS even after 48 h. Therefore, NPs do not induce an oxidative stress. In contrast, cells exposed to LL37 for 5 h or 48 h generate ROS, mainly for concentrations above 10  $\mu\text{g/mL}$ . (e) Measurement of the membrane potential by flow cytometry of HaCaT cells after 24 h of contact with soluble LL37, Au NPs or LL37-Au NPs. Cells upon hyperpolarization, when the interior becomes more electronegative with respect to the exterior, take up more dye and therefore have high fluorescence. Conversely, cells that have undergone depolarization take up less dye (therefore have low fluorescence). As positive control, we have used gramicidin (10  $\mu\text{M}$ ), a non-selective ionophore that causes cell depolarization, and as negative control, we have used valinomycin (10  $\mu\text{M}$ ), a  $\text{K}^+$  ionophore that causes cell hyperpolarization. Our results show that HaCaT cells become hyperpolarized after 5 h of contact with LL37. This effect was not observed after 48 h. A depolarisation was observed in HaCaT cells exposed to Au NPs for 5 h or 48 h while cells exposed to LL37-Au NPs are depolarised only at 48 h. All Results are average  $\pm$  SEM,  $n=3$ .

### 3.2.3 LL37-Au NPs are mostly internalized by scavenger receptor-mediated endocytosis in keratinocytes.

Internalization of LL37-Au NPs and Au NPs by human keratinocytes was monitored after 5 h and 48 h of exposure by inductively coupled plasma mass spectrometry (ICP-MS) (Fig. 3.9 a1,a2). HaCaT cells internalized higher amount of Au NPs than LL37-Au NPs (2 to 7-fold higher, depending in the initial concentration and time of contact). The internalization of the NPs occurred essentially during the first 5 h since no significant increase was observed after 48 h of NP contact with the cells.

Next, we studied the mechanism of NP internalization in HaCaT cells. Cells were incubated in the presence of endocytosis chemical inhibitors on concentrations that were not cytotoxic for the cells (Fig. 3.10a), after which, rhodamine-labeled LL37-Au NPs or rhodamine-labeled LL37 were added and the internalization process monitored by flow cytometry. Filipin III inhibits cholesterol dependent internalization mechanisms, nocodazole inhibits microtubule dependent pathways, cytochalasin D inhibits all pathways dependent on actin, dynasore inhibits clathrin-mediated endocytosis polyinosinic acid and dextran sulfate inhibit scavenger receptors and EIPA inhibits macropinocytosis [59], [261], [262], [114]. Whenever possible molecules that enter by a specific internalization pathway were used as positive controls to show the efficacy of our inhibitors (Fig. 3.10b). Our results show that the internalization of LL37-Au NPs and LL37 was mediated by endocytosis since significant inhibition was observed at 4 °C. Our results further show that LL37-Au NPs and LL37 were internalized mainly by scavenger receptors, since keratinocytes inhibited with polyinosinic acid or dextran sulfate had no significant NPs or LL37 peptide internalization (Fig. 3.9 b1,b2). To confirm that NP are internalized by an endocytic mechanism, keratinocytes were transfected with siRNAs to down-regulate key components of different endocytic mechanisms (Fig. 3.9 c1,c2). We observed a 70% and 60% reduction of LL37-Au NPs and LL37 uptake, respectively, upon downregulation of class-A scavenger receptor 3 (SCARA3), confirming a role of scavenger receptors in NP internalization.

Overall, our results show that HaCaT cells internalize higher concentrations of Au NPs than LL37-Au NPs however this might be due to the higher propensity of Au NPs to sediment in cell culture media as compared with LL37-Au NPs. Our results further show that LL37-Au NPs and LL37 are mainly internalized by scavenger receptors as confirmed by chemical or siRNA knockdown studies. Class-A scavenger receptors (SCARA) are a family of cell surface glycoproteins able to bind modified lipoproteins and polyanionic ligands such as oligonucleotides and double-

stranded RNA [263], [264]. The expression of SCARA3 in keratinocytes has been described [265] as well as the involvement of this receptor in the internalization of oligonucleotide-conjugated Au NPs in HaCaT cells [266]. It is likely that the negative charge of LL37-Au NPs in cell medium facilitates the interaction with scavenger receptors in comparison with other endocytic pathways as previously described for cell penetrating peptide nanocomplexes and DNA-functionalized Au NPs [114].

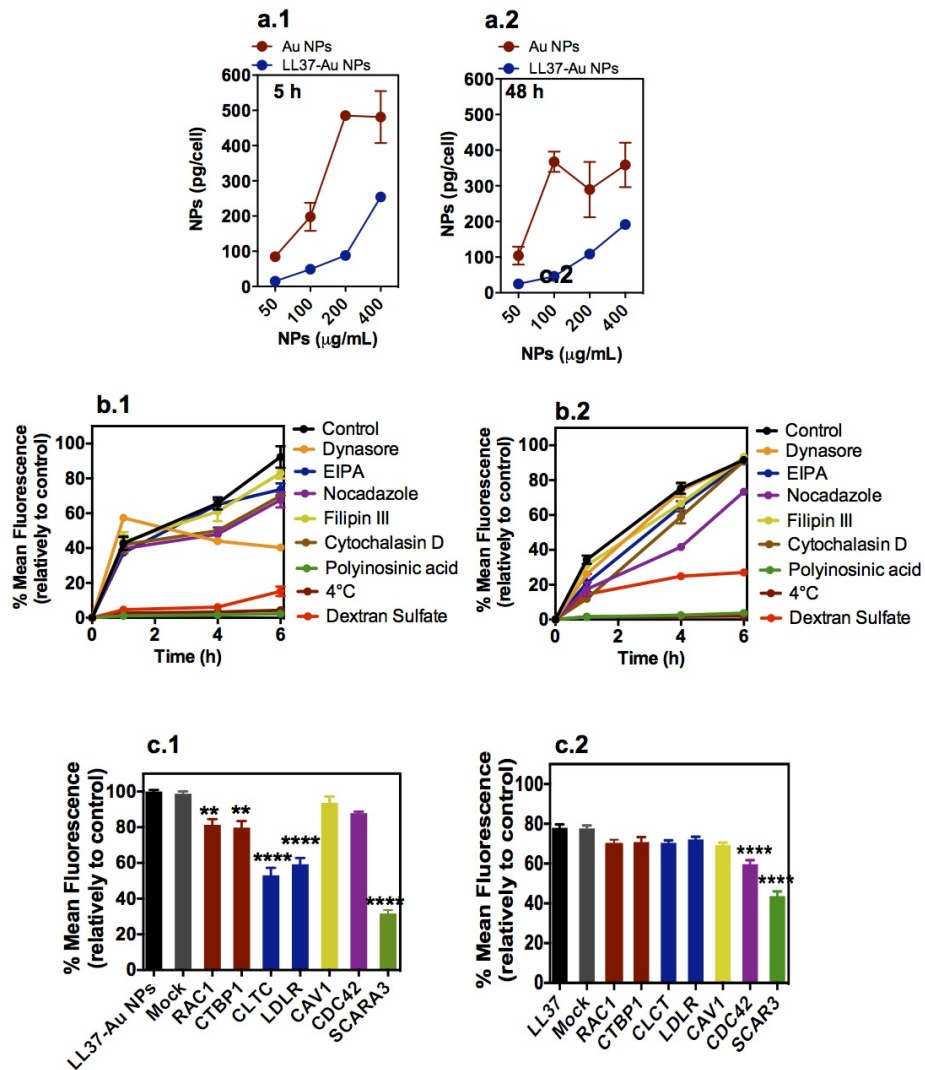


**Figure 3.9: Internalization mechanism of LL37-Au NPs.** (a) ICP-MS quantification of NPs (100-400  $\mu\text{g/mL}$ ) uptake by HaCaT cells after 5 h (a.1) and 48 h (a.2). The results are presented in mass of NPs and not mass of gold. Results are  $Mean \pm SEM$  ( $n = 3$ ). (b and c) Internalization mechanism of LL37 AuNPs and LL37. Uptake of rhodamine-labeled LL37-Au NPs (15  $\mu\text{g/mL}$ ) (b.1 and c.1) and rhodamine-labeled LL37 (1  $\mu\text{g/mL}$ ) (b.2 and c.2) in HaCaT cells after chemically inhibition or after silencing key regulators of clathrin-mediated endocytosis (CLTC and LDLR), caveolin-mediated endocytosis (CAV1), GPI-anchored protein-enriched early endocytic compartment/clathrin-independent carriers (GEEC-CCLIC) pathway (CDC42), macropinocytosis (RAC1 and CTBP1) and scavenger receptors (SCAR3) with siRNAs. In both cases, HaCaT cells were incubated with NPs or LL37 for different times in the presence of the inhibitor. As controls, cells incubated with NPs or LL37 without inhibitors were used. The results are expressed as  $Mean \pm SEM$  ( $n = 3$ ). \* $P < 0.05$ , \*\* $P < 0.01$ , \*\*\* $P < 0.001$ , \*\*\*\* $P < 0.0001$  indicates statistical significance relatively to control (cells exposed to LL37-Au NPs or LL37 without any inhibitor).

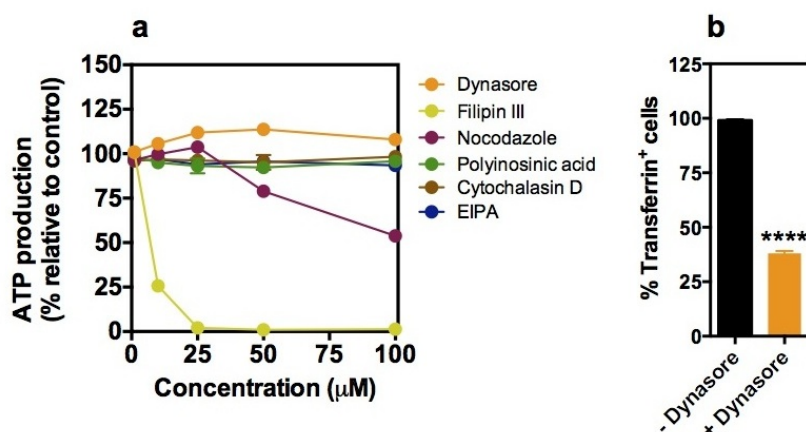


**Figure 3.10: Internalization mechanism of NPs.** (a) Toxicity of chemical inhibitors used for NPs internalization studies. HaCaT were exposed for 6 h to chemical inhibitors of several internalization pathways. The quantification of cell metabolism was assessed by an ATP kit. Results are average  $\pm$  SEM,  $n=3$ . (b) Inhibitory activity of Dynasore in the internalization of transferrin. Transport of FITC-labeled transferrin ( $1 \mu\text{g}/\text{mL}$ ) known to selectively enter cells via clathrin-mediated endocytosis. Dynasore at concentration of  $80 \mu\text{M}$  inhibits the internalisation of transferrin in HaCaT cells. Cells were exposed to culture medium with and without dynasore for 30 min, exposed to FITC-labeled transferrin for 3 min, at  $4^\circ\text{C}$ , and finally characterized by FACS. \*\*\*\* $P < 0.0001$  indicates statistical significance between groups.

### 3.2.4 LL37-Au NPs accumulate in the endolysosomal compartment.

In some cases, the bioactivity of LL37 requires its intracellular internalization. For example, the expression of IL8 by epithelial cells exposed to LL37 requires the internalization of the peptide [268]. In addition, the differentiation of human monocytes into M1 phenotype might be related to LL37 internalization [269]. Moreover, the maturation of dendritic cells likely requires LL37 internalization [270]. Therefore, we examined the intracellular trafficking of LL37-Au NPs and LL37 by confocal microscopy. For this purpose, cells were exposed for 30 min, 4 h and 24 h to rhodamine-labeled LL37-Au NPs ( $100 \mu\text{g}/\text{mL}$ ) or rhodamine-labeled LL37 ( $1 \mu\text{g}/\text{mL}$ ). Early and late endosomes were stained with EEA1 and Rab7 respectively, and cell membrane stained with anti-human EGFR (Figs. 3.11a, 3.12a, 3.13a). Images of cells reconstructed from z-stacks of confocal images indicated extensive cellular uptake of NPs. Our results showed that the highest co-localization of LL37-Au NPs with EEA1 vesicles peaked at 4 h (ca. 25%) while co-localization with Rab7 peaked at 24 h (ca. 33%) (Fig. 3.12b). Some co-localization of LL37-Au NPs was also observed



with EGFR. We further characterized the cellular uptake of LL37-Au NPs in HaCaT cells by TEM analyses (Fig. 3.11b). TEM results confirm that NPs are taken up by HaCaT and localize within endolysosomal vesicles already after 30 min of NPs incubation. NPs are taken up by HaCaT cells with large membrane ruffles engulfing aggregates of NPs when incubation time increases. We complement these studies by evaluating the internalization of rhodamine-labeled LL37 (Fig. 3.13a). LL37 is internalized by HaCaT and 50% of LL37 was within the endolysosomal compartment (EEA1 and Rab7 positive compartments) up to 24 h (Fig. 3.13b).

Taken together, our results show that a significant percentage of both LL37 and LL37-Au NPs accumulate in the endolysosomal compartment. These results are in line with the results obtained recently for macrophages that showed that LL37 accumulated in the endolysosomal compartment [267]. The accumulation of LL37 conferred high bacterial killing activity by enhancing macrophage ROS activity (interestingly high ROS levels were also observed in our results in keratinocytes, please see Fig. 3.8. It is possible that the accumulation of LL37 or LL37-Au NPs in keratinocytes is related to its antimicrobial activity.

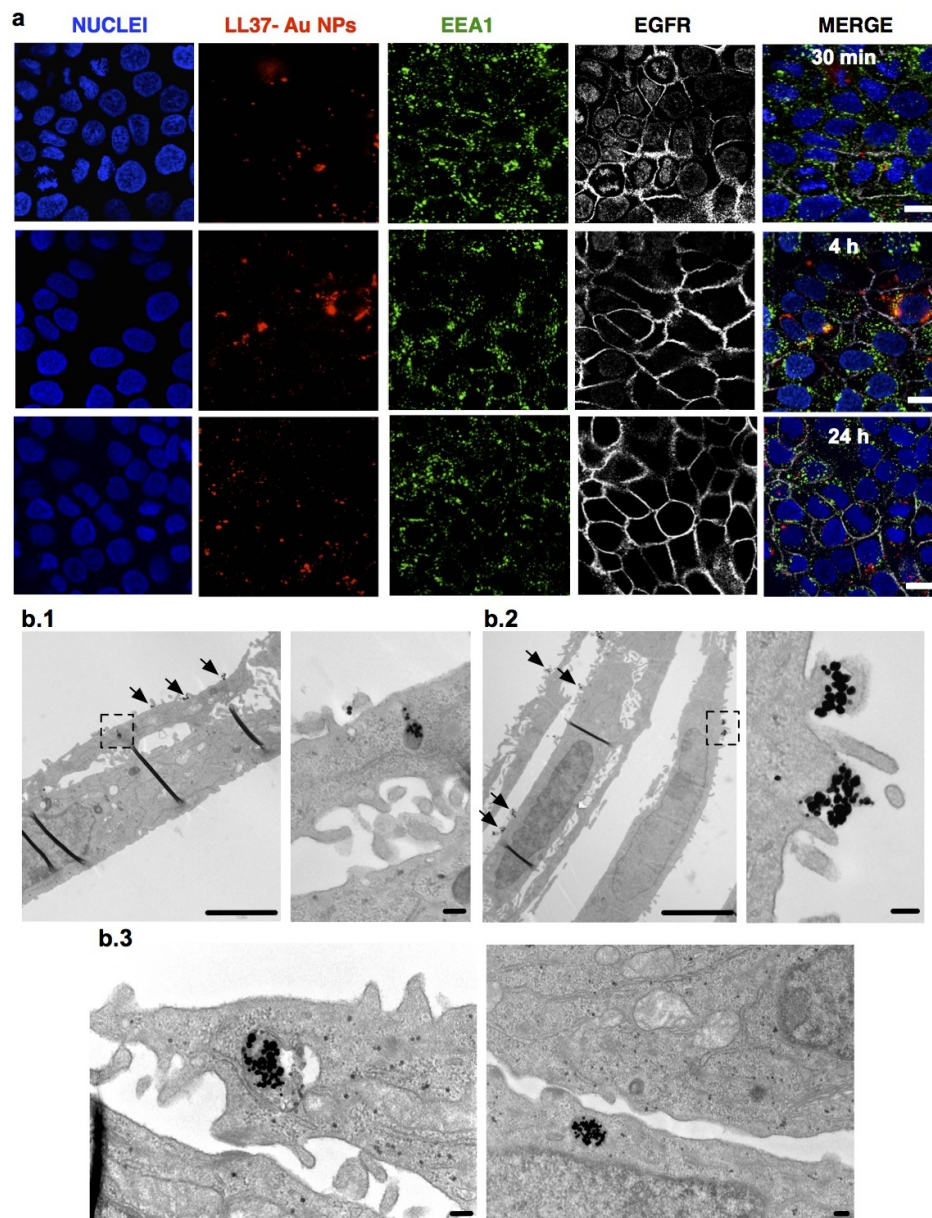


**Figure 3.11: Intracellular trafficking of LL37-Au NPs.** (a) HaCaT cells were exposed for 30 min, 4 h or 24 h to fluorescently labeled LL37-Au NPs ( $100 \mu\text{g}/\text{mL}$ ). At the end of each time, cells were washed with PBS and stained for endolysosomal compartment markers as early endosome EEA1 and late endosome/lysosome marker protein Rab7 (see results of Fig. 2.12) (cell membrane was stained for EGFR). Confocal microscopy was performed to identify the intracellular location of the NPs. Bar corresponds to  $15 \mu\text{m}$ . (b) Characterization of LL37-Au NPs intracellular trafficking in HaCaT by transmission electron microscopy (TEM). TEM results confirm that NPs are taken up by HaCaT and localize within endolysosomal structures after 30 min (b1), 4 h (b2) and 24 h (b3). Arrows indicate sites of internalization. Cell spots defined by a dashed square means areas of magnification. In b.1 and b.2, bar corresponds to 2000 nm (left) and 100 nm (right, magnification). In b.3, bar corresponds to 100 nm.

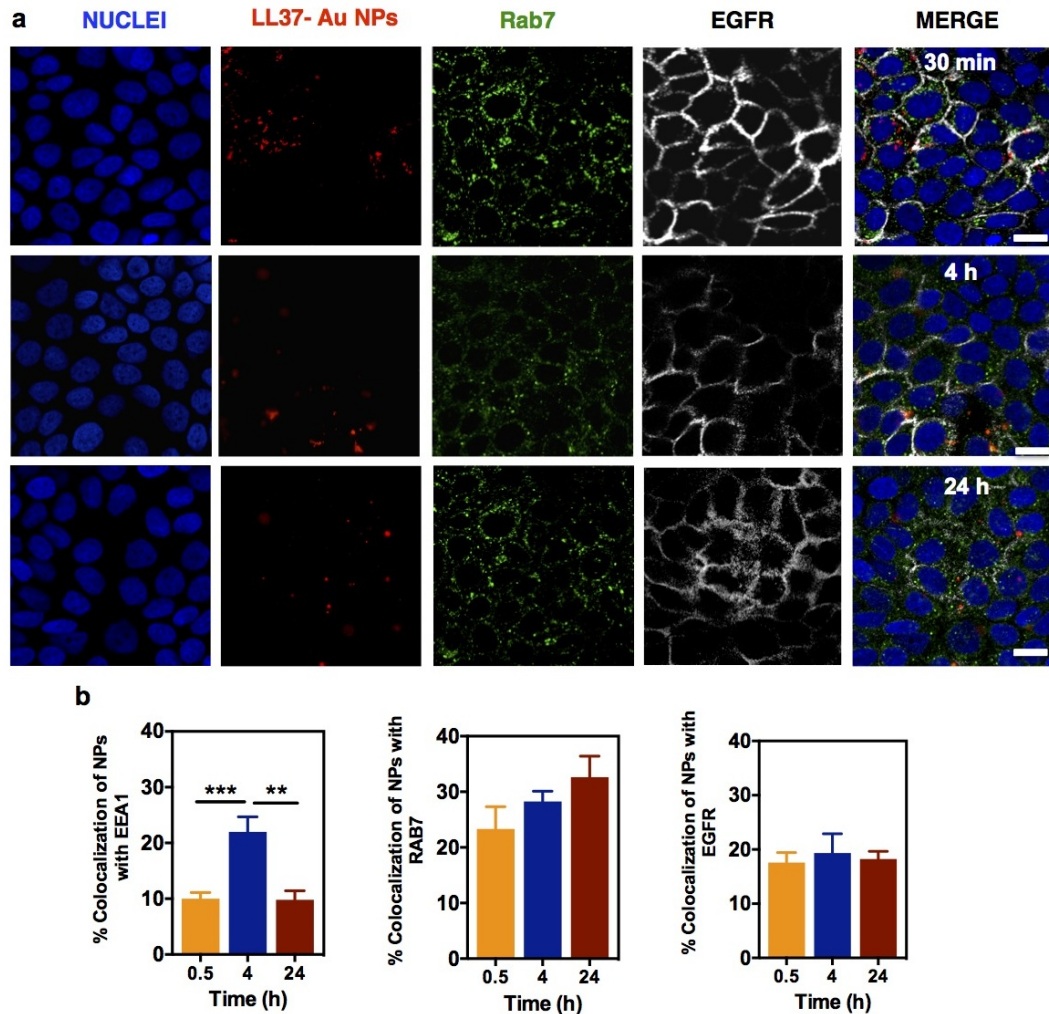


**Figure 3.12: Intracellular trafficking of LL37-Au NPs in HaCaT cells.** (a) HaCaT cells were exposed for 30 min, 4 h or 24 h to fluorescently labeled LL37-Au NPs (100  $\mu\text{g}/\text{mL}$ ). At the end of each time, cells were washed with PBS and stained for endolysosomal compartment markers as early endosome EEA1 (see results of Fig. 2.11) and late endosome/lysosome marker protein Rab7 (cell membrane was stained for EGFR). Confocal microscopy was performed to monitor the intracellular location of the NPs following internalization. Bar corresponds to 15  $\mu\text{m}$ . (b) Quantification of the co-location of NPs with EEA1, Rab7 or EGFR. Results are Average  $\pm$  SEM, from 6 different confocal images (40x objective).  $**P < 0.01$  and  $***P < 0.001$  indicates statistical significance between groups.



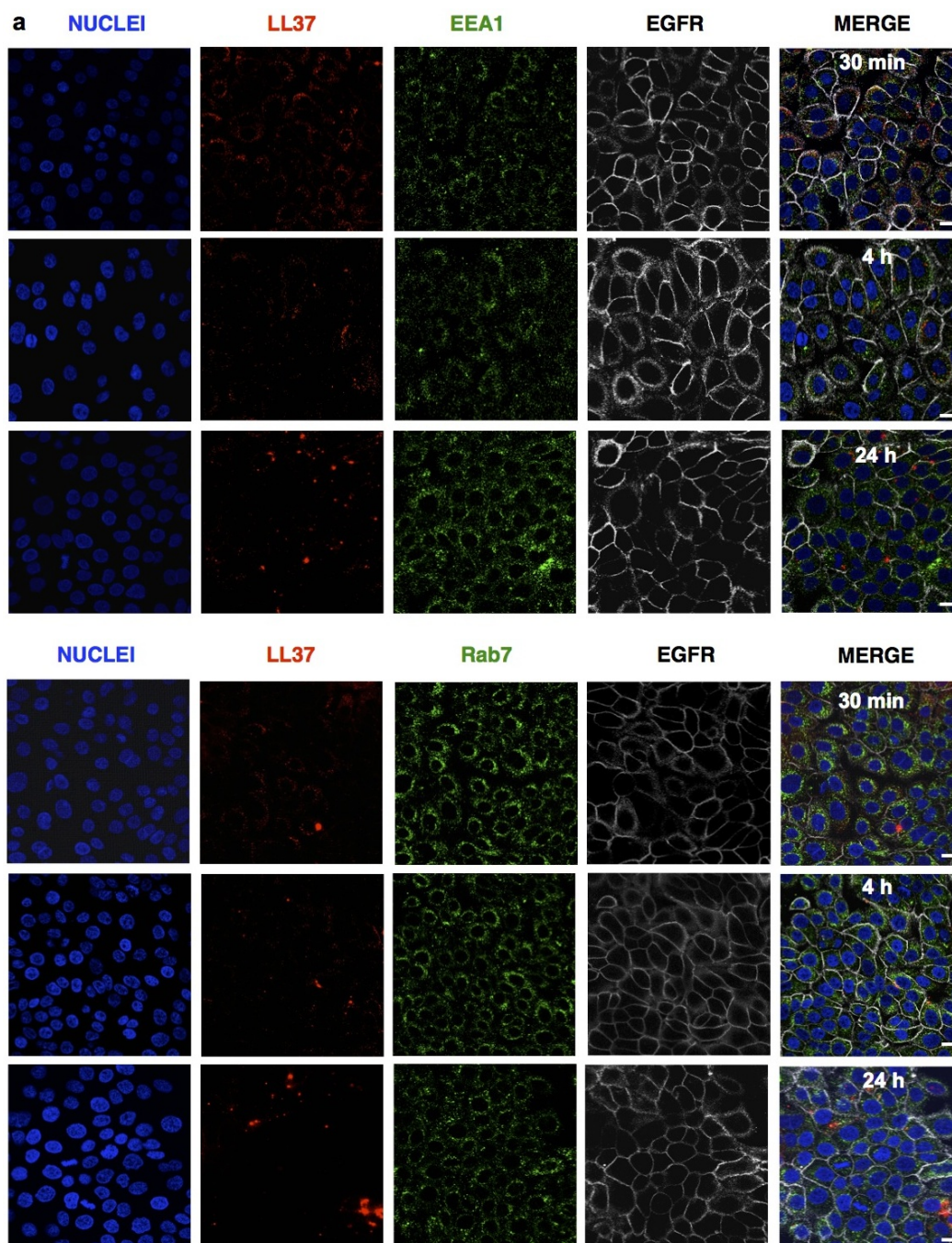


**Figure 3.13: Intracellular trafficking of soluble LL37 in HaCaT cells.** Cells were exposed for 30 min, 4 h and 24 h to fluorescently-labeled LL37 (1  $\mu\text{g}/\text{mL}$ ). At the end of each time, HaCaT were washed with PBS, fixed and stained for endolysosomal compartment markers as early endosome EEA1 and late endosome/lysosome marker protein Rab7 (cell membrane was stained for EGFR). Confocal microscopy was performed to monitor the intracellular location of LL37 following internalization. Bar corresponds to 15  $\mu\text{m}$ . (b) Quantification of the co-location of NPs with EEA1, Rab7 or EGFR. Results are Average  $\pm$  SEM, from 6 different confocal images (40x objective) (see results in the next page).

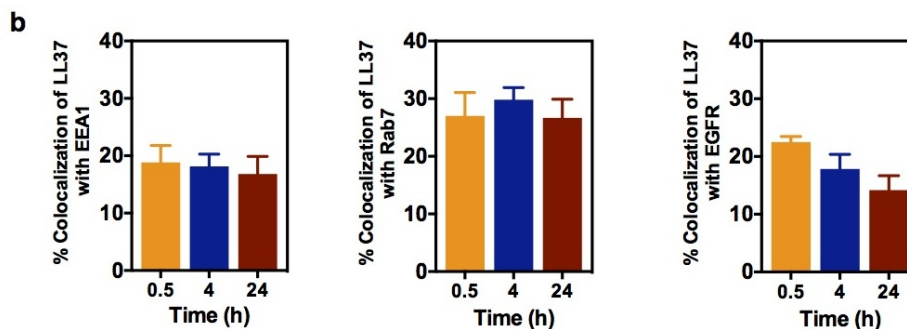
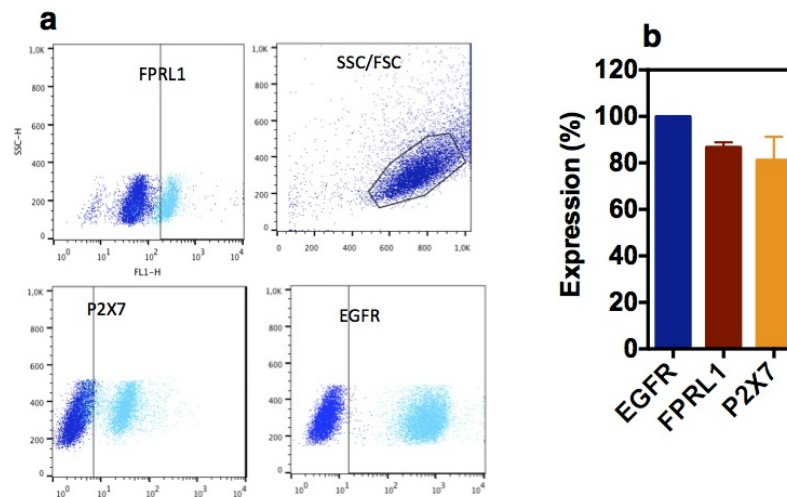


Figure 3.14: (See caption above)

### 3.2.5 LL37-Au NPs, as LL37 peptide, promote HaCaT migration through P2X, ADAM17 and EGFR.

Migration of keratinocytes is an important step in skin wound healing [225], [234]. Previous studies have shown that LL37 activates keratinocyte migration by the transactivation of epidermal growth factor receptor (EGFR) [225] (Fig. 3.16a). This process involves the activation of metalloproteinases (likely ADAM10 and/or ADAM17) that releases EGF anchored to cell membrane into a heparin-binding EGF (HB-EGF), which in turn binds to EGFR [271]. This leads to the phosphorylation of ERK1/2 [272] and STAT3, translocation of STAT3 into the nucleus and finally the initiation of the transcription of target genes. So far little is known about how this cascade is initiated. Recent studies suggest that P2X receptors might be the first target of LL37 in keratinocytes [241], [267]; however, no experimental evidence has been described. It has been hypothesized that LL37 binds non-specifically to purinergic receptors on the basis of their cationic [241] or hydrophobic [267] properties. Furthermore, it is unclear which pathway/molecule links purinergic receptors with the activation of metalloproteases [227]. In this work, we have studied the pro-migratory properties of LL37 peptide, LL37-Au NPs and Au NPs by an *in vitro* scratch assay in HaCaT cells for 72 h (Fig. 3.18). Initially, we evaluate whether EGFR was expressed in HaCaT cells by flow cytometry. HaCaT cells express high levels of EGFR, FPRL1, a receptor that has been described to be involved in the biological action of LL37 in endothelial cells [183], and P2X7 (Fig. 3.15).



**Figure 3.15: Expression of EGFR, FPRL1 and P2X7 receptors in HaCaT cells.** (a) Flow cytometry plots for the expression of FPRL1, P2X7 and EGFR. Positive cells (light blue) were calculated based in the isotype control (dark blue). (b) Quantification of receptor expression. Results are average  $\pm$  SEM, n=3.

Next, we evaluated whether the migration of keratinocytes was due to the transactivation of EGFR. Both LL37 peptide and LL37-Au NPs induce the migration of HaCaT cells (Fig. 3.16). The inhibition of FPRL1 by the antagonist WRW4 [274] had no measurable effect in the migration of keratinocytes; however, the inhibition of EGFR by Erlotinib decreased significantly the migration of keratinocytes treated with LL37 peptide or LL37-Au NPs (Figs. 3.16 b1, b2).

To show the involvement of metalloproteases in the transactivation of EGFR we have performed the scratch assay in the presence of Marimastat, a general ADAM inhibitor (Fig. 3.16 b3). The pro-migratory properties of both LL37 and LL37-Au NPs significantly decreased in the presence of the ADAM inhibitor. Because recent studies have shown the involvement of ADAM17 in the transactivation of EGFR [272] we performed knockdown studies for ADAM17 using siRNA (Fig. 3.16 b4). Our results clearly show that the inhibition of ADAM17 decreased the migratory properties of keratinocytes after activation by LL37 or LL37-Au NPs.

To show the involvement of purinergic receptors in the transactivation of EGFR we have performed the scratch assay in the presence of pyridoxalphosphate-6-azophenyl-2'4'-disulfonic acid tetrasodium salt (PPADS) [227], [228], a broad-spectrum purinergic receptor antagonist (Fig. 3.16 b5). Our results show that keratinocyte migration was inhibited after activation with LL37 or LL37-Au NPs. In addition, PPADS

treatment decreased significantly the phosphorylation of ERK1/2 a downstream target of the transactivation of EGFR (Fig. 3.18b). Because it has been hypothesized recently that LL37 binds non-specifically to P2X7 receptors [267] [273], we inhibited chemically the receptor by A-740003 [275], [276] (Fig. 3.16 b5) or siRNA (Fig. 3.16 b6). In both cases, keratinocyte migration was inhibited after activation with LL37 or LL37-Au NPs.

To further confirm the involvement of P2X receptors in the LL37-Au NPs and LL37 activity in keratinocytes we performed electrophysiological recordings. In whole-cell patch-clamped HaCaT cells at an holding potential of -70 mV, the exposure to either LL37 peptide (1  $\mu\text{g}/\text{mL}$ ) or LL37-Au NPs (200  $\mu\text{g}/\text{mL}$  which corresponds to 50  $\mu\text{g}/\text{mL}$  of immobilized LL37) or Au NPs (200  $\mu\text{g}/\text{mL}$ ) elicited an inward current (Fig. 3.17a). We next attempted to evaluate if the observed inward currents were mediated by ATP-gated P2X channels. For that purpose, we evaluated the impact of apyrase, an enzyme that catalyses the sequential hydrolysis of ATP to ADP and ADP to AMP, to the inward-currents elicited by different compounds. We observed that the presence of apyrase reduced the charge transfer (Q) triggered by Au NPs and LL37-Au NPs but not by LL37 (Fig. 3.17 b1). Whole-cell patch clamp recordings showed that LL37-Au NPs (Fig. 3.17 a3) or Au NPs (Fig. 3.17 a1) triggered the release of extracellular ATP from HaCaT cells, which in turn activated P2X receptors. If cells were treated with apyrase after the pulse with LL37-Au NPs or Au NPs there was a significant decrease in the inward electric current. In contrast, whole-cell patch-clamp recordings showed that LL37 peptide (Fig. 3.17 a2) did not trigger the release of extracellular ATP because no decrease in the inward electric current was observed after treatment with apyrase.

Overall, our functional data indicate that both LL37 and LL37-Au NPs activate keratinocyte migration by the transactivation of EGFR while Au NPs have no bioactivity. Our functional data further suggests that P2X receptors are involved in the initial stages of the process followed by the activation of ADAM17 and EGFR. HaCaT cells inhibited by general purinergic receptor antagonists or by specific P2X7 receptor inhibitors (chemical or genetic) have decreased migration after activation by LL37 peptide or LL37-Au NPs. Our electrophysiology results suggest that the activation of P2X receptors by LL37 does not involve extracellular ATP. Indeed recent experimental results in mononuclear cells suggest that the biological role of LL37 is likely mediated by a complex between LL37 and P2X7R [267]. P2X7R forms a large multimolecular complex with several proteins in the plasma membrane such as  $\beta$ -actin, integrin  $\beta$ 2, heat shock proteins and non-muscle myosin [267]. Moreover,

the direct or indirect (by one of the co-associated molecules) activation of P2X7R can trigger PLD, MAPK- or PI3K-mediated downstream signaling pathways [277]. From our results and data in the literature is still unclear whether there is a specific domain(s) of P2X7R or some co-associated adhesion molecule that mediates the binding of LL37. Importantly, in case of LL37-Au NPs, the activation of P2X receptors seems to be mediated in part by extracellular ATP. Cell treatment with apyrase decreased significantly, but not all, the inward electric current. Because Au NPs also induce the release of extracellular ATP but have no significant effect in the migratory properties of keratinocytes it is likely that the activation mechanism of LL37-Au NPs might involve other mechanisms than extracellular ATP. Therefore, we speculate that the activation of P2X receptors by LL37-Au NPs is due to a combinatorial effect by extracellular ATP and the direct/indirect interaction of LL37 of the surface of the NP with P2X7R. Further studies are necessary to clarify this issue.



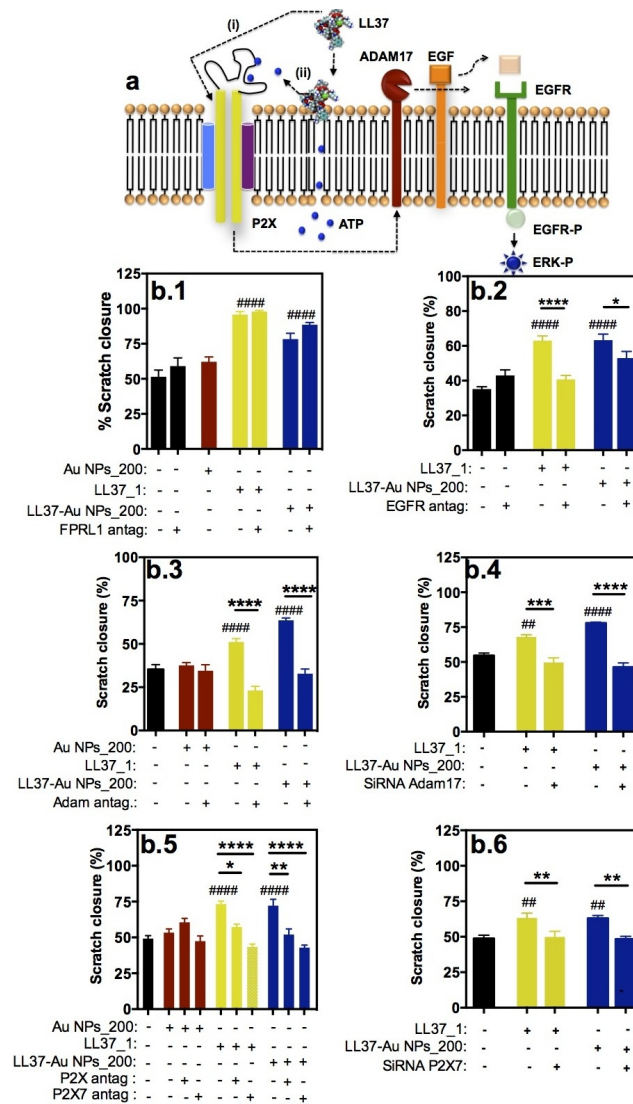


**Figure 3.16: Bioactivity of LL37-Au NPs: functional studies.** (a) Schematic representation of the transactivation mechanism of EGFR. (b) HaCaT migration studies by a scratch assay. Confluent HaCaT cells were starved for 15 h in DMEM with 0.5% FBS and then incubated for 1 h with specific chemical inhibitors or transfected with siRNA for 24 h followed by the incubation for 5 h with LL37 (1  $\mu\text{g}/\text{mL}$ ; referred as LL37\_1 in the graph), LL37-Au NPs (200  $\mu\text{g}/\text{mL}$  which corresponds to 50  $\mu\text{g}/\text{mL}$  of immobilized LL37; referred as LL37-Au NPs\_200 in the graph) or Au NPs (200  $\mu\text{g}/\text{mL}$ ; Au NPs\_200). Cells were then washed with PBS, a scratch was created, the plates re-coated with fibronectin, cells were again washed and maintained in starvation medium up to 72 h. Cell migration was monitored by a high-content microscope. Wound area at 48 h post-treatment was normalized by initial wound area. Results are average  $\pm$ SEM,  $n=6$ . The following chemical inhibitors have been used: FPRL1 receptor inhibitor (WRW4), EGFR receptor inhibitor (Erlotinib), ADAM metalloprotease inhibitor (Marimastat), P2X receptor inhibitor (PPADS) and P2X7 receptor inhibitor (A-740003). # $P < 0.05$ , ## $P < 0.01$ , ### $P < 0.001$  and #### $P < 0.0001$  indicates statistical significance relatively to control (cells without treatment). \* $P < 0.05$ , \*\* $P < 0.01$ , \*\*\* $P < 0.001$  and \*\*\*\* $P < 0.0001$  indicates statistical significance between treatment groups.

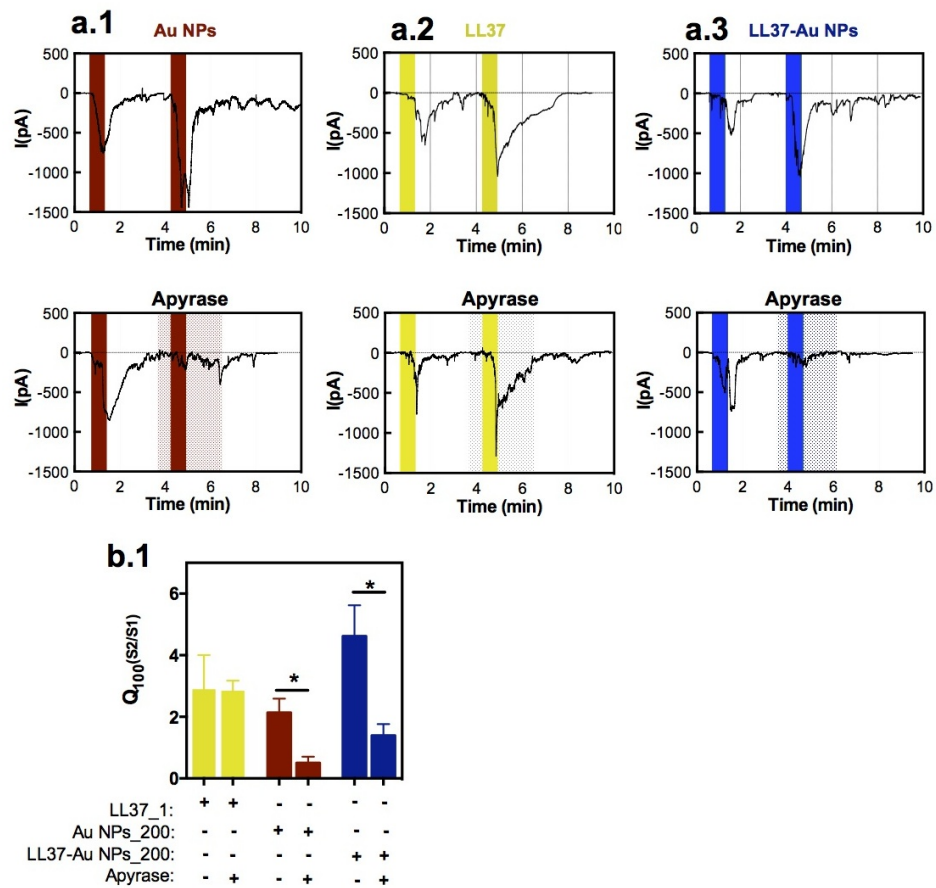


**Figure 3.17: Bioactivity of LL37-Au NPs: electrophysiology studies.** (a) Representative traces of inward-currents recorded in whole cell patch-clamped HaCaT cells at a holding potential of  $-70$  mV exposed to (a1) Au NPs ( $200 \mu\text{g}/\text{mL}$ ), (a2) LL37 ( $1 \mu\text{g}/\text{mL}$ ) or (a3) LL37-Au NPs ( $200 \mu\text{g}/\text{mL}$  which corresponds to  $50 \mu\text{g}/\text{mL}$  of immobilized LL37). Cells were fast perfused twice to the different treatments and the inward currents recorded presented a reproducible ratio between the charge transfer measured in the first 100 s ( $Q_{100}$ ) in the second exposure (S2) over the first exposure (S1) as quantified in (b1). The inward currents triggered by Au NPs and LL37-Au NPs, but not by LL37 were attenuated by the presence of apyrase ( $20 \text{ U}/\text{mL}$ ), as observed by a reduced charge transfer in S2 in the presence of apyrase (darker background), as depicted in the lower traces in (a) and quantified by a reduced S2/S1 ratio shown in (b). Data are presented as mean  $\pm$  SEM of the ratio of ( $Q_{100}$ ) in S2 over S1 measured from 4-5 different cells per condition.  $*P < 0.05$  unpaired t-test.

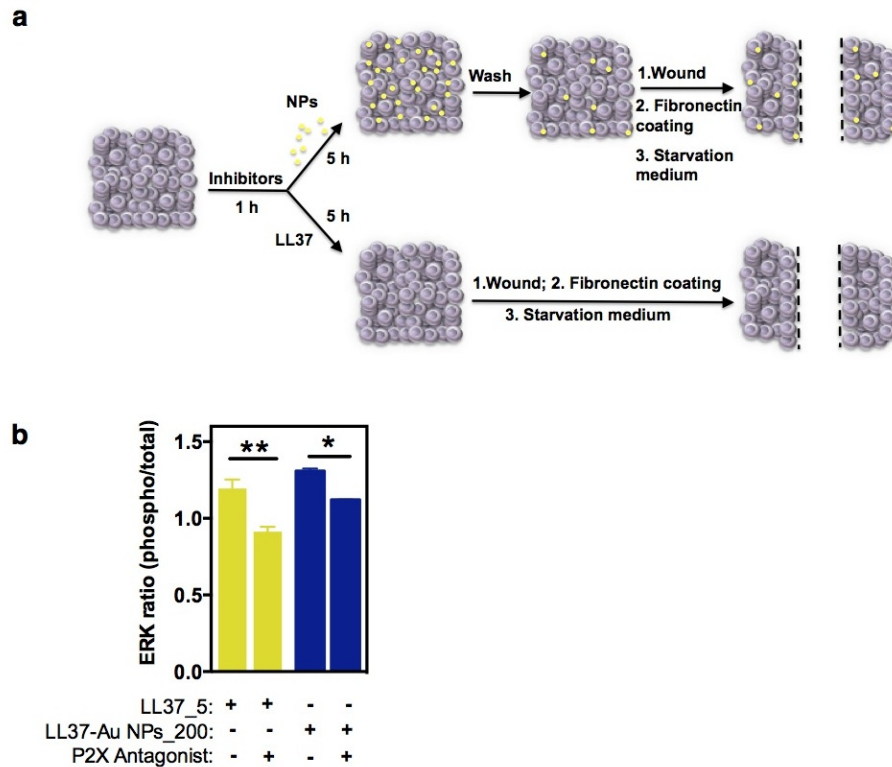


**Figure 3.18: In vitro wound model.** (a) Experimental protocol of the scratch assay. Confluent HaCaT cells were starved for 15 h in DMEM with 0.5% FBS and then incubated for 1 h with specific inhibitors followed by the incubation for 5 h with LL37 (1  $\mu\text{g}/\text{mL}$ ), LL37-Au NPs or Au NPs (both at 200  $\mu\text{g}/\text{mL}$  which corresponds to 50  $\mu\text{g}/\text{mL}$  of immobilized LL37). Cells were then washed with PBS, a starch was created, the plates re-coated with fibronectin, cells were again washed and maintained in starvation medium up to 72 h. Cell migration was monitored by a high-content microscope. (b) ERK phosphorylation in the presence or absence of P2X antagonist. HaCaT cells were incubated with P2X antagonist PPADS (100  $\mu\text{M}$ ) and then activated with LL37 (5  $\mu\text{g}/\text{mL}$ ) or LL37-Au NPs (200  $\mu\text{g}/\text{mL}$ ) for 4 min or 8 min, respectively. Following activation, the cells were lysed and protein extracted. The levels of ERK (phosphorylated and total) were determined by an ELISA kit. Results are average  $\pm$  SEM,  $n=3$ . \*, \*\* means statistical significance of  $P < 0.05$  and  $P < 0.01$ .

### 3.2.6 LL37-Au NPs prolong EGFR and ERK phosphorylation and HaCaT migration compared to LL37 peptide.

Epithelial wounding induces activation of EGFR and its two major downstream effectors PI3K and extracellular signal-regulated kinase ERK [278]. We have evaluated the phosphorylation of EGFR in HaCaT mediated by LL37 peptide and LL37-Au NPs. In line with previous results [225], the phosphorylation of EGFR by LL37

peptide was rapid (peaked at 8 min) and persisted for 10 min (Fig. 3.19 a1). Interestingly, the phosphorylation of EGFR by LL37-Au NPs peaked at 10 min of contact and persisted for at least 60 min. The phosphorylation level was not significantly affected using a lower concentration of LL37-Au NPs (15  $\mu\text{g}/\text{mL}$ ) (data not shown). In addition, LL37-Au NPs lose their capacity to prolong the phosphorylation of EGFR in HaCaT cells if washed after 10 min of contact, indicating that NP contact with cells is required for EGFR phosphorylation (Fig. 3.19 a2).

Next, we examined whether the prolonged phosphorylation of EGFR was correlated with a prolonged phosphorylation of ERK1/2 [272]. The phosphorylation of ERK1/2 in HaCaT cells by LL37 peptide peaked at 4 min and then decreased at time 30 min, while the phosphorylation of ERK1/2 in cells by LL37-Au NPs peaked at 30 min (Fig. 3.19b). Thus, our results confirm a correlation between EGFR and ERK1/2 phosphorylation.

To evaluate the functional impact of the prolonged phosphorylation of EGFR we have conducted a scratch assay in which the wound was large enough to evaluate the long-term migratory activity of keratinocytes. Remarkably, HaCaT cells treated with LL37-Au NPs (15  $\mu\text{g}/\text{mL}$ ) had significantly higher migratory capacity than cells activated with LL37 or the other controls (Figs. 3.19 c1, c2).

Taken together, our results show that LL37-Au NPs but not LL37 peptide have the capacity to prolong the phosphorylation of EGFR and ERK1/2 (from few minutes up to 1 h) and thus enhancing the migratory properties of keratinocytes in a large in vitro wound model. To the best of our knowledge, this is the first study documenting the long-lasting phosphorylation of keratinocytes activated through purinergic receptors. However, it is known that cells cultured in the presence of EGF have long-lasting phosphorylation of EGFR and ERK (2 to 24 h) [279]. The differences in the phosphorylation of EGFR between EGF and ligands of purinergic receptors is explained by differences in the recruitment of growth factor receptor-bound protein 2 (Grb2) and other molecular players. The prolongation of EGFR phosphorylation observed in our studies may be explained by (i) an increased recycling rate of EGFR or (ii) retention of the phosphorylated EGFR at the plasma membrane preventing EGFR desphosphorylation [280]. Prolongation of EGFR phosphorylation has been described in some studies associated with the prevention of EGFR desphosphorylation (mechanism ii). For example, the association of EGFR with the receptor erbB2, a major interaction partner and coactivator of EGFR, is sufficient to prolong and enhance the net phosphorylation of EGFR [281]. The prolongation of EGFR is caused by erbB2-mediated retention of phosphorylated EGFR at the plasma mem-

brane thereby preventing EGFR desphosphorylation and signal termination. In addition, it is known that CTEN, a focal adhesion molecule of tensin family, is able to extend the life of phosphorylated EGFR by decreasing EGFR reduction through the decrease of EGFR ubiquitination [282]. Moreover, EGF immobilized in two-dimensional surfaces is able to prolong the phosphorylation of EGFR [283]. Our results indicate that LL37-Au NPs contribute for the long-term phosphorylation of EGFR by plasma membrane contact and not by NP internalization. It is tempting to speculate that LL37-Au NPs before internalization induce a constant activation of purinergic receptors (by both direct/indirect binding of LL37 or ATP release), which in turn prolong the activation of EGFR and downstream signaling.

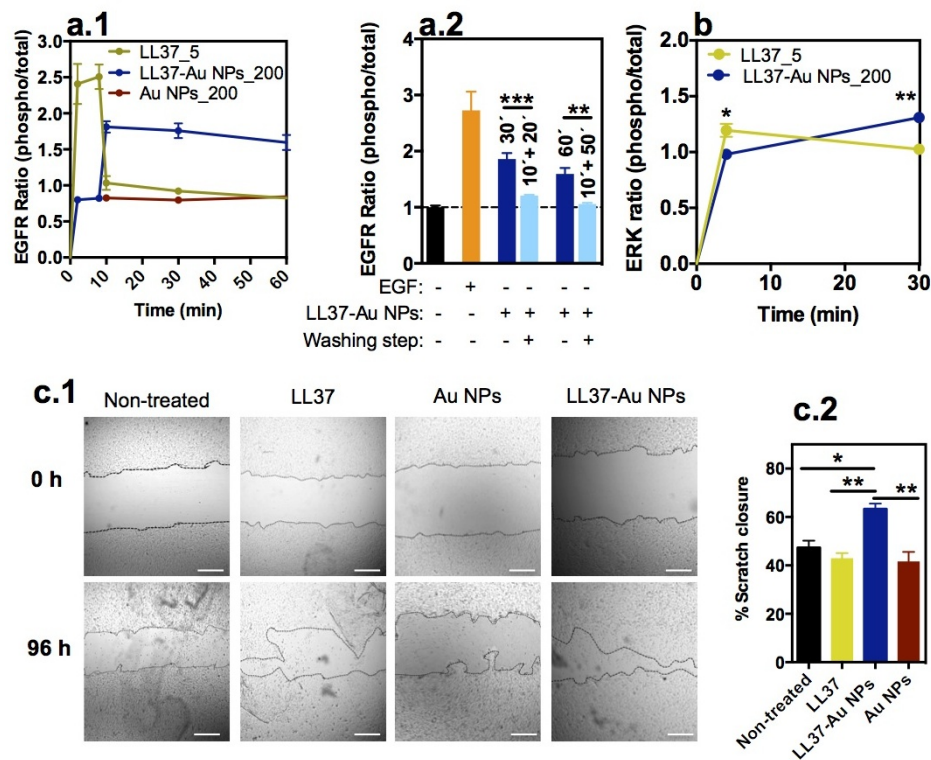


**Figure 3.19: Bioactivity of LL37-Au NPs:molecular studies.** (a.1) Phosphorylation profile (phospho/total protein) of EGFR in HaCaT cells after contact with LL37 (5  $\mu\text{g}/\text{mL}$ ), LL37-Au NPs (200  $\mu\text{g}/\text{mL}$  which corresponds to 50  $\mu\text{g}/\text{mL}$  of immobilized LL37) or Au NPs (200  $\mu\text{g}/\text{mL}$ ) for a certain time (up to 60 min). (a.2) Phosphorylation profile of EGFR in HaCaT cells after contact with LL37-Au NPs (200  $\mu\text{g}/\text{mL}$ ) with or without washing the LL37-Au NPs. The “10’+20’” on top of the column means that cells were washed after 10 min of contact with LL37-Au NPs and then cultured for more 20 min in medium without NPs. Epidermal growth factor (EGF) has been used as positive control. Results are average  $\pm$  SEM,  $n=3$ . (b) Phosphorylation profile (phospho/total protein) of ERK without washing the LL37-Au NPs in contact with HaCaT cells. Results are average  $\pm$  SEM,  $n=3$ . (c) Scratch assay of HaCaT cells after 96 h of incubation with LL37 peptide (1  $\mu\text{g}/\text{mL}$ ), Au NPs (15  $\mu\text{g}/\text{mL}$ ) and LL37-Au NPs (15  $\mu\text{g}/\text{mL}$ ). (c.1) Light microscopy images of the healing of the scratch at 96 h. Bars correspond to 1 mm. (c.2) Quantification of scratch closure at 96 h. Results are average  $\pm$  SEM,  $n=3$ . In graphs a, b and c,  $*P < 0.05$ ,  $**P < 0.01$ ,  $***P < 0.001$  indicate statistical significance between treatment groups.

### 3.2.7 LL37-Au NPs have higher in vivo wound healing activity than LL37 peptide.

To further verify the biological effects of LL37-Au NPs wound healing experiments were performed in a splinted mouse full thickness excisional model. The

freshly created wounds were immediately treated with LL37 peptide (70  $\mu\text{g}$ ), LL37-Au NPs (200  $\mu\text{g}$ ) or Au NPs (200  $\mu\text{g}$ ). Wound area was monitored over a period of 10 days. At day 5, LL37-Au NP-treated mice showed an acceleration of wound healing as compared to the control (Figs. 3.20a, 3.22). LL37-Au NP-treated mice showed complete wound healing after 10 days, whereas LL37 peptide-treated mice showed 70% healing after 10 days. No adverse effects on body weight, general health, or behavior of the mice were observed after NP treatment. The effect of LL37-Au NPs on wound healing was assessed by histological and immunohistochemical examination of epithelial gap closure. Skin sections were stained with hematoxylin and eosin (H&E) for general observation of skin layers and the extent of collagen deposition in healed tissue was determined by Masson's Trichrome (MT) staining. On day 5, the thick scab and the epithelium layer were formed in wounds treated with LL37-Au NPs compared to LL37 and Au NP-treated wounds (Fig. 3.20e). In addition, the wounds treated with LL37-Au NPs have higher levels of collagen than the ones treated with LL37 and Au NP-treated wounds, as shown by the sircol collagen results (Fig. 3.20b). At day 10, a prominent thick epithelium layer was developed in LL37-Au NPs group and wound re-epithelization and deposition of connective tissue processes were mostly completed, leading to closure of wound (Fig. 3.20e).

It has been shown that IL6 is involved in wound healing by regulating leukocyte infiltration, angiogenesis, collagen accumulation and LL37-mediated keratinocyte migration [284], [184]. Epidermal keratinocytes have been identified as the main source of IL6 production in the skin and several host defense peptides including LL37 have been shown to stimulate IL6 expression [186], [285]. Therefore, we evaluated the expression of IL6 in the wounds of all the experimental groups by qRT-PCR. Our results show that wounds treated with LL37-Au NPs have higher expression of IL6 than wounds treated with LL37 or Au NPs (Fig. 3.20c). We extended these studies to quantify neutrophil infiltration in wounds by myeloperoxidase (MPO) analysis. Myeloperoxidase is an enzyme that is found predominantly in the azurophilic granules of neutrophils and can be used as a quantitative index of inflammatory infiltration [286]. MPO activity in wound tissue was significantly decreased after treatment with LL37 peptide and LL37-Au NPs on day 10, demonstrating anti-inflammatory properties of LL-37 peptide (Fig. 3.20d). No reduction in MPO activity was found in wound tissue treated with Au NPs.

Next, we assessed the impact of LL37 and LL37-Au NPs in the vascularization of the wounds. The levels of VEGF were quantified by qRT-PCR and expressed as percentage relatively to the control condition (Fig. 3.21a). Our results show wounds

treated with LL37-Au NPs have higher expression of VEGF at day 10 than wounds treated with LL37 or Au NPs. We complemented these studies by assessing CD31 expression by immunostaining at day 10. Wounds treated with LL37-Au NPs have higher levels of CD31 than wounds treated with LL37 or Au NPs (Fig. 3.21b).

The interactions between skin and colloidal Au NPs of different physicochemical characteristics have been previously investigated [101], [287]. We decided to investigate the accumulation of LL37-Au NPs in the skin and in the main organs of the mouse full thickness excisional model such as liver, lungs, spleen and kidney by ICP-MS. LL37-Au NPs (200  $\mu\text{g}/\text{mL}$  in water) were administered intradermally at several sites around the wound. Our results clearly show that LL37-Au NPs accumulated in the skin, being 74% of the initial concentration of the NPs found in the skin at day 2; however, only 10% of the initial concentration of NPs was found at day 15 (Fig. 3.23a). Less than 1% of the topical dose was found in the main organs at days 2 and 15. The toxic effects of the LL37-Au NPs against liver (transaminase-GPT), kidney (urea), lung and general damage (lactate dehydrogenase) were also measured after 48 h of exposure (Fig. 3.23b). Our results showed that the topical administration of the LL37-Au NPs did not elevate the levels of these key parameters, indicating that the NPs did not cause significant damage to organ functions at the tested doses.

Overall, our results show that LL37-Au NPs have higher wound healing activity than LL37 peptide. Our results further show that LL37-Au NPs are eliminated from the skin and likely excreted through the urine since they do not accumulate in the spleen, lung, liver or kidneys. The wound healing mechanism of LL37-Au NPs was mediated by an increased of IL6 production, decreased inflammation (as evaluated by myeloperoxidase activity) and increased neovascularization. Although our work is the first study to demonstrate the *in vivo* wound healing properties of immobilized LL37, the *in vivo* wound healing properties of LL37 peptide have been previously demonstrated in animal models [183], [233], [234] and in phase I/II clinical trials [236]. The primary safety and tolerability end-point for LL37 was met for patients with venous leg ulcers. The results further show that patients treated with LL37 (twice per week; 0.5 mg/mL) had a statistically significant improved healing rate compared with placebo. However, the peptide was administered twice per week and new systems for the sustained release of the peptide while potentiating its activity may be need. Recently, we have reported a delivery system of LL37 based on the encapsulation of the peptide in poly(lactic-co-glycolic acid) nanoparticles [129]. We have shown that the sustained release of LL37 could accelerate wound



healing. It is likely that the therapeutic effect observed was primarily due to the protection of LL37 against proteases in the wound area. In fact LL37 is degraded in a few hours after exposure to fluid isolated from chronic wounds [288]. In the current work, we have a nanoformulation that does not release the LL37 since the peptide is chemically conjugated to the NP. The higher in vivo therapeutic effect of LL37-Au NPs as compared to LL37 peptide is likely based in differences of the mechanism. According to our in vitro functional and molecular studies LL37-Au NPs activate keratinocytes by a prolongation of EGFR and ERK phosphorylation which leads to a higher migratory activity of the cells than the one observed with LL37 activation. It is possible that the superior wound healing properties of LL37-Au NPs to LL37 might involve different cells of the skin and not only keratinocytes. Work is in progress to elucidate the effect of LL37-Au NPs in endothelial cells, a key player in skin regeneration. Another important result in our study is the demonstration that LL37-Au NPs are eliminated from the skin in a few days and therefore the risks of Au NP accumulation in the skin are relatively low.

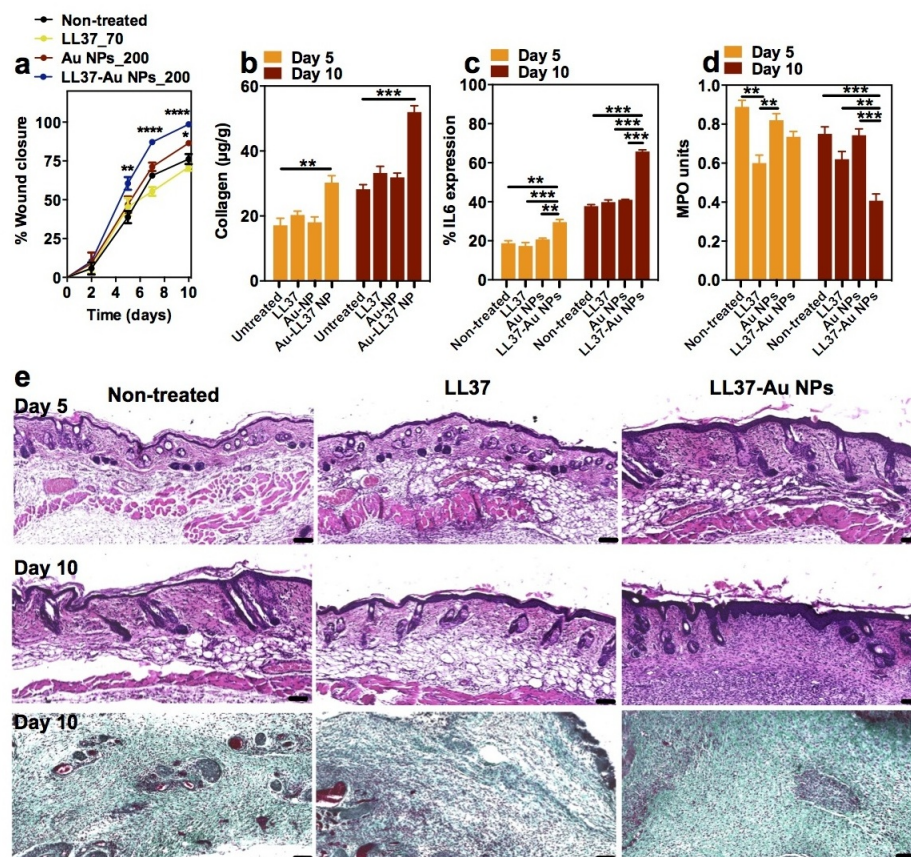


**Figure 3.20: In vivo wound healing properties of LL37-Au NPs: granulation tissue and inflammation.** (a) Wound closure in wounds treated with vehicle (0.9% NaCl), LL37 peptide (70 µg per wound), Au NPs (200 µg per wound) or LL37-Au NPs (200 µg per wound). The formulations were administered intradermally at several sites around the wound. Ten animals (therefore 20 wounds) were used per each group. Wound areas were quantified by a high definition camera. Results are average ± SEM, n=20. (b) Quantification of collagen at days 5 and 10 by a sircol assay. Results are average ± SEM, n=10. (c) Quantification of IL6 by qRT-PCR at days 5 and 10. Results are average ± SEM, n=10. (d) Quantification of myeloperoxidase (MPO) activity at days 5 and 10. Results are average ± SEM, n=10. (e) Histological analysis (Hematoxylin & Eosin staining and Masson trichrome staining) of wound tissues at day 5 and 10 of treatment. In graphs a, b, c and d, \* $P < 0.05$ , \*\* $P < 0.01$ , \*\*\* $P < 0.001$  and \*\*\*\* $P < 0.0001$  indicates statistical significance between treatment groups. In graph a statistical significance is against non-treated animals.

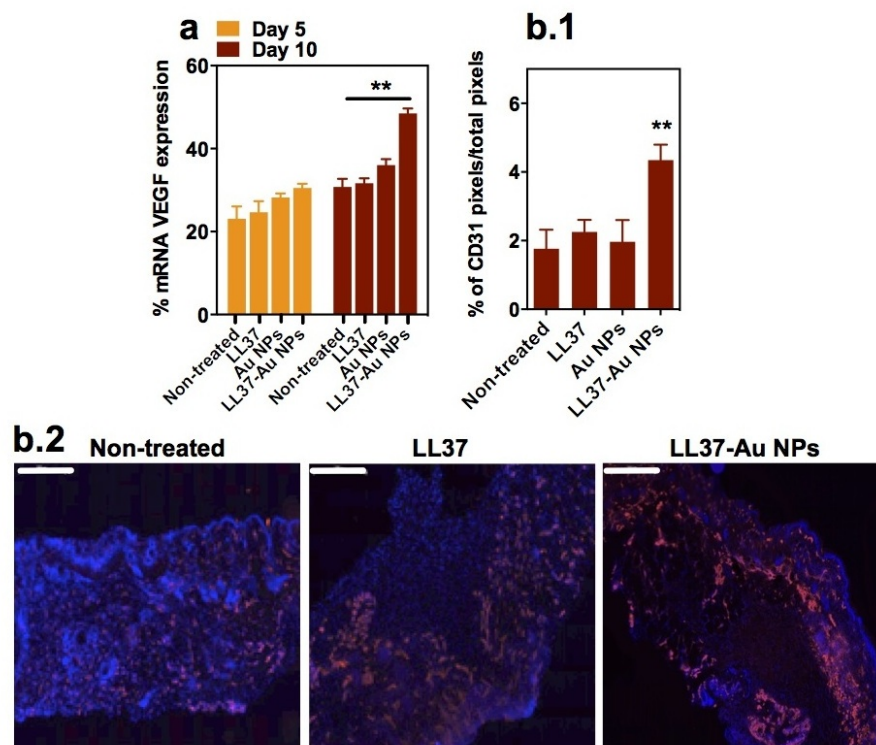


**Figure 3.21: In vivo wound healing properties of LL37-Au NPs: neovascularization.** (a) qRT-PCR VEGF expression in wounds treated with LL37 peptide, LL37-Au NPs or Au NPs at day 5 and 10. Results are average  $\pm$  SEM,  $n=10$ . Expression results were normalized for control condition. (b) Expression of CD31 in wounds treated with LL37 peptide, LL37-Au NPs or Au NPs at day 10. (b.1) Quantification of CD31 staining. The percentage of red pixel represents both endothelial and red blood cells. Results were expressed as percentage of red pixels over the total amount of pixels within the analyzed surface. Results are average  $\pm$  SEM,  $n=10$ . (b.2) Representative immunofluorescent images for each experimental group. Bars correspond to  $500 \mu\text{m}$ . \*\* $P < 0.01$  indicates statistical significance between treatment groups (a) or between LL37-Au NPs and Non-treated.

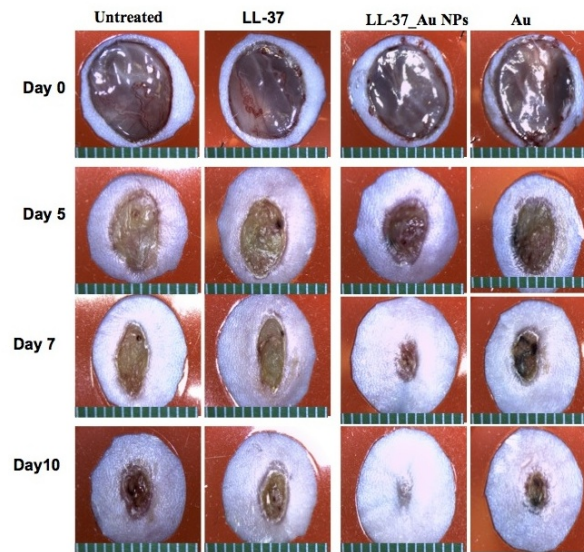


**Figure 3.22: In vivo wound area closure.** Optical images of full-thickness excisional wounds up to 10 days for the different experimental groups

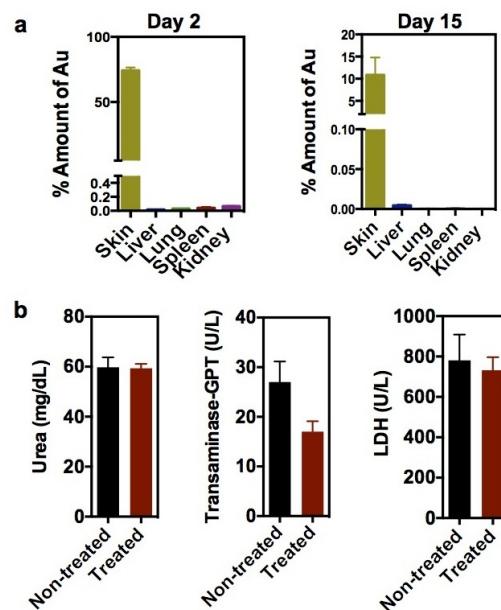


**Figure 3.23: In vivo distribution of LL37-Au NPs.** (a) Au content in different organs of mice at day 2 and 15, as quantified by ICP-MS. Animals were injected with a single dose (1 mg per animal) of LL37-Au NPs. Results are average  $\pm$  SEM,  $n=5$ . (b) In vivo evaluation of biochemical parameters after 2 days exposure to LL37 Au NPs. Blood Serum collected at day 2 was analyzed for the following biochemical parameters: urea, transaminase-GPT and LDH. This analysis showed no relevant changes compared with untreated animal values demonstrating absence of cytotoxic effect in vivo.

### 3.3 Conclusions

Although the wound healing properties of soluble LL37 peptide have been previously demonstrated, it is unknown the bioactivity of permanently immobilized LL37. Here we report a new formulation based on LL37 conjugated to Au NPs that have a gold (Au) core and a hydrophilic cationic LL37 peptide shell, made in a quick one-step synthetic process. NPs have controlled size (21 nm) and low polydispersity. Typically for the production of peptide conjugated Au NPs, Au NPs are produced and then peptides are conjugated. In some cases this requires multiple steps and the aggregation of NPs is a major issue. In the current work we proposed a novel methodology to produce stable Au NPs conjugated with thiol-terminated AMPs where the AMP acts as capping agent during NP formation. These NPs incorporate approximately 250  $\mu\text{g}$  of LL37 per mg of NP, they have an average diameter of 21 nm and a positive zeta potential (15 mV). When these NPs are exposed to keratinocytes, they activate purinergic receptors which in turn trigger ADAM17 activity, the consequent release of EGF anchored to cell membrane and finally the activation of EGFR. Our results show that LL37-Au NPs are rapidly internalized mainly by scavenger receptor endocytosis and accumulate in the cellular endolysosomal compartment. The work conducted in this study is significant because it (i) shows that LL37 chemically conjugated to Au NPs have superior wound healing activity and lower cytotoxicity than LL37, a peptide that is currently being evaluated in clinical trials for wound repair, (ii) it shows for the first time that both LL37 and LL37-Au NPs mediate the migratory activity of keratinocytes through purinergic receptors and (iii) the activation of purinergic receptors by LL37-Au NPs but not LL37 peptide leads to long-lasting phosphorylation of EGFR and ERK which enhances the migratory properties of keratinocytes. The results presented here are an exciting first step toward the development of antimicrobial peptide-based nanotherapeutics for skin disorders paving the way for additional studies in more complex animal models.

### 3.4 Material and Methods

**Materials.**  $\text{HAuCl}_4 \cdot 3\text{H}_2\text{O}$ ,  $\text{Na}_3\text{C}_6\text{H}_5\text{O}_7$  and HEPES, all acquired to Sigma-Aldrich, were used as received. Lyophilized LL37 peptide modified with a C-terminal cysteine (LLGDFFRKSKEKIGKEFK-RIVQRIKDFLRNLVPRTEESC-NH<sub>2</sub>) was purchased from Caslo Laboratory, Denmark. The peptide was synthesized by conventional

solid-phase synthesis, purified by high performance liquid chromatography, and characterized by matrix assisted laser desorption ionization time-of-flight (MALDI-TOF) mass spectroscopy. The purity of the peptide was 96%. Rhodamine B isothiocyanate and HEPES were purchased from Sigma.

**NP preparation.** LL37 (0.5 mM, 1 mg/mL) were dissolved initially in DMF (100  $\mu$ L) followed by addition of HEPES (950  $\mu$ L, 100 mM, pH 5).  $HAuCl_4 \cdot 3H_2O$  ( $10^{-2}$  M, 50  $\mu$ L) was added to a peptide solution (0.25 mM, 950 mL; therefore the final concentration of  $HAuCl_4$  was 0.5 mM) and the NP synthesis was carried out at 25  $^{\circ}$ C. LL37-Au NPs were also synthesized using  $HAuCl_4 \cdot 3H_2O$  (final concentration 0.25 mM, 0.5 mM and 1 mM), and HEPES (100 mM, pH 6 and pH 7.5) by the same procedure at 25  $^{\circ}$ C. The synthesized Au NPs were centrifuged at 14.000 rpm for 20 min at 4  $^{\circ}$ C followed by washing with Milli-Q water to remove unreacted peptides and HEPES, frozen and freeze-dried at 223 K using a Snijders Scientific freeze-dryer. Spherical Au NPs were also synthesized via citrate reduction method [83]. An aqueous  $HAuCl_4$  solution (0.5 mM, 100 mL of water) was boiled in a 250 mL round bottom flask while being stirred after which an aqueous sodium citrate solution (2%, w/v, in water) was added. The reaction was allowed to run until the solution reached a wine red color, indicating the reaction was completed. Fluorescent Au NPs and LL37-Au NPs were prepared by addition of DMSO (0.5 mM) solution of Rhodamine to achieve a final concentration of 25  $\mu$ M for flow cytometry and confocal microscopy studies. Free Rhodamine molecules in the colloidal gold solution were removed by centrifugation at 12000 rpm for 15 min at 4 $^{\circ}$ C followed by two washings with Milli-Q water. The pellet obtained after centrifugation was redispersed in Milli-Q water and then dialysed.

**NP characterization: general analyses.** The reduction of  $HAuCl_4 \cdot 3H_2O$  was monitored by UV-visible spectroscopy using a BioTek synergy MX microplate reader. TEM images were obtained using a Jeol JEM-1011 microscope operating at an accelerating voltage of 100 kV. A drop of NPs solution was placed on a 300 mesh copper grid with a carbon-coated Formvar membrane and dried overnight before examination by TEM. A minimum of 100 NPs was measured using Image J software for the particle size analysis. FTIR spectroscopy analyses were performed in ATR mode using a JASCO spectrophotometer at 4  $cm^{-1}$  resolutions with 64 scans. The hydrodynamic diameter and Zeta potential of Au NPs and LL37-Au NPs suspended in water and in cell culture medium (EGM-2) were measured via a Zeta PALS Zeta Potential Analyzer (Brookhaven Instruments Corporation). The amount of gold in Au NPs and LL37-Au NPs was quantified by ICP-MS, using a 7700x ICP-MS (Agilent



Technologies). The content of LL37 in LL37-Au NPs was estimated by High Resolution Thermogravimetric analyses (Hi-Res-TGA), using a TA Instruments Q500 thermogravimetric analyzer (thermobalance sensitivity:  $0.1 \mu\text{g}$ ). The temperature calibration was performed by measuring the Curie point of a nickel standard and using open platinum crucibles and a dry nitrogen purge flow of  $100 \text{ mL min}^{-1}$ . This procedure was performed at the heating rate and temperature range used throughout the experimental work, i.e.  $2 \text{ }^\circ\text{C min}^{-1}$  over the  $30\text{-}600 \text{ }^\circ\text{C}$  temperature interval. The amount of immobilized peptide was determined indirectly by estimating the peptide that remained in solution after NP synthesis. The concentration of the peptide used for the synthesis of NPs is calculated by spectrophotometry at  $257 \text{ nm}$  using the Beer-Lambert law and an extinction coefficient of  $195 \text{ M}^{-1}\text{cm}^{-1}$ . The synthesized LL37-Au NPs ( $1 \text{ mL}$ ) were centrifuged at  $20000 \text{ rpm}$  for  $30 \text{ min}$  to settle all NPs as a pellet. The supernatant was collected carefully. The ICP-MS analysis of the collected pellet was performed to estimate the number of LL37-Au NPs present in the pellet (or in  $1 \text{ mL}$  of the synthesized NPs). ICP-MS value provides the number of gold ions present in the pellet and we know theoretically the number of gold ions present in single NP and therefore the number of NPs present in the pellet or given volume of solution can be estimated. Simultaneously, the amount of LL 37 peptide in supernatant ( $1 \text{ mL}$ ) is estimated using Beer-Lambert law. The amount of immobilized peptide is estimated by subtracting the amount of peptide in supernatants from the initial added amount. The number of peptide per Au NP is obtained by dividing the number of immobilized peptide per mL of solution by the number of Au NPs per mL of solution.

**NP characterization: MD analyses.** MD simulations were performed using GROMACS 4.6.5 code [289]. A  $6.0 \text{ nm}$  diameter Au NP in water was modeled based on the force field parameters described elsewhere. The ff99SB force field was used to model the peptides. In the case of water molecules, the TIP3P model was used. The peptides were first relaxed in aqueous solution  $50 \text{ ns}$  at  $323.15 \text{ K}$  and then at  $298.15 \text{ K}$  for another  $50 \text{ ns}$ . The resulting conformations were then used as the initial structure for the subsequent simulations. Several independent systems were simulated in view of obtaining data with statistical significance. Hence, a total of 6 peptide positions relative to the Au NP were prepared by rotation of the backbone. All systems were pre-equilibrated using energy minimization simulations. Box volume was relaxed for  $100 \text{ ps}$  in NPT ensemble under periodic boundary conditions (PBC). The simulations were carried out for  $100 \text{ ns}$ , with a  $2 \text{ fs}$  time step, in NVT ensemble under PBC. The temperature was fixed at  $298.15 \text{ K}$  using the Nose-Hoover

thermostat. The electrostatic interactions were treated with the particle mesh Ewald (PME) method and a real space cutoff of 1.0 nm. A cutoff of 1.2 nm was applied to Lennard-Jones interactions. Hydrogen bonds were constrained with the LINCS algorithm.

**NP characterization: antimicrobial properties.** *Escherichia coli* (ATCC 25922) was grown at 37 °C and maintained on LB plates (Luria-Bertani broth with 1.5% agar). LL37-Au NPs, autoclaved LL37-Au NPs and soluble LL37 (5 µg/mL) were evaluated against  $10^5$  bacteria (in 1 mL of PBS buffer) and incubated for up to 4 h at 37 °C. Aliquots (100 µL) were taken out from the respective suspensions at 2 h intervals and diluted in PBS buffer to give  $10^3$  bacteria per mL and plated on LB agar plates followed by incubation at 37 °C. Colonies were counted after 24 h of incubation. The collected supernatant was tested for antimicrobial activity as described above.

**Cell Culture.** A human keratinocyte cell line (HaCaT cell line, CLS, Eppelheim, Germany) was cultured as recommended by the vendor. Briefly, cells were cultivated using DMEM supplemented with 1% (v/v) penicillin and streptomycin (Invitrogen) and 10% (v/v) fetal bovine serum (FBS, Invitrogen) until 90% of confluence. For passage, HaCaT cells were initially trypsinized and then scraped. The cells were sub-cultured at a ratio of 1:3 until achieving the number of cells required for the experiment.

**NP cytotoxicity: viability, metabolism and ROS analyses.** HaCaT cells were seeded at a density of  $2 \times 10^4$  cells per well in a 96 well plate and cultured for 24 h. After that time, the medium was removed and cells were incubated with medium containing LL37 (0.5, 1, 10, 30, 60 µg/mL), or LL37-Au NPs or Au NPs (in both cases: 25, 50, 100 and 200 µg/mL). After 5 and 24 h, CellTiter-Glo® luminescent cell viability assay (Promega) was used to assess the ATP production in cells according to the supplier's instructions. For ROS quantification, cells were seeded at a density of  $4 \times 10^4$  cells/cm<sup>2</sup> in a 24 well plate and cultured for 24 h. After that time, the medium was removed and cells were incubated with medium containing LL37-Au NPs or Au NPs (in both cases: 25, 50, 100 and 200 µg/mL) for 5 h or 48 h. At the end, cells were exposed to 6-carboxy-2'-7'-dichlorodihydrofluorescein diacetate (DCFH-DA, 100 µM, Sigma), a dye commonly used to measure intracellular changes in ROS, for 1 h. Then, cells were washed twice with PBS, trypsinized, centrifuged and resuspended in PBS for further characterization by flow cytometry (FACS Calibur, BD Biosciences). Hydrogen peroxide (1 mM) was used as a positive control for ROS production. In addition, propidium iodide (PI) (1 µg/mL final concentration) was



used to quantify cell viability and to exclude the dead cells (i.e. PI positive cells) from the DCFH analysis.

**NP cytotoxicity: membrane potential.** HaCaT cells were seeded at a density of  $4 \times 10^4$  cells/cm<sup>2</sup> per well in a 24 well plate and cultured for 24 h. After that time, the medium was removed and cells were incubated with culture medium containing LL37-Au NPs, or LL37, or Au NPs at different concentrations. After 5 and 48 h, cells were harvested, resuspended in medium with 5 nM of DiOC5(3) (Sigma-Aldrich) and incubated for 5 min at room temperature in the dark, prior to the analysis with the flow cytometer (FACS Calibur, BD Biosciences). Cells treated with gramicidin (10  $\mu$ M, Sigma) or valinomycin (10  $\mu$ M, Sigma) were used as controls for cell depolarization and hyperpolarization, respectively.

**NP internalization: ICP-MS studies.** HaCaT cells were seeded at a density of  $3 \times 10^5$  cells per well in a 6-well plate and cultured for 24 h. LL37-Au NPs and Au NPs (50, 100, 200, 400  $\mu$ g/mL) suspended in serum-containing medium were incubated with cells for 5 h or 24 h. After incubation, cells were washed three times with PBS to remove non-internalized NPs. Cells were then detached using 0.2% (v/v) trypsin in PBS, centrifuged, counted and resuspended in nitric acid solution (1 mL, 69%, v/v). After acidic digestion, samples were diluted to 4 mL in Milli-Q water and gold was quantified by ICP-MS, using a Bruckner 820-MS instrument (Fremont, CA, USA). Elemental analysis detection of Au<sup>197</sup> was performed after a calibration of the apparatus using gold (Panreac) as standard at 5, 10, 50, 100, 250, 500 and 1000  $\mu$ g/L. Iridium (Panreac) was used as internal standard at 20  $\mu$ g/L. Considering the total cell number in each conditions, data analysis permitted to quantify total Au<sup>197</sup> per cell and NPs per cell.

**Internalization studies: endocytosis chemical inhibition studies.** HaCaT cells were cultured on 24 well plates ( $2 \times 10^5$  cells per well) and inhibited by one of the following chemicals during 30 min before adding a suspension of rhodamine-labelled NPs (15  $\mu$ g/mL) or rhodamine-labelled LL37 (1  $\mu$ g/mL): dynasor (100  $\mu$ M), cytochalasin D (100  $\mu$ M), nocodazole (25  $\mu$ M), filipin III (1  $\mu$ M) and polyinosinic acid (100  $\mu$ g/mL), EIPA (100  $\mu$ g/mL) or dextran sulfate (2,5  $\mu$ g/mL). The inhibitor concentrations were based in values reported in literature and further validated by us to have no cytotoxic effect over the period of the assay (6 h), as confirmed by a ATP assay. The incubation of the cells with NPs for different times was performed in the presence of the inhibitor. As controls, we used HaCaT keratinocyte cells without NPs or LL37 and cells incubated with NPs or LL37 without inhibitor. At the end of each time point, cells were centrifuged at 1.000 rpm, 20°C for 5 min, washed 3 times

with cold PBS and then resuspended in PBS containing 2.5% FBS (400  $\mu$ L) for FACS analysis. A total of 10.000 events were obtained per measurement. To validate the inhibitory activity of dynasor we performed uptake studies of FITC-labeled transferrin, known to selectively enter cells via clathrin-mediated endocytosis. Briefly, HaCaT keratinocyte cells were cultured on 24 well plates ( $3 \times 10^5$  cells per well) and treated or not with dynasor (80  $\mu$ M, 30 min pre-incubation), followed by addition of 1  $\mu$ g/mL FITC-labeled transferrin (Life Technologies). The transferrin was allowed to bind for 3 min at 4°C. Cells were then evaluated as before.

**Internalization studies: endocytosis siRNA studies.** The NP uptake mechanism was also studied on HaCaT cells by silencing specific proteins of clathrin-mediated endocytosis (CLTC and LDLR), caveolin-mediated endocytosis (CAV1), GEEC-CCLIC pathways (CDC42), macropinocytosis (RAC1 and CTBP1) and scavenger receptors (SCARA3) by siRNA (Thermo Fisher). Transfection was performed in a 24 well plate with  $1 \times 10^5$  cells per well in antibiotic-free complete medium with 100 nM siRNA and 1.5  $\mu$ L of Lipofectamine RNAiMAX (Life Technologies) transfection reagent for 24 h. After this initial period, the transfection medium was replaced by complete medium and the cells incubated for another 24 h. Then, cells were cultured with Rhodamine-labelled NPs (15  $\mu$ g/mL) or Rhodamine-labelled LL37 (1  $\mu$ g/mL) for 4 h. Once the incubations were terminated, the cells were centrifuged at 1.000 rpm, 20 °C for 5 min, washed 3 times with cold PBS and then resuspended in PBS containing 2.5 % FBS (400  $\mu$ L) for FACS analysis. Non-transfected cells were used as controls. In all FACS analysis, a total of 10.000 events were recorded per run. All conditions were performed in triplicate.

**Intracellular trafficking: confocal microscopy analyses.** HaCaT cells  $3 \times 10^4$  were plated on a  $\mu$ -slide 8 well (ibiTreat, Ibidi, Germany) and left to adhere overnight before adding rhodamine LL37-Au NPs (100  $\mu$ g/mL) or rhodamine-labeled LL37 (at 1  $\mu$ g/mL). After 30 min, 4 h or 24 h of NPs incubation, cells were washed three times with PBS and were fixed with paraformaldehyde (4% (v/v)) for 10 min, at room temperature, and washed two times with PBS. After blocking with BSA (1%, w/v in PBS) for 1 h, fixed HaCaT were incubated with anti-EGFR antibody (Abcam, dilution 1:1000) for 2 h, washed three times with PBS and permeabilized with 0.3% Triton X-100/PBS, and blocked with BSA solution for 1 h. Cells were incubated with primary antibodies early endosomal marker EEA1 (Cell Signaling C45B10, 1:100 dilution) and the late endosome/lysosome marker protein RAB7 (Cell Signaling D95F2, 1:100 dilution) diluted in BSA solution according to the manufacturer's instructions and incubated for 2 h at room temperature. Secondary antibodies were

anti-mouse Alexa fluor 647 and anti-rabbit Alexa fluor 488 (both from Life technologies 1:1000 dilution). Un-bound antibody was removed by washing two times with PBS before staining the nucleus of cells with Hoechst (Life technologies, dilution 1:1000) for 10 min. Six confocal images (40 objective) for each condition were taken, using the optimal pinhole for better discrimination between foci and assuring no overexposure or bleed-through between channels. Usually images were composed of four channels (blue, green, red, and far-red), where different interactions were analyzed. Images were exported to ImageJ, and colocalization analysis was performed using the automated co-localization tools available named JACOP.

**Intracellular trafficking: TEM analyses.** HaCaT ( $1 \times 10^5$  cells/cm<sup>2</sup>) were plated in a 56 cm<sup>2</sup> cell culture Petri dishes until confluency. The cells were then exposed to 100  $\mu$ /mL of LL37-Au NPs for 30 min, 4 h or 24 h. After incubation, cells were washed three times with PBS to remove the NPs not internalized by cells and then fixed for 45 min with 2.5% (v/v) glutaraldehyde in PBS (0.1 M, pH 7.4). The fixative was then removed, and new fixative solution (1.5 mL) was added to the plate to scrap the cells. Floating cells were then collected in the eppendorf and centrifuged at 3.000 rpm to obtain a pellet and the supernatant discarded. The samples were then post-fixed with a solution of PBS containing 1% OsO<sub>4</sub> and 0.8% C<sub>6</sub>N<sub>6</sub>FeK<sub>4</sub>, for 2 h at room temperature, washed with PBS 0.1 M, and finally dehydrated (in a graded concentration of acetone). The dehydrated samples were then embedded in resin and sliced in blocs for visualization. TEM images were recorded with a JEOL 1010 microscope that operates at 80 kV.

**FACS analyses.** Cells were dissociated from the culture plate by exposure to Cell Dissociation Buffer (Life Technologies) for 3-5 min and gentle pipetting, centrifuged and finally resuspended in PBS supplemented with 0,1% (v/v) BSA. The single cell suspensions were aliquoted ( $1.5 \times 10^5$  cells per condition) and stained with either isotype controls and antigen-specific primary antibodies: Anti-EGFR antibody (ab30, Abcam, dilution 1:200) and Anti-P2X7 antibody (H-265) (sc-25698, Santa Cruz Biotechnology, dilution 1:100) for 30 min at 4°C and. After the incubation with primary antibodies, cells were washed 3 times and incubated with anti-mouse Alexa fluor 488 and anti-rabbit Alexa fluor 488 (both Life technologies 1:1000 dilution) for 30 min, respectively. Once the incubations were terminated, the cells were centrifuged at 1000 rpm, 20 °C for 5 min, washed 3 times with cold PBS and then resuspended in PBS containing 0,1% BSA (400  $\mu$ L) for FACS analysis. Differently for FPRL1 quantification, cells were fixed with 0,1% (v/v) paraformaldehyde (PFA) for 10 min, washed, permeabilized with saponin 0,02% (v/v) for 20 min and

then stained with either isotype controls and antigen-specific primary antibodies Anti-FPRL1 antibody (ab101702, Abcam, dilution 1:200) for 30 min at 4°C. After the incubation with primary antibodies, cells were washed 3 times and incubated with anti-rabbit Alexa fluor 488 (Life technologies 1:1000 dilution) for 30 min. All conditions were performed in triplicate. FACS Calibur (BD Biosciences, San Diego, CA) and Cyflogic software were used for the acquisition and analysis of the data.

**NP bioactivity: scratch assay.** HaCaT cells (passage 35-40) were seeded at a density of  $2 \times 10^4$  cells/well in fibronectin-coated 96-well plate in DMEM supplemented with 1% (v/v) penicillin and streptomycin and 10% (v/v) FBS. After 48 h, cells were initially starved for 15 h in DMEM with 0.5% FBS, inactivated with mitomycin (5  $\mu\text{g}/\text{mL}$ ) for 2 h, and then incubated with LL37 (1  $\mu\text{g}/\text{mL}$ ), LL37- Au NPs or Au NPs (both at 200  $\mu\text{g}/\text{mL}$ ) for 5 h at 37 °C and 5% CO<sub>2</sub>. In case of chemical inhibition, the chemical inhibitors for FPRL1 (WRW4, Calbiochem, 10  $\mu\text{M}$ ), EGFR (Erlotinib HCL, OSI-744, Selleck Chemicals, 2 nM), ADAM17 (Marimastat, Sigma, 10  $\mu\text{M}$ ), P2X (PPADS, Sigma, 100  $\mu\text{M}$ ) and for P2X7 (A-740003, Sigma, at a concentration of 500 nM) were added to the cells 1 h before the incubation with LL37 peptide and LL37-Au NPs and then maintained during the assay. We tested all inhibitors used in our study, and none of them showed any significant toxicity to cells under our experimental conditions (data not shown). After the 5 h treatment, cells were washed twice with PBS to remove non-internalized NPs and a scratch was created with a sterile pipette tip. The detached cells were washed twice with PBS and then plates were re-coated with fibronectin (10  $\mu\text{g}/\text{mL}$  in starvation medium) for 1 h at 37 °C. Cells were washed and maintained in starvation medium up to 72 h. Cell migration was monitored overtime by a In Cell Microscope 2000 (GE Healthcare) (objective 2x). The cells treated with LL37 peptide were cultured with starvation medium containing LL37 for the entire duration of the experiment. Scratch areas were quantified using the AxioVision software (Carl Zeiss). Wound areas were normalized by the initial area (n= 6 images). In case of siRNA knock-down studies, on-target plus human ADAM17 siRNA or P2X7R siRNA (both from Dharmacon) were used to silence ADAM17 or P2X7 before performing the scratch assay. HaCaTs were transfected with 50 nM siRNA using 0.25  $\mu\text{L}$  of Lipofectamine RNAiMAX (Life Technologies) for 24 h in antibiotic-free complete medium before starting the scratch assay. To test the prolonged effect of LL37-Au NPs on HaCaT migration, cells were plated in fibronectin-coated 24-well plate ( $2 \times 10^5$  cells/well), after 48 h cells were starved for 15 h in DMEM with 0.5% FBS and then the scratch was made with a sterile pipette tip. Only after this step, the cells were incubated with LL37 (1  $\mu\text{g}/\text{mL}$ ),

LL37-Au NPs and Au NPs (15  $\mu\text{g}/\text{mL}$ ) in starvation medium up to 96 h. During this time, cell migration was monitored by scratch area quantification.

**NP bioactivity: EGFR and ERK1/2 phosphorylation.** The activation of EGFR receptor in HaCaT (80% confluency, in 6-well plates) was induced by starving the cells for 24 h in DMEM supplemented with 1% (v/v) penicillin and adding soluble LL37, LL37-Au NPs and Au NPs for a given period of time. Following treatment, the plates were immersed in ice and the medium was discarded. Then the proteins were isolated from the cells. The levels of EGFR (phosphorylated EGFR and total EGFR) were determined by ELISA kit (R&D Systems). The activation of ERK signaling pathways in HaCaT (80% confluency, in one 96-well cell culture clear-bottom black microplate) were obtained starving the cells for 24 h in DMEM supplemented with 1% (v/v) penicillin and then stimulating them with soluble LL37 (5  $\mu\text{g}/\text{mL}$ ), LL37-Au NPs and Au NPs (200  $\mu\text{g}/\text{mL}$ ). After treatments the level of ERK were determined using a phosphoprotein and total protein ELISA kit (R&D Systems ref. KCB1018) according to the manufacture's instructions. Data were acquired with a BioTek synergy MX microplate reader.

**NP bioactivity: electrophysiological recordings.** Whole-cell patch-clamp recordings of HaCaT cells were performed using borosilicate glass patch pipettes with a resistance of 2-5 M $\Omega$  and compensating the series resistance by 50-60% with a List EPC-7 amplifier, as described previously [315]. The pipettes were filled with (in mM): 135 K-gluconate, 10 CsCl, 0.4  $\text{NaH}_2\text{PO}_4$ , 0.73  $\text{CaCl}_2$ , 1  $\text{MgCl}_2$ , 1 EGTA, and 14 HEPES (pH 7.4). The external solution contained (mM): 140 NaCl, 3 KCl, 2  $\text{CaCl}_2$ , 1  $\text{MgCl}_2$ , 15 HEPES and 10 glucose (pH 7.4). Cells were rapidly perfused as previously described [316] and all experiments were carried out at RT (22-25  $^\circ\text{C}$ ). The currents were recorded at -70 mV, filtered (2-pole Butterworth filter, -12 dB/octave) and digitized to a personal computer at a sampling rate of 1 kHz for analysis using pCLAMP software (AXON instruments). Charge transfer was calculated by the integration of the area under the current in the first 100 s ( $Q_{100}$ ) from the beginning of the exposure to Au NPs, LL37 or LL37-Au NPs in the absence or presence of apyrase (darker background; 20U/mL; Sigma).

**In vivo wound healing and tissue collection.** 6-7 week old RjHan:NMRI female mice (Janvier, BE) were anesthetized with isoflurane and the dorsal area was shaved using a depilatory cream a day before the surgery. Two 0.5-mm-thick silicone (Grace biolabs, UK) donut-shaped splints (OD=20 mm, ID= 10 mm) were fixed on either side of the dorsal midline, approximately 3.5 cm from the ears and positioned with 6-0 nylon sutures (Monosof, USA). Full-thickness excisional wounds were made

using an 8 mm round skin biopsy punch (Kai Europe GMBH, DE), centered within each splint. 10 mice were randomly assigned per group and were administered intradermally at several sites around the wound with only vehicle (0.9% w/v NaCl, Mini-Plasco, BE), 70  $\mu\text{g}$  of LL-37, 200  $\mu\text{g}$  of LL-37 Au NPs, and 200  $\mu\text{g}$  of Au NPs in autoclaved water by sterile insulin syringe (BD medical, France) as a dispersion in 30  $\mu\text{l}$  of vehicle. Two wounds were made on each mouse to increase sample size and to avoid cross-contamination both wounds were administered with the same treatment. Thus, n=10 animals (20 wounds) per group. Wounds were covered with transparent sterile adhesive bandage (IV3000, Smith & Nephew, UK) followed by adhesive fabric tape (BSN medical, France) to prevent the chewing of splints by mice. On days 0, 2, 5, 7, 10, 13 and 16 wounds were digitally photographed by Leica IC80 HD camera (Leica, Swiss). Optical zoom was maintained identical throughout the experiments. Wound areas were quantified using the Jmicro Vision software developed by N.Roduit at University of Geneva, Switzerland. Wound sizes are expressed as percentage of the initial respective wound. On day 5 and 10, three animals per group were sacrificed and wounds along with surrounding tissue were collected for further experiments and bisected into two halves. Remaining animals were sacrificed on day 16. The animal studies were approved by the animal care and ethical committee of health science sector, Université Catholique de Louvain.

**In vivo study: histology and immunohistochemistry.** The wound halves were immediately fixed with paraformaldehyde (4% in PBS, 0.01 M, pH 7.4) and after 24 h, the samples were transferred to PBS buffer at 4 °C. Wound tissue was embedded in paraffin blocks and sequentially sectioned at 5  $\mu\text{m}$  using a MICROM 17M325 microtome (Thermo Fisher Scientific, DE). Skin sections were stained with hematoxylin and eosin (H&E) to assess the predominant stages of healing and with Masson's Trichrome (MT) green staining to study the extent of collagen deposition in healed tissue during the course of wound healing. Images were taken with an AxioCam camera on an Axioplan microscope (Carl Zeiss GmbH, Oberkochen, DE). All histological analyses were performed on at least 3 wounds per group per time point and images presented are representative of all replicates. A semi-quantitative estimation of MT green staining was performed using FRIDA software (developed by Johns Hopkins University, USA) and the staining values were expressed as staining per unit area. The wound halves (n=3) were embedded in Tissue-Tek O.C.T. compound (Sakura Finetek, CA) and frozen. Sections were cut at 10  $\mu\text{m}$  thickness using a cryostat (Leica Microsystems, GE). An antibody directed against the murine endothelial cell surface marker (CD31) was used to determine the extent of endothe-

lial cell growth in the wound sections. After permeabilization (Triton X-100 0.1% (v/v) in PBS) and blocking (5% (w/v) BSA in PBS), the primary antibody (rat anti-CD31 (1:50, BD Biosciences, USA)) was applied for 1 h at 37 °C. Secondary antibody (Alexa Fluor 568 goat anti-rat (1:500, Invitrogen)) was used to visualize the antigen. Finally, sections were incubated with DAPI (Invitrogen) (50 ng/ml) for 5 min to visualize the cell nuclei. Images of entire sections were acquired by a MIRAX microscope (Zeiss, USA). Fluorescence of CD31 and red blood cells was quantified on whole sections using a script of FRIDA software (developed by Johns Hopkins University, USA). Results were expressed as percentage of red pixels over the total amount of pixels within the analyzed surface.

**In vivo study: collagen (sircol) assay.** The homogenate of wound tissue was used to measure the total acid-soluble collagen (types I-V) colorimetrically using a Sircol Collagen Assay kit (Newtown Abbey, UK) following the manufacturer's instructions. Briefly, wound tissue sample (n=3) of 10th day, was homogenized in lysis buffer (100 mM potassium phosphate, 0.1% Triton X-100, pH 7.8) and tissue debris was removed by centrifugation at 12000 x g for 10 min (Biofuge 15 R, Heraeus Sepatech, Chandler, Arizona, USA). Sircol dye reagent was added to tissue extracts, stirred for 30 min at room temperature and centrifuged at 12000 x g for 10 min. Absorbance of the bound dye was measured at 560 nm in a spectrophotometer (Spectramax M2e & program SoftMax Pro, Molecular Devices, LLC, USA). The amount of collagen protein in skin samples was adjusted to the amount of total protein using the BCA Protein Assay kit (Pierce, Rockford, IL, USA). Collagen concentrations were expressed as  $\mu\text{g}$  collagen per gram of total protein.

**In vivo study: MPO assay.** The tissue-associated myeloperoxidase (MPO) assay was performed to quantify the degree of inflammatory infiltration in the wounds [290]. Briefly, wound specimens from each group (n=3) on day 5 and day 10 were collected as described in section 2.5 and snap frozen in liquid N<sub>2</sub> at the time of sacrifice and stored for later assessment. For determination of MPO activity, tissue was placed in hexadecyltrimethylammonium bromide (HTAB) buffer (0.5% HTAB in 50 mM potassium phosphate buffer, pH 6) on ice and gently homogenized. The homogenate was centrifuged (Allegra X-15R, Beckman Coulter, CA) at 2000 x g for 10 min and subsequently ultracentrifuged (Biofuge 15 R, Heraeus Sepatech, Chandler, Arizona, USA) at 18.393 x g for 20 min at 4 °C. The supernatant (7  $\mu\text{L}$ ) was added to 96-well plates (Nunc, Roskilde, DK) together with 200  $\mu\text{l}$  of a 50 mM potassium phosphate buffer containing 0.167 mg/mL O-dianisidine (Sigma Aldrich, DE) and 500 ppm hydrogen peroxide (Merck, DE). Samples were analyzed in triplicate. MPO

activity in the supernatant was measured spectrophotometrically at 460 nm for 30 min. The results were expressed as MPO units per gram of tissue, and one unit of MPO activity was defined as the amount that degrades 1 mmol/min of hydrogen peroxide at 25 °C.

**In vivo study: RNA isolation and quantitative RT-PCR.** Total RNA was isolated from collected wounded tissues using TRIzol® reagent (Ambion, Invitrogen, USA). RNA samples were subjected to DNase I (Promega, USA) treatment to remove genomic DNA contamination in the presence of RNase inhibitor. The quality and quantity of RNA were evaluated by nanospectrophotometer (NanoDrop 2000, Thermo Scientific, DE). 1 µg RNA was reverse transcribed using first standard synthesis system (SuperScript™, Invitrogen, BE) and oligo (dT) primer (Eurogentec, BE) following the supplier protocol. The resulting cDNA was used as template for 30 cycles of semi-quantitative polymerase chain reaction (PCR) in a T100™ thermo cycler, Bio-Rad, BE. Primers of  $\beta$ -actin (internal control), IL6 and VEGF were used to amplify respective cDNA by PCR. PerlPrimer software was used to design the primers which are mentioned below. The PCR products were subjected to electrophoresis on Syber™ Safe (Invitrogen, BE) stained 1% agarose gel. All samples were analyzed in triplicates. The fluorescence of DNA was measured by ImageJ software and the semi-quantitative fluorescence values were expressed as relative mRNA expression. The sequence of the primers were (sequence 5' to 3'): TACAATGAGCTGCGTGTGGCCC (IL6, forward), AGGATGGCGTGAGGGAGAGCAT (IL6, reverse), TTCGGGAACCAGACCTCTCA (VEGF, forward), AATGGCGAATCCAGTCCCAC (VEGF, reverse), CCGGAGAGGAGACTTCACAG ( $\beta$ -actin, forward), TCCACGATTTCCCAGAGAAC ( $\beta$ -actin, reverse).

**Statistical analyses.** Statistical analyses were performed by a t-test or one-way ANOVA test with a Newman-Keuls test applied post hoc for paired comparisons of means (GraphPad Prism 5.0 software).

**Acknowledgements.** The authors would like to thank the financial support of European Commission (Marie Curie Initial Training Network NANODRUG, project n° 289454, FP7-PEOPLE 2011-2015 and ERC grant, project n° 307384, Nanotrigger). Michela Comune is an early stage researcher (ESR) of FP7 Marie Curie ITN NANODRUG network.



# Interaction of antimicrobial peptide-conjugated nanoparticles with endothelial cells.

## 4.1 Introduction

Ischemic diseases such as myocardial infarction, chronic wounds, stroke, cause a high morbidity with important social impact. Platforms to promote angiogenesis and thus new blood vessel formation in order to deliver oxygen and nutrients are thus required. One of the angiogenic therapies being tested to treat patients suffering from these diseases is based on the delivery of growth factors such as vascular endothelial growth factor (VEGF<sub>165</sub>), placenta growth factor (PlGF), fibroblast growth factor (FGF), among others [291]. Because of the fast plasma clearance and short half-life of these growth factors [292] several controlled release systems have been developed [293]- [298]. However, because of growth factor potency and, in some cases, limitations in the control release of the growth factor, pathological processes may occur [299], [300]. Furthermore, these approaches are relative expensive. Therefore, alternative approaches based in pro-angiogenic small molecules (e.g. peptides, chemicals) have been studied in the last few years [301], [302]. In some cases, the pro-angiogenic drugs have been immobilized in nanoparticles to increase their bioavailability [301] or to increase their targeting and bioactivity [250]. In other cases the bulk of the nanoparticle has been identified as the pro-angiogenic component [251], [303].

LL37 is an antimicrobial peptide (AMP) predominantly found in human skin and part of the innate immune defense system, with pro-angiogenic properties [204], [304].

Exogenous application of LL37 in a chorioallantoic membrane assay or in a rabbit model of hind-limb ischemia resulted in neovascularization [183]. In endothelial cells, the LL37 induced angiogenesis by the interaction with formyl peptide receptor-like 1 [183] and downstream by the activation of cyclooxygenase 1 and prostaglandin E<sub>2</sub> synthesis [304]. Yet, it is unknown whether immobilized LL37 has pro-angiogenic activity. Recently, we have shown that LL37-conjugated gold nanoparticles (LL37-Au NPs) have superior wound healing properties than LL37 peptide both in vitro (keratinocyte migratory properties) and in vivo (splinted mouse full thickness excisional model) [Chapter 3]. These superior properties were likely due to the capacity of LL37-Au NPs to prolong the phosphorylation of the epidermal growth factor receptor (EGFR) and ERK1/2 (from few minutes up to 1 h) in keratinocytes and thus to enhancing their migratory properties.

Here, we have evaluated the pro-angiogenic potential of LL37-Au NPs. We have selected Au NPs because it is relatively easy the immobilization of high concentrations of LL37 per surface area, the modification of their properties (including size, charge and morphology), and they have been used in the clinic for many years [70]. The production of our nanoparticulate formulation involved only a processing step (which included the mixing of the peptide with gold salts, at room temperature) for 1 day followed by a centrifugation step. The simplicity of the process makes possible the large-scale production of LL37-conjugated NPs at a relative low cost. The cytotoxicity properties of LL37-Au NPs and LL37 peptide against endothelial cells have been evaluated by cell viability, metabolism, stress oxidative and cell membrane assays. The internalization and intracellular trafficking of LL37-Au NPs have been evaluated in endothelial cells by mass spectrometry and immunofluorescence analyses. Activation of endothelial cells by LL37 peptide and LL37-Au NPs was monitored by the phosphorylation of receptors mediating the biological role of LL37 and by the intracellular levels of Ca<sup>2+</sup>. The pro-angiogenic properties of LL37 and LL37-Au NPs were further evaluating by their capacity to promote the formation of tube-like structures on an extracellular matrix and by induction of VEGF synthesis. Finally, we have evaluated in vivo the pro-angiogenic potential of LL37 and LL37-Au NPs in a chorioallantoic membrane assay.

## 4.2 Results and discussion

LL37-conjugated Au NPs were prepared in a one-step procedure using a procedure developed by us [313] (Fig. 4.1a). Briefly, a solution of  $HAuCl_4 \cdot 3H_2O$  (0.5

mM) was added to a solution of LL37 peptide (0.25 mM) in HEPES bufer (pH 5.0) and reacted for 4 h. The synthesized Au NPs were centrifuged, washed to remove unreacted peptides and HEPES, frozen and freeze-dried before use. The LL37-Au NPs have a surface plasmon resonance (SPR) band centered at 530 nm, a dominant spherical morphology with an average diameter of  $21 \pm 8$  nm ( $n \geq 100$ , by TEM analyses) (Fig. 4.1 b.1), a zeta potential of  $+15.4 \pm 2$  mV and 25% of organic mass in the NPs (as evaluated by TGA). Au NPs without LL37 were synthesized by a citrate buffer reduction procedure to obtain NPs with a SPR band centered at 530 nm, spherical shape with an average diameter of  $17.4 \pm 1.8$  nm ( $n \geq 100$ , by TEM analyses) (Fig. 4.1 b.2) and a zeta potential of  $-23.9 \pm 3.4$  mV.

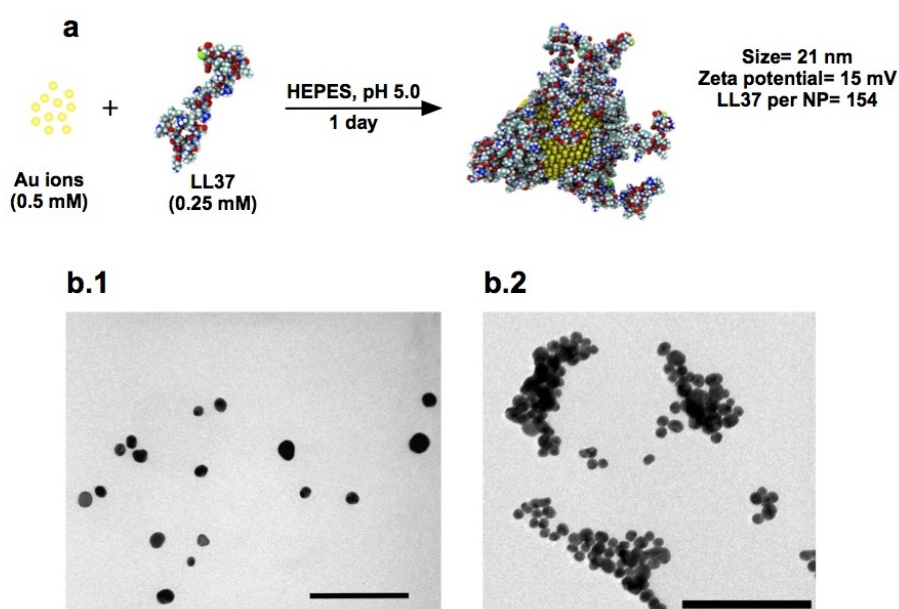


**Figure 4.1: Preparation and characterization of LL37-Au NPs.** (a) Schematic representation of Au NP synthesis in the presence of LL37 peptide. (b) Representative TEM images of LL37-Au NPs (b.1) and Au NPs (b.2). Bar corresponds to 200 nm.

#### 4.2.1 LL37-Au NPs are less cytotoxic to endothelial cells than LL37 peptide.

The physicochemical properties of NPs like size, shape and stability can be altered when resuspended in cell culture media and so influence their cytotoxicity and bioactivity. Therefore, we studied the zeta potential, size and stability of Au NPs and LL37-Au NPs in endothelial cell medium (EGM-2 containing 2% FBS) by dynamic light scattering (DLS). According to DLS studies, the LL37-Au NPs were positively

charged when resuspended in HEPES; however, they became negatively charged after resuspension in cell culture medium likely due to formation of biomolecule corona on the surface of NPs (Fig. 4.2a). In contrast, the Au NPs resuspended in HEPES or cell culture media were negatively charged. Au NPs were more susceptible to sedimentation in cell culture media than LL37-Au NPs (Fig. 4.2b). Low counts of Au NPs were already observed at time zero, which shows that a significant part of the NPs were already sedimented. LL37-Au NPs did not sediment but show some aggregation in cell culture media.

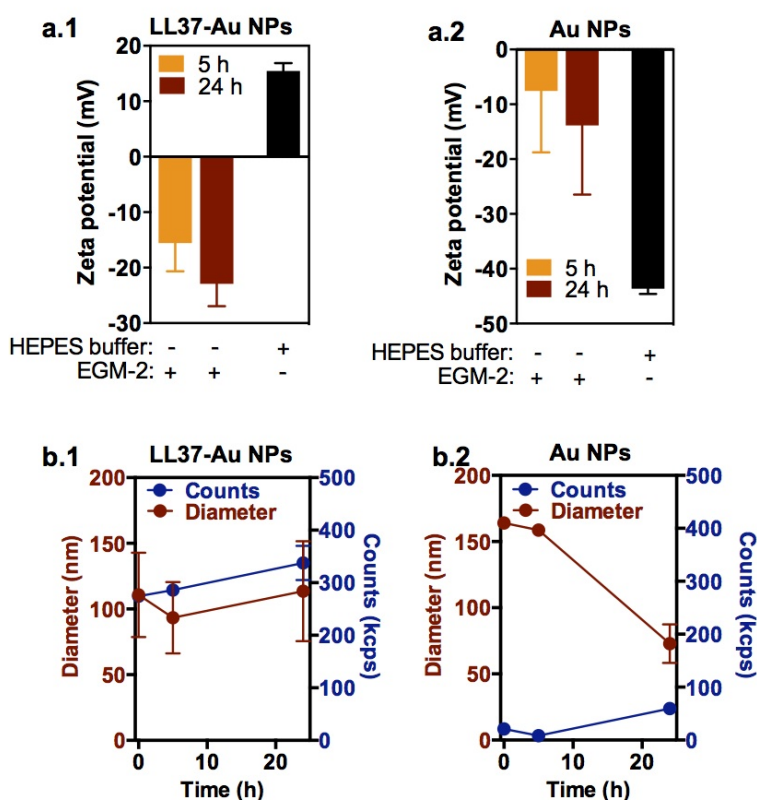


**Figure 4.2: Stability of LL37-Au NPs suspended in culture medium.** (a) Zeta potential of LL37-Au NPs (a.1) and Au NPs (a.2) suspended in HEPES or EGM-2 medium containing 2% (v/v) FBS (endothelial cell medium). (b) Diameter and counts (Kcps) of LL37-Au NPs (b.1) and Au NPs (b.2) in EGM-2 containing 2% (v/v) FBS. The average diameter of NPs (200  $\mu\text{g}/\text{mL}$ ) suspended in 2 mL of cell culture media was determined by a dynamic light scattering method (DLS) using a Zeta Plus analyzer (Brookhaven), from six independent measurements. In a and b, results are Average  $\pm$  SEM, n=3.

To assess the cytotoxic effect of LL37-Au NPs in endothelial cells, human vein endothelial cells (HUVECs) were incubated with increasing amounts of LL37-Au NPs

from 25 to 400  $\mu\text{g}/\text{mL}$  for 5 and 48 h. LL37 peptide and Au NPs were used as control. Cell viability was monitored by propidium iodide (PI) incorporation (Fig. 4.3a), cell metabolism by ATP production (Fig. 4.3b), and cellular oxidative stress by the production of reactive oxygen species (ROS) (Fig. 4.3c) using flow cytometry. HUVECs treated with LL37 or LL37-Au NPs up to a concentration of 10-30  $\mu\text{g}/\text{mL}$  and 400  $\mu\text{g}/\text{mL}$  (ca. 100  $\mu\text{g}/\text{mL}$  of LL37), respectively, have no significant decrease in cell viability or increase in ROS production. Yet, a decrease in cell viability and an increase in ROS production were observed for concentrations of LL37 equal or above 30  $\mu\text{g}/\text{mL}$ . Au NPs were also cytotoxic for concentrations of 400  $\mu\text{g}/\text{mL}$ .

We complemented the previous studies by measuring the impact of soluble LL37, Au NPs and LL37-Au NPs on cell membrane (Fig. 4.3d). For that purpose, we labeled cell membranes with 3,3'-dipentylloxacarbocyanine iodide ( $\text{DiOC}_5(3)$ ), a charged lipophilic dye that emits a fluorescent signal proportional to the membrane potential [305], and exposed the cells to soluble LL37, Au NPs or LL37-Au NPs. Cells upon hyperpolarization (i.e., cell interior becomes more electronegative with respect to the exterior) take up more dye and therefore have higher fluorescence. Conversely, cells that have undergone depolarization take up less dye (therefore have lower fluorescence). As controls, we used gramicidin (10  $\mu\text{M}$ ), a non-selective ionophore that causes cell depolarization, and valinomycin (10  $\mu\text{M}$ ), a  $\text{K}^+$  ionophore that causes cell hyperpolarization. Membrane potential of HUVECs is not altered for LL37-Au NPs or Au NPs up to concentrations of 400  $\mu\text{g}/\text{mL}$ . HUVECs become hyperpolarized after 5 h exposure to LL37 peptide in solution at concentrations below 30  $\mu\text{g}/\text{mL}$ , while depolarized for concentrations above 30  $\mu\text{g}/\text{mL}$ .

Overall, our results show that LL37-Au NPs are relatively non-cytotoxic to HUVECs for concentrations up to 400  $\mu\text{g}/\text{mL}$  (this means 100  $\mu\text{g}/\text{mL}$  of immobilized LL37). In contrast, LL37 peptide was cytotoxic for concentrations equal or above 30  $\mu\text{g}/\text{mL}$ . These results are in line with LL37 peptide expression in a disease setting. For example, LL37 expression has been detected at 30  $\mu\text{g}/\text{mL}$  and 5  $\mu\text{g}/\text{mL}$  in infants with pulmonary infections and in individuals with cystic fibrosis lung disease, respectively [306], [307]. In addition, LL37 has pro-survival or pro-apoptotic effects at certain concentrations depending on the cell type [308]. LL37 is a potent inhibitor of human neutrophil apoptosis through P2X7 receptors and G-protein-coupled receptors, and thus not involving formyl peptide receptor-like 1 downstream signaling. Yet, at the same concentration (25  $\mu\text{g}/\text{mL}$ ), LL37 induces caspase-mediated apoptosis of epithelial cells. The underlying mechanisms that result in divergent consequences of LL37 in different cell types remain unclear. However, it is known

that at low concentrations LL37 peptide exhibits a non-pore formation carpet mode on zwitterionic vesicles while at high concentrations penetrate the membrane [309]. Our results show that the cytotoxicity of LL37 at 30  $\mu\text{g}/\text{mL}$  in endothelial cells was mediated by an increase in membrane depolarization and ROS levels. Similar behavior was not observed for equivalent concentrations of LL37 peptide once immobilized on top of the nanoparticles. This suggests that LL37-conjugated nanoparticles have minimal impact in cell membrane and is not able to penetrate the membrane; however further research is necessary to clarify this issue.

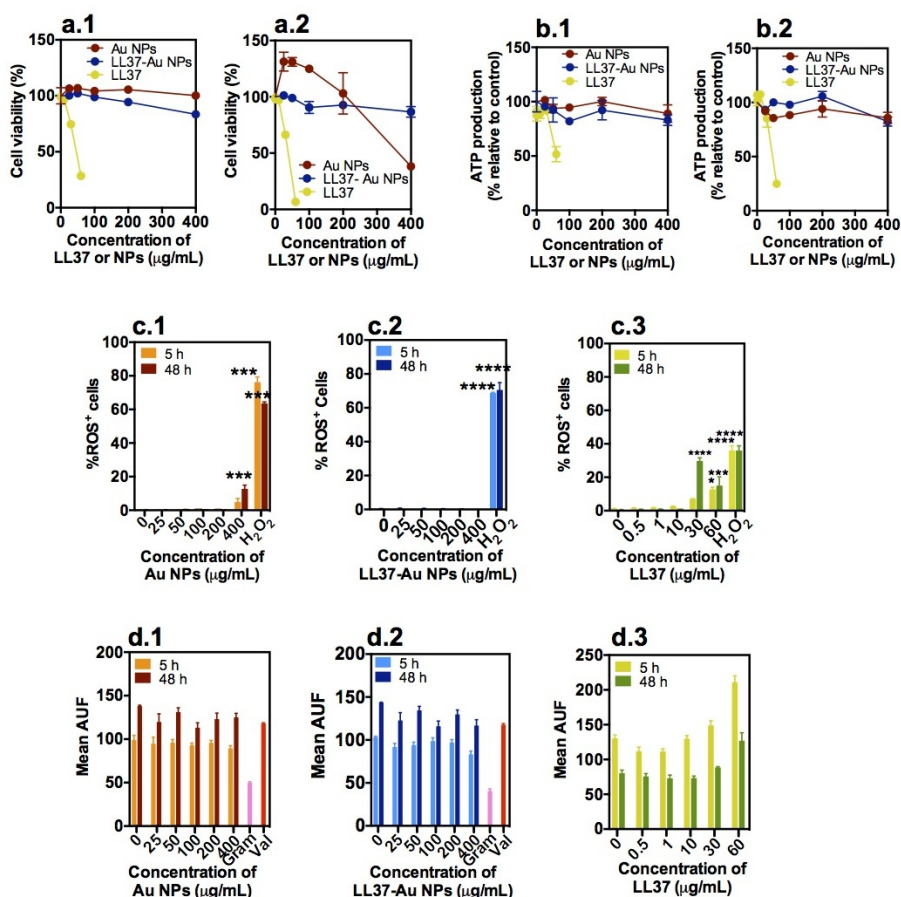


**Figure 4.3: Cytotoxicity of LL37 and LL37-Au NPs.** (a, b) HUVECs were exposed for 5 (a.1 and b.1) or 48 h (a.2 and b.2) to different concentrations of soluble LL37, Au NPs and LL37-Au NPs, followed by the quantification of viability (PI staining followed by flow cytometry evaluation) (a) or ATP by an ATP kit (b). Results are average  $\pm$  SEM,  $n=3$ . (c) Percentage of HUVECs expressing ROS. Non-treated cells and hydrogen peroxide-treated cells were used as negative and positive controls, respectively. Results are average  $\pm$  SEM,  $n=3$ . \* $P < 0.05$ , \*\* $P < 0.01$ , \*\*\* $P < 0.001$  and \*\*\*\* $P < 0.0001$  indicates statistical significance between sample and non-treated cells. (d) Measurement of the membrane potential. Results are average  $\pm$  SEM,  $n=3$ . Gramicidin ( $10 \mu\text{M}$ ), a non-selective ionophore that causes cell depolarization, was used as positive control. Valinomycin ( $10 \mu\text{M}$ ), a  $\text{K}^+$  ionophore that causes cell hyperpolarization, was used as negative control.

#### 4.2.2 Uptake and intracellular accumulation of LL37-Au NPs.

Internalization of LL37-Au NPs and Au NPs by HUVECs at 5 and 48 h post-exposure was monitored using inductively coupled plasma mass spectrometry (ICP-MS). The internalization of the Au NPs occurred essentially during the first 5 h since

similar levels of Au NPs were quantified at time 48 h (Figs. 4.4 a1, 4.4 a2). In contrast, the internalization of LL37-Au NPs increased significantly from 5 h to 48 h. At 48 h, no significant differences in NPs internalization were observed in HUVECs exposed to Au NPs or LL37-Au NPs.

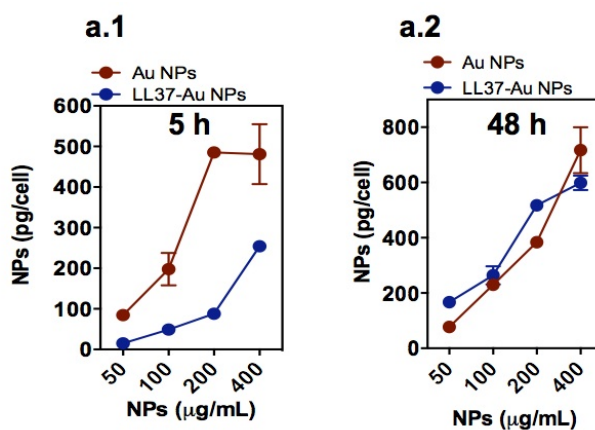


**Figure 4.4: Internalization of LL37-Au NPs.** (a) ICP-MS study of internalization of Au NPs and LL37-Au NPs by HUVECs at 5 h (a.1) and 48 h (a.2). The results are presented in mass of NPs and not mass of gold. Results are Average  $\pm$  SEM (n=3).

Next, we examined the intracellular trafficking of LL37-Au NPs and LL37 by confocal microscopy. For this purpose, cells were exposed for 30 min, 4 h and 24 h to rhodamine-labeled LL37-Au NPs (100  $\mu\text{g}/\text{mL}$ ) and rhodamine-labeled LL37 (1  $\mu\text{g}/\text{mL}$ ). Early and late endosomes were stained with Rab7 and EEA1 and cell membrane stained with CD31. Images of cells reconstructed from z-stacks of confocal images indicated cellular uptake of NPs (Fig. 4.5) and LL37 (Fig. 4.6). Co-localization of LL37-Au NPs with EEA1- or Rab7-positive compartments increased during 24 h (maximum time evaluated) while co-localization of the NPs with CD31-positive regions peaked at 30 min (Fig. 4.5b). In contrast, co-localization of LL37 peptide with EEA1-, Rab7- or CD31-positive regions peaked upon to 4 h (Fig. 4.6b).

Overall, our results show that endothelial cells internalize higher concentrations of Au NPs than LL37-Au NPs at time 5 h but similar concentrations were found at time 48 h. The faster internalization of Au NPs by endothelial cells might be due to the higher propensity of Au NPs to sediment in cell culture media as compared with LL37-Au NPs. Our intracellular trafficking results in HUVECs suggest that up to 30-35% of LL37-Au NPs and LL37 accumulate in the EEA1 and Rab7-positive endolysosomal compartments upon 24 h. No significant differences exist in the intracellular accumulation of LL37 and LL37-Au NPs at least in the EEA1 and



Rab7-positive compartments; however, the kinetics of the process seems different in both cases. It is important to note that the intracellular accumulation of LL37 in the endolysosomal compartment has been described previously in other cells such as macrophages [267].

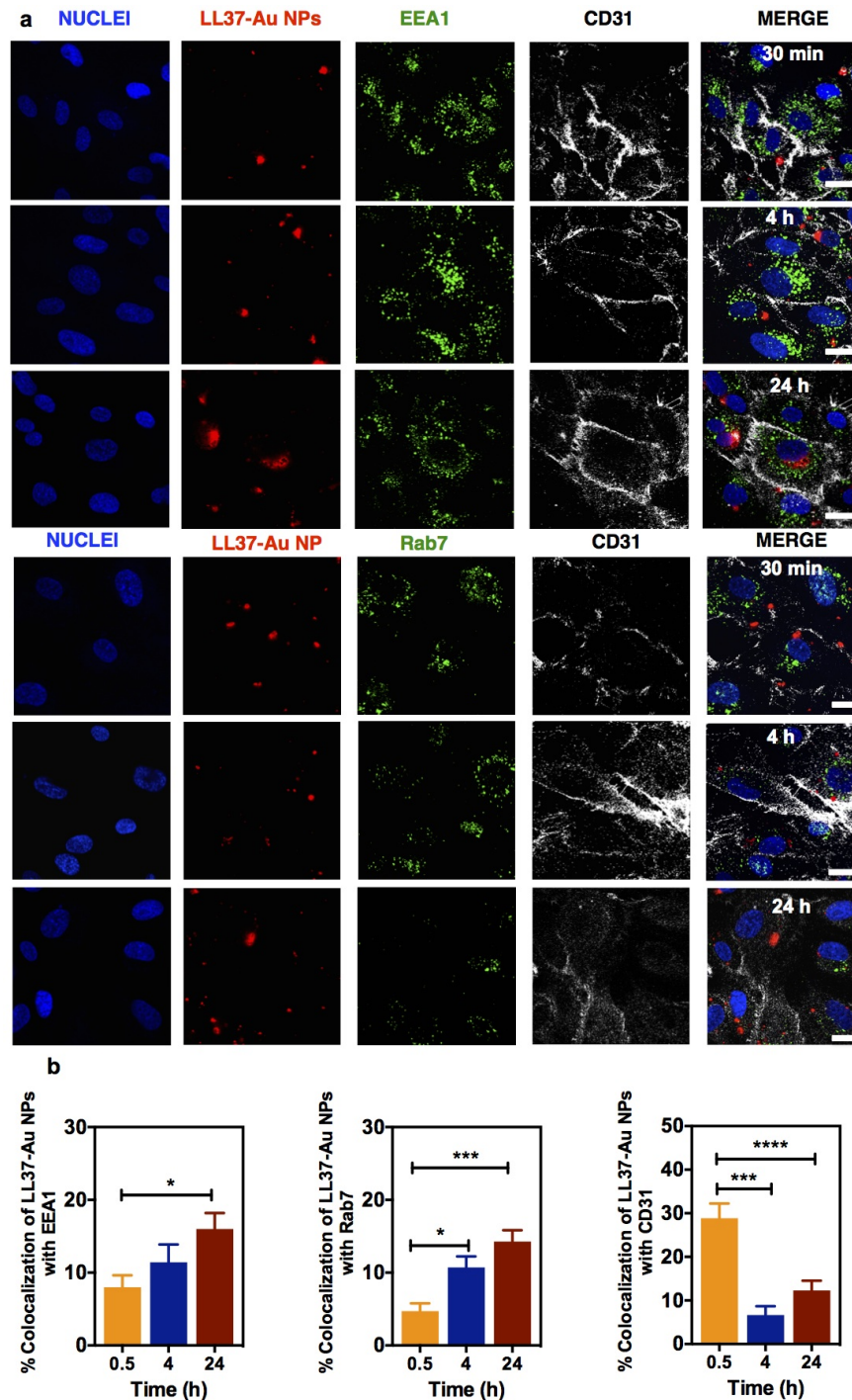


**Figure 4.5: Intracellular trafficking of LL37-Au NPs.** HUVECs were exposed for 30 min, 4 h and 24 h to fluorescently-labeled LL37-Au NPs (100  $\mu\text{g}/\text{mL}$ ). At the end of each time, cells were washed with PBS and stained for endolysosomal compartment markers as early endosome EEA1 and late endosome/lysosome marker protein Rab7 (cell membrane was stained for CD31). (b) Quantification of the co-location of LL37-Au NPs with EEA1, Rab7 or CD31. Results are average  $\pm$  SEM, from 6 different confocal images (40x objective). \* $P < 0.05$ , \*\* $P < 0.01$ , \*\*\* $P < 0.001$  and \*\*\*\* $P < 0.0001$  indicate statistical significance between groups. Bars correspond to 15  $\mu\text{m}$ .

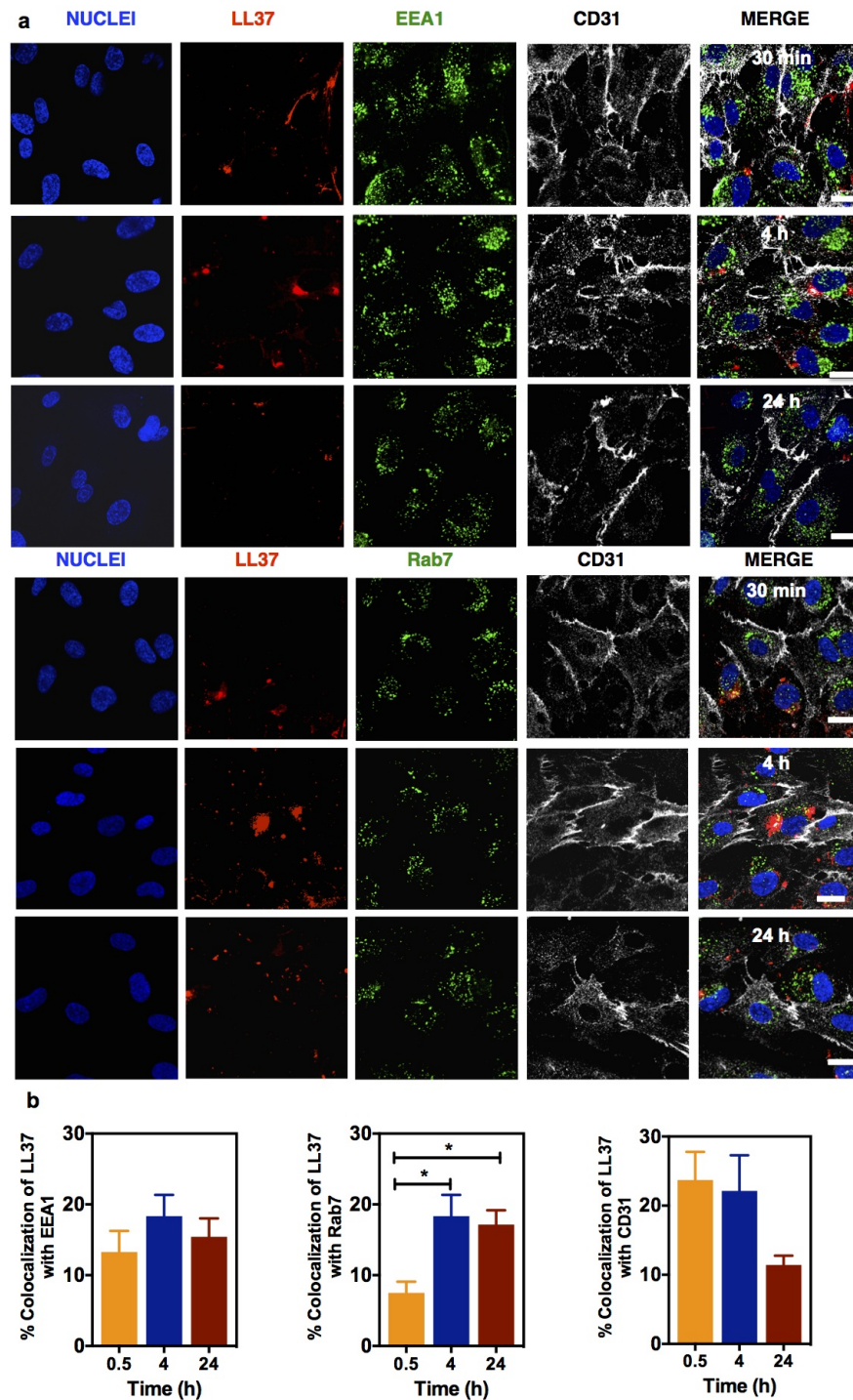


**Figure 4.6: Intracellular trafficking of soluble LL37.** HUVECs were exposed for 30 min, 4 h and 24 h to fluorescently-labeled LL37 (1  $\mu\text{g}/\text{mL}$ ). At the end of each time, HUVECs were washed with PBS and stained for endolysosomal compartment markers as early endosome EEA1 and late endosome/lysosome marker protein Rab7 (cell membrane was stained for CD31). (b) Quantification of the co-location of LL37-Au NPs with EEA1, Rab7 or CD31. Results are average  $\pm$  SEM, from 6 different confocal images (40x objective). \* $P < 0.05$  indicates statistical significance between groups. Bars correspond to 15  $\mu\text{m}$ .

### 4.2.3 LL37 peptides but not LL37-Au NPs trigger an increase in intracellular levels of $\text{Ca}^{2+}$ in HUVECs.

Two main receptors have been described to mediate the biological role of LL37 in many cells: FPRL1 and P2X7 receptors that mediate the transactivation of epidermal growth factor receptor (EGFR) [225], [229], [183]. HUVECs express both receptors although the expression is higher for FPRL1 than EGFR (Figs. 4.7a, 4.7b).

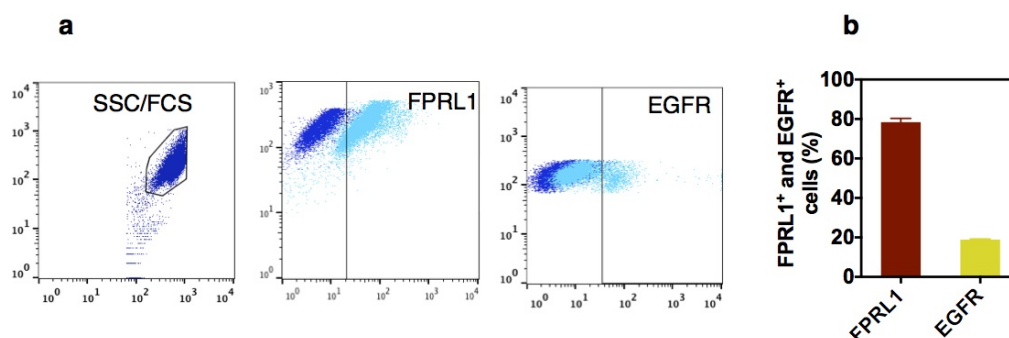


**Figure 4.7: Expression of EGFR and FPRL1 in HUVECs.** (a) Flow cytometry plots for the expression of FPRL1 and EGFR. Positive cells (light blue) were calculated based in the isotype control (dark blue). (b) Quantification of receptor expression. Results are average  $\pm$  SEM,  $n=3$ .

FPRL1 has been described as the natural receptor for LL37 in endothelial cells [183], leading to an increase in intracellular calcium and the activation of cytosolic phospholipase A2, PI3K, and PLC [310]. To assess the bioactivity of LL37 and LL37-Au NPs we evaluated its ability to induce an increase in intracellular free  $\text{Ca}^{2+}$  in endothelial cells (Figs. 4.8a, 4.8b). HUVECs were cultured in serum-free medium for 7 h, loaded with a fluorescent dye to monitor the free intracellular  $\text{Ca}^{2+}$  concentration and then activated with LL37, LL37-Au NPs or VEGF<sub>165</sub> as positive control. As expected, LL37 added to the cell culture medium at final concentration of 50 or 100  $\mu\text{g}/\text{mL}$  lead to an increase of intracellular  $\text{Ca}^{2+}$  (Fig. 4.8 a.1). Curiously, the FPRL1 antagonist WRW4 [311] inhibited partial but not fully the intracellular levels of  $\text{Ca}^{2+}$ , which indicates that other signaling pathways are responsible for the intracellular accumulation of  $\text{Ca}^{2+}$ . In addition, LL37-Au NPs had no inductive effect in the intracellular accumulation of  $\text{Ca}^{2+}$  up to 600  $\mu\text{g}/\text{mL}$  (Fig. 4.8 a.2 and data not shown).

Next, we evaluated whether LL37 or LL37-Au NPs could activate epidermal growth factor receptor (EGFR). Previous studies have shown that LL37 leads to the transactivation of EGFR [225] (Fig. 4.8b). This process involves the activation of

metalloproteinases (likely ADAM10 and/or ADAM17) that releases EGF anchored to cell membrane into a heparin-binding EGF (HB-EGF), which in turn binds to EGFR [271]. This leads to the phosphorylation of ERK1/2 [272] and STAT3, translocation of STAT3 into the nucleus and finally the initiation of the transcription of target genes. So far little is known about how this cascade is initiated [227]. We have evaluated the phosphorylation of EGFR in HUVECs mediated by LL37 peptide and LL37-Au NPs. In contrast to LL37 peptide, LL37-Au NPs did activate the phosphorylation of EGFR, thus showing that soluble and immobilized LL37 activate different signaling pathways.

All together, our results are in line with previous data showing that soluble LL37 peptide activates FPRL1 receptor in endothelial cells [183]. However, other signaling pathways may contribute for the accumulation of  $\text{Ca}^{2+}$  since WRW4 peptide, an antagonist of FPRL1, only partially inhibits the intracellular levels of  $\text{Ca}^{2+}$ . According to our results the transactivation of EGFR does not occur in endothelial cells cultured in the presence of LL37; however, it is known that LL37 may exert its biological role through other molecules/receptors such as GAPDH [274] or insulin-like growth factor 1 receptor [312]. This issue should be further investigated in the near future. In contrast, LL37-Au NPs have not the capacity to induce the intracellular concentration of  $\text{Ca}^{2+}$  in endothelial cells; however, the NPs have the capacity to induce the phosphorylation of EGFR. It is tempting to speculate that the absence of  $\text{Ca}^{2+}$  intracellular accumulation by endothelial cells exposed to LL37-Au NPs is due to the inability of the immobilized LL37 to interact with FPRL1. In line with our recent data obtained in keratinocytes (chapter 2), LL37-Au NPs are able to transactivate EGFR. The mechanism is not yet known for endothelial cells but, as it was observed in keratinocytes, it may involve the activation of P2X receptors with the consequent activation of metalloproteases that shed HB-EGF.



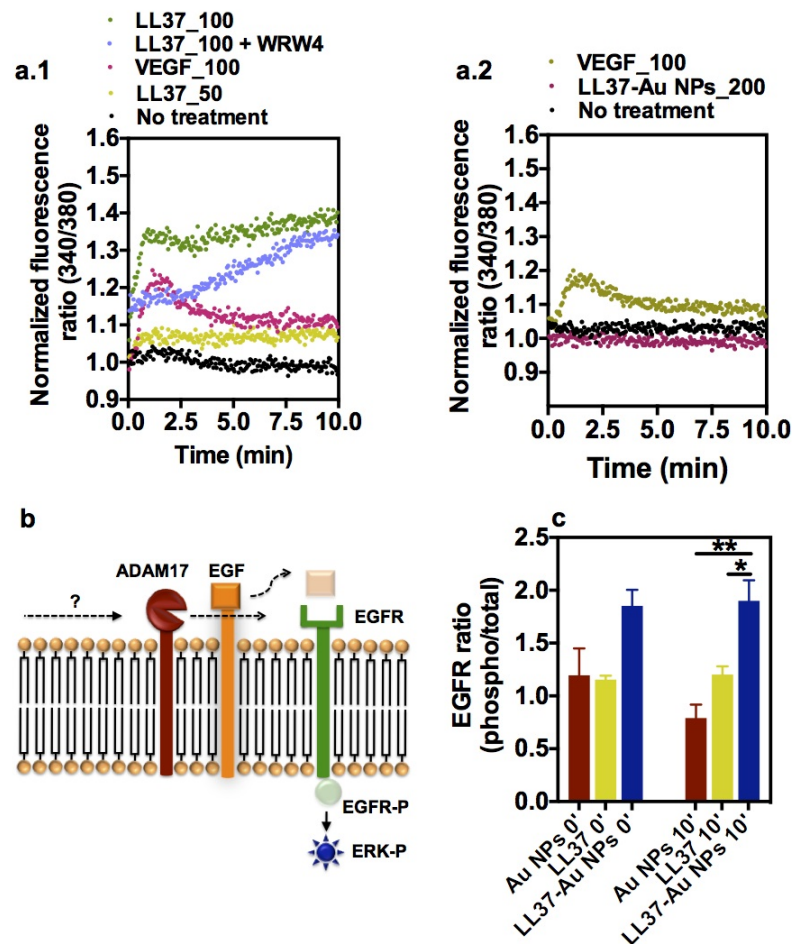


**Figure 4.8: Bioactivity of LL37 and LL37-Au NPs: molecular studies.** (a) Capacity of LL37 and LL37-Au NPs to induce intracellular  $\text{Ca}^{2+}$  accumulation in HUVECs. HUVECs were starved for 7 h, loaded with Fura-2 dye for 1 h, and exposed to LL37 (LL37\_50 means LL37 at 50  $\mu\text{g}/\text{mL}$ ; LL37\_100 means LL37 at 100  $\mu\text{g}/\text{mL}$ ) or LL37-Au NPs (LL37\_200 means LL37 at 200  $\mu\text{g}/\text{mL}$ ). VEGF<sub>165</sub> (VEGF\_100 means VEGF<sub>165</sub> at 100 ng/mL) was used as a positive control. (b) Schematic representation of the transactivation mechanism of EGFR. This process involves the activation of metalloproteinases (likely ADAM10 and/or ADAM17) that releases EGF anchored to cell membrane into a heparin-binding EGF (HB-EGF), which in turn binds to EGFR. This leads to the phosphorylation of ERK1/2 and STAT3, translocation of STAT3 into the nucleus and finally the initiation of the transcription of target genes. (c) Phosphorylation profile (phospho/total protein) of EGFR in HUVECs after contact with LL37 (5  $\mu\text{g}/\text{mL}$ ), LL37-Au NPs (200  $\mu\text{g}/\text{mL}$ ) or Au NPs (200  $\mu\text{g}/\text{mL}$ ) up to 10 min. Results are mean  $\pm$  SEM (n=3). \* $P < 0.05$ , \*\* $P < 0.01$  indicates statistical significance between samples.

#### 4.2.4 Both LL37 peptide and LL37-Au NPs induce angiogenesis in a CAM assay.

The pro-angiogenic properties of LL37, LL37-Au NPs and Au NPs were evaluated in a *in vitro* Matrigel assay (Fig. 4.9a). In this assay, the number of cord-like structures was quantified by microscopy after 4 h of seeding HUVECs in the presence of LL37, LL37-Au NPs or Au NPs on top of Matrigel. LL37 and LL37-Au NPs treatment induced endothelial cord formation by HUVECs, similar as VEGF, a pro-angiogenic factor (Fig. 4.9b). In contrast, HUVECs treated with Au NPs formed similar number of cord-like structures as non-treated cells. Next, we evaluated the inhibitory effect of FPRL1 antagonist WRW4 on the pro-angiogenic activity of LL37 and LL37-Au NPs in the *in vitro* Matrigel assay. As shown in Fig. 4.9b, WRW4 significantly impairs the LL37-induced tube formation, but has low effect in the LL37-Au NP-induced tube formation.

We further assessed the pro-angiogenic activity of LL37, Au NPs and LL37-Au NPs in a chorioallantoic membrane (CAM) assay for 3 days (Figs. 4.10a, 4.10b). Both LL37 and LL37-Au NPs induced vessel growth. In both cases, the mesenchymal region of CAM was dilated and a higher number of blood vessels and inflammatory precursor cells were observed than in control (CAM treated with vehicle). This reaction was similar to the one observed for basic fibroblast growth factor (bFGF) (data not shown), a pro-angiogenic factor. Interestingly, Au NPs without LL37 are also able to induce a pro-angiogenic and inflammatory response. A quantitative analysis revealed that LL37, Au NPs and LL37-Au NPs induced an increase in erythrocyte-filled blood vessels (Fig. 4.10c).

To investigate whether LL37 peptide or LL37-Au NPs might influence angiogenesis by induction of VEGF synthesis, we determined VEGF levels in HUVEC supernatants by ELISA after cell contact for 24 h with LL37, Au NPs or LL37-Au NPs (Fig. 4.10d). LL37 induced higher secretion of VEGF<sub>165</sub> in HUVECs as compared to non-treated cells, but this superior secretion is abolished after FPRL1 inhibition. In contrast, cells treated with LL37-Au NPs or Au NPs had lower secretion of VEGF<sub>165</sub> than non-treated cells. Cells treated with Au NPs had the lowest secretion of VEGF<sub>165</sub>.

All together, our results suggest that the pro-angiogenic properties of LL37 peptide and LL37-Au NPs are mediated by different mechanisms. LL37 activates primarily FPRL1 receptor that leads to an increase of intracellular levels of Ca<sup>2+</sup> and the secretion of VEGF<sub>165</sub>, followed by an increase in the formation of cord-like structures. In contrast, LL37-Au NPs activate the transactivation of EGFR but has no ef-

fect on FPRL1 receptor and consequent increase of intracellular levels of  $\text{Ca}^{2+}$  and secretion of  $\text{VEGF}_{165}$ .

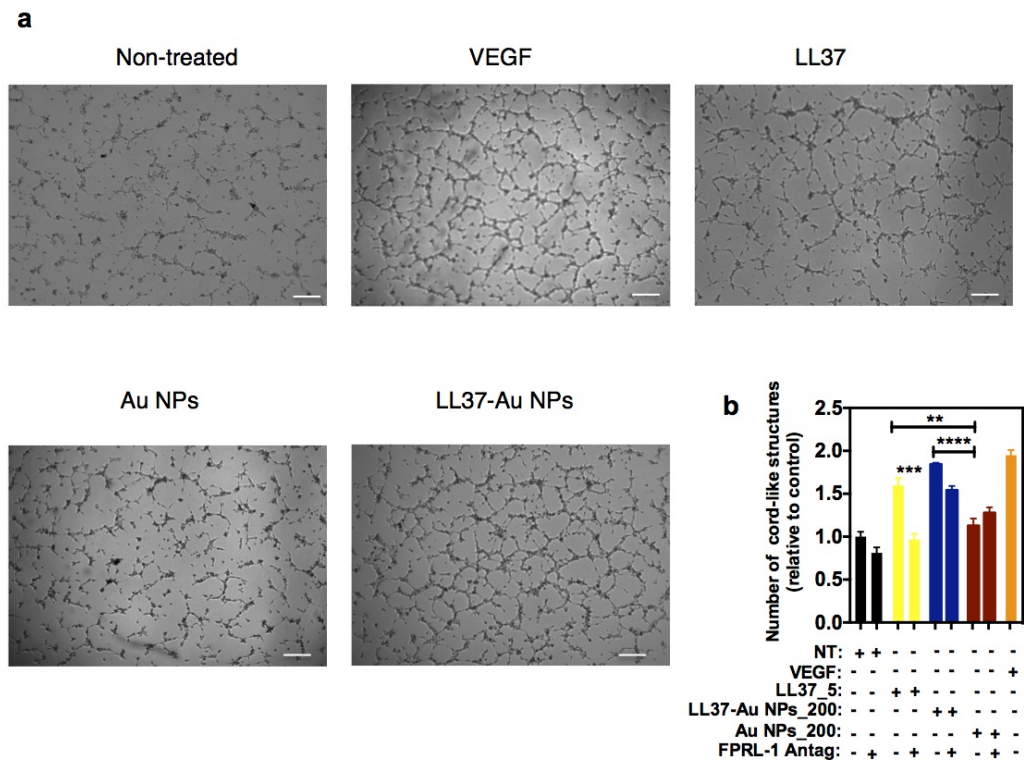


**Figure 4.9: Formation of cord-like structures on Matrigel by HUVECs treated with LL37 or LL37-Au NPs.** Cells were exposed to LL37-Au NPs (200  $\mu\text{g}/\text{mL}$  which corresponds to 50  $\mu\text{g}/\text{mL}$  of immobilized LL37), Au NPs (200  $\mu\text{g}/\text{mL}$ ), LL37 (5  $\mu\text{g}/\text{mL}$ ) or VEGF (50  $\text{ng}/\text{mL}$ ) with and without FPRL1 Antagonist WRW4 (10  $\mu\text{M}$ ). After 4 hours images were taken by a In Cell Microscope 2000 (GE Healthcare) (Objective 2x) (a) and then ImageJ was used to calculate the number of cord-enclosed regions for each conditions relative to control (b). Bars correspond to 50  $\mu\text{m}$ . Results are mean  $\pm$  SEM (n=3-6). \*\*  $P < 0.01$ , \*\*\*  $P < 0.001$ , \*\*\*\*  $P < 0.0001$  indicates statistical significance between groups.



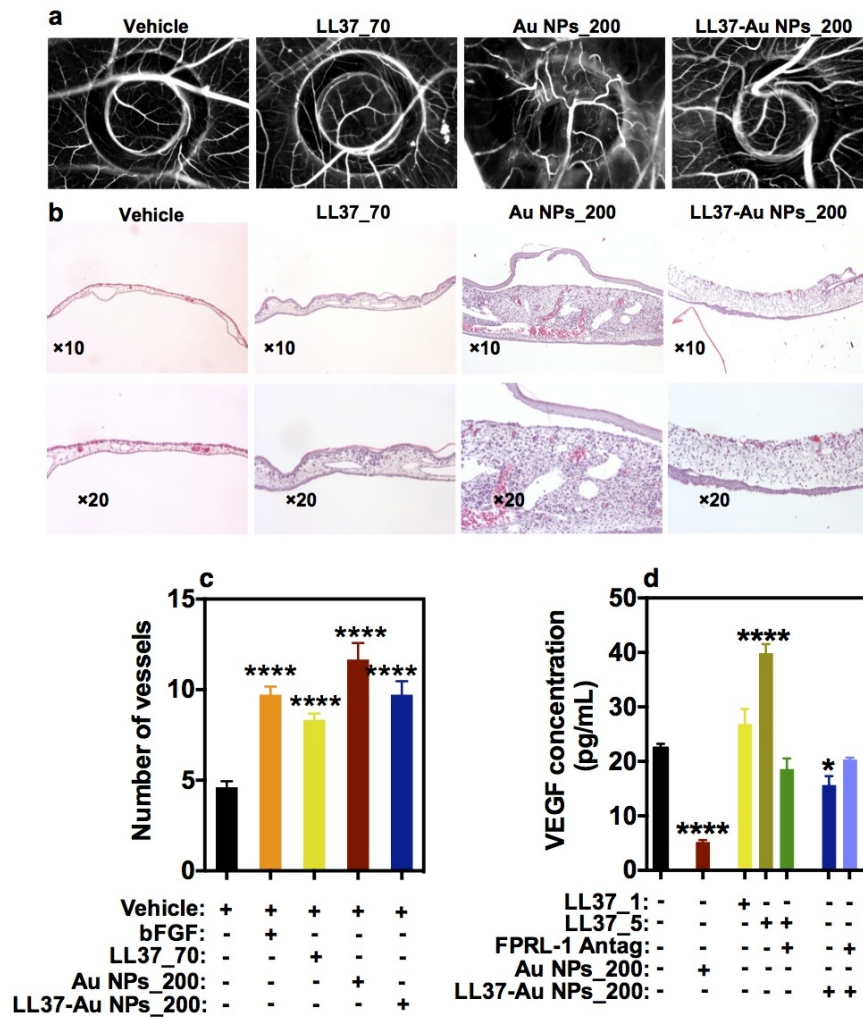


**Figure 4.10: Pro-angiogenic activity of LL37 and LL37-Au NPs.** Pro-angiogenic activity of LL37 (70  $\mu\text{g}$  per egg), Au NPs (200  $\mu\text{g}$  per egg), bFGF (400 ng per egg), vehicle (water) and LL37-Au NPs (200  $\mu\text{g}$  per egg which corresponds to 50  $\mu\text{g}/\text{mL}$  of immobilized LL37) in a chorioallantoic membrane (CAM) assay during 3 days. (a) Light microscopy images showing the region that received the treatment (the ring has 3 mm of diameter). (b) Hematoxylin eosin staining of CAMs. (c) Quantification of number of vessels with less than 20  $\mu\text{m}$  that are recruited for the region that received the treatment (within the ring). Results are mean  $\pm$  SEM (n=11-13). \*\*\*\* $P$  < 0.0001 indicates statistical significance between samples and vehicle. (d) Secretion of (VEGF<sub>165</sub>) in HUVECs exposed to LL37 or LL37-Au NPs or Au NPs as assessed by ELISA. Results are mean  $\pm$  SEM (n=5). \* $P$  < 0.05 and \*\*\*\* $P$  < 0.0001 indicate statistical significance between samples and non-treated.

## 4.3 Conclusions

Although the angiogenic properties of soluble LL37 peptide have been previously demonstrated, it is unknown the bioactivity of permanently immobilized LL37. Here we report a new formulation based on LL37 conjugated to Au NPs that have a Au core and a hydrophilic cationic LL37 peptide shell, made in a quick one-step synthetic process. These NPs incorporate approximately 250  $\mu\text{g}$  of LL37 per mg of NP, they have an average diameter of 21 nm and a positive zeta potential (15 mV). Our results show that LL37-Au NPs are relatively non-cytotoxic to HUVECs for concentrations up to 400  $\mu\text{g}/\text{mL}$  (i.e., 100  $\mu\text{g}/\text{mL}$  of immobilized LL37). In contrast, LL37 peptide was cytotoxic for concentrations equal or above 30  $\mu\text{g}/\text{mL}$ . Our results further show that LL37-Au NPs are rapidly internalized and both LL37 and NPs stay confined within the cellular endolysosomal compartment up to 24 h. When these NPs are exposed to endothelial cells, they activate the transactivation of EGFR but had no capacity to activate FPRL1 and downstream signals such as the accumulation of intracellular  $\text{Ca}^{2+}$ . In contrast, LL37 activates primarily FPRL1 receptor that leads to an increase of intracellular levels of  $\text{Ca}^{2+}$  and the secretion of  $\text{VEGF}_{165}$ . Importantly, both LL37 and LL37-Au NPs have pro-angiogenic properties as demonstrated in a Matrigel and CAM assays. This work highlights some important points: (i) LL37-Au NPs have lower cytotoxicity than LL37, (ii) LL37 maintains the ability to form cord-like structures and pro-angiogenic activity after the immobilization on the NPs even if they cannot induce intracellular  $\text{Ca}^{2+}$  accumulation and  $\text{VEGF}_{165}$  secretion as soluble LL37, (iii) this divergence suggests that pro-angiogenic activity of LL37-Au NPs are regulated by a different receptor and signaling than soluble LL37. Future studies are required to further characterize the mechanism of action of LL37-Au NPs in endothelial cells and hence their potential for therapeutic angiogenesis.

## 4.4 Methods

**Materials.**  $\text{HAuCl}_4 \cdot 3\text{H}_2\text{O}$ ,  $\text{Na}_3\text{C}_6\text{H}_5\text{O}_7$  and HEPES, all acquired to Sigma-Aldrich, were used as received. Lyophilized LL37 peptide modified with a C-terminal cysteine (LLGDFFRKSKEKIGKEFK-RIVQRIKDFLRNLVPRTESSC-NH<sub>2</sub>) was purchased from Caslo Laboratory, Denmark. The peptide was synthesized by conventional solid-phase synthesis, purified by high performance liquid chromatography, and characterized by matrix assisted laser desorption ionization time-of-flight (MALDI-

TOF) mass spectroscopy. The purity of the peptide was 96%. Rhodamine B isothiocyanate and HEPES were purchased from Sigma.

**NP preparation.** LL37 (0.5 mM, 1 mg/mL) were dissolved initially in DMF (100  $\mu$ L) followed by addition of HEPES (950  $\mu$ L, 100 mM, pH 5).  $HAuCl_4 \cdot 3H_2O$  ( $10^{-2}$  M, 50  $\mu$ L) was added to a peptide solution (0.25 mM, 950  $\mu$ L; therefore the final concentration of  $HAuCl_4$  was 0.5 mM) and the NP synthesis was carried out at 25 °C. LL37-Au NPs were also synthesized using  $HAuCl_4 \cdot 3H_2O$  (final concentration 0.25 mM, 0.5 mM and 1 mM), and HEPES (100 mM, pH 6 and pH 7.5) by the same procedure at 25 °C. The synthesized Au NPs were centrifuged at 14.000 rpm for 20 min at 4 °C followed by washing with Milli-Q water to remove unreacted peptides and HEPES, frozen and freeze-dried at 223 K using a Snijders Scientific freeze-dryer. Spherical Au NPs were also synthesized via citrate reduction method [83]. An aqueous  $HAuCl_4$  solution (0.5 mM, 100 mL of water) was boiled in a 250 mL round bottom flask while being stirred after which an aqueous sodium citrate solution (2%, w/v, in water) was added. The reaction was allowed to run until the solution reached a wine red color, indicating the reaction was completed. Fluorescent Au NPs and LL37-Au NPs were prepared by addition of DMSO (0.5 mM) solution of Rhodamine to achieve a final concentration of 25  $\mu$ M for flow cytometry and confocal microscopy studies. Free Rhodamine molecules in the colloidal gold solution were removed by centrifugation at 12000 rpm for 15 min at 4 °C followed by two washings with Milli-Q water. The pellet obtained after centrifugation was redispersed in Milli-Q water and then dialysed.

**NP characterization: general analyses.** The reduction of  $HAuCl_4 \cdot 3H_2O$  was monitored by UV-visible spectroscopy using a BioTek synergy MX microplate reader. TEM images were obtained using a Jeol JEM-1011 microscope operating at an accelerating voltage of 100 kV. A drop of NPs solution was placed on a 300 mesh copper grid with a carbon-coated Formvar membrane and dried overnight before examination by TEM. A minimum of 100 NPs was measured using Image J software for the particle size analysis. FTIR spectroscopy analyses were performed in ATR mode using a JASCO spectrophotometer at 4  $cm^{-1}$  resolutions with 64 scans. The hydrodynamic diameter and Zeta potential of Au NPs and LL37-Au NPs suspended in water and in cell culture medium (EGM-2) were measured via a Zeta PALS Zeta Potential Analyzer (Brookhaven Instruments Corporation). The amount of gold in Au NPs and LL37-Au NPs was quantified by ICP-MS, using a 7700x ICP-MS (Agilent Technologies). The content of LL37 in LL37-Au NPs was estimated by High Resolution Thermogravimetric analyses (Hi-Res-TGA), using a TA Instruments Q500 ther-

mogravimetric analyzer (thermobalance sensitivity: 0.1  $\mu\text{g}$ ). The temperature calibration was performed by measuring the Curie point of a nickel standard and using open platinum crucibles and a dry nitrogen purge flow of 100 mL  $\text{min}^{-1}$ . This procedure was performed at the heating rate and temperature range used throughout the experimental work, i.e. 2  $^{\circ}\text{C min}^{-1}$  over the 30-600  $^{\circ}\text{C}$  temperature interval.

**Cell Culture.** Human umbilical vein endothelial cells (HUVECs, Lonza, Walkersville, Maryland, USA) were cultured in endothelial growth medium (EGM-2, Lonza). Cells after 6 passages were used in all experiments. The cells were sub-cultured at a ratio of 1:3 until achieving the number of cells required for the experiment.

**Cytotoxicity studies.** HUVECs were seeded at a density of  $1 \times 10^4$  cells per well and cultured in a 96-well plate for 24 h and then incubated with LL37, LL37-Au NPs or Au NPs suspended in culture medium at different concentrations. After 5 and 48 h, CellTiter-Glo Luminescent Cell Viability Assay (Promega) was used to assess the ATP production of the cells according to the supplier's instructions. For ROS quantification, cells were seeded at a density of  $4 \times 10^4$  cells/ $\text{cm}^2$  in 24-well plates and cultured for 24 h. Either LL37-Au NPs or Au NPs suspended in culture medium at different concentrations were added to cells and left for 5 h and 48 h. Before the treatment ended, cells were exposed to 6-carboxy-2',7'-dichlorodihydrofluorescein diacetate (DCFH-DA, 100  $\mu\text{M}$ ), a dye commonly used to measure intracellular changes in ROS, for 1 h. After washing the cells twice, they were trypsinized, centrifuged and resuspended in PBS to proceed with flow cytometry analysis (FACS Canto II, BD Biosciences). Hydrogen peroxide (1 mM) was used as a positive control for ROS production. In addition, propidium iodide (PI) (1  $\mu\text{g}/\text{mL}$  final concentration) was used to quantify cell viability and to exclude the dead cells (i.e. PI positive cells) from the DCFH analysis.

**Membrane potential.** HUVECs were seeded at a density of  $4 \times 10^4$  cells/ $\text{cm}^2$  and in 24-well plates and cultured for 24 h. Then, LL37-Au NPs, Au NPs or LL37 peptide suspended/solubilized in culture medium at different concentrations were added to cells. After 5 and 48 h, cells were harvested, resuspended in medium with DiOC<sub>5</sub>(3) (5 nM, Sigma-Aldrich) and incubated for 5 min at room temperature in the dark, prior to the analysis with the flow cytometer (FACS Calibur, BD Biosciences). Cells treated with gramicidin (10  $\mu\text{M}$ ) or valinomycin (10  $\mu\text{M}$ ) were used as controls for cell depolarization and hyperpolarization, respectively.

**NP internalization studies.** HUVECs were seeded at a density of  $3 \times 10^5$  cells per well in 6-well plates and cultured for 24 h. Then, LL37-Au NPs or Au NPs sus-

pended in serum-containing medium were incubated with cells for 5 h or 48 h. After incubation, cells were washed three times with PBS to remove non-internalized NPs. Cells were then detached using 0.2% (v/v) trypsin in PBS, centrifuged, counted and resuspended in nitric acid solution (1 mL, 69%, v/v). After acidic digestion, samples were diluted to 4 mL in Milli-Q water and gold was quantified by ICP-MS, using a 7700x ICP-MS instrument (Agilent Technologies). Elemental analysis detection of Au<sup>197</sup> was performed after a calibration of the apparatus using gold (Panreac) as standard at 5, 10, 50, 100, 250, 500 and 1000 µg/L. Iridium (Panreac) was used as internal standard at 20 µg/L. The mass of NPs per cell was calculated based in the total Au<sup>197</sup> per cell, the Au<sup>197</sup> per mass of LL37-Au NPs and the total number of cells per experimental condition.

**Confocal microscopy analyses.** HUVECs were plated on a µ-slide 8 well, ibi-Treat (Ibidi, Germany) (3x10<sup>4</sup> cells per well) and left to adhere overnight before adding rhodamine-labeled LL37-Au NPs (at 100 µg/mL) or rhodamine-labeled LL37 (at 1 µg/mL) in EGM-2. After 30 min, 4 h or 24 h of NPs incubation, cells were washed three times with PBS and were fixed with paraformaldehyde (4% (v/v)) for 10 min, at room temperature, and washed two times with PBS. After blocking with BSA (1%, w/v in PBS) for 1 h, fixed HUVECs were incubated with mouse anti-human CD31 (Dako, dilution 1:50) for 2 h, washed three times with PBS and permeabilized with 0.3% Triton X-100/PBS, and blocked with BSA (1%, w/v in PBS) for 1 h. Cells were incubated with primary antibodies against early endosomal marker EEA1 (Cell Signaling C45B10, 1:100 dilution) and the late endosome/lysosome marker protein Rab7 (Cell Signaling D95F2, 1:100 dilution), diluted in BB according to the manufacturer's instructions, and incubated for 2 h at room temperature. Then, samples were washed and labeled with secondary antibodies anti-mouse Alexa fluor 647 and anti-rabbit Alexa fluor 488 (both from Life technologies 1:1000 dilution). Un-bound antibody was removed by washing three times with PBS before staining the nucleus of cells with Hoechst (Life technologies, dilution 1:1000) for 10 min. Six confocal images (40 objective) for each condition were taken, using the optimal pinhole for better discrimination between foci and assuring no overexposure or bleed-through between channels. Usually images were composed of four channels (blue, green, red, and far-red), where different interactions were analyzed. Images were exported to ImageJ, and colocalization analysis was performed using the automated co-localization tools available named JACOP.

**FACS analyses.** Cells were dissociated from the culture plate by exposure to Cell Dissociation Buffer (Life Technologies) for 3-5 min and gentle pipetting, centrifuged

and finally resuspended in PBS supplemented with 0,1% (v/v) BSA. The single cell suspensions were aliquoted ( $1.5 \times 10^5$  cells per condition) and stained with either isotype controls and antigen-specific primary antibodies Anti-EGFR antibody (ab30, Abcam, dilution 1:200) for 30 min at 4°C. After the incubation with primary antibodies, cells were washed 3 times and incubated with anti-mouse Alexa fluor 488 (Life technologies 1:1000 dilution) for 30 min. Once the incubations were terminated, the cells were centrifuged at 1000 rpm, 20 °C for 5 min, washed 3 times with cold PBS and then resuspended in PBS containing 0,1% BSA (400  $\mu$ L) for FACS analysis. Differently for FPRL1 quantification, cells were fixed with 0,1% (v/v) paraformaldehyde (PFA) for 10 min, washed, permeabilized with saponin 0,02% (v/v) for 20 min and then stained with either isotype controls and antigen-specific primary antibodies Anti-FPRL1 antibody (ab101702, Abcam, dilution 1:200) for 30 min at 4°C. After the incubation with primary antibodies, cells were washed 3 times and incubated with anti-rabbit Alexa fluor 488 (Life technologies 1:1000 dilution) for 30 min. All conditions were performed in triplicate. FACS Calibur (BD Biosciences, San Diego, CA) and Cyflog software were used for the acquisition and analysis of the data.

**Evaluation of  $\text{Ca}^{2+}$  intracellular release.** HUVECs were seeded at a density of  $1.5 \times 10^4$  cells per well and cultured for 48 h in black opaque 96-well plates. After a period of starvation (7 h, in EBM-2), cells were loaded with Fura-2 calcium fluorescent indicator by incubation with 5  $\mu$ M of the membrane permeable acetoxymethyl (AM) derivative Fura-2/AM (Molecular Probes), using basal medium as vehicle (35  $\mu$ L/well) for 1 h at 37 °C in 5%  $\text{CO}_2$ . The medium was replaced and cells were incubated in the same conditions for more 30 min to allow hydrolysis of the acetoxymethyl (AM) esters by cellular esterases, resulting in intracellular capture of the probe. Cells were then washed twice with 100  $\mu$ L sodium salt solution (140 mM NaCl, 5 mM KCl, 1 mM  $\text{CaCl}_2$ , 1 mM  $\text{MgCl}_2$ , 10 mM Glucose, 10 mM HEPES- $\text{Na}^+$  pH 7.4) and again immediately before the incubation or not with test compounds. Fluorescence reading was performed at 25 °C (Spectramax Gemini EM, Molecular Devices, with SoftMax Pro Software) by measuring emission at 510 nm, using two alternating excitation wavelengths (340 and 380 nm). Cells were then exposed to different concentrations of LL37 peptide, LL37-Au NPs and Au NPs. VEGF (100 ng/ml) was used as positive control for intracellular calcium release. For measurements in the presence of FPRL1 receptor inhibitor, cells were pretreated with the antagonist WRW4 (Calbiochem, 10  $\mu$ M), for 1 h before Fura-2/AM probe incubation.

**EGFR phosphorylation.** The activation of EGFR receptor in HUVECs (80% confluency, in 6-well plates) was induced by starving the cells for 24 h in EBM2 supplemented with 1% (v/v) penicillin and adding soluble LL37 (5  $\mu\text{g}/\text{mL}$ ), LL37-Au NPs (200  $\mu\text{g}/\text{mL}$ ) and Au NPs (200  $\mu\text{g}/\text{mL}$ ) for 10 minutes. Following treatment, the plates were immersed in ice and the medium was discarded. Then the proteins were isolated from the cells. The levels of EGFR (phosphorylated EGFR and total EGFR) were determined by ELISA kit (R&D Systems). Data were acquired with a BioTek synergy MX microplate reader.

**Evaluation of cord-like structure formation on Matrigel.** HUVECs were seeded at a density of  $2 \times 10^5$  per well in 6-well plates and cultured for 24 h in EGM-2. Cells were exposed to LL37-Au NPs (200  $\mu\text{g}/\text{mL}$ ) or Au NPs (200  $\mu\text{g}/\text{mL}$ ) for 4 h and then washed, trypsinized, counted and seeded again at a concentration of  $1 \times 10^4$  cells per well (in 50  $\mu\text{L}$  of M199 medium) on 15-well slide (IBIDI GmbH, Munich, Germany). Each well was previously coated with 10  $\mu\text{L}$  of Matrigel (BD Biosciences) and incubated for 30 min at 37 °C. For measurements in the presence of FPRL1 receptor inhibitor, cells were pretreated with FPRL1 antagonist WRW4 (Calbiochem, 10  $\mu\text{M}$ ) for 1h before adding NPs. In addition,  $1 \times 10^4$  cells in 50  $\mu\text{L}$  of M199 medium were seeded on top of the polymerized Matrigel in the presence of LL37 (5  $\mu\text{g}/\text{mL}$ ) with or without 10  $\mu\text{M}$  of FPRL1 Antagonist WRW4. VEGF at the concentration of 50 ng/mL was used as positive control. After 4 h one image of each well (n=3-6) for experimental condition was taken by a In Cell Microscope 2000 (GE Healthcare) (objective 2x) and then the ImageJ cell counter tool was used to calculate the number of cord-enclosed regions for each conditions relative to control.

**Measurement of VEGF by Elisa.** HUVECs were seeded at a density of  $4 \times 10^4$  cells/cm<sup>2</sup> in 24-well plates and cultured for 24 h in EGM-2 without VEGF. Then cells were exposed to LL37 (5  $\mu\text{g}/\text{mL}$ ), LL37-Au NPs (200  $\mu\text{g}/\text{mL}$ ) or Au NPs (200  $\mu\text{g}/\text{mL}$ ) suspended in culture medium without VEGF at different concentrations were added to cells. LL37 (5  $\mu\text{g}/\text{mL}$ ) and LL37-Au NPs (200  $\mu\text{g}/\text{mL}$ ) were also incubated in the presence of 10  $\mu\text{M}$  of FPRL1 Antagonist WRW4 (Calbiochem). After 24 h of incubation, cell medium from all the conditions was collected and used to quantify VEGF secretion. Supernatant content was measured by a human VEGF ELISA development Kit (PeproTech) according to the manufactures instruction. A calibration curve was established for the calculation.

**CAM assay.** CAM assays were performed in chicken eggs as described previously [183]. Water (5  $\mu\text{L}$ , vehicle, per egg), LL37 (70  $\mu\text{g}$  per egg), LL37-Au NPs (200  $\mu\text{g}$  per egg), Au NPs (200  $\mu\text{g}$  per egg) or bFGF (400 ng per egg) were mixed with

1% methylcellulose (5  $\mu$ L) and placed onto the CAMs and incubated for 3 days. After injection of 20% Luconyl black 0600 (BASF, Ludwigshafen, Germany), photographs were taken. CAMs were fixed, embedded in paraffin, sectioned, stained with a Masson-Goldner solution, and vessels were counted in hot spots as described previously [314].

**Statistical analyses.** Statistical analyses were performed by a t-test or one-way ANOVA test with a Newman-Keuls test applied post hoc for paired comparisons of means (GraphPad Prism 5.0 software).

**Acknowledgements.** The authors would like to thank the financial support of European Commission (Marie Curie Initial Training Network NANODRUG, project n° 289454, FP7-PEOPLE 2011-2015 and ERC grant, project n° 307384, Nanotrigger). Michela Comune is an early stage researcher (ESR) of FP7 Marie Curie ITN NANODRUG network.



## General Conclusions

The development of new and efficient treatments for wound healing is of utmost importance to satisfy the unmet clinical need. In fact, impaired wound healing and its medical complications remain one of the most prevalent and economically burdensome healthcare issue in the world [1]. Current therapies are limited, costly and ineffective. Some advanced technology have been developed over the last few decades, including the use of topic growth factors or cell-based therapies, but even the most innovative and sophisticated product requires proper wound care and wound bed preparation in order to function optimally, contributing to the huge economic burden of this medical area. Other exploratory methodologies have been proposed consisting on different drugs and delivery systems for growth factors, siRNA, miRNA, genetic material and other biomolecules with the aim to target different phases of wound healing and to improve outcome. Despite these advances, the proposed technologies have shown limited effectiveness due to fast degradation of growth factor and biomolecule by proteases or dilution by tissue fluid [51]. Moreover, they are able to target just a molecular pathway but since wound repair is the result of a complex set of interactions among cytokines, formed blood elements extracellular matrix and cells, there is the need of innovative therapies based on correcting multiple deficits simultaneously. Therefore, the combination of therapeutic molecules with NPs has shown huge potential to overcome these lacks and lead the development of a new successful formulation for chronic wound healing. This thesis focused in the development of a novel nanomaterial for wound healing. It comprises the immobilization of a therapeutic molecule, specifically the cationic antimicrobial peptide LL37, in a core of gold NPs. The main hypothesis of this thesis is that LL37- Au NPs have superior regenerative properties and less cytotoxicity than LL37 peptide.

This work shows for the first time the chemical immobilization of LL37 on Au NPs by a one-pot synthesis method. The methodology is relatively simple to allow the preparation of NP conjugates with relatively low size (21 nm) and polydispersity, with high stability in cell culture media or aqueous solutions and presenting antimicrobial and mammalian cell activity. We have screened several parameters to obtain low size and relatively low polydispersed Au NPs with high incorporation of AMPs, including aqueous conditions, time, pH, initial concentration of LL37 peptide and Au ions. Previous studies have reported the physical immobilization of antimicrobial peptides in NPs [245]. In this case, the antimicrobial peptide was adsorbed to a NP formulation and released overtime. Although, this approach prolongs the activity of the antimicrobial peptide, it is insufficient to yield a high local density of peptide on the NPs to enhance their interactions with the bacterial membranes and to enhance its potential bioactivity against mammalian cells. Recently, an alternative strategy has been developed based in the covalent immobilization of antimicrobial peptides in the NP formulation [246] [247]. An antimicrobial peptide conjugated with cholesterol and a TAT peptide easily formed core-shell structured nanoparticles (micelles; average diameter of 177 nm) having a hydrophobic cholesterol core and a hydrophilic cationic peptide shell. Despite the advances, it was unclear the in vivo effectiveness of the nanoformulation compared to free peptide. In fact, to the best of our knowledge, no study has compared in vivo the antimicrobial activity of antimicrobial peptide-conjugated NPs relatively to free antimicrobial peptides.

This work shows in different cell models (keratinocytes and endothelial cells) that LL37-Au NPs have lower cytotoxicity than LL37. LL37-Au NPs are relatively low cytotoxic against endothelial cells and keratinocytes for concentrations up to 400  $\mu\text{g}/\text{mL}$  (i.e, ca. 100  $\mu\text{g}/\text{mL}$  of immobilized LL37). Our results show that the cytotoxicity of LL37 at 10-30  $\mu\text{g}/\text{mL}$  in endothelial cells and keratinocytes was mediated by an increase in membrane depolarization and ROS levels. Similar behavior was not observed for equivalent concentrations of LL37 peptide once immobilized on top of the NPs. This suggests that LL37-Au nanoparticles have minimal impact in cell membrane and is not able to penetrate the membrane; however further research is necessary to clarify this issue.

LL37-Au NPs have high biological activity against mammalian cells. Our results indicate that LL37-Au NPs have superior biological activity than LL37 peptide against

keratinocytes. Keratinocytes exposed to LL37-Au NPs have prolonged migratory properties than keratinocytes exposed to LL37 peptide. The enhanced migratory properties of HaCaT cells, after exposure to LL37-Au NPs, was mediated by a prolonged transactivation of the EGFR via ADAM17 and prolonged ERK signaling activation. Our results further demonstrate that LL37-Au NPs have high pro-angiogenic activity against endothelial cells. We show for the first time that LL37 immobilized to a biomaterial still preserves its angiogenic activity and the mechanism mediating this biological action is different from non-immobilized LL37. LL37 activates primarily FPRL1 receptor that leads to an increase of intracellular levels of  $Ca^{2+}$  and the secretion of  $VEGF_{165}$ . In contrast, LL37-Au NPs activate the transactivation of EGFR but has no effect on FPRL1 receptor and consequent increase of intracellular levels of  $Ca^{2+}$  and secretion of  $VEGF_{165}$ . Importantly, both LL37 and LL37-Au NPs have pro-angiogenic properties as demonstrated in a CAM assay and in vitro Matrigel assays. So far it is unclear whether LL37-Au NPs have superior pro-angiogenic activity than free LL37 peptide. Further studies are required to address this issue.

Endothelial cells and keratinocytes internalize LL37-Au NPs. In case of keratinocytes, the internalization is mediated by scavenger receptors. Despite some differences in the internalization kinetics and magnitude in the internalization of LL37-Au NPs and Au NPs, the most significant aspect of our work is to demonstrate that LL37-Au NPs are internalized by mammalian cells without killing them. Our results further show that LL37-Au NPs are mainly internalized in keratinocytes by scavenger receptors, and at lower extent by clathrin-mediated endocytosis, as confirmed by chemical or siRNA knockdown studies. It is likely that the negative charge of LL37-Au NPs in cell medium facilitates the interaction with scavenger receptors in comparison with other endocytic pathways as previously described for cell penetrating peptide nanocomplexes and DNA-functionalized Au NPs [116]. The internalized LL37-Au NPs tend to accumulate in the endolysosomal compartment in both keratinocytes and endothelial cells; yet differences in the magnitude of the accumulation in both cells have been observed.

The current work shows for the first time the involvement of purinergic receptors in the biological role of LL37-Au NPs and LL37 in keratinocytes. Only recently, some studies have reported the use of NPs to modulate the activity of purinergic receptors [238] [239]. It is well known that purinergic receptors are not only widely expressed in the nervous system but also in non-neural cells such as adult and fetal

keratinocytes, fibroblasts, melanocytes, mast cells, Langerhans cells, and Meissners corpuscles, as well as in hair follicles, sweat glands, and smooth muscle and endothelial cells of skin vessels [237]. Consequently, purinoreceptors are involved in many non-neuronal mechanisms including exocrine and endocrine secretion, immune responses, inflammation, pain, platelet aggregation and endothelial-mediated vasodilatation. Cell proliferation, differentiation and death that occur in development and regeneration are also mediated by purinergic receptors. Purinergic signaling is involved also in skin pathology including psoriasis, scleroderma, skin cancer and wound healing defect, since extracellular nucleotides take part in all phases of wound repair [240]. The majority of studies involving purinergic signaling has been concerning their role in short-term events, such as neurotransmission, secretion, or regulation of the vascular hemostasis. However, there is growing interest in the long-term trophic effects of extracellular nucleotides on cell growth, proliferation, migration and contraction and in the therapeutic potential of compounds that act through purinergic receptors for modulating these phenomena and hence treating a wide range of diseases. Previous studies have demonstrated evidence that purinergic receptors have an essential bridging role in the AMP-ADAM/EGFR stimulatory effect [227] [241]. Other studies have indicated involvement of purinergic receptors in mediating the EGFR transsignaling effects of LL37 with the direct activation of P2X7 by LL37 in monocytes [229]. In the present work, we have performed electrophysiology studies on keratinocytes perfused with soluble LL37 and LL37-Au NPs to evaluate whether their biological effect was initiated by extracellular ATP release. Our results show that the biological role of LL37-Au NPs, but not LL37 peptide, is in part due to extracellular ATP released from keratinocytes. Therefore, both LL37 peptide and LL37-Au NPs have different mechanisms to modulate/activate P2X7 receptor. It is possible that LL37 peptide activates directly P2X7 as suggested by previous studies, without the release of ATP. Another possibility is that LL37 inserts in the cell membrane disturbing it without involving ATP release but leading to the release of other intracellular molecules such as  $Ca^{2+}$  [232].

This work is the first to demonstrate the superior wound healing activity of immobilized LL37 than soluble LL37 in the context of skin wound healing. In fact, results obtained in a splinted mouse full thickness excisional model showed that mice wounds treated with LL37-Au NPs have a faster wound closure than the ones treated with soluble LL37, showing a complete wound healing after 10 days, whereas LL37 peptide-treated mouse showed 70% healing after 10 days. LL37-Au NPs have

---

also superior bioactivity than soluble LL37 concerning collagen synthesis, IL-6 and VEGF expression and angiogenic activity. Further, no adverse effects on body weight, general health, or behavior of the mice were observed after NP treatment and there was no accumulation of NPs in spleen, lung, liver and kidney after 15 days and organs functionality was not altered.

The LL37-Au NPs formulation developed in the current work may have a great potential to treat chronic wounds. The formulation combines elements (LL37 and Au NPs) that have a biomedical history that facilitates the regulatory pathway. Importantly, the formulation is effective in addressing wound healing at multiple levels such as fighting bacterial infection, inducing angiogenesis and inducing the migration of keratinocytes to facilitate skin epithelization. In addition, the formulation has superior efficacy and lower cytotoxicity than LL37 peptide. This is the first technology that combines wound-healing efficacy and antimicrobial activity in the same formulation, it is cheaper than the actual advanced therapies, and may be administered only one time. Although the nanomedicine platform described in this work has significant biomedical potential, further studies are needed before its translation into clinical studies.

### **Perspective and Future work**

One of the most significant contributions of the current work is to highlight the possibility of a piercing mechanism underlying the biological mechanism of LL37-Au NPs. This piercing mechanism is responsible for the release of intracellular ATP that activates P2X receptors. So far, it is unclear the importance of this ATP in the long-lasting activity of LL37-Au NPs. Future studies should be performed to address this issue. A potential experiment will be to evaluate the effect of apyrase in a keratinocyte migration assay. If the piercing mechanism and ATP release is important for the long-lasting activity of LL37-Au NPs we have identified a new signaling strategy to potentiate keratinocyte migration. It is tempting to speculate that such principle could be used in the near future to coat medical devices for cutaneous treatments like patches.

At the moment, it is unclear whether LL37-Au NPs have superior pro-angiogenic properties than LL37 peptide. This requires further testing using different angiogenic models, endothelial proliferation and cycle studies [8], endothelial migration

---

studies, among others. In addition, it will be very important to evaluate the long-term activity of LL37-Au NPs and LL37, as it was shown for keratinocytes. Moreover, further tests are needed to elucidate the mechanism of action of LL37-Au NPs in endothelial cells. For example, it is not known the effect of the inhibition of EGFR signaling in the angiogenic properties of LL37-Au NPs.

So far we have demonstrated the bioactivity of LL37-Au NPs in a non-diabetic model with a single administration. Next steps include the evaluation of the therapeutic effect of LL37-conjugated NPs in a diabetic wound healing animal models. In fact, diabetic patients have a down-regulation in the expression of LL37 [220], and thus it is of utmost importance to compare the regenerative effect of our NP formulation in those patients. In fact, even if most animal studies indicate that LL37 accelerates wound healing, there are some conflicting results in diabetic animal models. Treatment with LL37 in wounds of diabetic ob/ob mice, showed a beneficial effect in one study [234], while another study in diabetic db/db mice failed to show any significant improvement [184]. For the clinical translation of our NP formulation, further pre-clinical tests in GMP conditions are necessary to validate the experimental results obtained in both normal and future diabetic mouse models.

Future studies may also explore LL37-Au NPs in the context of other diseases. For example LL37-Au NPs are very promising for the activation/modulation of purinergic receptors in neurological disorders where they have been shown to display a neuroprotective role [252]. Another aspect could be explored is the use of LL37 gold NPs to delivery miRNAs. miRNAs are important players in angiogenesis, cell proliferation and migration, which are essential components of proper healing of wounds. A recent comparison of skin tissue from normal and diabetic mice showed that 14 miRNAs were differentially expressed in diabetic skin; miR-146b and miR-21 were the most noteworthy [242]. Specifically, miRNA-21 showed a distinct character with increased expression in diabetic skin but decreased expression in diabetic wound healing. A recent study showed that miRNA-21 acts as a negative modulator of angiogenesis [243]. So far, there are some studies about the use of siRNA therapies, but not miRNA therapies, to improve wound healing.

# Bibliography

- [1] C.K. Sen, G.M. Gordillo, S. Roy, R. Kirsner, L. Lambert, T.K. Hunt, et al., Human skin wounds: a major and snowballing threat to public health and the economy, *Wound Repair Regen*, 2009, 176:763-71.
- [2] C.E. Fife, M.J. Carter, D. Walker, B. Thomson, Wound care outcomes and associated cost among patients treated in US outpatient wound centers: data from the US Wound Registry, *Wounds*, 2012, 24(1):10-17.
- [3] PREVADIAB2009. Estudo de prevalencia de diabetes em Portugal, 2012, Available from: [www.min-saude.pt/NR/rdonlyres/219DAD78CD13-43CE-9221-42744B24176C/0/EstudoprevalenciaDiabetesemPortugal.pdf](http://www.min-saude.pt/NR/rdonlyres/219DAD78CD13-43CE-9221-42744B24176C/0/EstudoprevalenciaDiabetesemPortugal.pdf).
- [4] Gronberg A1, Mahlapuu M, Stahle M, Whately-Smith C, Rollman O Treatment with LL-37 is safe and effective in enhancing healing of hard-to-heal venous leg ulcers: a randomized, placebo-controlled clinical trial., *Wound Repair Regen*, 2014 22(5):613-21.
- [5] D. Upton, Psychological aspects of wound care: implications for clinical practice, *JCN*, 2014, 28:2.
- [6] R. Diegelman, M.C. Evans, Wound Healing: An Overview of Acute, Fibrotic and Delayed Healing, *Frontiers in Bioscience*, 2004, 9:283-289.
- [7] A.J. Singer, R.A. Clark, Cutaneous wound healing, *N. Engl. J. Med.*, 1999, 341:738-746.
- [8] P. Martin, Wound healing aiming for perfect skin regeneration, *Science*, 1997, 276:75-81.

- [9] W.K. Stadelmann, A.G. Digenis, G.R. Tobin, Physiology and healing dynamics of chronic cutaneous wounds, *The American Journal of Surgery*, 1998, 176:26S-38S.
- [10] D.L. Steed, The role of growth factors in wound healing, *Surgical Clinics of North America*, 1997, 77:575-586.
- [11] G. Hubner, M. Brauchle, H. Smola, M. Madlener, R. Fassler, S. Werner, Differential regulation of pro-inflammatory cytokines during wound healing in normal and glucocorticoid-treated mice, *Cytokine*, 1996, 8:548-556.
- [12] M. Simpson, R. Ross, The neutrophilic leukocyte in wound repair a study with antineutrophil serum, *Journal of Clinical Investigation*, 1972, 8:2009-2023.
- [13] J.E. Park, A. Barbul, Understanding the role of immune regulation in wound healing, *Am J Surg.*, 2004, 187:11S-16S.
- [14] B. Witte, A. Barbul, General principles of wound healing, *Surgical Clinics of North America*, 1997, 77:509-528.
- [15] D.M. Cooper, Optimizing wound healing. A practice within nursings domain, *Nursing Clinics of North America*, 1990, 25:165-180.
- [16] A. Young, C.E. McNaught, The physiology of wound healing, *Surgery*, 2011, 29:475-479.
- [17] G.S. Lazarus, D.M. Cooper, D.R. Knighton, D.J. Margolis, R.E. Pecoraro, G. Rodeheaver, et al., Definitions and guidelines for the assessment of wounds and evaluation of healing, *Arch Dermatol* , 1997, 130:489-493.
- [18] T.N. Demidova-Rice, M.R. Hamblin, I.M. Herman, Acute and Impaired Wound Healing: Pathophysiology and Current Methods for Drug Delivery, Part 1: Normal and Chronic Wounds: Biology, Causes, and Approaches to Care, *Adv Skin Wound Care*, 2012, 25:304-314.
- [19] M.Y. Sieggreen, R.A. Kline, Arterial insufficiency and ulceration: diagnosis and treatment options, *Nurse Pract*, 2004, 29:46-52.
- [20] V. Falanga, Wound healing and its impairment in the diabetic foot, *Lancet*, 2005, 366:1736-1743.
- [21] D.J. Walker, Venous stasis wounds, *Orthopaedic Nursing*, 1999, 18:65-74.



- [22] H. Brem, M. Tomic-Canic, Cellular and molecular basis of wound healing in diabetes, *The Journal of Clinical Investigation*, 2007, 117(5):1219-1222.
- [23] G.S. Schultz, R.G. Sibbald, V. Falanga, E. A. Ayello, C. Dowsett, K. Harding, et al., Wound bed preparation: a systematic approach to wound management, *Wound Repair Regen.*, 2003, 11:1-28.
- [24] M. Tomic-Canic, E.A. Ayello, O. Stojadinovic, M.S. Golinko, H. Brem, Using gene transcription patterns (bar coding scans) to guide wound debridement and healing, *Adv Skin Wound Care.*, 2008, 21:487-492.
- [25] M. Ehrenreich, Z. Ruszczak, Tissue-engineered temporary wound coverings. Important options for the clinician, *Acta Dermatovenerol. Alp. Panonica Adriat.*, 2006, 15:5-13.
- [26] M.B. Dreifke, A.A. Jayasuriya, A.C. Jayasuriya, Current wound healing procedures and potential care, *Materials Science and Engineering*, 2015, 48:651-662.
- [27] J.S. Boateng, K.R. Matthews, H.N.E. Stevens, G.M. Eccleston , Wound Healing Dressings and Drug Delivery Systems: A Review, *Journal of Pharmaceutical Sciences*, 2008, 97:1-8.
- [28] A. Langer, W. Rogowski, Systematic review of economic evaluations of human cell-derived wound care products for the treatment of venous leg and diabetic foot ulcers, *BMC Health Services Research*, 2009, 9:115.
- [29] P.S. Murphy, G.R.D. Evans, Advances in Wound Healing: A Review of Current Wound Healing Products, *Plastic Surgery International*, 2012, 9:1-8.
- [30] O.Z. Lerman, R.D. Galiano, M. Armour, J.P. Levine, G.C. Gurtner, Cellular Dysfunction in the Diabetic Fibroblast, *American Journal of Pathology*, 2003, 162:1.
- [31] B.C. Kim, H.T. Kim, S.H. Park, J.S. Cha, T. Yufit, S.J. Kim et al., Fibroblasts from chronic wounds show altered TGF-beta signaling and decreased TGF-beta type II receptor expression, *J. Cell. Physiol.*, 2003, 6:331-6.
- [32] A.B. Wysocki, L. Staiano-Coico, F. Grinnell, Wound fluid from chronic leg ulcers contains elevated levels of metalloproteinases MMP-2 and MMP-9, *J. Invest. Dermatol.*, 1993 ,101(1):64-68.

- [33] K.C. Ongena, T.J. Phillips, H.Y. Park, Level of fibronectin mRNA is markedly increased in human chronic wounds, *Dermatol. Surg.*, 2000, 26:447-451.
- [34] M.I. Morasso, M. Tomic-Canic, Epidermal stem cells: the cradle of epidermal determination, differentiation and wound healing, *Biol Cell.*, 2005, 97(3):173-183.
- [35] M.A. Cohen, W.H. Eaglstein, Recombinant human platelet-derived growth factor gel speeds healing of acute full-thickness punch biopsy wounds, *Journal of the American Academy of Dermatology*, 2001, 12: 857-862.
- [36] J.M. Smiell, Clinical safety of becaplermin (rhPDGF-BB) gel. Becaplermin Studies Group, *Am. J. Surg.*, 1998, 176:68S-73S.
- [37] L.M. Mai, C.Y. Lin, C.Y. Chen, Y.C. Tsai, Synergistic effect of bismuth subgallate and borneol, the major components of Sulbogin1 on the healing of skin wound, *Biomaterials*, 2003, 24:3005-3012.
- [38] A. L. Badryia, H. Mohamed, A. Al-Ali, B. Kherallah, Are all wound products created equally: The re-emergence of natural honey, *The Journal of Diabetic Foot*, 2015, 7:26-41.
- [39] R. Khundkar, C. Malic, T. Burge, Use of Acticoat(TM) dressings in burns: what is the evidence?, *Burns*, 2010, 36:751-758.
- [40] B.N. Patrick, M.P. Rivey, D.R. Allington, Acute renal failure associated with vancomycin- and tobramycin-laden cement in total hip arthroplasty, *Annals of Pharmacotherapy*, 2006, 40(11):2037-2042.
- [41] The Annual UK Drug Tariff., 1988 (Nov), 1998 (May), 2007 (Feb) The Stationary Office The UK Drug Tariff.
- [42] H.J. Rutten, P.H. Nijhuis, Prevention of wound infection in elective colorectal surgery by local application of gentamicin-containing collagen sponge, *Eur J Surg Suppl*, 1997, 578:31-35.
- [43] Y. Sawada, M. Ara, T. Yotsuyanagi, K. Sone, Treatment of dermal depth burn wounds with an antimicrobial agent-releasing silicone gel sheet, *Burns*, 1990, 16(5):347-352.
- [44] Y. Sawada, O. Tadashi, K. Masazumi, S. Kazunobu, O. Koichi, J. Sasaki, An evaluation of a new lactic acid polymer drug delivery system: A preliminary report, *Br J Plast Surg*, 1994, 47(3):158-161.

- [45] S. Aoyagi, H. Onishi, Y. Machida, Novel chitosan wound dressing loaded with minocycline for the treatment of severe burn wounds, *Int J Pharm*, 2007, 330(1-2):138-145.
- [46] C. Yao, P. Yao, H. Wu, Z. Zha, Acceleration of wound healing in traumatic ulcers by absorbable collagen sponge containing recombinant basic fibroblast growth factor, *Biomed. Mater.*, 2006, 1:33-37.
- [47] S. Singla, R. Garg, A. Kumar, C. Gill, Efficacy of topical application of beta urogastrone (recombinant human epidermal growth factor) in Wagner Grade 1 and 2 diabetic foot ulcers: comparative analysis of 50 patients, *J. Nat. Sci. Biol. Med.*, 2014, 5:273-277.
- [48] Y. Wu, S. Huang, J. Enhe, K. Ma, S. Yang, T. Sun, et al., Bone marrow-derived mesenchymal stem cell attenuates skin fibrosis development in mice, *Int. Wound J.*, 2014, 11(6):701-10.
- [49] J.M. Gimble, A.J. Katz, B.A. Bunnell, Adipose-derived stem cells for regenerative medicine, *Circ. Res.*, 2007, 100:1249-1260.
- [50] R. Shohara, A. Yamamoto, S. Takikawa, A. Iwase, H. Hibi, F. Kikkawa, et al., Mesenchymal stromal cells of human umbilical cord Wharton's jelly accelerate wound healing by paracrine mechanisms, *Cytotherapy*, 2012, 14:1171-1181.
- [51] V.P. Mantripragada, A.C. Jayasuriya, IGF-1 release kinetics from chitosan microparticles fabricated using environmentally benign conditions, *Mater. Sci. Eng. C Mater. Biol. Appl.*, 2014, 42:506-516.
- [52] R. Feynman, There's Plenty of Room at the Bottom, *Engineering and Science*, 1960, 23(5):22-36.
- [53] E. Drexler, *Engines of Creation: The Coming Era of Nanotechnology*, Anchor Books, 1986.
- [54] J. Ramsden, What is nanotechnology?, *Nanotechnology Perceptions*, 2005, 1:3-17.
- [55] Moghimi SM, Hunter AC, Murray JC, Nanomedicine: current status and future prospects., *FASEB J*, 2005, 19:311-330.

- [56] S. Sandhiya, S.A. Dkhar, A. Surendiran, Emerging trends of nanomedicine: an overview, *Fundamental and Clinical Pharmacology*, 2009, 23:263-269.
- [57] L. Medintz, H. Mattousi, A.R. Clapp, Potential clinical applications of quantum dots, *International Journal of Nanomedicine*, 2008, 3:151-167.
- [58] K. Donaldson, V. Stone, C.L. Tran, W. Kreyling, P.J. Borm, *Nanotoxicology, Occup Environ Med.*, 2004, 61:727-8.
- [59] C.S.O. Paulo, M.M. Lino, A.A. Matos, L.S. Ferreira, Differential internalization of amphotericin B e Conjugated nanoparticles in human cells and the expression of heat shock protein 70, *Biomaterials*, 2013, 34(21):5281-5293.
- [60] N. Lewinski, V. Colvin, R. Drezek, Cytotoxicity of nanoparticles, *Small*, 2008, 4(1):26-49.
- [61] A. Albanese, W.C.W. Chan, Effect of gold nanoparticle aggregation on cell uptake and toxicity, *ACS Nano*, 2011, 5(7):5478-89.
- [62] E. Connor, J. Mwamuka, A. Gole, C. Murphy, M. Wyatt, Gold nanoparticles are taken up by human cells but do not cause acute cytotoxicity, *Small*, 2005, 1(3):325-327.
- [63] B. Chithrani, A. Ghazani, W. Chan, Determining the size and shape dependence of gold nanoparticle uptake into mammalian cells, *Nano Lett*, 2006, 6(4):662-668.
- [64] B. Semete, L. Booyesen, Y. Lemmer, L. Kalombo, L. Katata, J. Verschoor, et al., In vivo evaluation of the biodistribution and safety of PLGA nanoparticles as drug delivery, *Nanomedicine: Nanotechnology, Biology and Medicine*, 2010, 6(5):662-671.
- [65] D.F. Moyano, M. Goldsmith, D.J. Solfiell, D. Landesman-Milo, O.R. Miranda, et al., Nanoparticle hydrophobicity dictates immune response, *J Am Chem-Soc*, 2012, 134(9):3965-3967.
- [66] G.R. Monteith, D. McAndrew, H.M. Faddy, S.J. Roberts-Thomson, Calcium and cancer: targeting  $Ca^{2+}$  transport, *Nat Rev Cancer*, 2007, 7(7):519-530.
- [67] S.J. Xiong, S. George, H.Y. Yu, R. Damoiseaux, B. France, K.W. Ng, et al., Size influences the cytotoxicity of poly (lactic-co-glycolic acid) (PLGA) and titanium dioxide ( $TiO_2$ ) nanoparticles, *Arch Toxicol*, 2013, 87(6):1075-1086.

- [68] S. Mura, H. Hillaireau, J. Nicolas, B. Le Droumaguet, C. Gueutin, S. Zanna, et al., Influence of surface charge on the potential toxicity of PLGA nanoparticles towards Calu-3 cells, *Int J Nanomedicine*, 2011, 6:2591-2605.
- [69] C. Murphy, A. Gole, J. Stone, P. Sisco, A. Alkilany, E. Goldsmith, et al., Gold nanoparticles in biology: beyond toxicity to cellular imaging, *AccChem Res*, 2008, 41(12):1721-1730.
- [70] A. Thakor, J. Jokerst, C. Zavaleta, T. Massoud, S. Gambhir, Gold nanoparticles: a revival in precious metal administration to patients, *Nano Lett*, 2011, 11(10):4029-4036.
- [71] V. Sumbayev, I. Yasinska, C. Garcia, D. Gilliland, G. Lall, B. Gibbs, et al., Gold nanoparticles downregulate interleukin-1beta- induced pro-inflammatory responses, *Small*, 2013, 9(3):472-477.
- [72] Z. Deng, M. Liang, M. Monteiro, I. Toth, R. Minchin, Nanoparticle-induced unfolding of fibrinogen promotes Mac-1 receptor activation and inflammation, *Nat Nanotechnol*, 2011, 6(1):39-44.
- [73] C.Y. Tsai, S.L. Lu, C.W. Hu, C.S. Yeh, G.B. Lee, H.Y. Lei, Size-dependent attenuation of TLR9 signaling by gold nanoparticles in macrophages, *J Immunol*, 2012, 188(1):68-76.
- [74] M. Semmler-Behnke, W. Kreyling, J. Lipka, S. Fertsch, A. Wenk, S. Takenaka, et al., Biodistribution of 1.4- and 18-nm gold particles in rats, *Small*, 2008, 4(12):2108-2111.
- [75] N. Khlebtsov, L. Dykman, Biodistribution and toxicity of engineered gold nanoparticles: a review of in vitro and in vivo studies, *ChemSoc Rev*, 2011, 40(3):1647-1671.
- [76] R.R. Arvizo, O.R. Miranda, D.F. Moyano, C.A. Walden, K. Giri, R. Bhattacharya, et al., Modulating Pharmacokinetics, Tumor Uptake and Biodistribution by Engineered Nanoparticles, *Plos One*, 2011, 6(9):24374.
- [77] W.S. Cho, M. Cho, J. Jeong, M. Choi, H.Y. Cho, B.S. Han et al., Acute toxicity and pharmacokinetics of 13 nm-sized PEG-coated gold nanoparticles, *Toxicol Appl Pharmacol*, 2009, 236(1):16-24.
- [78] E. Froehlich, The role of surface charge in cellular uptake and cytotoxicity of medical nanoparticles, *Int J Nanomedicine*, 2012, 7:5577-5591.

- [79] J. Aaseth, M. Haugen, O. Forre, Rheumatoid arthritis and metal compounds perspectives on the role of oxygen radical detoxification, *Analyst*, 1998, 123:3-6.
- [80] S. Chen, Z. Wang, J. Ballato, S. Foulger, D. Carroll, Monopod, Bipod, Tripod, and Tetrapod Gold Nanocrystals, *J. Am. Chem. Soc.*, 2003, 125(52):16186-16187.
- [81] D.A. Giljohann, D.S. Seferos, W.L. Daniel, M.D. Massich, P.C. Patel, C.A. Mirkin, Gold Nanoparticles for Biology and Medicine, *Angew. Chem. Int. Ed.*, 2010, 49:3280-3294.
- [82] C.F. Shaw III, Gold-based therapeutic agents, *Chem Rev*, 1999, 99:2589-2600.
- [83] J. Turkevich, J. Hillier, P.C. Stevenson, A study of the nucleation and growth processes in the synthesis of colloidal gold, *Discuss. Faraday Soc.*, 1951,11:55-57.
- [84] G. Frens, Controlled Nucleation for the Regulation of the Particle Size in Monodisperse Gold Suspensions, *Nature Phys. Sci.*, 1973, 241:20-22.
- [85] MC Daniel, D. Astruc, Gold Nanoparticles: Assembly, Supramolecular Chemistry, Quantum-Size-Related Properties, and Applications toward Biology, Catalysis, and Nanotechnology, *Chem. Rev.*, 2004, 104:293-346.
- [86] E. Crew E, MA Tessel, S. Rahman, A. Razzak-Jaffar, D. Mott, M. Kamundi, et al., MicroRNA conjugated gold nanoparticles and cell transfection, *Anal Chem*, 2012, 84(1):26-29.
- [87] N. Chandaa, V. Kattumurib, R. Shukla, A. Zambre, K. Katti, A. Upendran, et al., Bombesin functionalized gold nanoparticles show in vitro and in vivo cancer receptor specificity, *PNAS*, 2010, 107(19):8760-8765.
- [88] K. Shimojo, T. Nilde, T. Taguchi, H. Naganawa, N. Kamiya, M. Goto, et al., Facile, rapid and efficient biofabrication of gold nanoparticles decorated with functional proteins, *Analyst*, 2012, 137(10): 2300-2303.
- [89] B. Duncan, C. Kim, VM Rotello, Gold nanoparticle platforms as drug and biomacromolecule delivery systems, *J. Contr. Release*, 2010, 148:122-127.
- [90] CY Tsai, AL Shiau, SY Chen, YH Chen, PC Cheng, MY Chang, et al., Amelioration of collagen induced arthritis in rats by nanogold, *Arthritis and Rheumatism*, 2007, 56(2): 544-554.

- [91] Han G, You CC, Kim BJ, Turingan RS, Forbes NS, Martin CT, et al., Light Regulated Release of DNA and its delivery to nuclei by means of photolabile gold nanoparticles, *Angewandte Chemie*, 2006, 118(19): 3237-3241.
- [92] Hong R, Han G, Fernandez JM, Kim BJ, Forbes NS, Rotello VM, Glutathione-mediated delivery and release using monolayer protected nanoparticle carriers, *Journal of the American Chemical Society*, 2006, 128(4): 1078-1079.
- [93] Boisselier E, Astruc D, Gold nanoparticles in nanomedicine: preparations, imaging, diagnostics, therapies and toxicity, *Chemical Society Review*, 2009, 38(6):1759-1782.
- [94] Dean HJ, Haynes J, Schmaljohn C, The role of particle-mediated DNA vaccines in biodefense preparedness, *Advanced Drug Delivery Reviews*, 2005, 57(9):1315-1342.
- [95] Lu W, Xiong C, Zhang G, Huang Q, Zhang R, Zhang JZ, et al., Targeted photothermal ablation of murine melanomas with melanocyte-stimulating hormone analog-conjugated hollow gold nanospheres, *Clin Cancer Res*, 2009, 15:876-886.
- [96] Sokolov K, Follen M, Aaron J, Pavlova I, Malpica A, Lotan R, et al., Real-time vital optical imaging of precancer using anti-epidermal growth factor receptor antibodies conjugated to gold nanoparticles, *Cancer Research*, 2003, 63:1999-2004.
- [97] Chen SA, Chen HM, Yao YD, Hung CF, Tu CS, Liang YJ, Topical treatment with anti-oxidants and Au nanoparticles promote healing of diabetic wound through receptor for advance glycation end-products, *European Journal of Pharmaceutical Sciences*, 2012, 47(5):875-883.
- [98] Zhou Y, Kong Y, Kundu S, Cirillo JD, Liang H, Antibacterial activities of gold and silver nanoparticles against *Escherichia coli* and *Bacillus Calmette-Guarin*, *Journal of Nanobiotechnology*, 2012, 10(19):1-9.
- [99] Li X, Robinson SM, Gupta A, Saha K, Jiang Z, Moyano DF, et al., Functional gold nanoparticles as potent antimicrobial agents against multi-drug-resistant bacteria, *ACS nano*, 2014, 8(10):10682-10686.
- [100] Charafeddine RA, Makdisi J, Schairer D, O'Rourke BP, Diaz-Valencia JD, et al., Fidgetin-Like 2: A Microtubule-Based Regulator of Wound Healing, *Journal of Investigative Dermatology*, 2015.

- [101] Randeria PS, Seeger MA, Wang XQ, Wilson H, Shipp D, Mirkin CA, et al., siRNA-based spherical nucleic acids reverse impaired wound healing in diabetic mice by ganglioside GM3 synthase knockdown, *Proceedings of the National Academy of Sciences*, 2015, 112(18):5573-5578.
- [102] Chen H, Dorrigan A, Saad S, Hare DJ, Cortie MB, Valenzuela SM, In vivo study of spherical gold nanoparticles: inflammatory effects and distribution in mice, *PLoS One*, 2013, 8(2):e58208.
- [103] Dykman LA, Khlebtsov NG, Uptake of engineered gold nanoparticles into mammalian cells, *Chemical reviews*, 2013, 114(2):1258-1288.
- [104] Zhu ZJ, Ghosh PS, Miranda OR, Vachet RW, Rotello VM, Multiplexed Screening of Cellular Uptake of Gold Nanoparticles Using Laser Desorption/Ionization Mass Spectrometry, *Journal of the American Chemical Society*, 2008, 130(43):14139-14143.
- [105] Jiang W, KimBetty YS, Rutka JT, ChanWarren CW, Nanoparticle-mediated cellular response is size-dependent, *Nat Nano*, 2008, 3(3):145-150.
- [106] Ferreira L, Nanoparticles as tools to study and control stem cells, *J Cell Biochem*, 2009, 108(4):746-52.
- [107] Doherty GJ, McMahon HT, Mechanisms of endocytosis, *Annu Rev Biochem*, 2009, 78:857-902.
- [108] Paulo CS, das Neves RP, Ferreira LS, Nanoparticles for intracellular-targeted drug delivery, *Nanotechnology*, 2011, 22(49):494002.
- [109] Tkachenko AG, Xie H, Liu Y, Coleman D, Ryan J, Glomm WR, et al., Cellular trajectories of peptide-modified gold particle complexes: comparison of nuclear localization signals and peptide transduction domains, *Bioconjugate chemistry*, 2004, 15(3):482-490.
- [110] Yang C, Neshatian M, van Prooijen M, Chithrani DB, Cancer nanotechnology: enhanced therapeutic response using peptide-modified gold nanoparticles, *J. Nanosci. Nanotechnol.*, 2014, 14(7):4813-4819.
- [111] Yang C, Chithrani DB, Peptide-modified smaller nanoparticles for improved cancer therapy, *J. Pharm. Pharmacol.*, 2014 (In press).



- [112] Nativo P, Prior IA, Brust M, Uptake and intracellular fate of surface-modified gold nanoparticles, *ACS Nano*, 2008, 2:1639-1644.
- [113] Krpetic Z, Saleemi S, Prior IA, See V, Qureshi R, Brust M, Negotiation of intracellular membrane barriers by TAT-modified gold nanoparticles, *ACS nano*, 2011, 5(6):5195-5201.
- [114] Ezzat K, Langel A, Scavenger receptor mediated uptake of cell penetrating peptide nanocomplexes with oligonucleotides, *The Fazeb Journal*, 2012, 26:1172-1180.
- [115] Peiser L, Gordon S, The function of scavenger receptors expressed by macrophages and their role in the regulation of inflammation, *Microbes Infect.*, 2001, 3(2):149-159.
- [116] Patel PC, Giljohann DA, Daniel WL, Zheng D, Prigodich AE, Mirkin CA, Scavenger receptors mediate cellular uptake of polyvalent oligonucleotide-functionalized gold nanoparticles, *Bioconjugate Chem*, 2010, 212250-2256.
- [117] Shi J, Votruba AR, Farokhzad OC, Langer R, Nanotechnology in drug delivery and tissue engineering: from discovery to applications, *Nano letters*, 2010, 10(9):3223-3230.
- [118] Torchilin VP, Recent advances with liposomes as pharmaceutical carriers, *Nature reviews Drug discovery*, 2005, 4(2):145-160.
- [119] Duncan R, Polymer conjugates as anticancer nanomedicines, *Nature Reviews Cancer*, 2006, 6(9):688-701.
- [120] Zhang L, Gu FX, Chan JM, Wang AZ, Langer RS, Farokhzad OC, Nanoparticles in medicine: therapeutic applications and developments, *Clinical pharmacology & therapeutics*, 2008, 83(5):761-769.
- [121] Danhier F, Ansorena E, Silva JM, Coco R, Le Breton A, Prat V, PLGA-based nanoparticles: an overview of biomedical applications, *Journal of controlled release*, 2012, 161(2):505-522.
- [122] Debbage P, Jaschke W, Molecular imaging with nanoparticles: giant roles for dwarf actors, *Histochemistry and cell biology*, 2008, 130(5):845-875.
- [123] Tocco I, Zavan B, Bassetto F, Vindigni V, Nanotechnology-based therapies for skin wound regeneration, *Journal of Nanomaterials*, 2012, 2012:4.

- [124] DeLouise LA, Applications of nanotechnology in dermatology, *Journal of investigative dermatology*, 2012, 132:964-975.
- [125] Schaeffer MR, Tantry U, Efron PA, Ahrendt GM, Thornton FJ, Barbul A, Diabetes-impaired healing and reduced wound nitric oxide synthesis: a possible pathophysiologic correlation, *Surgery*, 1997, 121(5):513-519.
- [126] Han G, Nguyen LN, Macherla C, Chi Y, Friedman JM, Nosanchuk JD, Martinez LR, Nitric oxide releasing nanoparticles accelerate wound healing by promoting fibroblast migration and collagen deposition, *The American journal of pathology*, 2012, 180(4):1465-1473.
- [127] Cortivo R, Vindigni V, Iacobellis L, Abatangelo G, Pinton P, Zavan B, Nanoscale particle therapies for wounds and ulcers, *Nanomedicine*, 2010, 5(4):641-656.
- [128] Chereddy KK, Coco R, Memvanga PB, Ucar B, des Rieux A, Vandermeulen G, et al., Combined effect of PLGA and curcumin on wound healing activity, *Journal of Controlled Release*, 2013, 171(2):208-215.
- [129] Chereddy KK, Her CH, Comune M, Moia C, Lopes A, Porporato PE, et al., PLGA nanoparticles loaded with host defense peptide LL37 promote wound healing, *Journal of Controlled Release*, 2014, 194:138-147.
- [130] Vignoni M, de Alwis Weerasekera H, Simpson MJ, Phopas J, Mah TF, Griffith M, et al., LL37 peptide silver nanoparticles: combining the best of the two worlds for skin infection control, *Nanoscale*, 2014, 6(11):5725-5728.
- [131] Vigderman L, Zubarev ER, Therapeutic platforms based on gold nanoparticles and their covalent conjugates with drug molecules, *Advanced drug delivery reviews*, 2013, 65(5):663-676.
- [132] Daniel MC, Astruc D, Gold nanoparticles: assembly, supramolecular chemistry, quantum-size-related properties, and applications toward biology, catalysis, and nanotechnology, *Chem. Rev.*, 2004, 104(1):293-346.
- [133] Love JC, Estroff LA, Kriebel JK, Nuzzo RG, Whitesides GM, Self-assembled monolayers of thiolates on metals as a form of nanotechnology, *Chemical reviews*, 2005, 105(4):1103-1170.
- [134] Delehanty JB, Boeneman K, Bradburne CE, Robertson K, Bongard JE, Medintz, IL, Peptides for specific intracellular delivery and targeting of nanoparticles:

- implications for developing nanoparticle-mediated drug delivery, *Therapeutic delivery*, 2010, 1(3):411-433.
- [135] Lia T, Heab X, Wang Z, The application of peptide functionalized gold nanoparticles, In ACS symposium series, 2012, 11130:55-68.
- [136] Kogan MJ, Olmedo I, Hosta L, Guerrero AR, Cruz LJ, Albericio F, Peptides and metallic nanoparticles for biomedical applications, *Nanomedicine*, 2007, 2(3):287-306.
- [137] Levy R, Thanh NT, Doty RC, Hussain I, Nichols RJ, Schiffrin DJ, et al., Rational and combinatorial design of peptide capping ligands for gold nanoparticles, *Journal of the American Chemical Society*, 2004, 126(32):10076-10084.
- [138] Serizawa T, Hirai Y, Aizawa M, Novel synthetic route to peptide-capped gold nanoparticles, *Langmuir*, 2009, 25(20):12229-12234.
- [139] Nasrolahi Shirazi A, Mandal D, Tiwari RK, Guo L, Lu W, Parang K, Cyclic peptide-capped gold nanoparticles as drug delivery systems, *Molecular pharmaceuticals*, 2012, 10(2):500-511.
- [140] Lai HZ, Wang SG, Wu CY, Chen YC, Detection of *Staphylococcus aureus* by Functional Gold Nanoparticle-Based Affinity Surface-Assisted Laser Desorption/Ionization Mass Spectrometry, *Analytical chemistry*, 2015, 87(4):2114-2120.
- [141] Parween S, Ali A, Chauhan VS, Non-natural amino acids containing peptide-capped gold nanoparticles for drug delivery application, *ACS applied materials & interfaces*, 2013, (5):6484-6493.
- [142] Tan YN, Lee JY, Wang DI, Uncovering the design rules for peptide synthesis of metal nanoparticles, *Journal of the American Chemical Society*, 2010, 132(16):5677-5686.
- [143] Yan X, Blacklock J, Li J, Moihwald, One-pot synthesis of polypeptide gold nanoconjugates for in vitro gene transfection, *ACS nano*, 2011, 6(1):111-117.
- [144] De la Fuente JM, Berry CC, Riehle MO, Curtis SG, NPs targeting at cells, *Langmuir*, 2006, 22:3286-3293.
- [145] Tkachenko AG, Xie H, Coleman D, Glomm W, Ryan J, Anderson MF, et al., Multifunctional gold nanoparticle-peptide complexes for nuclear targeting, *Journal of the American Chemical Society*, 2003, 125(16):4700-4701.

- [146] Liu Y, Shipton MK, Ryan J, Kaufman ED, Franzen S, Feldheim DL, Synthesis, stability, and cellular internalization of gold nanoparticles containing mixed peptide-poly (ethylene glycol) monolayers, *Analytical chemistry*, 2007, 79(6):2221-2229.
- [147] Bartczak D, Kanaras AG, Preparation of Peptide-Functionalized Gold Nanoparticles Using One Pot EDC/Sulfo-NHS Coupling, *Langmuir*, 2011, 27(16):10119-10123.
- [148] Slocik JM, Naik RR, Probing peptide-nanomaterial interactions, *Chem Soc Rev.*, 2010, 39(9):3454-63.
- [149] Bhattacharjee RR, Das AK, Haldar D, Si S, Banerjee A, Mandal TK, Peptide-assisted synthesis of gold nanoparticles and their self-assembly, *J Nanosci Nanotechnol*, 2005, 5(7):1141-7.
- [150] Sperling RA, Parak WJ, Surface modification, functionalization and bioconjugation of colloidal inorganic nanoparticles, *Philosophical Transactions of the Royal Society of London A: Mathematical, Physical and Engineering Sciences*, 368(1915):1333-1383.
- [151] Kumar A, Ma H, Zhang X, Huang K, Jin S, Liu J, et al., Gold nanoparticles functionalized with therapeutic and targeted peptides for cancer treatment, *Biomaterials*, 2012, 33(4):1180-1189.
- [152] de la Fuente JM, Berry CC, Tat peptide as an efficient molecule to translocate gold nanoparticles into the cell nucleus, *Bioconjug Chem*, 2005, 16(5):1176-80.
- [153] Arosio D, Manzoni L, Araldi EM, Scolastico C, Cyclic RGD functionalized gold nanoparticles for tumor targeting, *Bioconjugate chemistry*, 2011, 22(4):664-672.
- [154] Chanda N, Kattumuri V, Shukla R, Zambre A, Katti K, Upendran A, et al., Bombesin functionalized gold nanoparticles show in vitro and in vivo cancer receptor specificity, *Proceedings of the National Academy of Sciences*, 2010, 107(19):8760-8765.
- [155] Tran NTT, Wang TH, Lin CY, Tsai YC, Lai CH, Tai Y, et al., Direct synthesis of rev peptide-conjugated gold nanoparticles and their application in cancer therapeutics, *Bioconjugate chemistry*, 2011, 22(7):1394-1401.

- [156] Patel PC, Giljohann DA, Seferos DS, Mirkin CA, Peptide antisense nanoparticles, *Proceedings of the National Academy of Sciences*, 2008, 105(45):17222-17226.
- [157] Scara G, Porta F, Fascio U, Avvakumova S, Dal Santo V, De Simone M, et al., Gold nanoparticles capped by a GC-containing peptide functionalized with an RGD motif for integrin targeting, *Bioconjugate chemistry*, 2012, 23(3):340-349.
- [158] Koczulla AR, Bals R, Antimicrobial peptides, *Drugs*, 2003, 63(4):389-406.
- [159] Jones FS, Simms HS, The bacterial growth inhibitor (lactenin) of milk: I. The preparation in concentrated form, *J Exp Med*, 1930, 51(2):327-339.
- [160] Antimicrobial Sequences Database: //www.bbcm.univ.trieste.it/ tossi/pag1.htm.
- [161] Peters BM, Shirliff ME, Jabra-Rizk MA, Antimicrobial Peptides: Primeval Molecules or Future Drugs?, *PLoS Pathogens*, 2010, 6(10):e100167.
- [162] Wang G, Mishra B, Lau K, Lushnikova T, Golla R, Wang X, Antimicrobial Peptides in 2014, *Pharmaceuticals*, 2015, 8(1):123-150.
- [163] Schroeder JM, Harder J, Antimicrobial peptides in skin disease, *Drug Discovery Today: Therapeutic Strategies*, 2006, 3(1), 93-100.
- [164] Lupetti A, Wellng MW, Pauwels EKJ, Nibbering PH, Radiolabelled antimicrobial peptides for infection detection, *The Lancet Infectious Diseases*, 2003, 3:223-229.
- [165] Braff MH, Bardan A, Nizet V, Gallo RL, Cutaneous Defense Mechanisms by Antimicrobial Peptides, *J Invest Dermatol*, 2005, 125:9-13.
- [166] Shai Y, From innate immunity to de-novo designed antimicrobial peptides, *Curr Pharm Des*, 2002, 8:715-725.
- [167] Moser C, Weiner DJ, Lysenko E, Bals R, Weiser JN, Wilson JM., beta-Defensin 1 contributes to pulmonary innate immunity in mice, *Infect Immun*, 2002, 70(6):3068-72.
- [168] Giuliani A, Pirri G, Nicoletto S, Antimicrobial peptides: an overview of a promising class of therapeutics, *Cent Eur J Biol*, 2007, 2:1-33.

- [169] Nizet V, Ohtake T, Lauth X, Trowbridge J, Rudisill J, Dorschner RA, et al., Innate antimicrobial peptide protects the skin from invasive bacterial infection, *Nature*, 2001, 414 (6862):454-457.
- [170] Zaiou M, Multifunctional antimicrobial peptides: therapeutic targets in several human diseases, *J Mol Med*, 2007, 85:317-329.
- [171] Van Wetering S, Mannesse-Lazeroms SP, Dijkman JH, Hiemstra PS., Effect of neutrophil serine proteinases and defensins on lung epithelial cells: modulation of cytotoxicity and IL-8 production, *J Leukoc Biol*, 1997, 62(2):217-26.
- [172] Chertov O, Michiel DF, Xu L, Wang JM, Tani K, Murphy WJ, et al., Identification of defensin-1, defensin-2, and CAP37/azurocidin as T-cell chemoattractant proteins released from interleukin-8-stimulated neutrophils, *J Biol Chem*, 1996, 271(6):2935-40.
- [173] Lillard Jr JW, Boyaka PN, Chertov O, et al., Mechanisms for induction of acquired host immunity by neutrophil peptide defensins, *Proc Natl Acad Sci*, 1999, 96(2):651-6.
- [174] Yang D, Chen Q, Chertov O, Oppenheim JJ, Human neutrophil defensins selectively chemoattract naive T and immature dendritic cells, *J Leukoc Biol*, 2000, 68(1):9-14.
- [175] Yang D, Chen Q, Schmidt AP, Anderson GM, Wang JM, Wooters J, et al., LL-37, the neutrophil granule- and epithelial cell-derived cathelicidin, utilizes formyl peptide receptor-like 1 (FPRL1) as a receptor to chemoattract human peripheral blood neutrophils, monocytes, and T-cells, *J Exp Med*, 2000, 192(7):1069-74.
- [176] Bardan A, Nizet V, Gallo RL., Antimicrobial peptides and the skin, *Expert Opin Biol Ther*, 2004, 4(4):543-549.
- [177] Ong PY, Ohtake T, Brandt C, Strickland I, Boguniewicz M, Ganz T, et al., Endogenous antimicrobial peptides and skin infections in atopic dermatitis, *N Engl J Med*, 2002, 347(15):1151-60.
- [178] Yamasaki K, Di Nardo A, Bardan A, Masamoto Murakami, Takaaki Ohtake, Alvin Coda et al., Increased serine protease activity and cathelicidin promotes skin inflammation in rosacea, *Nat Med*, 2007, 13:975-980.

- [179] Nakatsuji T, Gallo RL, Antimicrobial Peptides: Old Molecules with New Ideas, *Journal of Investigative Dermatology*, 2012, 132:887-895.
- [180] Kenshi Y, Gallo RL, Antimicrobial peptides in human skin disease, *Eur J Dermatol.*, 2008, 18(1):11-21.
- [181] Cole AM, Shi J, Ceccarelli A, Kim YH, Park A, Ganz T, Inhibition of neutrophil elastase prevents cathelicidin activation and impairs clearance of bacteria from wounds, *Blood*, 2001, 97:297-304.
- [182] Steinstraesser L, Klein RD, Aminlari A, Fan MH, Khilanani V, Remick DG, et al., *Protegrin-1 enhances bacterial killing in thermally injured skin*, *Crit Care Med*, 2001, 29:1431-1437.
- [183] Koczulla R, von Degenfeld G, Kupatt C, Krotz F, Zahler S, Gloe T, et al., An angiogenic role for the human peptide antibiotic LL-37/hCAP-18, *J Clin Invest*, 2003, 111:1665-1672.
- [184] Steinstraesser L, Lam MC, Jacobsen F, Porporato PE, Chereddy KK, Becerikli M, et al., Skin electroporation of a plasmid encoding hCAP-18/LL-37 host defense peptide promotes wound healing, *Mol. Ther.*, 2014, 22;734-742.
- [185] Gonzalez-Curiel I, Trujillo V, Montoya-Rosales, Rincon K, Rivas-Calderon B, deHaro-Acosta J, et al., 1,25-Dihydroxyvitamin D3 induces LL-37 and HBD-2 production in keratinocytes from diabetic foot ulcers promoting wound healing: An in vitro model, *PLoS One*, 2014, 9:e111355.
- [186] Niyonsaba, F, Ushio H, Nakano N, Ng W, Sayama K, Hashimoto K, et al., Antimicrobial peptides human defensins stimulate epidermal keratinocyte migration, proliferation and production of proinflammatory cytokines and chemokines, *Journal of Investigative Dermatology*, 2007, 127(3):594-604.
- [187] Heilborn JD, Nilsson MF, Kratz G, Weber G, Sorensen O, Borregaard N, et al., The cathelicidin anti-microbial peptide LL-37 is involved in reepithelialization of human skin wounds and is lacking in chronic ulcer epithelium, *J Invest Dermatol*, 2003, 120:379-389.
- [188] L. Bi, Yang L, Narsimhan G, Bhunia AK, Yao Y, Designing carbohydrate nanoparticles for prolonged efficacy of antimicrobial peptide, *J Control Release*, 2011, 150(2):150-156.

- [189] Eby DM, Farrington KE, Johnson GR, Synthesis of bioinorganic antimicrobial peptide nanoparticles with potential therapeutic properties, *Biomacromolecules*, 2008, 9:2487-2494.
- [190] L. Liu, Xu K, Wang H, Tan PK, Fan W, Venkatraman SS, et al., Self-assembled cationic peptide nanoparticles as an efficient antimicrobial agent, 2009, *Nat Nanotechnol* 4(7):457-463.
- [191] H. Wang, Xu K, Liu L, Tan JP, Chen Y, Li Y, et al., The efficacy of self-assembled cationic antimicrobial peptide nanoparticles against *Cryptococcus neoformans* for the treatment of meningitis, *Biomaterials*, 2010, 31(10):2874-2881.
- [192] Piras AM, Maisetta G, Sandreschi S, Gazzarri M, Bartoli C, Grassi L, et al., Chitosan nanoparticles loaded with the antimicrobial peptide temporin B exert a long-term antibacterial activity in vitro against clinical isolates of *Staphylococcus epidermidis*, *Frontiers in microbiology*, 2015, 6.
- [193] Water JJ, Smart S, Franzyk H, Foged C, Nielsen HM, Nanoparticle-mediated delivery of the antimicrobial peptide plectasin against *Staphylococcus aureus* in infected epithelial cells, *European Journal of Pharmaceutics and Biopharmaceutics*, 2015, 92:65-73.
- [194] Medeiros KA, Joanitti GA, Silva LP, Chitosan nanoparticles for dermaseptin peptide delivery toward tumor cells in vitro, *Anticancer Drugs*, 2014, 25:323-331.
- [195] Miao D, Jiang M, Liu Z, Gu G, Hu Q, Kang T, et al., Co-administration of dual-targeting nanoparticles with penetration enhancement peptide for antiglioblastoma therapy, *Mol. Pharm.*, 2014, 11:90-101.
- [196] Ahmad A, Ranjan S, Zhang W, Zou J, Pykka, Kinnunen PK, Novel endosomolytic peptides for enhancing gene delivery in nanoparticles, *Biochimica et Biophysica Acta (BBA)-Biomembranes*, 2015, 1848(2):544-553.
- [197] Benson HA, Namjoshi S, Proteins and peptides: strategies for delivery to and across the skin, *Journal of pharmaceutical sciences*, 2008, 97(9):3591-3610.
- [198] Frick IM, Akesson P, Rasmussen M, Schmidtchen A, Björck L., SIC, a secreted protein of *Streptococcus pyogenes* that inactivates antibacterial peptides, *J Biol Chem*, 2003, 278(19):16561-16566.



- [199] Thwaite JE, Hibbs S, Titball RW, Atkins TP, Proteolytic degradation of human antimicrobial peptide LL-37 by *Bacillus anthracis* may contribute to virulence, *Antimicrob Agents Chemother*, 2006, 50(7):2316-2322.
- [200] Fox JL, Antimicrobial peptides stage a comeback, *Nat Biotechnol*, 2013, 31(5):379-382.
- [201] Lee IH, Cho Y, Lehrer RI, Effects of pH and salinity on the antimicrobial properties of clavanins *Infect Immun*, 1997, 65(7):2898-2903.
- [202] Larrick JW, Hirata M, Balint RF, Lee J, JZhong J, Wright SC, Human CAP18: a novel antimicrobial lipopolysaccharide-binding protein, *Infect. Immun.*, 1995, 63:1291-1297.
- [203] Burton MF, Steel PG, The chemistry and biology of LL-37, *Natural product reports*, 2009, 26(12):1572-1584.
- [204] Vandamme D, Landuyt B, Luyten W, Schoofs L, A comprehensive summary of LL-37, the factotum human cathelicidin peptide, *Cellular Immunology*, 2012, 280:22-35.
- [205] Porcelli F, Verardi R, Shi L, Henzler-Wildman KA, Ramamoorthy A, Veglia G, NMR structure of the cathelicidin-derived human antimicrobial peptide LL-37 in dodecylphosphocholine micelles, *Biochemistry*, 2008, 47:5565-5572.
- [206] G. Wang, Structures of human host defense cathelicidin LL-37 and its smallest antimicrobial peptide KR-12 in lipid micelles, *J. Biol. Chem.*, 2008, 283:32637-32643.
- [207] Park K, Elias PM, Oda Y, Mackenzie D, Mauro T, Holleran WM, Regulation of cathelicidin antimicrobial peptide expression by an endoplasmic reticulum (ER) stress signaling, vitamin D receptor- independent pathway, *J. Biol. Chem.*, 2011, 286:34121-34130.
- [208] Li X, Li Y, Han H, Miller DW, Wang G, Solution structures of human LL-37 fragments and NMR-based identification of a minimal membrane-targeting antimicrobial and anticancer region, *J. Am. Chem. Soc.*, 2006, 128:5776-5785.
- [209] Byfield FJ, Kowalski M, Cruz K, Leszczyna K, Namniot A, Savage PB, et al., Cathelicidin LL-37 increases lung epithelial cell stiffness, decreases transepithelial permeability, and prevents epithelial invasion by *Pseudomonas aeruginosa*, *The Journal of Immunology*, 2011, 187(12):6402-6409.

- [210] Thennarasu S, Tan A, Penumatchu R, Shelburne CE, Heyl DL, Ramamoorthy A, Antimicrobial and membrane disrupting activities of a peptide derived from the human cathelicidin antimicrobial peptide LL37, *Biophys. J.*, 2010, 98:248-257.
- [211] Ciornei CD, Sigurdardottir T, Schmidtchen A, Bodelsson M, Antimicrobial and chemoattractant activity, lipopolysaccharide neutralization, cytotoxicity, and inhibition by serum of analogs of human cathelicidin LL-37, *Antimicrob. Agents Chemother.*, 2005, 49:2845-2850.
- [212] Wuerth K, Hancock RE, New insights into cathelicidin modulation of adaptive immunity, *Eur. J. Immunol.*, 2011, 41:2817-2819.
- [213] Montreekachon P, Chotjumlong P, Bolscher JG, Nazmi K, Reutrakul V, Krisanaprakornkit S., Involvement of P2X(7) purinergic receptor and MEK1/2 in interleukin-8 up-regulation by LL-37 in human gingival fibroblasts, *J. Periodontal Res.*, 2011, 46:327-337.
- [214] Tjabringa GS, Aarbiou J, Ninaber DK, Drijfhout JW, Sorensen OE, Borregaard N, et al., The antimicrobial peptide LL-37 activates innate immunity at the airway epithelial surface by transactivation of the epidermal growth factor receptor, *J. Immunol.*, 2003, 171:6690-6696.
- [215] Coffelt SB, Marini FC, Watson K, Zvezdaryk KJ, Dembinski JL, LaMarca HL, et al., The pro-inflammatory peptide LL-37 promotes ovarian tumor progression through recruitment of multipotent mesenchymal stromal cells, *Proc. Natl. Acad. Sci.*, 2009, 106:3806-3811.
- [216] Zughailer SM, Shafer WM, Stephens DS, Antimicrobial peptides and endotoxin inhibit cytokine and nitric oxide release but amplify respiratory burst response in human and murine macrophages, *Cell. Microbiol.*, 2005, 7:1251-1262.
- [217] Pistolic J, Cosseau C, Li Y, Yu JJ, Filewod NC, Gellatly S, et al., Host defence peptide LL-37 induces IL-6 expression in human bronchial epithelial cells by activation of the NF-kappaB signaling pathway, *J. Innate. Immun.*, 2009, 1:254-267.
- [218] Scott MG, Davidson DJ, Gold MR, Bowdish D, Hancock RE, The human antimicrobial peptide LL-37 is a multifunctional modulator of innate immune responses, *J. Immunol.*, 2002, 169:3883-3891.

- [219] Nagaoka I, Tamura H, Hirata M, An antimicrobial cathelicidin peptide, human CAP18/LL-37, suppresses neutrophil apoptosis via the activation of formyl-peptide receptor-like 1 and P2X7, *J. Immunol.*, 2006, 176:3044-3052.
- [220] Rivas-Santiago B, Trujillo V, Montoya A, Gonzalez-Curiel I, Castaeda-Delgado J, Cardenas A, et al., Expression of antimicrobial peptides in diabetic foot ulcer, *Journal of dermatological science*, 2012, 65(1):19-26.
- [221] Pfosser A, El-Aouni C, Pfisterer I, Dietz M, Globisch F, Stachel G, et al., NF kappaB activation in embryonic endothelial progenitor cells enhances neovascularization via PSGL-1 mediated recruitment: novel role for LL37, *Stem Cells*, 2010, 28:376-385.
- [222] Park HJ, Cho DH, Kim HJ, Lee JY, Cho BK, Bang SI, et al., Collagen synthesis is suppressed in dermal fibroblasts by the human antimicrobial peptide LL-37, *J. Invest. Dermatol.*, 2009, 129:843-850.
- [223] Tokumaru S, Higashiyama S, Endo T, Nakagawa T, Miyagawa JI, Yamamori K, et al., Ectodomain shedding of epidermal growth factor receptor ligands is required for keratinocyte migration in cutaneous wound healing, *The Journal of cell biology*, 2000, 151(2):209-220.
- [224] Yin J, Fu-Shin XY, LL-37 via EGFR Transactivation to Promote High Glucose Attenuated Epithelial Wound Healing in Organ-Cultured Corneas, *Investigative ophthalmology and andvisual science*, 2010, 51(4):1891.
- [225] Tokumaru S, Sayama K, Shirakata Y, Komatsuzawa H, Ouhara K, Hanakawa Y, et al., Induction of keratinocyte migration via transactivation of the epidermal growth factor receptor by the antimicrobial peptide LL-37, *J Immunol.*, 2005, 175(7):4662-8.
- [226] Reiss K, Bhakdi S, Pore-forming bacterial toxins and antimicrobial peptides as modulators of ADAM function, *Med Microbiol Immunol*, 2012, 201(4):419-26.
- [227] Sommer A, Fries A, Cornelsen I, Speck N, Koch-Nolte F, Gimpl G, et al., Melittin modulates keratinocyte function through P2 receptor-dependent ADAM activation, *Journal of Biological Chemistry*, 2012, 287(28):23678-23689.
- [228] Tomasinsig L, Pizzirani C, Skerlavaj B, Pellegatti P, Gulinelli S, Tossi A, et al., The human cathelicidin LL-37 modulates the activities of the P2X7 receptor in a structure-dependent manner, *J. Biol. Chem.*, 2008, 283:30471-30481.

- [229] Ellsner A, Duncan M, Gavrilin M, Wewers MD, A novel P2X7 receptor activator, the human cathelicidin-derived peptide LL37, induces IL-1 beta processing and release, *J Immunol.*, 2004, 172(8):4987-4994.
- [230] Braff MH, Hawkins MA, Di NA, Lopez-Garcia B, Howell MD, Wong C, et al., Structure-function relationships among human cathelicidin peptides: dissociation of antimicrobial properties from host immunostimulatory activities, *J. Immunol.*, 2005, 174:4271-4278.
- [231] Nagaoka I, Tamura H, Hirata M., An antimicrobial cathelicidin peptide, human CAP18/LL-37, suppresses neutrophil apoptosis via the activation of formyl-peptide receptor-like 1 and P2X7, *J Immunol.*, 2006, 176(5):3044-52.
- [232] Pochet S, Tandel S, Querriere S, Tre-Hardy M, Garcia-Marcos M, De Lorenzi M, et al., Modulation by LL-37 of the responses of salivary glands to purinergic agonists, *Mol Pharmacol.*, 2006, 69(6):2037-2046.
- [233] Ramos R, Silva JP, Rodrigues AC, Costa R, Guardao L, Schmitt F, et al., Wound healing activity of the human antimicrobial peptide LL37, *Peptides*, 2011, 32(7):1469-76.
- [234] Carretero M, Escamez MJ, Garcia M, Duarte B, Holguin A, Retamosa L, et al., In vitro and in vivo wound healing-promoting activities of human cathelicidin LL-37, *J Invest Dermatol*, 2008, 128(1):223-36.
- [235] Gabriel M, Nazmi K, Veerman EC, Nieuw Amerongen AV, Zentner A, Preparation of LL-37-grafted titanium surfaces with bactericidal activity, *Bioconjug Chem.*, 2006, 17(2):548-50.
- [236] Gronberg A1, Mahlapuu M, Stahle M, Whately-Smith C, Rollman O Treatment with LL-37 is safe and effective in enhancing healing of hard-to-heal venous leg ulcers: a randomized, placebo-controlled clinical trial., *Wound Repair Regen*, 2014 22(5):613-21.
- [237] Geoffrey Burnstock, Gillian E. Knight, Aina V.H. Greig, Purinergic Signaling in Healthy and Diseased Skin, *Journal of Investigative Dermatology Volume 132* 526-546, 2012,
- [238] L Baron, A Gombault, M Fanny, B Villeret, F Savigny, N Guillou, et al., The NLRP3 inflammasome is activated by nanoparticles through ATP, ADP and adenosine, *Cell Death and Disease*, 2015:1-15

- [239] Leifert A., Pan Y, Kinkeldey A, Schiefer F, Setzler J, Scheel O, et al, Differential hERG ion channel activity of ultrasmall gold nanoparticles, PNAS, 2013
- [240] Gendaszewska-Darmach E1, Kucharska M., Nucleotide receptors as targets in the pharmacological enhancement of dermal wound healing, Purinergic Signalling, 2011
- [241] Sperrhacker M., Fischer J1, Wu Z1, Klunder S1, Sedlacek R2, Schroeder JM, et al., SPINK9 Stimulates Metalloprotease/EGFR-Dependent Keratinocyte Migration via Purinergic Receptor Activation, Journal of Investigative Dermatology, 2014, 134: 1645-1654
- [242] Madhyastha R., Madhyastha H, Nakajima Y, Omura S, Maruyama M. MicroRNA signature in diabetic wound healing: promotive role of miR-21 in fibroblast migration, Int Wound J, 2011.
- [243] Sabatel C., Malvaux L, Bovy N, Deroanne C, Lambert V, Gonzalez ML, et al., MicroRNA-21 exhibits antiangiogenic function by targeting RhoB expression in endothelial cells, PLoS One, 2011 6(2):16979.
- [244] Rai A., Pinto S, Paulo C, Comune M, Ferreira L, Biocompatibility Issues of Organic and Inorganic Nanomaterials, eBook Frontiers in Biomaterials, Publisher Bentham Science 2014:274-304
- [245] Bi, L., Yang L, Narsimhan G, Bhunia AK, Yao Y., Designing carbohydrate nanoparticles for prolonged efficacy of antimicrobial peptide, J Control Release ,2011, 150:150-6.
- [246] Liu, L., Xu K, Wang H, Tan PK, Fan W, Venkatraman SS, et al., Self-assembled cationic peptide nanoparticles as an efficient antimicrobial agent, Nat Nanotechnol ,2009, 4:457-63.
- [247] Wang, H., Xu K, Liu L, Tan JP, Chen Y, Li Y., The efficacy of self-assembled cationic antimicrobial peptide nanoparticles against *Cryptococcus neoformans* for the treatment of meningitis, Biomaterials ,2010, 31:2874-81.
- [248] Salvati, A., Pitek AS, Monopoli MP, Prapainop K, Bombelli FB, Hristov DR, et al., Transferrin-functionalized nanoparticles lose their targeting capabilities when a biomolecule corona adsorbs on the surface, Nat Nanotechnol ,2013, 8:137-43.

- [249] Monopoli, M.P., Christoffer Aberg, Anna Salvati, Kenneth A. Dawson, Biomolecular coronas provide the biological identity of nanosized materials, *Nat Nanotechnol*, 2012, 7:779-86.
- [250] Bartczak, D., Otto L. Muskens, Tilman Sanchez-Elsner, Antonios G. Kanaras, Timothy M. Millar, Manipulation of in vitro angiogenesis using peptide-coated gold nanoparticles, *ACS Nano*, 2013, 7:5628-36.
- [251] Patra, C.R., R. Bhattacharya, S. Patra, N.E. Vlahakis, A. Gabashvili, Y. Koltypin, et al., Pro-angiogenic properties of europium(III) hydroxide nanorods, *Advanced Materials*, 2008, 20:753.
- [252] Cunha RA, Neuroprotection by adenosine in the brain: From A1 receptor activation to A2A receptor blockade, *Purinergic Signalling*, 2005, 1:111-134.
- [253] Wiesner J, Vilcinskis A, Molekularbiologie Fi, Bio-ressourcen P, The ancient arm of the human immune system, *Antimicrobial peptides*, 2010,1:440-464.
- [254] Liu X1, Atwater M, Wang J, Huo Q, Extinction coefficient of gold nanoparticles with different sizes and different capping ligands, *Colloids Surf B Biointerfaces*, 2007,58:3-7.
- [255] Ramos R, Domingues L, Gama M, LL37, a human antimicrobial peptide with immunomodulatory properties, *Science against microbial pathogens: communicating current research and technological advances* 2011:915-25.
- [256] Heinz H, Farmer BL, Pandey RB, Slocik JM, Patnaik SS, Pachter R, et al., Nature of molecular interactions of peptides with gold, palladium, and Pd-Au bimetal surfaces in aqueous solution, *J Am Chem Soc*, 2009, 131:9704-14.
- [257] Heinz H, Computational screening of biomolecular adsorption and self-assembly on nanoscale surfaces, *J Comput Chem*, 2010, 31:1564-8.
- [258] Yu J, Becker ML, Carri GA, A molecular dynamics simulation of the stability-limited growth mechanism of peptide-mediated gold-nanoparticle synthesis, *Small*, 2010,6:2242-5.
- [259] Lobanov M, Bogatyreva NS, Galzitskaia OV, Radius of gyration is indicator of compactness of protein structure *Mol Biol*, 2008,42:701-6.
- [260] Johansson J, Gudmundsson GH, Rottenberg ME, Berndt KD, Agerberth B, Conformation-dependent antibacterial activity of the naturally occurring human peptide LL-37, *J Biol Chem*, 1998, 273:3718-24.

- [261] dos Santos T, Varela J, Lynch I, Salvati A, Dawson KA, Effects of transport inhibitors on the cellular uptake of carboxylated polystyrene nanoparticles in different cell lines, *PLoS One*, 2011, 6:e24438.
- [262] Lunov O, Syrovets T, Loos C, Beil J, Delacher M, Tron K, et al., Differential uptake of functionalized polystyrene nanoparticles by human macrophages and a monocytic cell line, *ACS Nano*, 2011,5:1657-69.
- [263] Limmon GV, Arredouani M, McCann KL, Corn Minor RA, Kobzik L, Imani F, Scavenger receptor class-A is a novel cell surface receptor for double-stranded RNA, *FASEB J*, 2008, 22:159-67.
- [264] Platt N, Gordon S, Scavenger receptors: diverse activities and promiscuous binding of polyanionic ligands, *Chem Biol*, 1998, 5:R193-203.
- [265] MacLeod DT, Nakatsuji T, Yamasaki K, Kobzik L, Gallo RL, HSV-1 exploits the innate immune scavenger receptor MARCO to enhance epithelial adsorption and infection, *Nat Commun*, 2013, 4:1963.
- [266] Choi CH, Hao L, Narayan SP, Auyeung E, Mirkin CA, Mechanism for the endocytosis of spherical nucleic acid nanoparticle conjugates, *Proc Natl Acad Sci U S A*, 2013, 110:7625-30.
- [267] Tang X, Basavarajappa D, Haeggstrom JZ, Wan M, P2X7 Receptor Regulates Internalization of Antimicrobial Peptide LL-37 by Human Macrophages That Promotes Intracellular Pathogen Clearance, *J Immunol*, 2015, 195:1191-201.
- [268] Lau YE, Rozek A, Scott MG, Goosney DL, Davidson DJ, Hancock RE, Interaction and cellular localization of the human host defense peptide LL-37 with lung epithelial cells, *Infect Immun*, 2005, 73:583-91.
- [269] van der Does AM, Beekhuizen H, Ravensbergen B, Vos T, Ottenhoff TH, van Dissel JT, et al., LL-37 directs macrophage differentiation toward macrophages with a proinflammatory signature, *J Immunol*, 2010, 185:1442-9.
- [270] Bandholtz L, Ekman GJ, Vilhelmsson M, Buentke E, Agerberth B, Scheynius A, et al. Antimicrobial peptide LL-37 internalized by immature human dendritic cells alters their phenotype, *Scand J Immunol*. 2006, 63:410-9.
- [271] Blobel CP, ADAMs: key components in EGFR signalling and development, *Nat Rev Mol Cell Biol*, 2005, 6:32-43.

- [272] Maretzky T, Evers A, Zhou W, Swendeman SL, Wong PM, Rafii S, et al., Migration of growth factor-stimulated epithelial and endothelial cells depends on EGFR transactivation by ADAM17, *Nat Commun*, 2011, 2:229.
- [273] Sperrhacker M, Fischer J, Wu Z, Klunder S, Sedlacek R, Schroeder JM, et al., SPINK9 stimulates metalloprotease/EGFR-dependent keratinocyte migration via purinergic receptor activation, *J Invest Dermatol*, 2014, 134:1645-54.
- [274] Mookherjee N, Lippert DN, Hamill P, Falsafi R, Nijnik A, Kindrachuk J, et al., Intracellular receptor for human host defense peptide LL-37 in monocytes, *J Immunol*, 2009, 183:2688-96.
- [275] Volonte C, Apolloni S, Skaper SD, Burnstock G, P2X7 receptors: channels, pores and more, *CNS Neurol Disord Drug Targets*, 2012, 11:705-21.
- [276] Honore P, Donnelly-Roberts D, Namovic MT, Hsieh G, Zhu CZ, Mikusa JP, et al., A-740003 [N-(1-[(cyanoimino)(5-quinolinylamino) methyl]amino)-2,2-dimethylpropyl)-2-(3,4-dimethoxyphenyl)acetamide], a novel and selective P2X7 receptor antagonist, dose-dependently reduces neuropathic pain in the rat, *J Pharmacol Exp Ther*, 2006, 319:1376-85.
- [277] Miller CM, Boulter NR, Fuller SJ, Zakrzewski AM, Lees MP, Saunders BM, et al., The role of the P2X(7) receptor in infectious diseases, *PLoS Pathog*, 2011, 7:e1002212.
- [278] Repertinger SK, Campagnaro E, Fuhrman J, El-Abaseri T, Yuspa SH, Hansen LA, EGFR enhances early healing after cutaneous incisional wounding, *J Invest Dermatol*, 2004, 123:982-9.
- [279] Boucher I, Kehasse A, Marcincin M, Rich C, Rahimi N, Trinkaus-Randall V, Distinct activation of epidermal growth factor receptor by UTP contributes to epithelial cell wound repair, *Am J Pathol*, 2011, 178:1092-105.
- [280] Tomas A, Futter CE, Eden ER, EGF receptor trafficking: consequences for signaling and cancer, *Trends Cell Biol*, 2014, 24:26-34.
- [281] Offterdinger M, Bastiaens PI, Prolonged EGFR signaling by ERBB2-mediated sequestration at the plasma membrane, *Traffic*, 2008, 9:147-55.
- [282] Hong SY, Shih YP, Li T, Carraway KL, Lo SH, CTEN prolongs signaling by EGFR through reducing its ligand-induced degradation, *Cancer Res*, 2013, 73:5266-76.



- [283] Fan VH, Tamama K, Au A, Littrell R, Richardson LB, Wright JW, et al., Tethered epidermal growth factor provides a survival advantage to mesenchymal stem cells, *Stem Cells*, 2007, 25:1241-51.
- [284] Lin Z-q, Kondo T, Ishida Y, Takayasu T, Mukaida N, Essential involvement of IL-6 in the skin wound-healing process as evidenced by delayed wound healing in IL-6-deficient mice, 2003, 73.
- [285] Sehgal PB, Interleukin-6: molecular pathophysiology, *J Invest Dermatol*, 1990, 94:2S-6S.
- [286] Hasmann A, Wehrsuetz-Sigl E, Marold A, Wiesbauer H, Schoeftner R, Gewessler U, et al., Analysis of myeloperoxidase activity in wound fluids as a marker of infection, *Annals of clinical biochemistry*, 2013, 50:245-54.
- [287] Fernandes R, Smyth NR, Muskens OL, Nitti S, Heuer-Jungemann A, Ardern-Jones MR, et al., Interactions of skin with gold nanoparticles of different surface charge, shape, and functionality, *Small*, 2015, 11:713-21.
- [288] McCrudden MTC, McLean DTF, Zhou M, Shaw J, Linden GJ, Irwin CR, et al., The Host Defence Peptide LL-37 is Susceptible to Proteolytic Degradation by Wound Fluid Isolated from Foot Ulcers of Diabetic Patients, *Int J Pept Res Ther*, 2014, 20:457-64.
- [289] Van Der Spoel D, Lindahl E, Hess B, Groenhof G, Mark AE, Berendsen HJ, GROMACS: fast, flexible, and free, *J Comput Chem*, 2005, 26:1701-18.
- [290] Peter P Bradley, Dennis A Priebat, RDC, Rothstein G, Measurement of cutaneous inflammation: estimation of neutrophil content with an enzyme marker, *Journal of Investigative Dermatology*, 1982, 78(3):206-9
- [291] Phelps, E.A., A.J. Garcia, Update on therapeutic vascularization strategies, *Regenerative Medicine*, 2009, 4(1):65-80
- [292] Eppler, S.M., Combs DL, Henry TD, Lopez JJ, Ellis SG, Yi JH, et al., A target-mediated model to describe the pharmacokinetics and hemodynamic effects of recombinant human vascular endothelial growth factor in humans. *Clin Pharmacol Ther*, 2002, 72(1):20-32.
- [293] Fischbach, C., D.J. Mooney, Polymeric systems for bioinspired delivery of angiogenic molecules, *Adv Polym Sci*, 2006:191

- [294] Shen, Y.H., M.S. Shoichet, M. Radisic, Vascular endothelial growth factor immobilized in collagen scaffold promotes penetration and proliferation of endothelial cells, *Acta Biomaterialia*, 2008, 4(3):477-489.
- [295] Sharon, J.L., D.A. Puleo, Immobilization of glycoproteins, such as VEGF, on biodegradable substrates, *Acta Biomaterialia*, 2008, 4(4):1016-1023.
- [296] Porter, A.M., C.M. Klinge, A.S. Gobin, Biomimetic hydrogels with VEGF induce angiogenic processes in both hUVEC and hMEC, *Biomacromolecules*, 2011, 12(1):242-6.
- [297] Leslie-Barbick J.E., J.J. Moon, J.L. West, Covalently-immobilized vascular endothelial growth factor promotes endothelial cell tubulogenesis in poly(ethylene glycol) diacrylate hydrogels, *J Biomater Sci Polym Ed*, 2009, 20(12):1763-79.
- [298] Phelps, E.A., Landazuri N, Thulé PM, Taylor WR, García AJ., Bioartificial matrices for therapeutic vascularization, *Proc. Nat. Acad. Sci. US*, 2010, 107(8):3323-8.
- [299] Ferrara, N., H.P. Gerber, and J. LeCouter, The biology of VEGF and its receptors, *Nat Med*, 2003, 9(6):669-76.
- [300] Vajanto, I., Rissanen TT, Rutanen J, Hiltunen MO, Tuomisto TT, Arve K et al., Evaluation of angiogenesis and side effects in ischemic rabbit hindlimbs after intramuscular injection of adenoviral vectors encoding VEGF and LacZ., *J Gene Med*, 2002, 4(4):371-80.
- [301] Margulis, K., Neofytou EA, Beygui RE, Zare RN, Celecoxib Nanoparticles for Therapeutic Angiogenesis, *ACS Nano*, 2015, 9(9): 9416-26.
- [302] Doorn, J., Fernandes HA, Le BQ, van de Peppel J, van Leeuwen JP, De Vries MR, et al., A small molecule approach to engineering vascularized tissue, *Biomaterials*, 2013, 34(12): 3053-63.
- [303] Patra, C.R., Kim JH, Pramanik K, d'Uscio LV, Patra S, Pal K, et al., Reactive Oxygen Species Driven Angiogenesis by Inorganic Nanorods, *Nano Letters*, 2011, 11(11):4932-4938.
- [304] Salvado, M.D., Di Gennaro A, Lindbom L, Agerberth B, Haeggstrom JZ. et al., Cathelicidin LL-37 induces angiogenesis via PGE2-EP3 signaling in endothe-

- lial cells, in vivo inhibition by aspirin, *Arterioscler Thromb Vasc Biol*, 2013, 33(8):1965-72.
- [305] Yount, N.Y., Kupferwasser D, Spisni A, Dutz SM, Ramjan ZH, Sharma S, et al., Selective reciprocity in antimicrobial activity versus cytotoxicity of hBD-2 and crotamine, *Proc Natl Acad Sci U S A*, 2009, 106:14972-7.
- [306] Schaller-Bals, S., A. Schulze, R. Bals, Increased levels of antimicrobial peptides in tracheal aspirates of newborn infants during infection, *Am J Respir Crit Care Med*, 2002, 165(7):992-5.
- [307] Chen, C.I., Schaller-Bals S, Paul KP, Wahn U, Bals R, Beta-defensins and LL-37 in bronchoalveolar lavage fluid of patients with cystic fibrosis, *J Cyst Fibros*, 2004, 3(1):45-50.
- [308] Barlow, P.G., Li Y, Wilkinson TS, Bowdish DM, Lau YE, Cosseau C, et al., The human cationic host defense peptide LL-37 mediates contrasting effects on apoptotic pathways in different primary cells of the innate immune system, *J Leukoc Biol*, 2006, 80(3):509-20.
- [309] Ding, B., Soblosky L, Nguyen K, Geng J, Yu X, Ramamoorthy A, et al., Physiologically-relevant modes of membrane interactions by the human antimicrobial peptide, LL-37, revealed by SFG experiments, *Sci Rep*, 2013, 3:1854.
- [310] Bae, Y.S., et al., The synthetic chemoattractant peptide, Trp-Lys-Tyr-Met-Val- D-Met, enhances monocyte survival via PKC-dependent Akt activation monocytes and neutrophils, 2002 71:329-338.
- [311] Bae, Y.S., Kim Y, Park JC, Suh PG, Ryu SH, Identification of peptides that antagonize formyl peptide receptor-like 1-mediated signaling, *Journal of Immunology*, 2004, 173(1):607-614.
- [312] Girnita, A., Zheng H, Gronberg A, Girnita L, Stahle M, Identification of the cathelicidin peptide LL-37 as agonist for the type I insulin-like growth factor receptor, *Oncogene*, 2012, 31(3):352-65.
- [313] A. Rai, S. Pinto, T. Velho, C. Moita, A. F. Ferreira, U. Trivedi, et al., One-step synthesis of high-density peptide-conjugated gold nanoparticles with antimicrobial efficacy in a systemic infection model, *Biomaterials*, submitted October 2015, 85:99-110.

- [314] Issbrucker K., Marti HH, Hippenstiel S, Springmann G, Voswinckel R, Gammann A, et al., p38 MAP kinase-a molecular switch between VEGF-induced angiogenesis and vascular hyperpermeability, *FASEB J.*, 2003, 17:262-264.
- [315] Marques JM, Rodrigues RJ, Valbuena S, Rozas JL, Selak S, Marin P, et al., CRMP2 tethers kainate receptor activity to cytoskeleton dynamics during neuronal maturation, *J Neuroscience*, 2013, 33:18298-18310
- [316] Paternain A.V., Cohen A., Stern-Bach Y., Lerma J., A role for extracellular Na<sup>+</sup> in the channel gating of native and recombinant kainate receptors, *J Neuroscience*, 2003, 33:8641-8648.

